ASIC GAS SENSORS BASED ON RATIOMETRIC PRINCIPLES

by

Jaleed Ejaz Khawaja

School of Engineering

University of Warwick

A thesis submitted to the University of Warwick

for the degree of Doctor of Philosophy

April 2009

Table of Contents

List of Figures

List of Tables

Summary

The wide-scale usage of VOCs in industrial processes requires monitoring the concentrations of these vapours to keep a safe operating environment. Most combustible hydrocarbons can be ignited as a gas-air mixture in the range of 0.5% to 15% by volume. This has led to the development of several portable air quality monitoring instruments. However, the high costs and lack of durability of these instruments has remained an issue to be addressed. This PhD thesis reports on the development and characterization of a novel low cost smart gas sensor technology adaptable for use in a portable instrument. The smart gas sensor devices have been developed to target four different VOCs in air.

The smart gas sensor device combines a smart ASIC (SRL 194 designed at SRL, Warwick University) fabricated in standard 0.7 µm CMOS technology and two alkyl-dithiol based self-assembled gold nanoparticle chemoresistive sensors (fabricated at Sony Deutschland GmbH) in a ratiometric array to offer a robust system which can address the common mode variations found in polymer based gas sensor systems. The ratiometric ASIC sensor array architecture allows for the reduction of the baseline value's dependence on environmental variations and the elimination of baseline drift due to long term application of DC voltage.

Three ratiometric array arrangements - mono-type uni-variate with only one chemosensor per device, mono-type bi-variate with two chemosensors of the same film material per device and duo-type with a polar and a non-polar chemosensor per device and their variations were characterized in an automated FIA test station against exposure to methanol, ethanol, propan-1-ol, and toluene at 30°C and 0-5% rh. It was determined that the devices' response output to VOC analytes was entirely dependent on the variation of the resistance ratio of the chemoresistive sensors in the ratiometric sensor array. The effects of variations of the temperature and rh on the smart sensor output were calibrated. The mono-type devices gave a high magnitude response to the vapours whereas the duo-type arrangement offered a high degree of discrimination between the test analytes with little post-processing steps.

Three different alkyl-dithiol chemoresistive sensor films on gold electrodes were successfully used as the VOC vapour sensitive elements in each arrangement. The effects of using a silicone sealant gel as a partitioning layer were characterized and it was observed that at vapour concentrations less than 3000 ppm the silicone encapsulated chemosensor devices reported a larger response to the VOC analytes as compared to those without the silicone. The test devices reported promising response repeatability and reproducibility with excellent return to baseline properties, a negligible hysteresis and an error margin of under 10%. Ideal operating temperature was determined to be 40°C at which rh variations were found to be minimal. The test devices were found to be robust with little variation in the quality of the device output over the course of 18 months.

The novel research demonstrated that it is possible to get high level of diversification between analytes from a low cost and robust gas sensor system for monitoring VOCs. The work carried out here has opened the opportunity to develop highly integrated programmable hand-held gas sensor and e-nose systems for environmental monitoring use in health and safety applications.

Acknowledgements

I would like to thank my academic supervisor Prof. Julian Gardner for allowing me the opportunity of studying in this field, and for his guidance and tuition during my PhD. I would also like to acknowledge the help and advice of my co-supervisor Dr. Marina Cole.

I am grateful to all members of the *Sensors Research Laboratory, School of Engineering, University of Warwick***,** including, Mr. Frank T. Courtney and Mr. Ian Griffiths for their assistance in mechanical matters. I benefited greatly from useful discussions with Dr. Gurmukh Sehra, Dr. Jesus Garcia-Guzman, Dr. Su-Lim (Forest) Tan, Dr. Irina I. Leonte, Dr. Takao Iwaki, Mr. Fauzan Che-Harun, Mr. Philip King, Ms. Marina Talib, Mr. James Taylor, Mr. Shrey Pathak and Ms. Cecilia Occhiuzzi for their help in technical matters. I would especially like to thank Dr. James Covington for his encouragement advice and support over the course of this research.

This project was made possible with the material and financial support of our collaborators Dr. Tobias Vossmeyer, Dr. Isabelle Raible and Dr. Anette Simonis from *Sony Deutschland (GmbH), Material Science Laboratory*.

Finally, I am short of words for the immeasurable support and patience of my family, friends and colleagues who helped me in one way or another, without which I would not have been able to do this.

Declaration

The work described in this thesis is entirely original and my own, except where otherwise indicated.

Parts of this work have been presented at international conferences and published in the scientific literature listed below:

1. Conference Paper

[1] J.E. Khawaja, M. Cole, *J. García-Guzmán,* J.W. Gardner, ***Gold Nanoparticle CMOS Sensor for VOC Detection***, Eurosensors XX Conference, Göteborg, Sweden17-20 September, 2006.

Selected Abbreviations and Acronyms

TERM	*DEFINITION*
AMIS	AMI Semiconductors
Au-HDT	Gold nanoparticle 1,16-hexadecanedithiol
Au-MAH	Gold nanoparticle - 2-Mercapto-N-[6-(2-mercapto-acetylamino)- hexyl]-acetamide
Au-NT	Gold nanoparticle - 1,9-nonanedithiol
ASIC	Application Specific Integrated Circuit
CMOS	Complementary Metal Oxide Semiconductor
DC	Direct Current
DAFC	Direct Alcohol Fuel Cell
E-nose	Electronic Nose
FET	Field Effect Transistor
FIA	Fluid Injection Analysis
IDE	Inter-digitated Electrodes
I/O	Input/Output
MEMS	Micro-Electro-Mechanical-System
MOS	Metal Oxide Semiconductor
MRSA	Methicillin Resistant Staphylococcus Aureus
NOC	Nose-On-a-Chip
PCA	Principal Component Analysis
PCB	Printed Circuit Board
PDMS	Poly (dimethylsiloxane)
PEDOT-PSS	Poly(3,4-ethylenedioxy)thiophene-poly(styrene sulfonate)
PEG	Poly (ethylene glycol)
PEMFC	Polymer Exchange Membrane Fuel Cell
PEVA	Poly (ethylene-co-vinyl acetate)
PG	Periglomerulus Cell
PP	Poly (pyrrole)
PPM	Parts-Per-Million
PPS	Poly (phenylene sulphide)
PPSA	Poly (phenylene sulphide-phenyleneamine)
PPX	Poly (*p*-xylylene)
PSB	Poly (styrene-co-butadiene)
PSF	Poly (sulfane)
PT	Poly (thiophene)
PVPH	Poly (4-vinyl phenol)
PTFE	Poly (tetrafluoroethylene)
PVC	Poly (9-vinylcarbazole)
PVPD	Poly (vinyl pyrrolidone)
PVPH	Poly (4-vinyl phenol)
PW	Pulse Width
QCM	Quartz Crystal Microbalance
rh	Relative Humidity
RISC	Reduced Instruction Set Computing

rr	Resistance ratio
Si	Silicon
SRL	Sensors Research Laboratory
USEPA	United States Environment Protection Agency
UV	Ultra-Violet
VI	Virtual Instrument
VOC	Volatile Organic Compound

Selected Symbol Reference

TERM	*DEFINITION*
Δrr	Change in resistance ratio
Δrr_0	y intercept for linear regression fit
ΔV	Change in voltage (V)
ΔV_{max}	Maximum change in voltage (V)
α	Langmuir constant (ppm^{-1})
C	Concentration (ppm)
F_k	Freundlich coefficient
K	Langmuir sorption sites (ppm)
L	Linear regression gradient (ppm^{-1})
M	Quadratic regression coefficient of C^2 (ppm^{-2})
n	Freundlich power constant
P	2 parameter exponential growth coefficient
Q	2 parameter exponential growth coefficient of C (ppm^{-1})

In loving memory of Halima Mahmooda, Qamar Bashir, Ruqayya and Yahya Butt, Mansoor-ul-Haq Malik, Abdul Khaliq bin Habib and Khadim Hussain for inspiring me,

and to my family and friends for their timeless support and encouragement

CHAPTER 1

1. Introduction

1.1. Introduction

This chapter introduces gas sensor technology. The concept of 'smart circuitry' is explained and recent developments in the field of 'smart gas sensors' are discussed here. The chapter describes ideal characteristics and applications of a smart gas sensor. The research objectives of the performed study followed by an outline of the thesis are presented at the end of this chapter.

1.2. Characteristics of Gas Sensors

A sensor converts a physical or chemical quantity, such as light intensity, displacement, pressure, gas concentration or reaction speed into a quantifiable electrical signal (Gardner, 1994) called the sensor output, which can be processed and analysed. In the case of gas sensors, the input signal is usually a gas concentration. Figure 1.1 shows a typical system where a measured quantity, the measurand, in this case the gas concentration, is converted into a sensor output signal after being processed by a gas

sensor. At all times prior to the exposure of the sensor to the gas concentration (time < t_1), the sensor output is represented by y_0, i.e. the baseline value.

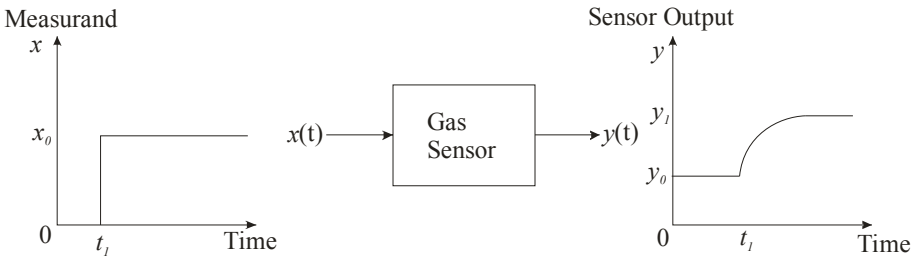

Figure 1.1 A simple gas sensor system with typical input (left) and output (right) signals (Pike 1996)

At time t_1, when the sensor is exposed to the gas concentration, the sensor output changes from y_0 to y_1 and the magnitude response given by the difference between the two signals (i.e. $\Delta y = y_1 - y_0$). The static response of a gas sensor may be described by a dimensionless parameter associated with the fractional response ($\Delta y/y_0$) of the sensor or by the absolute sensitivity of the sensor, which is the ratio of the change in output signal due to the change in the measurand (dy/dx) (Ingleby 1999). The dynamic response of a sensor system is exponential for a first order system and the response time is generally defined as the time required for the output signal to achieve a certain percentage of its steady–state value. The percentage employed for these measurements are usually 63% (τ_{63}) or 90% (τ_{90}).

An ideal gas sensor should have a high sensitivity to a particular measurand with repeatable and reproducible response outputs when exposed to the same gas concentrations. The sensor should show selectivity between different gases by having a different magnitude or frequency response. The sensor output should also return to the original baseline value once the measurand (gas concentration) is removed from the sensor environment.

Real gas sensors deviate from these ideal characteristics. The baseline value of the sensor output may be affected by ambient disturbances such as change in temperature, humidity, pressure, light, degradation of the gas sensor over time and long term application of DC voltage. These factors may result in a drift of the baseline value. Other common problems include variable sensitivity, slow response time and non-linear sensor output where the sensor output signal is not proportional to the input signal. The

problems are countered by modifying the sensing elements by changing the chemistry or the architecture of the sensing device or through signal modifications in post-processing steps (Holmin et al. 2001; Hui, Jun-hua & Zhong-ru 2003; Salit & Turk 1998; Yang, RD et al. 2007).

1.3. Smart Electronic Sensors

'*A sensor is a device that measures a physical quantity and converts it into a signal which can be read by an observer or by an instrument*' (Storey 2006). 'Smart sensors' are usually defined more loosely as there are a wide range of opinions amongst researchers as to what qualifies as 'smart'. Most authors would agree that as the most basic definition *"'Smart Sensors' are those sensors that include some logic function and/or are able make some type of decision"* (Giachino 1986). This definition emphasises on the decision making aspect of the function and excludes sensors only incorporating signal conditioning electronics. Corsi defines the term as '*sensors which contain both sensing and signal processing capabilities with objectives ranging from simply converting a physical viewing to sophisticated remote sensing, surveillance, search/track, weapon guidance, robotics, perceptronics and intelligence applications'* (Corsi 2007).

Millward suggests a smart sensor ASIC to be one in which one or more 'intelligent' elements or 'master cells' (e.g. control processing, digital signal processing, and data communication units) work along with a number of 'non-intelligent' elements or 'slave cells' which can be amplifiers, integrators, analogue multiplexors or analogue to digital converters (Millward 1992).

Where many individual sensors are linked to each other in the above mentioned way through some data processing unit, the integration of all individual components of the sensors is best achieved through standardised communications bus channels. The need for integrating all components of the sensing and signal processing or decision making units has led to the idea of 'Integrated Smart Sensors' where the sensing unit, processing or signal conditioning units are all combined into one package with a standard digital bus interface (Huijsing 1992) allowing large arrays of sensors to be connected using standardised interface technology. Such smart sensors and transducers being used in a networked environment have been defined in IEEE 1451.2-1997 (Kang 2000). One of the earliest smart sensors with a standardised bus was Honeywell's

primary air data transducer which offered the option of ARINC429 (point-to-point broadcast bus) which has been in operation since as early as 1984 (Prosser et al., 1999).

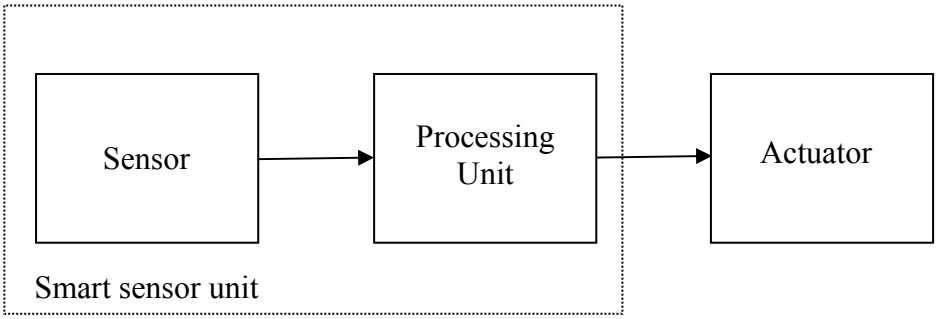

Figure 1.2 Basic elements of a smart sensor

Integrated smart sensors may be divided into two main categories, type I and type II, where type I smart sensors are those that include a sensing element and a pre-processing element and type II smart sensors are those that include a sensing element a pre-processing element and a processing element (Gardner et al., 2001). Figure 1.2 shows an integrated smart microsystem. If the processing unit only comprises of a pre-processing element then it forms a type I sensor, and if it contains a pre-processing and a processing element, then it is classified as a type II sensor. The integration of individual components into one system to form type I or type II smart sensors can have significant advantages when one of the following conditions is met:

a) It reduces cost per unit to manufacture

b) Offers substantial increase in performance

c) Device operation would otherwise not be possible

Out of the above three reasons the reduction in cost is by far the most significant driving factor in the desire for integrated smart sensors. Sensors with 'off-chip' micro-processing may be considered 'smart' as well. Thus the distinction between 'integrated sensors' and 'smart sensors' is made. A distinction between *smart* and *intelligent* instruments also needs to be drawn. An 'intelligent' instrument may be considered as one whose 'intelligence' is more associated with functionality rather than the high level of device integration. As long as a sensor can perform one of the following functions it may still be classified as a *smart* sensor:

a) Perform a logic function

b) Perform two-way communication

c) Automatic compensation

d) Decision making

For the purpose of this research work the smart electronics used are a combination of the sensing element and an ASIC based on the ratiometric principle, incorporating drift correction and temperature controlling elements.

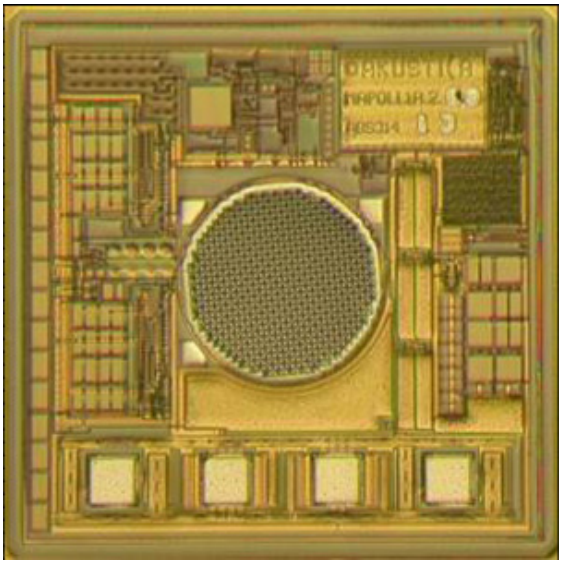

Figure 1.3 AKU 2000 CMOS MEMS microphone with integrated acoustic transducer and analogue output amplifier (Akustica 2008)

Figure 1.3 shows a smart single-chip digital microphone integrated with an acoustic transducer. The device measures 1 mm × 1 mm and is commonly found in laptop computer platforms. Variations of this chip are also being produced suitable for mobile phone use by Akustica's Sensory Silicon™. As the device integrates everything from the sensing element to the transducing element on one CMOS MEMS chip it can be integrated into small form factor products. As the device is based on CMOS MEMS technology it offers quick design cycles at relatively low per unit cost. Figure 1.4 below shows a fully integrated smart Vision System-on-Chip from NeuriCam. The device integrates a 32 bit RISC processor with a 32-node co-processor suitable for neural applications and a digital camera of 320 x 256 pixels and I/Os. The chip is fully functional with only one memory (static synchronous or asynchronous) and one flash to load the program and initials settings. The device uses conventional

CMOS technology and integrates video amplifier, analogue-to-digital converter and a bus interface. This device can be found in positional controllers, vehicle counters and biomedical inspection systems.

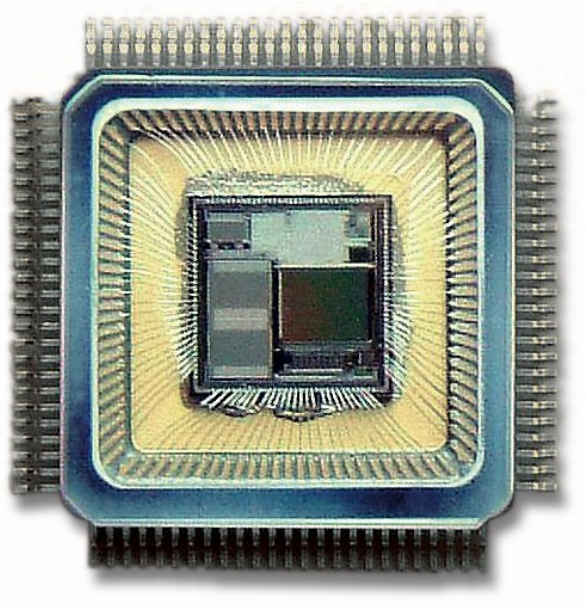

Figure 1.4 NC1503 CMOS Intelligent Vision System-on-Chip

(NeuriCam 2008)

1.3.1. Smart Gas Sensors

Smart gas sensors have been steadily gaining popularity with focus on technologies such as Lab-On-a-Chip and Nose-On-a-Chip. A single chip CMOS smart microsystem has been investigated by Baltes et al. at the Physical Electronics Laboratory at ETH Zurich. Their research has led to the combination of capacitive gas sensor (measuring capacitive changes in dielectric properties), a resonant cantilever (sensitive to mass changes) and a microcalorimeter (measuring the absorption or desorption heat upon interaction of VOCs with the polymer) onto a single CMOS chip (Hagleitner et al. 2001). Figure 1.5 shows a micrograph of this smart gas microsensor system. The architecture of this smart sensor consists of sensors, driving and signal-conditioning circuitry, analogue-to-digital converters, sensor control and power management unit, and a digital interface.

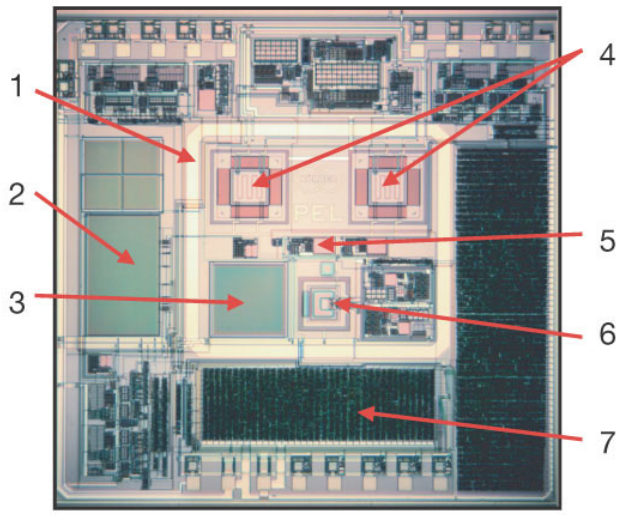

Figure 1.5 A single chip smart gas sensor. The different components include: 1, flip-chip frame; 2, reference capacitor; 3, sensing capacitor; 4, calorimetric sensor and reference; 5, temperature sensor; 6, mass-sensitive resonant cantilever; and 7, digital interface (Hagleitner et al. 2001).

Smart gas sensors find their use in air quality monitoring systems where it is vital to have real time or near real time information about any changes in the constituents of the environment. They are also utilized in monitoring the performance of a system to detect any VOC leaks. Such leaks can result in reduced efficiency of the system through contamination and wastage. A leak of a combustible hydrocarbon allowing it to mix with air or an oxygen supply can turn the resulting mixture explosive, resulting in damage to equipment and possible loss of human life.

In a project supported by the European Space Agency, Persaud et al. used conducting polymers and QCM sensors to form a smart gas sensor system to monitor environmental changes in the MIR space station (Persaud et al. 1999). This smart sensor provided real time information on any changes in the space station environment to the astronauts in an analyte concentration range of 10 to 1000 ppm. The system mapped the atmosphere of the space station for repeatable patterns related to onboard crew member activities such as physical exercises, meals, sleep periods, extra vehicular activity (preparation and return activities), shuttle docking, video/radio public relations activities test contaminations introduced for SGS control purposes, medical experiments, (e.g.,

disinfectants may be released) and other experiments. It also monitored the space stations activities which could have an impact on its internal atmosphere such as humidity control and temperature control, air circulation and oxygen generation. Extensive PCA pattern recognition technique was applied to the data and any leakages such as the one from the cooling system were immediately picked up.

CMOSSENS, a collaborative research project carried out between 1998-2002 funded by the European Commission aimed at developing a miniaturised gas sensor, which monolithically integrated signal processing electronics, driving circuitry and a microcontroller with the sensor array chip. This smart gas sensor array used drop-deposited nanocrystalline metal oxides (SnO_2) as sensitive layers on microplates.

Current research by Udrea et al. is being conducted at Cambridge University to develop a smart silicon-based chemical sensor using advanced nano-materials. These smart gas sensors are to be fully compatible with CMOS technology, use different nano-materials, such as doped carbon nanotubes, ZnO nanowires, and mesoporous WO_3 and aim to operate with a power consumption of less than 1 mW. The research will target pollutant gases such as H_2, NH_3, O_3, CO_2 and NO_2.

As commercial interest in gas sensors and smart gas sensor systems has increased a number of companies have entered the marketplace with their products. The major gas sensors manufacturers are City Technology Ltd., Alphasense, Membrapor, Dynament Ltd, Figaro, Nemoto & Co. LTD, Monox Sensor Group, Sixth Sense, Sensirion, Sierra Sensors, Smiths Detection, Airsense and Osmetech.

1.4. Practical Uses of Gas Sensors

The analysis of Volatile Organic Compounds (VOCs) is of great interest in many fields such as air quality monitoring in environmental chemistry, automotive industry, oil and gas exploration and chemical processing industries, food and beverage industries, cosmetics and health industries. Studies with gas sensors have been carried out to record pollution levels in urban areas (De Vito et al. 2008) for monitoring VOCs like benzene, excessive exposure to which can lead to respiratory illnesses. VOCs also form the principle components in odours (Gardner et al., 1999). Thus, environments where it is necessary to monitor the presence of unpleasant odours, such as water treatment units, drains and sewage pipes (Fuchs et al., 2008) it is more desirable to use a physical device rather than the human alternative.

The USEPA reports that indoor VOC levels may be 10 times higher than outdoor levels. Furthermore, after using certain products such as paint strippers or aerosols the VOC levels may be 1,000 times higher than the acceptable levels (Agency 1994). Exposure to such high levels of these vapours is related to symptoms such as nose and throat irritation, eye irritation and watering, headaches, nausea and vomiting, dizziness, asthma exacerbation, allergic skin reaction, memory impairment and visual disorders. Long term exposure to VOCs may also lead to more serious ailments such as cancer, damage to the liver, kidneys and central nervous system and loss of coordination. Recent studies have been carried out using gas sensors and their derivatives such as electronic noses (e-noses: a combination of sensor arrays and pattern recognition) with the aim to monitor VOC levels in the indoor environment (Grimsrud et al., 2006; Wen 2006; Wolfrum et al., 2006). At such high concentrations a mixture of certain hydrocarbons with air or an oxygen supply can become explosive. Monitoring the level of combustible hydrocarbons is of particularly necessary in an industrial environment where these VOCs may catch fire and result in damage to valuable equipment.

Combustible hydrocarbons are present in large quantities and high concentrations around oil and gas extraction and petrochemical processing plants. The four hydrocarbons tested in this study are methanol, ethanol, propan-1-ol and toluene. All four of these are in liquid form at room temperature. The minimum temperature required to form an ignitable mixture in air is called the *flashpoint*. All four of the discussed analytes have a flashpoint lower than room temperature. Table 1.1 shows the

flashpoints of the four analytes used in this study and their Lower Explosive Limits (LEL) and Upper Explosive Limits (UEL) shown as a percentage by volume in air.

Analyte	Flashpoint	LEL	UEL
Methanol	10°C	6%	36%
Ethanol	12°C	3.3%	19%
Propan-1-ol	15°C	2.1%	13.5%
Toluene	4.4°C	1.2%	6.75%

Table 1.1 Flashpoint and explosive limits of analytes

Advancement in fuel cell technology has resulted in the development of Direct Alcohol Fuel Cells (DAFCs) (Lamy et al., 2002) which use a stream of alcohol that reacts with water at the anode, while a stream of oxygen reacts with the hydrogen cations at the cathode. The two electrodes are separated by a semi-permeable membrane. The relevant reaction equations are given below:

Anode: $CH_3OH + H_2O \rightarrow CO_2 + 6H^+ + 6e^-$ (1.1)

Cathode: $(3/2)O_2 + 6H^+ + 6e^- \rightarrow 3H_2O$ (1.2)

Overall reaction: $CH_3OH + (3/2)O_2 \rightarrow CO_2 + 2H_2O$ (1.3)

The main problem that these fuel cells face is the alcohol molecules permeating through the membrane material into the cathode chamber (Antonucci et al., 2006). This drastically reduces the efficiency of the fuel cell (Chen et al., 2006). As alcohols are combustible hydrocarbons, a mixture of the alcohol molecules and oxygen can be dangerously explosive, making it necessary to monitor any presence of alcohols in the oxygen and hydrogen chamber. Studies have also been carried out to observe cathode degradation in Polymer Electrolyte Membrane Fuel Cells (PEMFCs) due to the presence of toluene (Li et al., 2008).

The advantage of using a portable gas sensor over conventional chemical analytical methods is the potential to provide a quick in situ evaluation of the environment and avoid long and complicated processes that often have a high economic cost. Portable gas sensors and e-noses also offer systems that are non-destructive and objective, at a relatively low cost.

Amongst medical practitioners it is a well-known fact that certain ailments can result in odorous symptoms such as ‘sweet’ smelling breath in a diabetic patient (Chang & Subramian 2008). Bacterial infections such as MRSA also result in a unique odour specific to the bacterial strain. A culture test to identify the bacterial strain takes two to three days and DNA testing can reduce the time to identify the bacteria to two hours. However, using an e-nose can give a positive result on MRSA in approximately 15 minutes (Marks 2005). Time is of the essence when identifying and stopping the spread of contaminants such as MRSA in a hospital environment. Gardner et al. have reported a 96% accurate detection rate using an e-nose. This has also been reported in popular media (Economist 2006). Similarly no two people have the exact same odour-identity or ‘smell fingerprint’ which is determined by many factors including: our genes, skin type, diet, medicine, mood state and even the weather. Thus, an odour sample from an individual can also be processed not only to identify the person, but also to identify any changes in the person’s health or mood.

Most commercially available e-noses are based on the change in electrical resistance of a semi-conductive material, such as a metal oxide semiconductor (Gardner et al., 1999) when exposed to vapours. Metal oxide semiconductors have an operating temperature of around 300°C. This makes them high in power consumption. On the other hand conducting polymers (Gruber et al., 2004) operate at room temperature and offer greater possibilities of structural variation.

Figure 1.6 GDA 2 (Gas Detector Array 2)
Portable detector for hazardous gases and chemical agents

In the recent past, commercial interest in gas sensor and e-nose devices has increased significantly. Some of the commercially available portable gas sensors

include the Gas Detector Array 2 (figure 1.6) from Airsense Analytics GmbH. This instrument has been designed to detect hazardous gases including chemical warfare agents. It uses an ion-mobility spectrometer, a photoionization detector, an electrochemical cell and two metal oxide sensors and can detect ammonia, inorganic sour gases, small chlorinated molecules as well as benzene, phosgene, vinyl chloride and chlorobenzene.

Earlier hand held e-nose systems were developed by Lewis et al. at the California Institute of Technology. Their research work led to the establishment of Cyrano Sciences (now Smiths Detection), which commercialised its product in the year 2000 as the Cyranose 320 (figure 1.7 (a)). The Cyranose 320 utilized a nano-composite sensor array with 32 sensors and advanced pattern recognition algorithms and offered accurate on-site analysis. This was a major breakthrough in the portability of such a device and brought the cost of such a system to $5500. At the same institution a system to monitor air was developed as an air quality monitoring system, jointly funded by the California Institute of technology and NASA's Jet Propulsion Laboratory. The third generation of this e-nose is shown in figure 1.7 (b). The e-nose sensor unit uses an array of non-specific chemical sensors controlled and analyzed electronically, mimicking the mammalian nose (Ryan et al., 2006).

Figure 1.7 (a) Cyranose 320

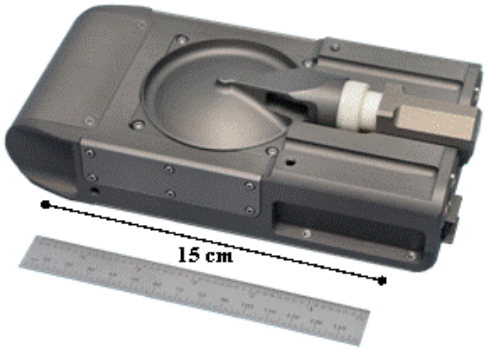

Figure 1.7 (b) 3rd Generation JPL E-nose Unit

Recent market research carried out by Frost & Sullivan shows that portable sensors account for 70.2% of the global gas sensors' market (Sankaranarayanan, 2007).

The demand for these gas sensors is expected to grow at a steady rate. The OEMs and the replacement market are expected to be the main driving factors. At the current growth rate the market capitalisation in the USA alone is expected to cross US $5 billion by 2012.

1.5. Developments in Gas Sensing

Interest has been growing in the field of gas sensing and artificial olfaction over the last twenty years. More recently developments in understanding the mammalian olfactory system has resulted in a lot of focus on gas sensing electronic nose systems which can mimic the human olfactory system. In 2004 Richard Axel and Linda Buck were awarded the Nobel Prize in Physiology or Medicine for their work on odorant receptors and the organization of the olfactory system (Buck, L & Axel 1991a, 1991b; Buck, LB 2005; Chess et al. 1992).

Recent activity at *Sensors Research Laboratory* at Warwick University has focussed on the development of an artificial olfactory mucosa by combining a silicon sensor array with a microfluidic package (Covington et al., 2007; Gardner et al., 2007; Sanchez-Montanes et al., 2008). The system uses an 80 element microsensor array, with five different sensor tunings to exploit the nasal chromatographic phenomena, which has been observed in the mammalian olfactory system. Research has also been carried out towards the development of a smart micronose. An array of 70 gas sensors (5 rows of 14 sensors each) based on a combined FET/resistive cell has been fabricated under a standard CMOS process and using different carbon black polymer composite materials (Covington, J. A. et al. 2003).

Work in the field of CMOS towards developing ASICs for sensing applications has been carried out at Swiss Federal Institute of Technology, Zurich (ETH Zurich). Baltes et al. have carried out work on microelectrode arrays integrated with analogue and digital circuitry with functions such as signal filtering, analogue and digital conversion, multiplexing, simultaneous recording and stimulation (Hierlemann & Baltes 2003; Hierlemann et al. 2003). The group has also reported on single chip micro-hotplate gas sensors capable of operating at 450°C, based on metal oxides in CMOS technology and (Barrettino et al., 2004a; Barrettino et al., 2004b). Gardner et al. have reported work on a ratiometric ASIC developed in CMOS technology which can be combined with chemoresistive gas sensitive elements to provide a complete gas sensing system (Cole et al., 2003; García-Guzmán et al., 2003). This ASIC can be driven by a 5

V power supply and includes data sampling, signal processing and temperature regulatory components which give a voltage output proportional to the resistive ratio change of the gas sensors.

1.6. Aims and Objectives of the Project

The aim for this research was to assemble and characterize an efficient gas sensor system based on the ratiometric principle, utilizing gold nanoparticle based chemoresistors as the gas sensitive elements. The gas sensing system should have very few post processing steps to make it ideally suitable for use in a portable hand-held instrument.

SRL 194 ASIC device fabricated using the *Europractice* scheme with an AMIS 0.8 μm standard CMOS process, developed from previous work at the *Sensors Research Laboratory* at Warwick University (García-Guzmán 2005), was identified as the ASIC of choice to be integrated with gas sensing elements. Self-assembled gold nanoparticle alkyl-dithiol linker films deposited layer by layer on gold IDEs on a silicon substrate were chosen as the VOC sensitive part of the gas sensing system. Three different models for arranging the chemoresistive array were tested. For each arrangement three different chemoresistive gas sensor materials were identified. The compatibility of these materials for a hybrid device was to be tested.

The behaviour of the gas sensor system when characterized against VOCs at different relative humidities and temperatures was of particular interest. The VOCs of interest for characterization were methanol, ethanol, propan-1-ol and toluene vapours in inert air. Initial characterization at 30°C and 0-5 % rh was to be carried out and compared with effects of changes in temperature up to 40°C and relative humidity up to 35-40 %rh. It was expected that the ratiometric architecture of the circuitry would compensate for any shifts in the temperature and relative humidity that the test devices are subjected to. The final gas sensor system was to be resilient to any other changes in the environment other than those of the effects of tested analytes on the sensing elements. The best fit regression models for the characterization results to the different VOCs were to be identified and plotted for the three different types of sensor arrangements. The repeatability and reproducibility of the device responses was to be tested by exposing them to first increasing concentrations and then decreasing concentrations and the hysteresis between the responses observed. Effects of drift and application of DC voltage over long periods of time ware to be observed and the

operating range of the compatible resistance ratio needed to be identified. The internal resistance of offset circuit of the SRL 194 ASIC was to be determined and effects of temperature changes on the resistance of the internal and connective circuitry were to be observed.

1.7. Outline of the Thesis

Figure 1.8 gives a graphical representation of how this thesis will proceed.

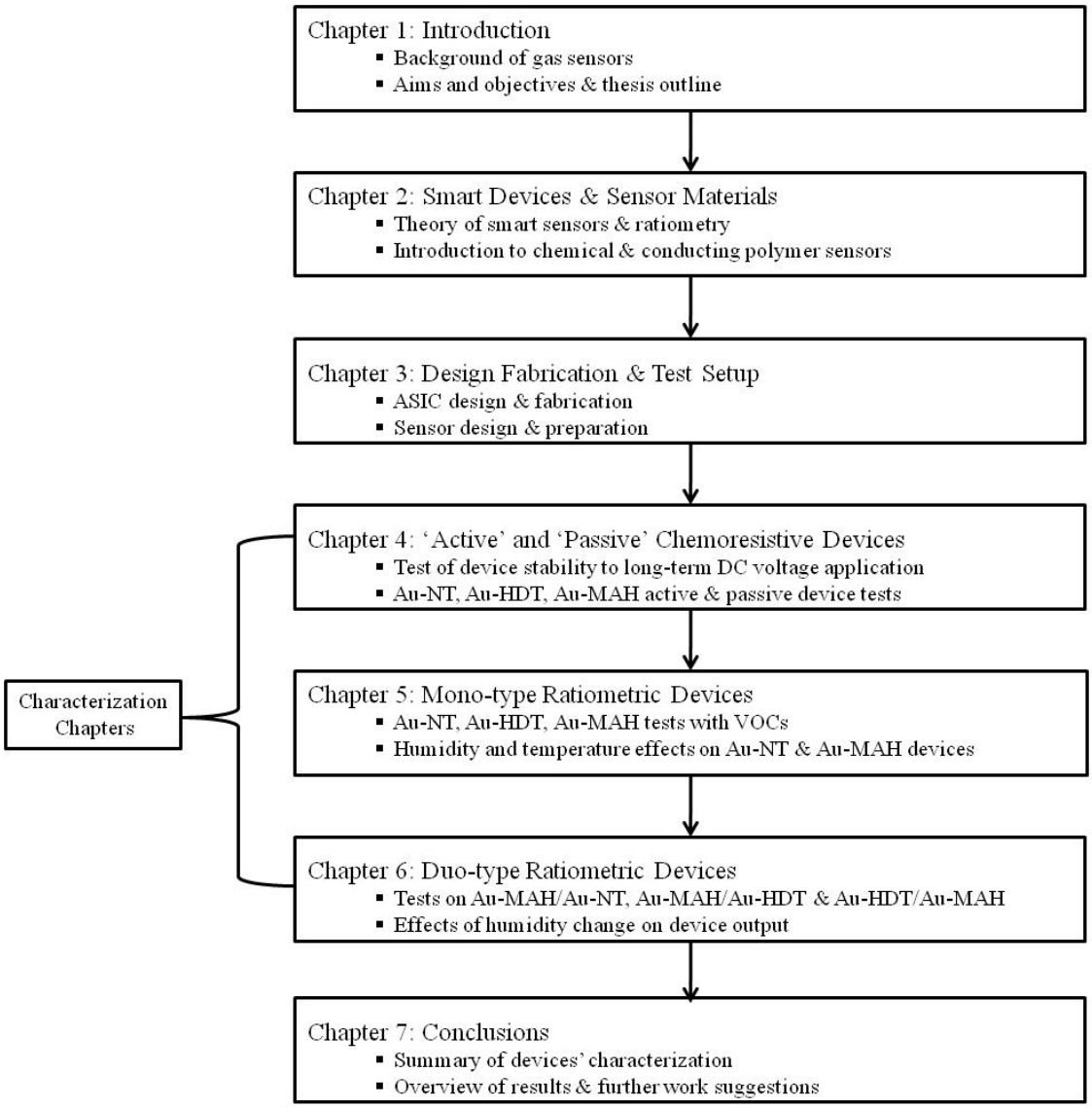

Figure 1.8 Summarized outline of the thesis

This thesis describes the design and characterization of a ratiometric gas sensor system using self-assembled gold nanoparticle alkyl-dithiol chemoresistive sensors in

various configurations. Chapter 1 reviews chemical and gas sensor systems and gives an overview of developments in gas sensor systems capable of identifying targeted groups of compounds. In this chapter the case is made for the need to develop smart gas sensors with the capability of monitoring alcohol and toluene concentrations. The chapter also gives an introduction to smart sensors and smart gas sensing systems and their applications.

Chapter 2 describes the ratiometric principle and various polymers utilized as odour and vapour sensors. The use of metal nanoparticle based composite polymer materials, and specifically gold nanoparticle based thiol sensors, is also described in this chapter. Chapter 3 explains the design, fabrication and test methodology used to characterize the various sensor systems tested in this study. The process of producing self-assembled gold nanoparticle dithiol films is described in detail. The test circuitry and the data acquisition hardware designs are also presented in this chapter. A brief introduction to the models used for data analysis in later chapters is also given in chapter 3.

Chapters 4, 5, and 6 present characterization observations from various arrangements of the gas sensor materials tested in this research project. Three particular arrangements are tested with the different kinds of gold nanoparticle based alkyl-dithiol chemoresistive film sensors. The chemoresistive sensors are combined with the SRL 194 ASIC to form the various types of sensors. In chapter 4 the devices characterized contain one chemoresistive sensor combined with the ratiometric ASIC and balanced by a constant resistance resistor. A variation of this arrangement is also tested in this chapter. In this modified arrangement the advantages of using silicone sealant gel encapsulation of the chemosensor, while under analyte exposure conditions, are observed.

Chapter 5 examines ratiometric sensor array based devices. The sensor devices are assembled by combining two chemoresistive sensors based on the same material with the SRL 194 ASIC. One of the two chemosensors in these *mono-type* devices is encapsulated in the silicone sealant gel used in chapter 4. A method to discriminate between analytes using statistical data from device results is also explained in chapter 5.

Chapter 6 describes the results obtained for ratiometric sensor devices which are formed by combining two chemoresistive sensors of different materials with the SRL 194 ASIC. One of the two chemoresistors in these *duo-type* devices is based on a

gold nanoparticle dithiol material with a polar content in the linker chain, while the other chemoresistor of the pair has a non-polar linker base.

Chapter 7 concludes the research discussing the results and how the objectives of the project are fulfilled. Last but not least, the latest developments are presented to highlight the possible future enhancements.

1.8. References

Agency, USEP 1994, 'Indoor Air Pollution: An Introduction for Health Professionals', *EPA 402-R-94-007*.

Akustica 2008, *Akustica's Sensory Silicon™*, viewed 22.08.2008 2008, <http://www.akustica.com/>.

Antonucci, V, Aricò, AS, Baglio, V, Brunea, J, Buder, I, Cabello, N, Hogarth, M, Martin, R & Nunes, S 2006, 'Membranes for portable direct alcohol fuel cells', *Desalination*, vol. 200, no. 1-3, pp. 653-5.

Barrettino, D, Graf, M, Kirstein, K, Hierlemann, A & Baltes, H 2004a, 'A monolithic fully-differential CMOS gas sensor microsystem for microhotplate temperatures up to 450 degrees C', *2004 Ieee International Symposium on Circuits and Systems, Vol 4, Proceedings*, pp. 888-91.

Barrettino, D, Graf, M, Zimmermann, M, Hagleitner, C, Hierlemann, A & Baltes, H 2004b, 'A smart single-chip micro-hotplate-based gas sensor system in CMOS-technology', *Analog Integrated Circuits and Signal Processing*, vol. 39, no. 3, pp. 275-87.

Buck, L & Axel, R 1991a, 'A Novel Multigene Family May Encode Odorant Receptors', *Journal of General Physiology*, vol. 98, no. 6, pp. A3-A.

Buck, L & Axel, R 1991b, 'A Novel Multigene Family May Encode Odorant Receptors', *Cell*, vol. 65, no. 1, pp. 175-87.

Buck, LB 2005, 'Unraveling the sense of smell (Nobel lecture)', *Angewandte Chemie-International Edition*, vol. 44, no. 38, pp. 6128-40.

Chang, JB & Subramian, V 2008, 'Electronic Noses Sniff Success', *IEEE Spectrum*, March 2008.

Chen, W, Sun, G, Guo, J, Zhao, X, Yan, S, Tian, J, Tang, S, Zhou, Z & Xin, Q 2006, 'Test on the degradation of direct methanol fuel cell', *Electrochimica Acta*, vol. 51, no. 12, pp. 2391-9.

Chess, A, Buck, L, Dowling, MM, Axel, R & Ngai, J 1992, 'Molecular-Biology of Smell - Expression of the Multigene Family Encoding Putative Odorant Receptors', *Cold Spring Harbor Symposia on Quantitative Biology*, vol. 57, pp. 505-16.

Cole, M, Ulivieri, N, Garcia-Guzman, J & Gardner, JW 2003, 'Parametric model of a polymeric chemoresistor for use in smart sensor design and simulation', vol. 34, pp. 865-75.

Corsi, C 2007, 'Smart Sensors', *Infrared Physics & Technology*, vol. 49, no. 3, pp. 192-7.

Covington, JA, Gardner, JW, Hamilton, A, Pearce, TC & Tan, SL 2007, 'Towards a truly biomimetic olfactory microsystem: an artificial olfactory mucosa', *Iet Nanobiotechnology*, vol. 1, no. 2, pp. 15-21.

Covington, JA, Tan, SL, Gardner, JW, Hamilton, A, Koickal, T & Pearce, T 2003, 'Combined smart chemFET/resistive sensor array', *Proceedings of the Ieee Sensors 2003, Vols 1 and 2*, pp. 1120-3.

De Vito, S, Massera, E, Piga, A, Martinotto, L & Di Francia, G 2008, 'On field calibration of an electronic nose for benzene estimation in an urban pollution monitoring scenario', *Sensors and Actuators B-Chemical*, vol. 129, pp. 750-7.

Economist, T 2006, 'What the nose knows', *The Economist*, Mar 9th 2006.

Fuchs, S, Strobel, P, Siadat, M & Lumbreras, M 2008, 'Evaluation of unpleasant odor with a portable electronic nose', *Materials Science & Engineering C-Biomimetic and Supramolecular Systems*, vol. 28, no. 5-6, pp. 949-53.

García-Guzmán, J 2005, 'Smart ratiometric ASIC chip for VOC monitoring', University of Warwick.

García-Guzmán, J, Ulivieri, N, Cole, M & Gardner, JW 2003, 'Design and simulation of a smart ratiometric ASIC chip for VOC monitoring', *Selected Papers from Eurosensors XVI*, vol. 95, no. 1-3, pp. 232-43.

Gardner, JW 1994, *Microsensors: Principles and Applications*, John Wiley & Sons Ltd.

Gardner, JW & Bartlett, PN 1999, *Electronic noses : principles and applications*, Oxford University Press, Oxford.

Gardner, JW & Taylor, JE 2007, 'Novel convolution based signal processing techniques for a simplified artificial olfactory mucosa', *Transducers '07 & Eurosensors Xxi, Digest of Technical Papers, Vols 1 and 2*, pp. U1245-U6.

Gardner, JW, Varadan, VK & Awadelkarim, OO 2001, *Microsensors, MEMS and Smart Devices*, John Wiley & Sons, Ltd.

Giachino, JM 1986, 'Smart Sensors', *Sensors and Actuators*, vol. 10, no. 3-4, pp. 239-48.

Grimsrud, D, Bridges, B & Schulte, R 2006, 'Continuous measurements of air quality parameters in schools', *Building Research and Information*, vol. 34, no. 5, pp. 447-58.

Gruber, J, Yoshikawa, EKC, Bao, Y & Geise, HJ 2004, 'Synthesis of a novel poly(p-phenylene-vinylene) derivative and its application in chemiresistive sensors for electronic noses with an unusual response to organic vapours', *E-Polymers*.

Hagleitner, C, Hierlemann, A, Lange, D, Kummer, A, Kerness, N, Brand, O & Baltes, H 2001, 'Smart single-chip gas sensor microsystem', *Nature*, vol. 414, no. 6861, pp. 293-6.

Hierlemann, A & Baltes, H 2003, 'CMOS-based chemical microsensors', *Analyst*, vol. 128, no. 1, pp. 15-28.

Hierlemann, A, Brand, O, Hagleitner, C & Baltes, H 2003, 'Microfabrication techniques for chemical/biosensors', *Proceedings of the Ieee*, vol. 91, no. 6, pp. 839-63.

Holmin, S, Krantz-Rulcker, C, Lundstrom, I & Winquist, F 2001, 'Drift correction of electronic tongue responses', *Measurement Science & Technology*, vol. 12, no. 8, pp. 1348-54.

Hui, D, Jun-hua, L & Zhong-ru, S 2003, 'Drift reduction of gas sensor by wavelet and principal component analysis', *Sensors and Actuators B: Chemical*, vol. 96, no. 1-2, pp. 354-63.

Huijsing, JH 1992, 'Integrated Smart Sensors', *Sensors and Actuators a-Physical*, vol. 30, no. 1-2, pp. 167-74.

Ingleby, P 1999, 'Modelling and Characterisation of Conduction Polymer Chemoresistors', University of Warwick.

Kang, L 2000, 'IEEE 1451: A standard in support of smart transducer networking', paper presented to Instrumentation and Measurement Technology Conference, 2000. IMTC 2000. Proceedings of the 17th IEEE.

Lamy, C, Lima, A, LeRhun, V, Delime, F, Coutanceau, C & Léger, J-M 2002, 'Recent advances in the development of direct alcohol fuel cells (DAFC)', *Journal of Power Sources*, vol. 105, no. 2, pp. 283-96.

Li, H, Zhang, J, Fatih, K, Wang, Z, Tang, Y, Shi, Z, Wu, S, Song, D, Zhang, J, Jia, N, Wessel, S, Abouatallah, R & Joos, N 2008, 'Polymer electrolyte membrane fuel cell contamination: Testing and diagnosis of toluene-induced cathode degradation', *Journal of Power Sources*, vol. 185, no. 1, pp. 272-9.

Marks, P 2005, 'E-nose to sniff out hospital superbugs', 22 September 2005.

Millward, SJ 1992, 'Approaches to the organisation of smart sensor ASICs', paper presented to ASICs for Measurement Systems, IEE Colloquium on.

NeuriCam 2008, *CMOS Intelligent Vision System-on-Chip*, viewed 22.08.2008 2008, <http://www.neuricam.com/main/product.asp?4M=NC1503>.

Persaud, KC, Pisanelli, AM, Szyszko, S, Reichl, M, Horner, G, Rakow, W, Keding, HJ & Wessels, H 1999, 'A smart gas sensor for monitoring environmental changes in closed systems: results from the MIR space station', *Sensors and Actuators B: Chemical*, vol. 55, pp. 118-26.

Pike, AC 1996, 'Design of chemoresistive silicon sensors for application in gas monitoring', University of Warwick.

Prosser, SJ & Schmidt, EDD 1999, 'Smart Sensors for Industrial Applications', *Microelectronics International*, vol. 16, no. 2, pp. 20-3.

Ryan, MA, Shevade, AV, Taylor, CJ, Homer, ML, Jewell, AD, Kisor, A, Manatt, KS, Yen, SPS, Blanco, M & Goddard, WA July 2006, 'Expanding the Capabilities of the JPL Electronic Nose for an International Space Station Technology Demonstration', paper presented to International Conference On Environmental Systems.

Salit, ML & Turk, GC 1998, 'A drift correction procedure', *Analytical Chemistry*, vol. 70, no. 15, pp. 3184-90.

Sanchez-Montanes, MA, Gardner, JW & Pearce, TC 2008, 'Spatio-temporal information in an artificial olfactory mucosa', *Proceedings of the Royal Society a-Mathematical Physical and Engineering Sciences*, vol. 464, no. 2092, pp. 1057-77.

Sankaranarayanan, V 20 Aug 2007, *Gas Sensors Market - An Overview*, Frost & Sullivan, viewed 26.08.08 2008, <http://www.frost.com/prod/servlet/market-insight-top.pag?docid=104185353>.

Storey, N 2006, *Electronics: A Systems Approach*, 3 edn, Pearson Education.

Wen, J 2006, 'A smart indoor air quality sensor network - art. no. 617440', *Smart Structures and Materials 2006: Sensors and Smart Structures Technologies for Civil, Mechanical , and Aerospace Systems, Pts 1 and 2*, vol. 6174, pp. 17440-.

Wolfrum, EJ, Meglen, RM, Peterson, D & Sluiter, J 2006, 'Calibration transfer among sensor arrays designed for monitoring volatile organic compounds in indoor air quality', *Ieee Sensors Journal*, vol. 6, no. 6, pp. 1638-43.

Yang, RD, Park, J, Colesniuc, CN, Schuller, IK, Trogler, WC & Kummel, AC 2007, 'Ultralow drift in organic thin-film transistor chemical sensors by pulsed gating', *Journal of Applied Physics*, vol. 102, no. 3, p. 034515.

CHAPTER 2

2. Ratiometric Design & Smart Sensor Materials

2.1. Introduction

This chapter introduces and defines the concept of ratiometry with the purpose to explain where ratiometry is present in electrical and electronic systems and how it may be of benefit for the purpose of research in chemical sensing. The chapter then describes the use of chemical sensors and the different types of chemical sensors that have been popularly developed and studied over the years. Next, an introduction to polymer based odour and gas sensors is given which develops the idea of composite material sensors, finally introducing the concept of the metal particle based composite polymer chemical sensors is studied here.

A detailed review of existing literature is given over the course of this chapter explaining how the electronic circuitry has been designed and integrated with chemical sensors in order to detect specific chemicals at a potentially low unit cost.

2.2. The Ratiometric Principle

In an electronic system the term *ratiometric* means that the output signal depends on the ratio of the input signals. If the input signals are resistance dependent then the ratio of the two resistances is referred to as the *resistance ratio* and denoted here by *rr*. Using this technique in a smart sensor offers the self-calibrating and error correction capabilities in the smart electronic circuitry.

$$rr = Resistance\ Ratio = \frac{R_1}{R_2} \tag{2.1}$$

In its most basic form, the ratiometric principle can be applied in the form of a voltage divider. The figure 2.1 below shows a set of *n* voltage dividers supplied by a common voltage supply (García-Guzmán 2005).

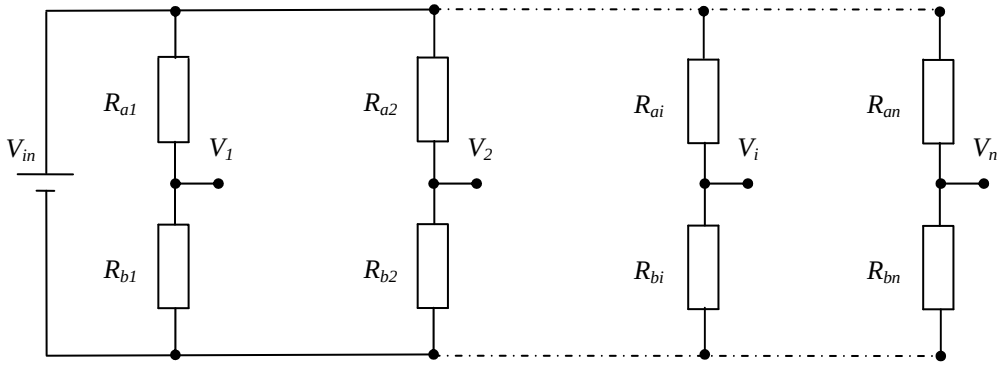

Figure 2.1 Voltage divider

Here the resistance ratio equals to the ratio of R_a and R_b. The circuit is said to be in a balanced condition when the resistance ratio of each arm is equal to the resistance ratio of the next one. Any change in one of the ratios can be picked up by the resulting change in the differential output.

$$\frac{R_{a1}}{R_{b1}} = \frac{R_{a2}}{R_{b2}} = \frac{R_{ai}}{R_{bi}} \qquad (i = 1, 2, 3 \ldots n) \tag{2.2}$$

In figure 2.1, the potential at the middle of every arm in the circuit is the same $V_1 = V_2 = V_i$. A change in the supply voltage will not have any effect on the resistance ratios of each arm and hence the potential difference between V_1 and V_i will always be zero, providing stability to the circuit. Thus, the two resistors in each arm act as output stabilisers. This factor is particularly important in the case of this study as chemoresistors are prone to effects of ageing. But for identical chemoresistors or chemoresistors from the same batch being tested at the same time the effects of ageing are expected to be similar. The ratiometric setup should cancel out such an affect including that of drift caused by long term application of DC voltage.

One of the most common forms of ratiometric circuits is in bridge circuits. A classical example of such a circuit is the Wheatstone bridge circuit. This circuit is essentially two ratiometric voltage dividers parallel to each other. Thus, the resistance ratios of the two voltage dividers can be represented as given in equation 2.2, where n = 2. The output from the circuit is taken at the halfway point of the two voltage dividers.

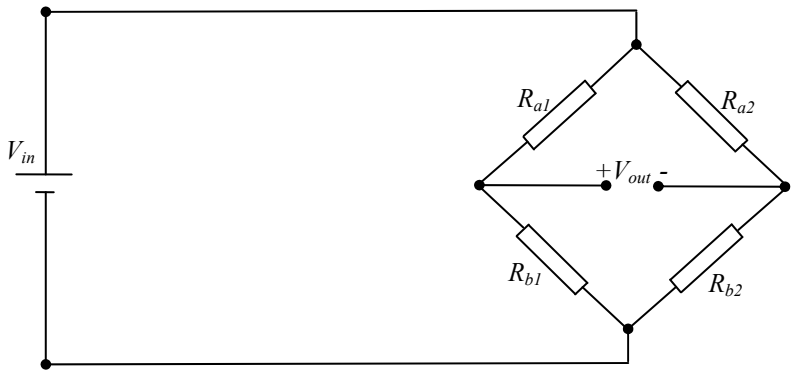

Figure 2.2 Wheatstone bridge circuit

The voltage output of the circuit in figure 2.2 can be calculated as follows:

$$V_{out=} \left(\frac{R_{b1}}{R_{a1}+R_{b1}}\right) - \left(\frac{R_{b2}}{R_{a2}+R_{b2}}\right) V_{in} \qquad (2.3)$$

The bridge circuit is balanced when the resistance ratios of the two voltage divider arms are balanced. The circuit is often used when one of the resistances is unknown. Adding a variable resistor in the same arm of the circuit as the unknown resistor (i.e. if R_{b1} is unknown, denoted in figure 2.3 as R_x, then R_{a1} is the variable resistor) allows the

balanced conditions to be reached and hence identifies the value of the unknown resistance.

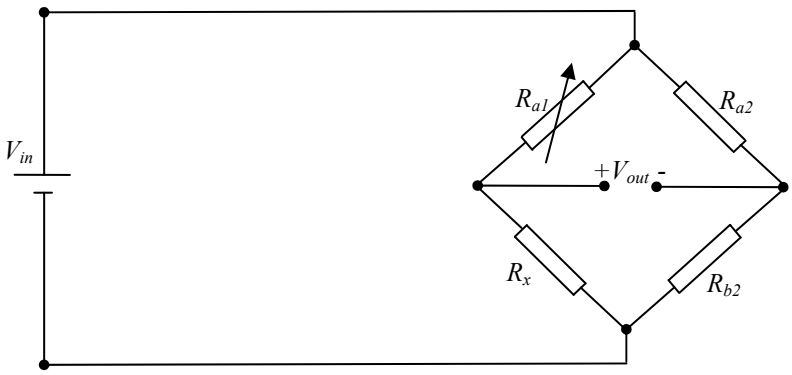

Figure 2.3 Wheatstone bridge circuit balanced with a variable resistor

Another important use of ratiometric circuits is in feedback circuits such as operational amplifiers. The two arrangements of standard operational amplifiers are given in the figures below:

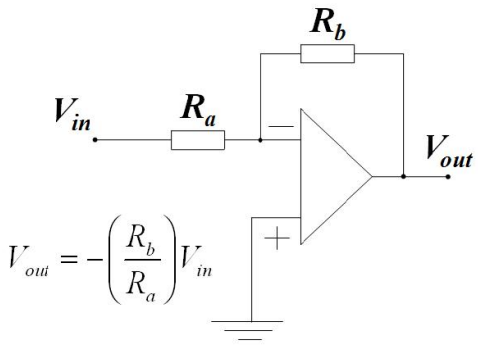

Figure 2.4 Inverting amplifier

The resistor R_b is connected from the output terminal to the inverting terminal of the amplifier providing negative feedback. When both the resistors used in the circuit are equal to each other the output voltage is simply the negative of the input voltage. The gain of this inverting amplifier is given as:

$$Gain = \frac{V_{out}}{V_{in}} = -\frac{R_b}{R_a} \tag{2.4}$$

If one of the resistors varies (R_b of the Inverting amplifier circuit in this case) its value in terms of the variation of resistance the output voltage is now given as:

$$V_{out} = -\frac{R_b + \Delta R}{R_a} V_{in} \tag{2.5}$$

Then for the condition $R_a = R_b = R$

$$V_{out} = -(1 + \frac{\Delta R}{R}) V_{in} \tag{2.6}$$

For the converse situation when R_a varies the voltage output for when $R_a = R_b = R$ is given by

$$V_{out} = -\left(\frac{R}{R + \Delta R}\right) V_{in} \tag{2.7}$$

The circuitry which is of particular interest to this study is the non-inverting ratiometric amplifier circuit. Here, the input voltage is applied to the non-inverting end of the operational amplifier. The amplifier is followed by a voltage divider circuit, the output of which is connected to the inverting input of the operational amplifier through a feedback loop.

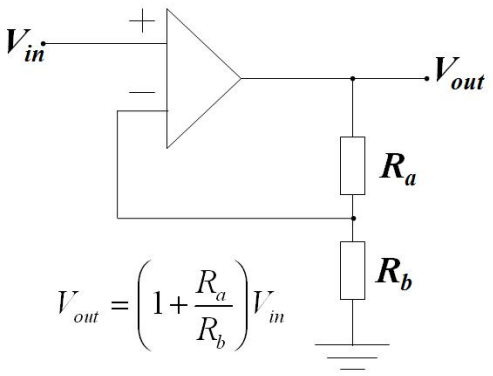

Figure 2.5 Non-Inverting amplifier

The voltage output is directly dependent on the ratio of the two resistors in the potential divider circuit and is given by:

$$V_{out} = (1 + \frac{R_a}{R_b})\, V_{in} \tag{2.8}$$

In the balanced condition when $R_a = R_b$ the output voltage is twice the input voltage. Visiting the same condition as for the inverting amplifier when $R_a = R_b = R$ and a variation in the resistance of R_a, the output voltage as a function of the resistance ratio is given as

$$V_{out} = \left(1 + \frac{R + \Delta R}{R}\right) V_{in} = (2 + \frac{\Delta R}{R}) V_{in} \tag{2.9}$$

Similarly, if R_b changes, the output voltage is given by:

$$V_{out} = \left(1 + \frac{R}{R + \Delta R}\right) V_{in} \tag{2.10}$$

And in the case when both resistors change simultaneously, but with different proportions, the relationship is given by:

$$V_{out} = \left(1 + \frac{R_a + \Delta R_a}{R_b + \Delta R_b}\right) V_{in} \tag{2.11}$$

The above relationship is explored in greater detail in chapter 3.

2.3. Odour Sensitivity in Polymers

Polymer based sensors respond to an interaction between the analyte substances and polymer materials generating a change of a physical parameter such as a change in electrical resistance (Bochenkov et al., 2004), capacitance (Albrecht et al., 2003; Steiner et al., 1995) or bulk size (Janata et al., 2003) amongst others, which can be recorded and measured and correlated to the stimulus. Previous studies have analysed various types of polymer based sensors for gas or vapour detection. PDMS hollow fibre membranes have been used for the detection of carbon dioxide/methane mixtures sensors suitable for biogas composition monitoring (Rego et al., 2004). PEG based chemoresistive sensors have been studied for their responsiveness to various organic vapours (Niu et al., 2007). Previous work at Warwick University has included research on conducting polymer gate FET sensors using carbon black polymer composites films, such as PSB (Covington et al., 2001), PVC and PEVA (Covington et al., 2001) for the analysis of toluene vapour. Tan et al. have used PSF and PVPH (Tan et al., 2004) in a Nose-on-a-Chip microsystem imitating the biological olfactory system. Chemoresistive properties of lead containing PPX films (Bochenkov et al., 2005; Bochenkov et al., 2004) have been studied for their response to ammonia.

In lieu with the use of these polymers in the wider field of sensors, a large number of gas sensors employ conducting or insulating polymers, and composites of the two in artificial olfactory and gas sensor systems. These sensors offer high sensitivity, a quick response time and have the advantage over metal oxide sensors of being operable at room temperatures (Shi et al., 2007). In addition to this, these composite polymers are highly flexible in their design, which can be tailored to be sensitive to specific stimuli such as an analyte vapour, a chemical group such as alcohols and phenols, or a particular odour class (Dowdeswell et al., 1999; Lonergan et al., 1996). They can also be used in an e-nose system where they can be designed to give a patterned response to odours. As each substance has its own unique odour this odour pattern can act as an olfactory fingerprint for a particular substance (Canhoto et al., 2005; Canhoto et al., 2004; Pinzari et al., 2004).

Previous studies have tried to integrate various sensor elements with differing characteristics to develop a smart hybrid multisensory application (Harsányi et al., 1999) by combining thick and thin film elements with inorganic and organic polymer based sensors and providing signal processing through an attached ASIC unit. The

polymers discussed in this study are alkyl-dithiol composite polymers with self-assembled gold nanoparticles which respond reversibly to the presence of an analyte through absorption or adsorption processes, resulting in a change in their resistance. As each resistive polymer can be designed to be broadly sensitive to a particular analyte, previous studies have reported the use of a matrix of chemically different polymers in conjunction with a conductive component such as Poly(3,4-ethylenedioxy)thiophene-poly(styrene sulfonate) (PEDOT-PSS) and compared the response with the corresponding carbon black filled composite polymer detectors to form an array of vapour sensitive detectors (Sotzing et al. 2000). The response output from such an array makes a characteristic fingerprint specific to each odour which can be processed with pattern recognition techniques.

In the field of conducting polymers, monomers can be synthesised either electrochemically or chemically to form a conducting polymer gas sensor with a dopant or anion to balance the charge. This type of conducting polymer can also be either ionically conducting or electronically conducting depending upon the mobility of the ions and localisation of electrons on the polymer. They have been successfully employed in electronic (Angelopoulos 2001), optoelectronic (Gazotti et al. 2001) and electromechanical devices (Otero 2000). They have also been applied in chemical sensors based on electronic, optical or mechanical transduction mechanisms (Janata & Josowicz 2003). Gas sensors based on metal polyacetylene, polyaniline, PT, PPSA (Janata & Josowicz 2003), PP and its derivatives (Babudri et al. 2004; Slater et al., 1993), polyphenylene, and PPS have been used extensively in previous studies (Mehamod et al., 2003; Naso et al., 2003; Persaud et al., 1996).

2.3.1. Composite polymer materials as odour and gas sensors

Composite polymer sensors have become increasingly popular over the last few years (Airoudj et al. 2008; Gao et al. 2006; Morohashi et al. 2006; Tai et al. 2007; Zee & Judy 2001). Initially they were distinctly different from gas-sensitive doped metal oxide films due to their inability to conduct electrical charge. With the introduction of conductive grains to form metal-polymer composites, the electrical conductivity was improved and these materials could be used as the resistive elements in gas sensors. The concept was first reported by Lewis at Caltech (Freund et al., 1995; Lewis 1996) and commercialised by Cyrano Sciences Inc. (now Smith Detection Pasadena). Lewis embedded carbon nanospheres to create a conducting matrix while

Sony and others embedded gold and platinum nanospheres (Joseph et al. 2003; Joseph, Yvonne et al. 2004).

Composite polymer sensors employing a sensitive film material interlaced with a conductive material are now a popular choice of materials for polymer-based gas sensors. The most common composite materials typically employ carbon-black as a conductive material, which has been the subject of extensive research as a gas sensor composite material (Burl et al. 2002; Doleman et al. 1998; Sisk et al., 2005; Zee et al., 2001). The carbon-black material and the polymer material are usually mixed in a solvent. On deposition the solvent evaporates and leaves the composite film behind. The carbon-black material provides the conductivity in these composites, whereas the polymer material offers the selectivity. Upon exposure to an analyte, the analyte diffuses into the polymer composite and the polymer swells to a certain degree depending on the interaction between the polymer and the analyte. This swelling causes the dispersed conductive carbon particles to move further apart from each other. This redistributes the conductive fillers in the composite polymer matrix and results in a change in the resistance of composites, which provides measurable signals characterizing the surrounding vapour-phase analytes (Chen et al., 2004; Lei et al., 2007). Research carried out by Lewis et al. demonstrates the carbon-black composite polymer sensor response based on percolation theory (Lonergan et al., 1996).

Conventionally, sensors were designed using a ‘lock and key’ approach where a specific sensor would respond and bind highly selectively to an analyte of interest. This required precise chemical design of the sensor which would only respond favourably to one analyte. This approach is feasible when a specific compound needs to be identified in a controlled environment. Using this approach if a number of compound analytes, such as those present in odours or food materials need to be identified, a separate selective receptor sensor would be needed for each compound of the analyte mixture. Complex odours can comprise of a composition of thousands of analyte compounds. Using the conventional approach would require the design of an equal number of receptor sensors to identify each compound. This, for obvious reasons, becomes impractical and uneconomical when dealing with complicated odours.

Using composite polymer materials has the added advantage of increasing the diversity of polymers that may be utilized to act as polymer sensors. Some polymers which may be sensitive to certain chemicals or compounds cannot be used as sensor materials in chemoresistive sensors due to their high resistivity or lack of conductivity.

This property can be manipulated by forming a composite of the polymer with a material of high conductivity, such as carbon-black or metal nanospheres. Thus, the breadth of polymers that may be used as polymer sensors, and hence, the number of chemicals that may be identified using the conducting composites of these polymers is increased (Lonergan et al., 1996). These composite polymer materials also offer the possibility to vary one property of the polymer at a time. In this manner a whole array of polymer materials can be created which have the same basic component but each polymer has had some addition or modification to increase its sensitivity to a different compound. The chemical diversity created in such an array is thus able to respond to a wide cross-section of analytes. The basic criteria for the elements of a gas sensor array can be categorized as follows:

1) It should easily convert environmental information into an easily monitored signal using minimum hardware and energy
2) It should give reversible, reproducible responses with minimum baseline drift
3) It should be tuneable to some extent and respond predictably to a wide range of chemicals and concentrations
4) It should be easily fabricated from inexpensive, commercially available materials using well-established techniques
5) It should allow miniaturisation to accommodate the construction of compact sensors with various elements
6) It should be robust and stable in a variety of environments

Metal oxide gas sensors, such as those made from tin oxide (SnO_2) (Corcoran et al., 1993; Gardner et al., 1991; Gardner et al., 1992) have been extensively researched and are amongst the most well-established. Several commercially available SnO_2 array based ‘electronic noses’ have also been available for some time (Gardner et al., 1994). However, there are certain disadvantages associated with the use of SnO_2 based gas sensors. These sensors suffer from low selectivity and stability. These sensors also have an operating temperature of ca. 300°C, thus, have a high power consumption and a long recovery time for vapours such as ethanol (Pourfayaz et al. 2005). Other sensors such as Surface Acoustic Wave (SAW) devices have high levels of sensitivity to the presence of vapours, which can be tailored by coating the SAW crystals with different polymer films with different gas-solid partition coefficients for the vapours of interest. A

disadvantage of both QCM and SAW sensors is their need for frequency detectors, whose resonant frequencies can drift as the active membrane ages.

2.3.2. Metal nanoparticle based polymer composite materials

Similar to the carbon black and SnO_2 materials metal nanoparticle based composite polymer material arrays have been the subject of much interest (Daniel et al., 2004; Shipway et al., 2000). In the polymer composite materials mentioned previously, it was the carbon black material which provided the conductivity in the otherwise mostly insulating polymer materials. In the metal nanoparticle polymer composites it is the metal colloidal structures encapsulated in the organic polymer materials that provide the enhancement in the material conductivity. The polymer composites respond to analyte sorption by swelling reversibly when exposed to various gases and hence, disrupting the conductive path, increasing the electron tunnelling distance and inducing a resistance change in the composite film (Sichel 1982), which can be measured when the film is deposited across two metal electrodes. This characteristic of these films makes their resistive properties dependent on the film thickness. Compared to the carbon black material the film deposition process for the metal nanoparticle polymer composites is relatively easy to control as they can be deposited through the well-established practice of layer by layer self-assembly.

The charge transport properties in these materials are dependent on the size of the metal particles and can be tuned by varying the size of the metal particles, molecular weight or structure of the organic component of these materials (Beverly, Sampaio & Heath 2002; Snow & Wohltjen 1998). The electronic properties of alkanethiol (Terrill et al. 1995; Wuelfing et al. 2000) and arenethiolate (Wuelfing et al., 2002) encapsulated gold nanoparticles, as discussed in detail by Murray et al., can be controlled through the size and structure of the organic ligands. Furthermore, Wessels et al. have shown that the conductivity of gold nanoparticle films can be tuned from semiconductor like to metallic behaviour by changing the structure of the organic linker molecules that connect these nanoparticles (Wessels et al. 2004). Brust et al. showed an inverse relationship between the length of the linker structure and their conductivity in gold nanoparticle alkylene-dithiol films (Bethell et al. 1996). The conductivity of these films strongly decreased with increasing linker structure length (Brust et al. 1998).

Vossmeyer and co-workers have shown that the chemical selectivity of these gold nanoparticle organic linker structure films can be tuned towards polar protic (R-

OH) compounds by balancing the hydrophobic and hydrophilic functional groups in the linker compound. Their study also demonstrates a lithographic method for patterning layer by layer assembled nanoparticle films on chip (Vossmeyer et al. 2004). Figure 2.6 shows a micrograph of a self-assembled gold nanoparticle nonane-dithiol film developed by Vossmeyer et al.

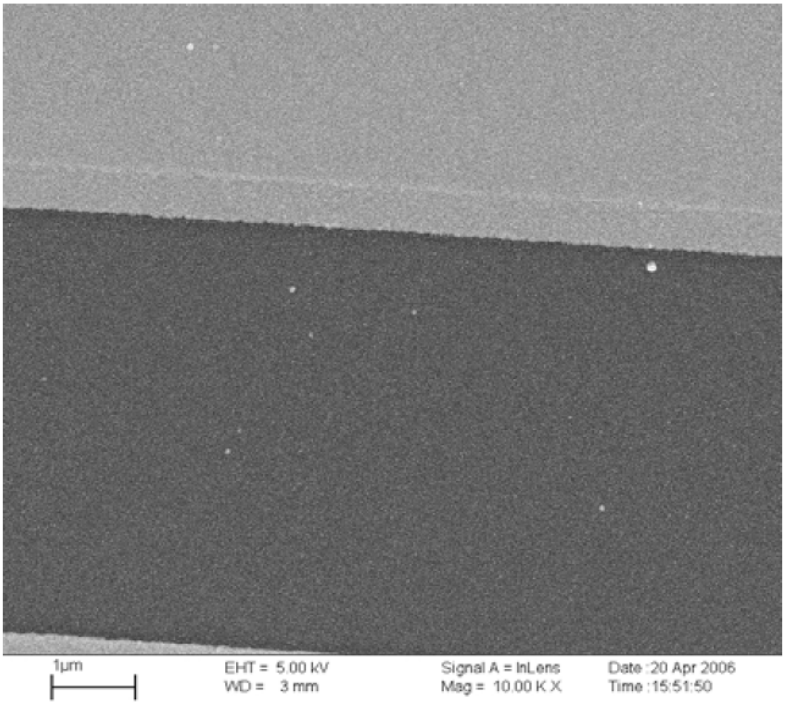

Figure 2.6 Micrograph of self-assembled Au-NT film showing good homogeneity including coverage of the gold electrodes (brighter areas)

2.4. Thiols as VOC sensitive materials

Thiols are organic compounds that contain the functional group composed of a sulphur and a hydrogen atom (-SH). Alkylthiols are also referred to as Sulfhydryls or Mercaptans. The thiol functional group is the sulphur analogue of the hydroxyl group. Hence, the synthesis of thiols is analogous to the method of making alcohols. Thiols are formed when a halogenoalkane is heated with a solution of sodium hydrosulphide.

$$CH_3CH_2Br + NaSH \text{ heated in ethanol (aq)} \rightarrow CH_3CH_2SH + NaBr \qquad (2.12)$$

Sulphur and oxygen are both in group VI of the periodic table. Sulphur is in period 3, whereas, oxygen is period 2. Therefore, thiols and alcohols share some of their chemical bonding properties. Sulphur anions are better nucleophiles than oxygen atoms as the sulphur nucleus exerts a lesser force on its electrons, hence, reactions to form thiols are quicker than those to form an alcohol and have a higher yield. The difference of electronegativity between sulphur and hydrogen is fairly low. This gives thiols a low dipole moment and makes them almost non-polar.

The advantage of using thiols as gas sensitive films is the flexibility to control their properties through molecular level design. This allows for the inclusion of a polar group to the otherwise non-polar thiol polymer. Thiols also bond readily with metal particles and studies of thiols bonding with gold particles have been carried out by Brust et al (Brust et al., 1998; Brust et al., 1995; Brust et al., 1994). The flexibility of thiols to allow polar and non-polar groups while acting as linker structures with gold particles, which provided an effective conductive channel in the films, was the reason derivatives of gold alkyl-thiols were used as the sensor film in this study.

2.4.1. Gold nanoparticle-Polymer composite films

The physical and chemical properties and thus the selectivity of the polymer films can be modified by forming composite materials with metal nanoparticle cores. The nanoparticles provide signal transduction and hence, enhance the conductivity of these materials, which otherwise may have a very high resistivity. This section focuses on the choice of colloidal gold as the metal nanoparticle material. Gold particles were chosen for their well established chemistry with organic ligands containing the thiol group (Alvarez et al. 1997) .

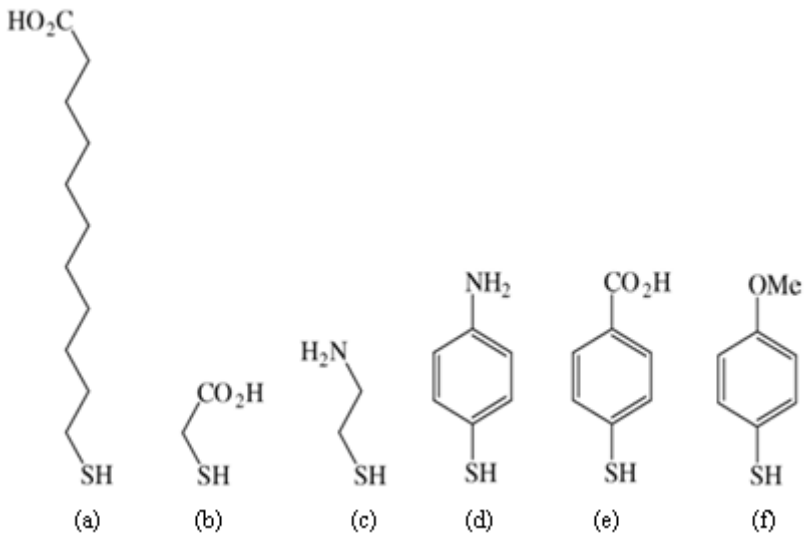

Figure 2.7 Examples of thiol molecules commonly used with functionalised gold surfaces. From left to right: (a) Mercaptoundecanoic acid, (b) Mercaptoacetic acid, (c) Cysteamine, (d) 4-mercaptoaniline, (e) 4-mercaptobenzoic acid and (f) 4-mercaptoanisole (Thery-Merland et al. 2006)

The growth of these crystals depends on the activation energy required and the availability of this activation force. Alvarez et al. show that the growth of gold nanoparticle clusters can be easily controlled and slowed down and singularly stable structures can be brought to a halt. The activation energy can be removed by lowering the temperature or by a weakly binding passivating agent that also acts as a mild etchant in an otherwise inert environment. Removal of this energy results in slowing down or halting the colloidal growth process, thus allowing control over the particle size. These gold clusters grow from atomic level dispersion and act as thermochemical 'sinks' as they accumulate. The weakly bound surface passivating monolayer has little or no effect on the stability of these particles which can be obtained as the exclusive product of the process.

Monodisperse colloids of CdS and CdSe have been grown by Murray et al. (Murray et al., 1993) and the kinetics of the growth processes have been worked on by Reiss (Reiss 1951). Gold nanocrystal growth over a range of 1.5-20 nm diameter have

been grown in a controlled surfactant concentration environment, i.e. by varying the gold to thiol ratio by Leff and co-workers (Leff et al., et al. 1995).

Gold clusters and its colloidal and compound forms are the best understood metallic systems. Gold is also mostly chemically inert and possesses low surface energy, which gives small gold crystallites extensive stability as compared to bulk gold. On a per-surface-atom basis gold's surface energy is about a tenth of that of the bulk cohesive energy (3.9 eV), 90% of which may be retained by gold clusters of as little as 75 atoms. Usually this is only 60% at aggregation. This property of gold allows using a weakly binding group such as alkylthiolates (SR) for protecting the nanometer scale gold surfaces of large clusters. This may be represented as Au-SR. Previous studies have shown n-Alkylthiolates (SR_n) to form protective compact, ordered monolayers where thiolates (-SR) or dialkydisulfides (RSSR) reversibly attach to various gold surfaces (Dubois et al., 1992). This behaviour is down to the gold surface atoms interacting with the non-bonding 's' orbital of an intact RSSR molecule (Fenter et al., 1994). This property can be observed amongst larger $Au_n(SR)_m$ clusters, where 'n' is much larger than 'm', and hence the molecule appears flat to the RSSR unit as in extended surface systems.

Thiols are well-known to form stable, self-assembled monolayers on gold surface (Camillone et al., 1991; Fenter et al., 1993; Laibinis et al., 1991). With the above mentioned properties of thiol as gas sensitive materials and the way gold particles behave in their presence, gold nanoparticle composite polymers based on this linker functional group were chosen for the purpose of this study.

2.5. Conclusions

In this chapter an introduction to the ratiometric principle was given. The presence of ratiometry in popularly used circuits was analysed. Furthermore, literature on odour sensitive polymers was reviewed and a comparison between various types of polymer sensors including carbon-black composite polymers and metal nanoparticle induced core composite polymers was carried out. Finally the flexibility offered by thiol molecules in designing a sensor and the stability gained from the mostly inert self-assembled gold nanoparticle linker structures was discussed.

The following chapter describes the design and fabrication of the smart ratiometric ASIC as well as the design and fabrication process associated with the chemical sensitive dithiol gold nanoparticle material. This chemoresistive material is combined with the ratiometric ASICs to form the smart gas sensor devices characterized in this research project.

2.6. References

Airoudj, A, Debarnot, D, Beche, B & Poncin-Epaillard, F 2008, 'A new evanescent wave ammonia sensor based on polyaniline composite', *Talanta*, vol. 76, no. 2, pp. 314-9.

Albrecht, BA, Benson, CH & Beuermann, S 2003, 'Polymer capacitance sensors for measuring soil gas humidity in drier soils', *Geotechnical Testing Journal*, vol. 26, no. 1, pp. 3-11.

Alvarez, MM, Khoury, JT, Schaaff, TG, Shafigullin, M, Vezmar, I & Whetten, RL 1997, 'Critical sizes in the growth of Au clusters', *Chemical Physics Letters*, vol. 266, no. 1-2, pp. 91-8.

Angelopoulos, M 2001, 'Conducting polymers in microelectronics', *IBM Journal of Research and Development*, vol. 45, no. 1, pp. 57-75.

Babudri, F, Naso, F, Colangiuli, D, Farinola, GM, Rella, R, Tafuro, R & Valli, L 2004, 'Chemical sensors based on electroactive polymers: First example of the use of a polyphenylenethienylene derivative', *Sensors and Microsystems, Proceedings*, pp. 140-5.

Bethell, D, Brust, M, Schiffrin, DJ & Kiely, C 1996, 'From monolayers to nanostructured materials: an organic chemist's view of self-assembly', *Journal of Electroanalytical Chemistry*, vol. 409, no. 1-2, pp. 137-43.

Beverly, KC, Sampaio, JF & Heath, JR 2002, 'Effects of size dispersion disorder on the charge transport in self-assembled 2-D Ag nanoparticle arrays', *Journal of Physical Chemistry B*, vol. 106, no. 9, pp. 2131-5.

Bochenkov, VE & Sergeev, GB 2005, 'Preparation and chemiresistive properties of nanostructured materials', *Advances in Colloid and Interface Science*, vol. 116, no. 1-3, pp. 245-54.

Bochenkov, VE, Zagorsky, VV & Sergeev, GB 2004, 'Chemiresistive properties of lead nanoparticles, covered by oxide and sulfide layer', *Sensors and Actuators B: Chemical*, vol. 103, no. 1-2, pp. 375-9.

Brust, M, Bethell, D, Kiely, CJ & Schiffrin, DJ 1998, 'Self-assembled gold nanoparticle thin films with nonmetallic optical and electronic properties', *Langmuir*, vol. 14, no. 19, pp. 5425-9.

Brust, M, Fink, J, Bethell, D, Schiffrin, DJ & Kiely, C 1995, 'Synthesis and reactions of functionalised gold nanoparticles', *Journal of the Chemical Society-Chemical Communications*, no. 16, pp. 1655-6.

Brust, M, Walker, M, Bethell, D, Schiffrin, DJ & Whyman, R 1994, 'Synthesis of thiol-derivatized gold nanoparticles in a 2-phase liquid-liquid system', *Journal of the Chemical Society-Chemical Communications*, no. 7, pp. 801-2.

Burl, MC, Sisk, BC, Vaid, TP & Lewis, NS 2002, 'Classification performance of carbon black-polymer composite vapor detector arrays as a function of array size and detector composition', *Sensors and Actuators B: Chemical*, vol. 87, no. 1, pp. 130-49.

Camillone, N, Chidsey, CED, Liu, GY, Putvinski, TM & Scoles, G 1991, 'Surface-structure and thermal motion of normal-alkane thiolsself-assembled on Au(111) studied by low-energy helium diffraction', *Journal of Chemical Physics*, vol. 94, no. 12, pp. 8493-502.

Canhoto, O & Magan, N 2005, 'Electronic nose technology for the detection of microbial and chemical contamination of potable water', *Sensors and Actuators B-Chemical*, vol. 106, no. 1, pp. 3-6.

Canhoto, O, Pinzari, F, Fanelli, C & Magan, N 2004, 'Application of electronic nose technology for the detection of fungal contamination in library paper', *International Biodeterioration & Biodegradation*, vol. 54, no. 4, pp. 303-9.

Chen, SG, Hu, JW, Zhang, MQ, Li, MW & Rong, MZ 2004, 'Gas sensitivity of carbon black/waterborne polyurethane composites', *Carbon*, vol. 42, no. 3, pp. 645-51.

Corcoran, P, Shurmer, HV & Gardner, JW 1993, 'Integrated tin oxide sensors of low-power consumption for use in gas and odor sensing', *Sensors and Actuators B-Chemical*, vol. 15, no. 1-3, pp. 32-7.

Covington, JA 2001, 'CMOS and SOI CMOS FET-based gas sensors', Dissertation/Thesis thesis.

Covington, JA, Gardner, JW, Briand, D & de Rooij, NF 2001, 'A polymer gate FET sensor array for detecting organic vapours', *Sensors and Actuators B: Chemical*, vol. 77, no. 1-2, pp. 155-62.

Daniel, MC & Astruc, D 2004, 'Gold nanoparticles: Assembly, supramolecular chemistry, quantum-size-related properties, and applications toward biology, catalysis, and nanotechnology', *Chemical Reviews*, vol. 104, no. 1, pp. 293-346.

Doleman, BJ, Lonergan, MC, Severin, EJ, Vaid, TP & Lewis, NS 1998, 'Quantitative Study of the Resolving Power of Arrays of Carbon Black-Polymer Composites in Various Vapor-Sensing Tasks', *Analytical Chemistry*, vol. 70, no. 19, pp. 4177-90.

Dowdeswell, RM & Payne, PA 1999, 'Odour measurement using conducting polymer gas sensors and an artificial neural network decision system', *Engineering Science and Education Journal*, vol. 8, no. 3, pp. 129-34.

Dubois, LH & Nuzzo, RG 1992, 'Synthesis, structure, and properties of model organic-surfaces', *Annual Review of Physical Chemistry*, vol. 43, pp. 437-63.

Fenter, P, Eberhardt, A & Eisenberger, P 1994, 'Self-assembly of n-alkyl thiols as disulfides on Au(111)', *Science*, vol. 266, no. 5188, pp. 1216-8.

Fenter, P, Eisenberger, P & Liang, KS 1993, 'Chain-length dependence of the structures and phases of CH3(CH2)N-1SH self-assembled on Au(111)', *Physical Review Letters*, vol. 70, no. 16, pp. 2447-50.

Freund, MS & Lewis, NS 1995, 'A chemically diverse conducting polymer-based "electronic nose"', *Proceedings of the National Academy of Sciences of the United States of America*, vol. 92, no. 7, pp. 2652-6.

Gao, T, Woodka, MD, Brunschwig, BS & Lewis, NS 2006, 'Chemiresistors for array-based vapor sensing using composites of carbon black with low volatility organic molecules', *Chemistry of Materials*, vol. 18, no. 22, pp. 5193-202.

García-Guzmán, J 2005, 'Smart ratiometric ASIC chip for VOC monitoring', University of Warwick.

Gardner, JW & Bartlett, PN 1994, 'A brief-history of electronic noses', *Sensors and Actuators B-Chemical*, vol. 18, no. 1-3, pp. 211-20.

Gardner, JW, Shurmer, HV & Corcoran, P 1991, 'Integrated tin oxide odor sensors', *Sensors and Actuators B-Chemical*, vol. 4, no. 1-2, pp. 117-21.

Gardner, JW, Shurmer, HV & Tan, TT 1992, 'Application of an electronic nose to the discrimination of coffees', *Sensors and Actuators B-Chemical*, vol. 6, no. 1-3, pp. 71-5.

Gazotti, WA, Nogueira, AF, Girotto, EM, Micaroni, L, Martini, M & das Neves, S 2001, *Handbook of Advanced Electronic and Photonic Materials and Devices*, vol. 10, Academic Press, New York.

Harsányi, G, Réczey, M, Dobay, R, Lepsényi, I, Illyefalvi-Vitéz, Z, Van den Steen, J, Vervaet, A, Reinert, W, Urbancik, J, Guljajev, A, Visy, C, Inzelt, G & Bársony,

I 1999, 'Combining inorganic and organic gas sensors elements: a new approach for multi-component sensing', *Sensor Review*, vol. 19, no. 2, pp. 128-34.

Janata, J & Josowicz, M 2003, 'Conducting polymers in electronic chemical sensors', *Nature Materials*, vol. 2, no. 1, pp. 19-24.

Joseph, Y, Besnard, I, Rosenberger, M, Guse, B, Nothofer, HG, Wessels, JM, Wild, U, Knop-Gericke, A, Su, DS, Schlogl, R, Yasuda, A & Vossmeyer, T 2003, 'Self-assembled gold nanoparticle/alkanedithiol films: Preparation, electron microscopy, XPS-analysis, charge transport, and vapor-sensing properties', *Journal of Physical Chemistry B*, vol. 107, no. 30, pp. 7406-13.

Joseph, Y, Guse, B, Yasuda, A & Vossmeyer, T 2004, 'Chemiresistor coatings from Pt- and Au-nanoparticle/nonanedithiol films: sensitivity to gases and solvent vapors', *Sensors and Actuators B: Chemical*, vol. 98, no. 2-3, pp. 188-95.

Laibinis, PE, Whitesides, GM, Allara, DL, Tao, YT, Parikh, AN & Nuzzo, RG 1991, 'Comparison of the structures and wetting properties of self-assembled monolayers of normal-alkanethiols on the coinage metal-surfaces, Cu, Ag, Au', *Journal of the American Chemical Society*, vol. 113, no. 19, pp. 7152-67.

Leff, DV, Ohara, PC, Heath, JR & Gelbart, WM 1995, 'Thermodynamic Control of Gold Nanocrystal Size: Experiment and Theory', *J. Phys. Chem.*, vol. 99, no. 18, pp. 7036-41.

Lei, H, Pitt, WG, McGrath, LK & Ho, CK 2007, 'Modeling carbon black/polymer composite sensors', *Sensors and Actuators B: Chemical*, vol. 125, no. 2, pp. 396-407.

Lewis, NS 1996, 'The Caltech Electronic Nose Project', *Engineering and Science*, no. LIX, pp. 2-113.

Lonergan, MC, Severin, EJ, Doleman, BJ, Beaber, SA, Grubbs, RH & Lewis, NS 1996, 'Array-Based Vapor Sensing Using Chemically Sensitive, Carbon Black-Polymer Resistors', *Chemistry of Materials*, vol. 8, no. 9, pp. 2298-312.

Mehamod, FS, Daik, R & Ahmad, M 2003, 'The potential application of poly(1,4-phenylene diphenylvinylene), p-PDV for oxygen detection based on fluorescence quenching', *Sensors and Actuators B-Chemical*, vol. 96, no. 3, pp. 537-40.

Morohashi, H, Nakanoya, T, Iwata, H, Yamauchi, T & Tsubokawa, N 2006, 'Novel contamination and gas sensor materials from amphiphilic polymer-grafted carbon black', *Polymer Journal*, vol. 38, no. 6, pp. 548-53.

Murray, CB, Norris, DJ & Bawendi, MG 1993, 'Synthesis and characterization of nearly monodisperse CdE (E = S, Se, Te) semiconductor nanocrystallites', *Journal of the American Chemical Society*, vol. 115, no. 19, pp. 8706-15.

Naso, F, Babudri, F, Colangiuli, D, Farinola, GM, Quaranta, F, Rella, R, Tafuro, R & Valli, L 2003, 'Thin film construction and characterization and gas-sensing performances of a tailored phenylene-thienylene copolymer', *Journal of the American Chemical Society*, vol. 125, no. 30, pp. 9055-61.

Niu, L, Luo, Y & Li, Z 2007, 'A highly selective chemical gas sensor based on functionalization of multi-walled carbon nanotubes with poly(ethylene glycol)', *Sensors and Actuators B: Chemical*, vol. 126, no. 2, pp. 361-7.

Otero, TF 2000, *Polymers in Sensors and Actuators*, Springer, Berlin.

Persaud, KC, Khaffaf, SM, Hobbs, PI & Sneath, RW 1996, 'Assessment of conducting polymer odour sensors for agricultural malodour measurements', *Chemical senses*, vol. 21, no. 5, pp. 495-505.

Pinzari, F, Fanelli, C, Canhoto, O & Magan, N 2004, 'Electronic nose for the early detection of moulds in libraries and archives', *Indoor and Built Environment*, vol. 13, no. 5, pp. 387-95.

Pourfayaz, F, Khodadadi, A, Mortazavi, Y & Mohajerzadeh, SS 2005, 'CeO2 doped SnO2 sensor selective to ethanol in presence of CO, LPG and CH4', *Sensors and Actuators B: Chemical*, vol. 108, no. 1-2, pp. 172-6.

Rego, R & Mendes, A 2004, 'Carbon dioxide/methane gas sensor based on the permselectivity of polymeric membranes for biogas monitoring', *Sensors and Actuators B: Chemical*, vol. 103, no. 1-2, pp. 2-6.

Reiss, H 1951, 'The Growth of Uniform Colloidal Dispersions', *Journal of Chemical Physics*, vol. 19, no. 4, pp. 482-7.

Shi, G & Bai, H 2007, 'Gas based sensors on conductin polymers', *Sensors*, vol. 7, no. 3, pp. 267-307.

Shipway, AN, Katz, E & Willner, I 2000, 'Nanoparticle arrays on surfaces for electronic, optical, and sensor applications', *Chemphyschem*, vol. 1, no. 1, pp. 18-52.

Sichel, EK 1982, 'Tunneling Conduction in Carbon-Polymer Composites', in Anonymous (ed.), *Carbon Black-Polymer Composites*, Marcel Decker, Inc., New York, vol. 1, pp. 51-78.

Sisk, BC & Lewis, NS 2005, 'Comparison of analytical methods and calibration methods for correction of detector response drift in arrays of carbon black-polymer composite vapor detectors', *Sensors and Actuators B: Chemical*, vol. 104, no. 2, pp. 249-68.

Slater, JM, Paynter, J & Watt, EJ 1993, 'Multi-layer conducting polymer gas sensor arrays for olfactory sensing', *The Analyst*, vol. 118, no. 4, pp. 379-84.

Snow, AW & Wohltjen, H 1998, 'Size-induced metal to semiconductor transition in a stabilized gold cluster ensemble', *Chemistry of Materials*, vol. 10, no. 4, pp. 947-+.

Sotzing, GA, Briglin, SM, Grubbs, RH, Lewis, NS & Fq 2000, 'Preparation and properties of vapor detector arrays formed from poly(3,4 ethylenedioxy)thiophene-poly(styrene sulfonate)/insulating polymer composites', *Analytical Chemistry*, vol. 72, no. 14, pp. 3181-90.

Steiner, FP, Hierlemann, A, Cornila, C, Noetzel, G, Bachtold, M, Korvink, JG, Gopel, W & Baltes, H 1995, 'Polymer Coated Capacitive Microintegrated Gas Sensor', paper presented to Solid-State Sensors and Actuators, 1995 and Eurosensors IX.. Transducers '95. The 8th International Conference on.

Tai, HL, Jiang, YD, Xie, GZ, Yu, JS & Zhao, MJ 2007, 'Self-assembly of TiO2/polypyrrole nanocomposite ultrathin films and application for an NH3 gas sensor', *International Journal of Environmental Analytical Chemistry*, vol. 87, no. 8, pp. 539-51.

Tan, SL, Covington, JA, Gardner, JW & Hesketh, PJ 2004, 'Ultra-fast/low volume odour delivery package for chemical microsystems', *Proceedings of the Ieee Sensors 2004, Vols 1-3*, pp. 1171-4.

Terrill, RH, Postlethwaite, TA, Chen, CH, Poon, CD, Terzis, A, Chen, AD, Hutchison, JE, Clark, MR, Wignall, G, Londono, JD, Superfine, R, Falvo, M, Johnson, CS, Samulski, ET & Murray, RW 1995, 'Monolayers in three dimensions: NMR, SAXS, thermal, and electron hopping studies of alkanethiol stabilized gold clusters', *Journal of the American Chemical Society*, vol. 117, no. 50, pp. 12537-48.

Thery-Merland, F, Méthivier, C, Pasquinet, E, Hairault, L & Pradier, CM 2006, 'Adsorption of functionalised thiols on gold surfaces: How to build a sensitive and selective sensor for a nitroaromatic compound?', *Sensors and Actuators B: Chemical*, vol. 114, no. 1, pp. 223-8.

Vossmeyer, T, Joseph, Y, Besnard, I, Harnack, O, Krasteva, N, Guse, B, Nothofer, HG & Yasuda, A 2004, 'Gold-nanoparticle/dithiol films as chemical sensors and first steps towards their integration on chip', *Physical Chemistry of Interfaces and Nanomaterials Iii*, vol. 5513, pp. 202-12.

Wessels, JM, Nothofer, HG, Ford, WE, von Wrochem, F, Scholz, F, Vossmeyer, T, Schroedter, A, Weller, H & Yasuda, A 2004, 'Optical and electrical properties of three-dimensional interlinked gold nanoparticle assemblies', *Journal of the American Chemical Society*, vol. 126, no. 10, pp. 3349-56.

Wuelfing, WP, Green, SJ, Pietron, JJ, Cliffel, DE & Murray, RW 2000, 'Electronic conductivity of solid-state, mixed-valent, monolayer-protected Au clusters', *Journal of the American Chemical Society*, vol. 122, no. 46, pp. 11465-72.

Wuelfing, WP & Murray, RW 2002, 'Electron hopping through films of arenethiolate monolayer-protected gold clusters', *Journal of Physical Chemistry B*, vol. 106, no. 12, pp. 3139-45.

Zee, F & Judy, JW 2001, 'Micromachined polymer-based chemical gas sensor array', *Sensors and Actuators B: Chemical*, vol. 72, no. 2, pp. 120-8.

CHAPTER 3

3. Design, Fabrication and Test Setup

3.1. Introduction

This chapter is divided into three sections. In the first part the design of the ASIC used as a ratiometric processing unit is described. The second part discusses the design and fabrication of the chemoresistive sensors and the results that can be expected from their use in three separate ratiometric configurations. These arrangements can be described as, a) mono-variable resistive units (where only one of the chemoresistors is exposed to the Volatile Organic Compound (VOC) vapour), b) bi-variable mono-type resistive units (where both of the chemoresistors exposed to VOC vapours in the ratiometric arrangement are made from the same chemoresistive sensor material but one of the two chemoresistors is encapsulated in a silicone sealant gel), and c) the duo-type sensor devices where two distinctive chemoresistors based on different chemoresistive film materials are combined with the ASIC. The third part of the chapter explains the design of the data acquisition hardware, the testing strategy used to collect the characterization data and the Flow Injection Analysis (FIA) station (Covington, 2001). All chemoresistors used over the course of the testing are based on self-assembled gold nano-particle linker structures. Three chemoresistive materials based on different linker structures were tested in this study. These were:

1. Au-NT: Gold nanoparticle - 1,9-nonanedithiol (Sheet resistance: 100 MΩ/□)
2. Au-MAH: Gold nanoparticle - 2-Mercapto-N-[6-(2-mercapto-acetylamino)-hexyl]-acetamide (Sheet resistance: 400 MΩ/□)
3. Au-HDT: Gold nanoparticle 1,16-hexadecanedithiol (Sheet resistance: 3.6GΩ/□)

The chemical and physical properties of these materials have been described by Vossmeyer et al. (Joseph et al., 2003; Joseph et al., 2004; Joseph et al. 2004b; Krasteva et al., 2002; Krasteva et al., 2003; Vossmeyer et al., 2002; Vossmeyer et al., 2004; Vossmeyer et al., 1994).

3.2. ASIC Design

The smart ASIC used for this research was fabricated using standard CMOS 0.7µm analogue fabrication technology. The ASICs were manufactured by AMI Semiconductors under the Europractice scheme. The design comprised of three main sections:

a) A gas sensor section
b) A temperature control section
c) A programmable microcontroller section to control the offset circuit properties

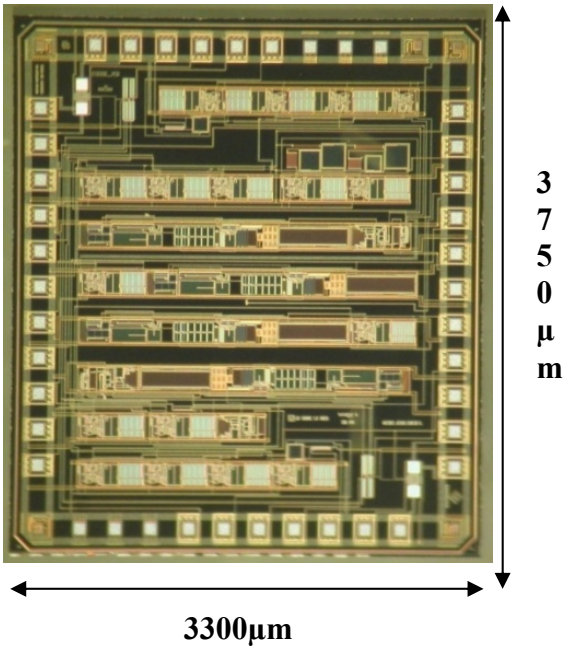

Figure 3.1 Picture of the ratiometric ASIC

The smart ASIC is pictured in figure 3.1 and is of dimensions 3300µm×3750µm. The programmable potentiometer circuitry was designed by Dr. Jesus García-Guzmán and a detailed account of the complete design and simulation of the components of the ASIC has been published (Cole et al. 2003; García-Guzmán 2005; García-Guzmán et al. 2003). For the purpose of this research only the gas sensor section of the ASIC and the programmable microcontroller sections are made use of. During testing the temperature of the testing chamber was kept constant by keeping it in a Techne 2D Dri-Bloc heater.

3.3. The Smart Gas Sensor Section

The gas sensor section of the ASIC used a common reference voltage point split between the gas sensor circuit and an offset circuit (figure 3.2). Two non-inverting amplifier circuits (i.e. the gas sensor circuit and the offset circuit) were connected to each other through an instrumentation amplifier circuit. The amplified output of the instrumentation amplifier was filtered through a fourth order Bessel filter before being output to the data acquisition system.

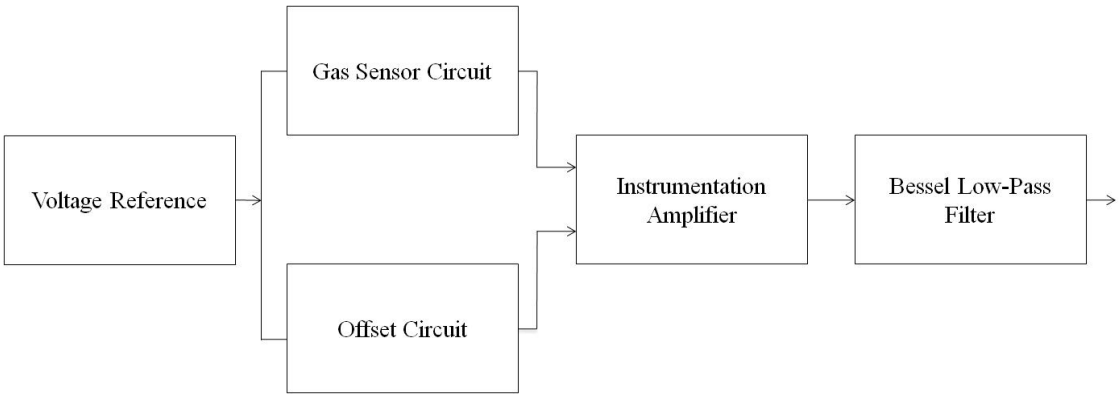

Figure 3.2 Schematics of the gas sensor section of the ASIC

Both the offset circuit as well as the gas sensor circuit were internally arranged in a non-inverting amplifier formation. Volatile Organic Compound (VOC) sensitive chemoresistors replaced conventional static resistors in the gas sensor circuit. The amplifier gain was determined by the ratio of these two VOC sensitive chemoresistors. Under ideal conditions this ratio is kept as close to unity as possible. However, a slight variation in matching this ratio was always present. In addition to this the resistance value of the chemoresistors was observed to drift randomly over long periods of time (over a year). The chemoresistors also responded to changing ambient conditions such as temperature, light and humidity.

The ratiometric arrangement cancelled many of the ageing and temperature variation effects. However, perfect cancellation of these effects was not achieved. Several configurations of these two resistors in the gas sensor circuit were tested to verify equations 2.9, 2.10 and 2.11, as described in chapter 2. Equation 2.9 reflected the

test situation where the chemoresistors which formed the R_a resistor in the amplifier circuit varied as it responded to analyte concentrations. This is represented in figure 3.3.

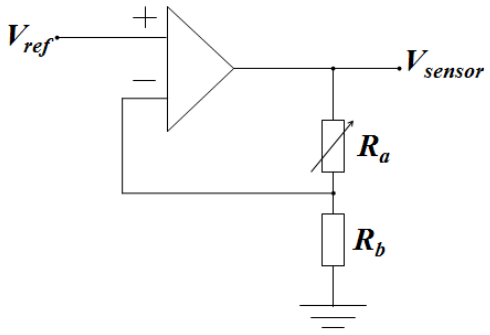

Figure 3.3 Non-inverting circuit for gas sensor with R_a as a chemoresistive sensor

The test circuit where the chemoresistive sensor was represented by R_b in the non-inverting amplifier was similar to the one used in the offset circuit in the ASIC and is shown in figure 3.4.

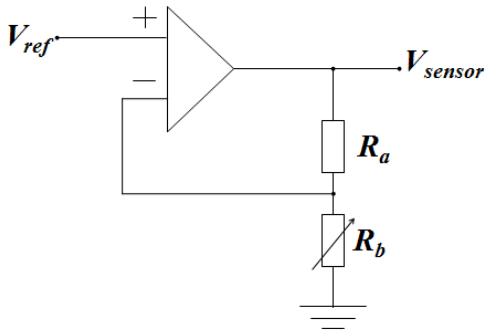

Figure 3.4 Internal non-inverting Amplifier Circuit for the Offset Circuit

The corresponding equation for the circuit shown in figure 3.3 is

$$V_{out} = \left(1 + \frac{R + \Delta R}{R}\right) V_{in} = \left(2 + \frac{\Delta R}{R}\right) V_{in} \quad (2.9)$$

One of the two resistors in the offset circuit was an externally programmable potentiometer which could be digitally set from within LabVIEW software. The advantage of this design was that it allowed setting the baseline output voltage prior to testing under non-exposure conditions. The circuit schematic for the offset circuit was the same as in the case of R_b forming a variable chemoresistor in a non-inverting amplifier circuit as in figure 3.4. For the offset circuit the offset resistor (R_b) is built into the ASIC (figure 3.4). The corresponding equation for that circuit is

$$V_{out} = \left(1 + \frac{R}{R + \Delta R}\right) V_{in} \quad (2.10)$$

A special case of the gas sensor circuit is also tested in this study where both the chemoresistors are exposed to the test vapour. In this arrangement the resistances of both the chemoresistors vary with the concentration of the vapours to which the chemoresistive sensors along with the ASICs are exposed. Two variations of this arrangement were used over the course of this study. The first one used both the sensors of the same basic material; however, the chemoresistor corresponding to R_b was coated with a silicone gel. The silicone gel is expected to act similar to a partitioning layer and expected to enhance the resulting resistance change due to exposure to some vapours.

The other variation of this setup used two chemoresistors based on different chemoresistive film materials. An enhanced signal output, for vapours with non-similar sorption properties with both the chemoresistors, and cancellation of the output for VOCs with similar sorption properties was expected as a result of using this setup. The circuit schematic of this arrangement is given in figure 3.5 below.

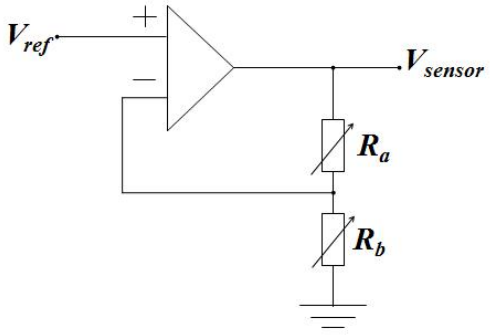

Figure 3.5 Non-inverting circuit for gas sensor with R_a and R_b representing the variable ratiometric arrangement

Both the offset circuit as well as the gas sensor circuit were supplied with the same 1.2 V reference voltage. Externally programmable potentiometers in the offset circuit set the baseline output voltage. The output from the gas sensor circuit and the offset circuit were fed into an instrumentation amplifier. This part of the circuit amplified any differences between the outputs of the two. The gain of the instrumentation amplifier (shown in figure 3.6) is given by equation 3.1. Here R_{gain} can be set through a programmable potentiometer. The value of this resistor was normally kept at 50 kΩ. The value of R_1 was 100 kΩ and was fabricated into the ASIC. Thus, a minimum gain of 5 was achievable through this setup. Due to slight variations in the actual fabricated devices, a gain of 7 was more commonly observed using LabVIEW software.

$$Gain = \frac{V_{out}}{V_{sensor} - V_{offset}} = \left(1 + \frac{2R_1}{R_{gain}}\right)\left(\frac{R_3}{R_2}\right) \tag{3.1}$$

The fabricated resistance values for the differential amplifier stage of the instrumentation amplifier were 100 kΩ for the feedback resistors (R_1) and 10 kΩ for the forward paths (R_2 *and* R_3). A circuit diagram of the instrumentation amplifier is given in figure 3.6.

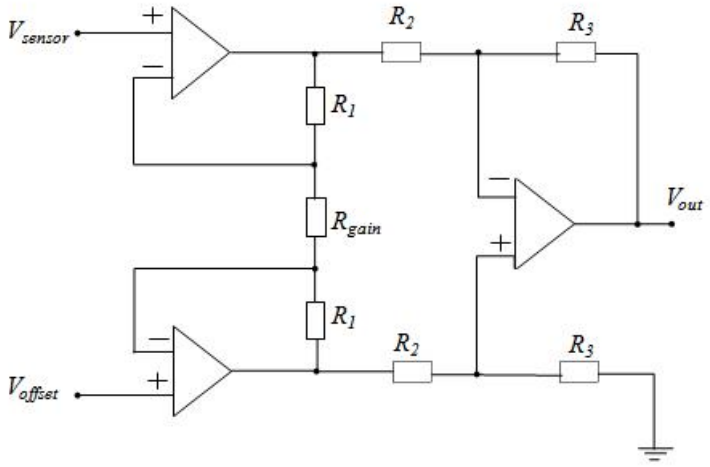

Figure 3.6 Instrumentation Amplifier

The ASIC circuit applies a fourth order Bessel low pass filter to the output of the instrumentation amplifier. This should remove any high frequency noise present in the output. The filter uses the values of capacitors and resistors given in table 3.1 for a cut-off frequency of f_c = 50 kHz as mentioned by García-Guzmán (García-Guzmán 2005). A circuit diagram of a fourth order Bessel low pass filter is given in figure 3.7.

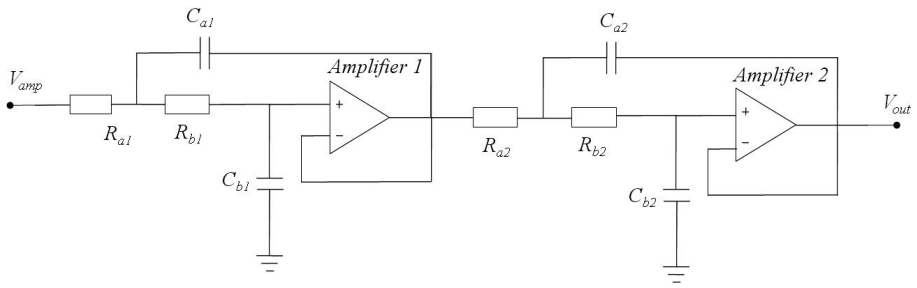

Figure 3.7 Fourth Order Bessel Low Pass Filter

The output from the Bessel filter is V_{out} which is the final device output. This voltage output is received by *National Instruments* Data Acquisition Card (NI-DAQ) and recorded as a *.txt file in the connected computer for further processing.

Component	Capacitance (pF)	Component	Resistance (Ω)
C_{a1}	20.0	R_{a1}	402 k
C_{b1}	14.7	R_{b1}	1.05 M
C_{a2}	20.0	R_{a2}	687 k
C_{b2}	7.5	R_{b2}	956 k

Table 3.1 Resistance and Capacitance used for the Bessel Low Pas Filter (García-Guzmán 2005)

3.4. Chemoresistive Gold nano-particle Sensors

This part of the chapter explores different odour sensitive polymer materials and explains the functional mechanisms of the polymer sensitive films used over the course of this study. An attempt will be made to explain the mechanisms behind odour sensitivity and the dependence of sensitivity on polymer chain length and the associated gold nanoparticle linker structures. This study focuses on the use of three different polymers based on the alkyl-dithiol group, R-$(SH)^2$. Two of the linker structures discussed here are nearly dipole neutral and the third one has been modified to include a polarized section in the linker chain. The chemical films incorporate self-assembled gold nanoparticles which allow the conductivity of the films to be modified by acting as conducting agents in the chemo-resistive films.

3.4.1. Preparation of the colloidal metal nanospheres

Faraday introduced the technique to prepare colloidal metals in a two-phase system (Faraday 1857), by reducing aqueous gold salt with phosphorus in carbon disulphide, to obtain a ruby coloured aqueous solution of dispersed gold particles. Brust et al. have reported (Brust et al. 1994) the combination of Faraday's two-phase technique with an ion extraction monolayer self-assembly method with alkane thiols (Porter et al. 1987), and prepared derivatised nanometre sized gold particles. The advantage of these thiol-derivatised metal nanoparticles is that they can be handled and characterised as a simple chemical compound. These particles have been shown to be very stable and not show any signs of decomposition, such as particle growth or loss of solubility (aggregation) after several months' storage in air, at room temperature. They can be precipitated using ethanol, redissolved using toluene, and chromatographed

without any change in their properties. It has also been reported that the gold-thiol bond is different in character from a gold sulphide bond (Brust et al. 1994).

The average gold nanoparticle diameter size obtained by Brust et al. was in the range of 1-3nm. Preparation of functionalised metal nanoparticle clusters which allow the chemical modification of their ligand shell has also been previously reported (BrustFink et al. 1995). These clusters can be utilised as building units for nanostructured materials. The electronic properties of these materials are heavily dependent on the particle size and the inter-particle spacing. Brust et al have also shown this inter-particle spacing to be adjustable by using different dithiol spacer molecules. The accuracy achieved is of the order of angstroms. Preparation of these dithiol linked gold-nanoparticles has been explained elsewhere (Brust et al., 1995).

The conductivity of the materials is reported to decrease exponentially with decreasing temperature, indicating the mechanism of activated charge transport. This means that at higher temperatures, electrons have gained enough energy to move from particle to particle as compared to lower temperatures, where the activation energy of the electrons has not been reached. The natural log of electronic conductivity (ln σ) was reported proportional to the reciprocal of absolute temperature (1/T). This relationship of the temperature dependence of electronic conductivity can be simplified using the Neugebauer and Webb equation (Neugebauer et al., 1962) (Eq. 3.2).

$$\sigma = \sigma_0 e^{\left(\frac{-E_a}{RT}\right)} \tag{3.2}$$

Where, σ_0 is a constant and E_a is the electrostatic activation energy of charge transport. The activation energy can be calculated from the electrostatic model developed by Abeles et al. (Abeles et al. 1975) (Eq. 3.3) for charge transport in cermets.

$$E_a = \left(\frac{1}{2}\right)\frac{e^2}{4\pi\varepsilon\varepsilon_0} \times [r^{-1} - (r+s)^{-1}] \tag{3.3}$$

Where, r is the radius of the small particle, s is the inter-particle spacing determined by the length of the dithiol spacer and ε is the dielectric constant of the embedding medium. The study showed that a decrease in conductivity for increasing lengths of linker chains, and an increase in effective activation energy for increasing linker chain lengths.

Several methods of production of gold nanoparticles are discussed by Bethell et al. (Bethell et al. 1996). A one step method using a two-phase liquid system has been explored. The method used ion-pair extraction and thiol self-assembly techniques giving a dark brown precipitate. This precipitate is reported to be soluble in toluene and re-precipitable in ethanol. The average particle size is reported to be in the range of 1.5 – 3 nm. If the addition of the alkanethiol is avoided the colloidal solution of gold nanoparticles is 'wine-red' in colour. This process produces slightly larger nanoparticle, reportedly around 8 ± 2 nm. These particles showed aggregation on solvent removal. Particularly with alkane*di*thiols an insoluble black precipitate containing gold nanoparticles is reported to have been produced with an average diameter of around 2.2 nm.

It has also been reported that the conductivity of the sensitive film materials may be controlled by the size of the linker molecules (Brust et al., 1995; Joseph et al., 2003; Joseph et al., 2004). The addition of three methylene units in a linker chain between gold nanoparticles, of 38 nanoparticle layers, is reported to have an increase of an order of magnitude in its resistivity (Bethell et al. 1996). Vossmeyer et al. report a nanoparticle/organic film composite and show the integration of cross-linking Polyphenylene dendrimers with gold nanoparticle to form a material with hydrophobic properties as well as good conductive properties when subjected to certain VOCs (Vossmeyer et al., 2002). The metal nanoparticles form a conductive path in the composite polymer material. It is also possible to make the nanoparticle films highly porous and thus enhance test vapour sorption into the material. A high sorption rate, coupled with a high surface to volume ratio offers a good signal transduction through the sensitive film.

3.4.2. Self-assembly in gold nanoparticles

The gold nanoparticle composite films used over the course of this study were formed using layer by layer self-assembly (Joseph et al., 2004). It has been shown by Brust et al. how gold nanoparticle get self-assembled into a three dimensional network using the dithiol molecules as inter-particle spacers (Brust et al., 1995). The accuracy achieved is of the order of angstroms. The same study also reports the self-assembly of gold nanoparticles into ordered structures. Bethell et al. report adding small quantities of alkanedithiol to the 'wine-red' gold nanoparticle solution in toluene, produced in the absence of any thiol, to produce ordered chains and globular supramolecular structures

of gold nanoparticles (Bethell et al. 1996). Typical features of these self-assembled particles are reported to be:

a) adjacent particles aligning themselves parallel to each other, with an inter-chain separation of ~1.5 nm

b) formation of strings of 'superclusters'

These self-assembled nanoparticles maintain their discrete character and do not merge together into larger units. The materials studied by Brust et al. show a characteristic similar to that of metal island films and cermets.

A layer by layer deposition technique of these gold nanoparticles is reported by Brust (Brust 1995). The slide on which the deposition is to take place is treated with 3-mercaptopropyl-trimethoxysilane to leave a free thiol group on the glass surface. On immersion of this slide into the 'wine-red' toluene (thiol free) solution of gold nanoparticles a monolayer of the gold particles is left on the slide surface. Further washing in the thiol free gold sol and repetition of the process is reported to have resulted in the deposition of several layers of these self-assembled gold nanoparticles onto the slide surface. This layer by layer deposition procedure is reported by Brust et al. to be the most robust of all the techniques to produce self-assembled metal nanoparticles and is employed by Vossmeyer et al. to produce the self-assembled gold nanoparticle alkanedithiol films used over the course of this study.

3.4.3. Gold nanoparticle-dithiol composite materials

Gold nanoparticles as composite core nanoparticle material have gained considerable attention over recent years (Han et al. 2001; Krasteva et al. 2002; Wohltjen & Snow 1998). As the gold nanoparticles offer a high surface to volume ratio in these composite films, the properties of the materials investigated are dominated by surface properties. A strong response is obtained through interactions with analyte molecules coming into contact with the gold nanoparticle/polymer composite materials.

Evans et al. and Zhang et al. show that the selectivity of these sensitive materials can be manipulated by changing or introducing different functional groups into the organic material surrounding the gold nanoparticles (Evans et al. 2000; Zhang et al. 2002). A dependence of resistivity on the size of the dendrimers was reported by Krasteva et al. (Krasteva et al. 2003). For this purpose, this study focused on the use of three different dithiol molecules as the linker structure in a gold nanoparticle composite.

3.4.4. Preparation of the Gold nanoparticle-Polymer composite films

Three different dithiol polymers were used over the course of this study. The main differences between the three polymers were the length of the carbon polymer chain and the inclusion of a polar amino group. The three polymer compound materials and their linker structures are as follows:

A. 1,9-nonanedithiol: HS-$(CH_2)_9$-SH or 'NT' for short (Joseph, Yvonne et al. 2004)

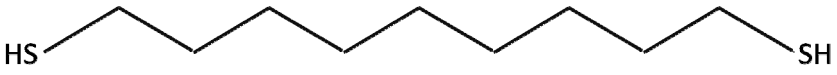

B. 1,16-hexadecanedithiol: HS-$(CH_2)_{16}$-SH or 'HDT' (Joseph, Y. et al. 2004)

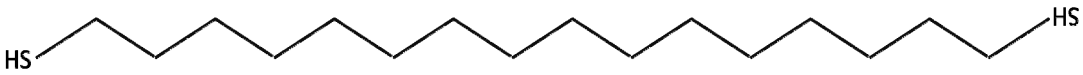

C. 2-Mercapto-N-[6-(2-mercapto-acetylamino)-hexyl]-acetamide
or 'MAH' (Vossmeyer et al. 2004):

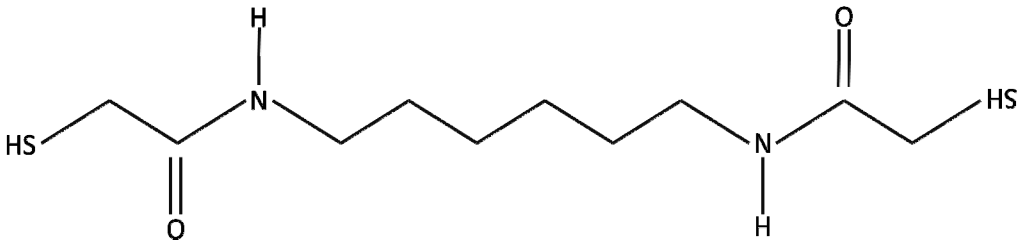

Figure 3.8 Linker Structures of the Sensor Film Materials

All three materials are interlaced with self-assembled gold nanoparticles of core size 4.0 ± 0.8nm. The NT and HDT materials are non-polar molecules, whereas the highly polar double bond in amide group of the MAH molecule gives it a strong dipole moment. This dipole increases the ability of the polymer material to form hydrogen bonds. Hence, a relatively high affinity for alcohols and water is expected for this material. Other properties of the materials can also be altered by forming composites

with other materials. All gold nanoparticle sensitive films used over the course of this study were prepared by Vossmeyer and co-workers at Sony Deutschland GmbH.

The layer by layer production of the self assembled polymer materials used the same procedure as Bethell et al. (Bethell et al. 1996). A detailed description of the deposition methodology is given by Joseph et al. (Joseph et al. 2003).

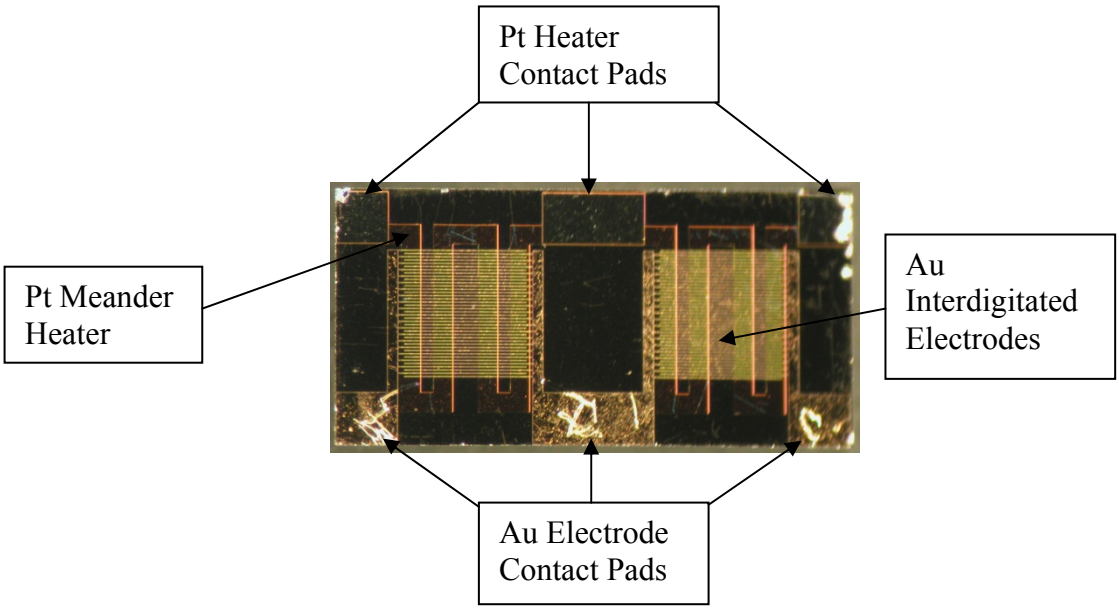

Figure 3.9 A chemoresistive sensor with 20 inter-digitated electrode pairs

The dodecylamine-stabilized gold nanoparticles, of core size 4.0 ± 0.8 nm (determined by TEM), were prepared by Vossmeyer et al. (Vossmeyer et al. 2002) by a method similar to that used by Leff et al. (Leff et al., 1996) and Brust et al. (Brust et al. 1994) using chemicals of reagent grade quality or better from Chempur, Fluka, Roth, Merck, Aldrich, ABCR or TCI and de-ionised water purified with a Millipore Milli Q system of 18.2MΩ resistivity. Oxidized silicon or BK7 glass incorporating 50 pairs of interdigitated gold electrodes was used as substrate. The dimensions of these gold interdigitated electrodes were 5 µm width, 100 nm height, 5 µm spacing, 1800 µm overlap and a 5 nm titanium adhesion layer. A 100 to 200 nm thick layer of calcium was deposited on to the glass substrate by thermal evaporation at the rate of ~5Å/s and oxidized by exposing to air to form Calcium Oxide (CaO). Using standard photolithographic techniques, the CaO film was patterned followed by a final etching step of the photoresist free CaO areas in water with an approximate pH of 5 adjusted with sulphuric acid (H_2SO_4). Acetone and propan-2-ol were used to remove the

remaining resist layer leaving behind a patterned water soluble CaO mask on the substrate surface. Oxygen plasma (PlasmaPrep5, from Gala Instrumente, Germany, for 4 mins at 30W and 0.24 mbar) was used to clean the substrate before the deposition of the nanoparticle film

Vossmeyer et al. describe the manufacturing process as follows: '*The substrates were then immersed into a solution of 50µL of 3-aminopropyldimethylethoxysilane in 5mL of toluene and heated to 60 °C for 30 min. The substrates were then washed with toluene and treated for 15 min with a solution of Au nanoparticles in toluene. The concentration of the particle solution corresponded to an absorbance of 0.4, measured at the maximum of the plasmon absorption band (λ_{max}) 514nm; 2mm path length). The substrates were washed again with toluene and treated with the linker solution, which contained 25µmol of alkanedithiol in 5mL of toluene. After 15 min, the substrates were washed with toluene, and then treated with particle and linker solutions. This whole process is counted as one deposition cycle and was repeated 13 times. The film deposition was finished by treating the substrates with the solution of alkanedithiol. The deposition of the gold particles was monitored by measuring the conductance of the films and their UV/vis spectra after each deposition cycle. Before such measurements, the films were briefly dried under a nitrogen stream.*'

Tencor Surface Profiler 10 was used to measure the thickness of the deposited film by determining the height profile at the edge of a scratch produced by moving a needle across the film and applying gentle pressure. The 1,9-nonanedithiol (NT) and the 1,16-hexadecanedithiol polymer material were purchased from Aldrich. The detailed preparation procedure is explained by Joseph et al. (Joseph et al. 2003).

3.5. The Test Setup

The test setup used for the characterization tests comprised of the sealable steel chamber containing the test sensor devices connected to the interface electronics. The output from the interface electronics was acquired through an NI-DAQ card and saved in a PC using LabVIEW software. The testing environment and exposure concentrations were provided by the FIA test station, schematics of which are given in Appendix B. The following sections explain the test setup in more detail.

3.5.1. Device Chamber and Interface Electronics

The testing chamber was made of stainless steel. Once placed inside the Dri bloc heater, it was allowed to stabilise at the heater temperature for six hours prior to testing. Figure 3.10 shows the top view of the sealed testing chamber. The chamber has the capacity to house two ratiometric ASIC devices with chemoresistors at the same time.

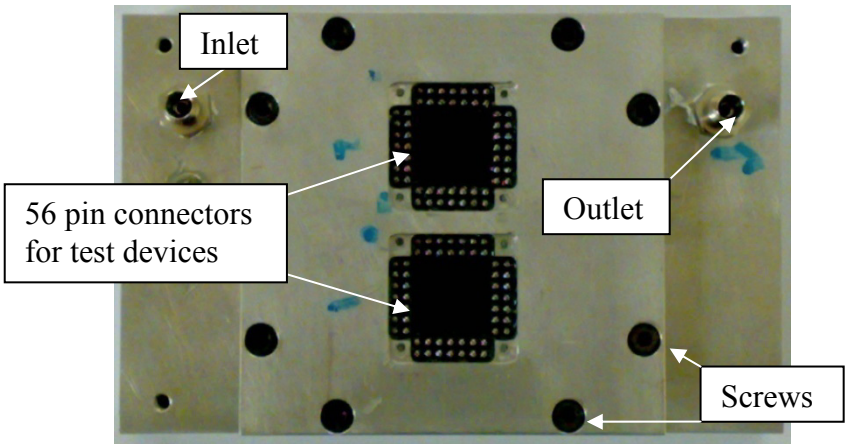

Figure 3.10 Sealed Chamber for Test Devices

The ASICs are packaged into a 68 pin Gold Ceramic Package by Spectrum Semiconductor Materials Inc. (PGA CPG06844), shown in figure 3.11, to provide pin outputs. The ASIC and the chemoresistors were glued to the CPG package with a Loctite Epoxy) and wire bonded with 25 µm gold wire to provide an electronic connection with the interface electronics.

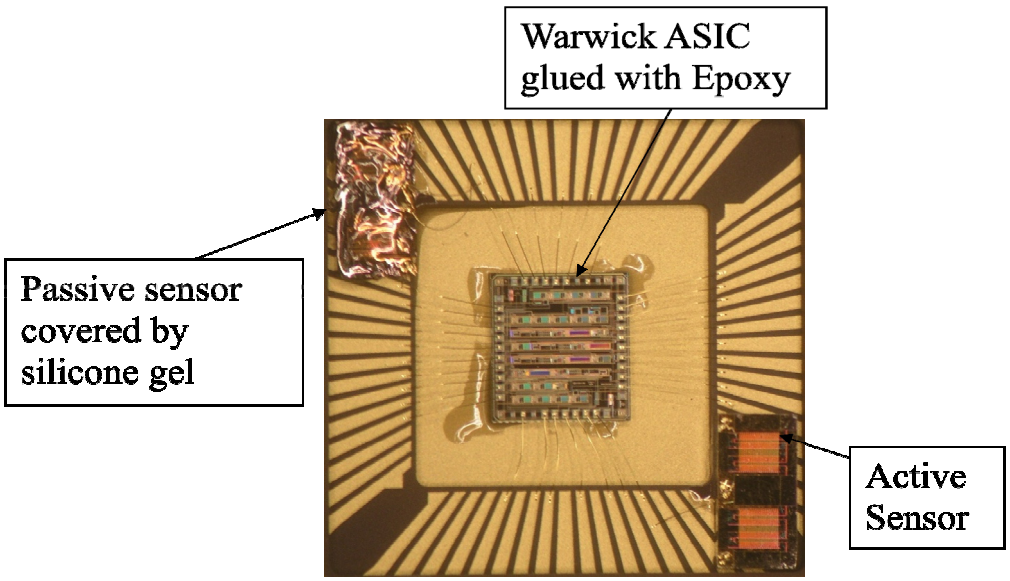

Figure 3.11 Layout of the ASIC Test Devices with Chemoresistors

Figure 3.11 shows the layout of wire-bonded ASICs and chemoresistors in the 68 pin ceramic gold package. 12 of the corner unutilised pins were cut and discarded to allow the gold package to fit into the connectors in the test chamber.

The resistance of the SRL 194 ASICs offset circuit is adjustable from an off-chip programmable potentiometer. This potentiometer is located on a printed circuit board (PCB), also referred here as the 'test board'. Figure 3.12 shows all the interface electronics connected to the sealed chamber with the electronic devices sealed inside. There are two circuit boards which make data transfer between the ASICs and the data acquisition system possible. The sensor test devices are sealed in a metal chamber which is connected to the test board using a connecting PCB as shown in figure 3.12.

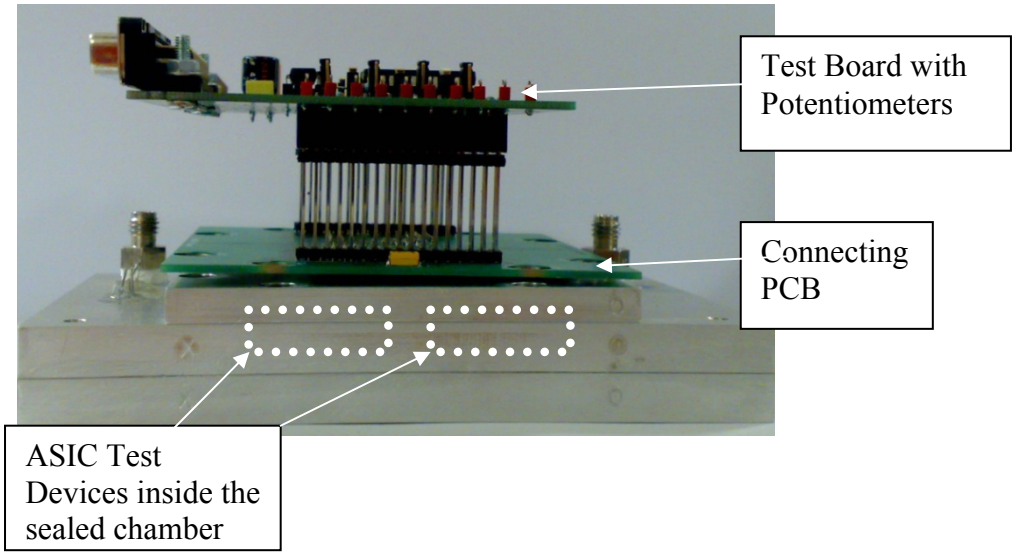

Figure 3.12 Test Chamber, Connecting PCB and the Test Board

Figure 3.13 shows the top view of the connecting PCB with the test chamber. This side of the connecting PCB links with the sealed test chamber. The initial design used a shielded cable between the connecting PCB and the test board. However, tests showed a poor signal to noise ratio with most of the output lost in the noise. The purpose of the shielded cable was to provide a significant distance between the block heater and the test board to avoid electronic noise from the Dri-Bloc heater. This would have protected the test board from exposure to the high temperatures generated by the Dri bloc heater and electromagnetic noise created by the heating coil. As the use of this cable was not possible, it was replaced by the connecting PCB. The maximum operating temperature of the bloc heater was therefore limited to 40ºC.

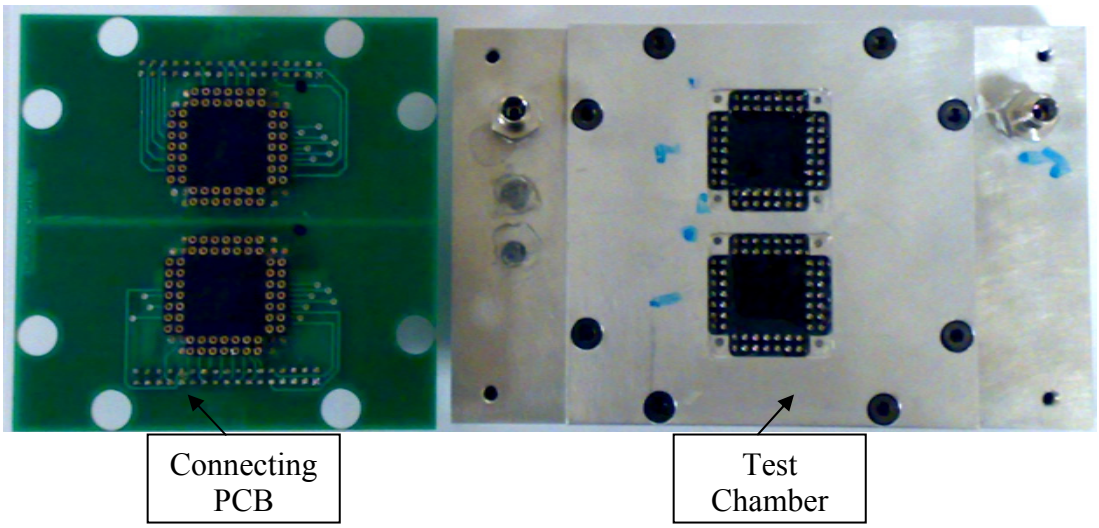

Figure 3.13 Connecting PCB (Top view) with the Test Chamber

Figure 3.14 shows the bottom view of the connecting PCB which plugs straight into the test board, as shown in figure 3.12. The connecting PCB as well as the test board, pictured in figure 3.15, included a ground plane which removed any unwanted electronic charge on the test board. This resulted in a significantly improved signal quality.

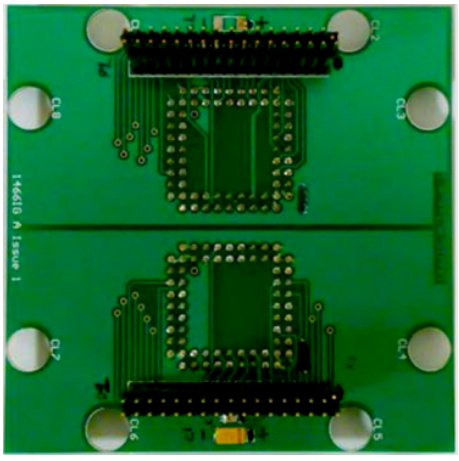

Figure 3.14 Connecting PCB (Bottom view)

Figure 3.15 shows the top view of the test board which interfaces with the data acquisition system and the connecting PCB. The test board allows access to the test sensordevices through 8 test points for each of the two devices inside the sealed test chamber. From these test points the offset voltage (V_{offset}), reference voltage (V_{ref}),

sensor voltage (V_{sensor}) and the output voltage (V_{out}) were measured using a gold precision voltmeter prior to starting each test. Two programmable potentiometers (Xicor X241AUP V0311ES) provided the resistance values for the offset resistors and the instrumentation amplifier. The jumpers on the test board give the option of using fixed resistors to test the functionality of the ASICs on their own or to utilise one or both of the chemoresistors placed with the ASICs inside the sealed test chamber. Two connectors connect the test board through two separate cables to the parallel port and the NI-DAQ card of a PC. The resistance values of the potentiometers can be set through the parallel port and output data of the test devices is collected using LabVIEW software.

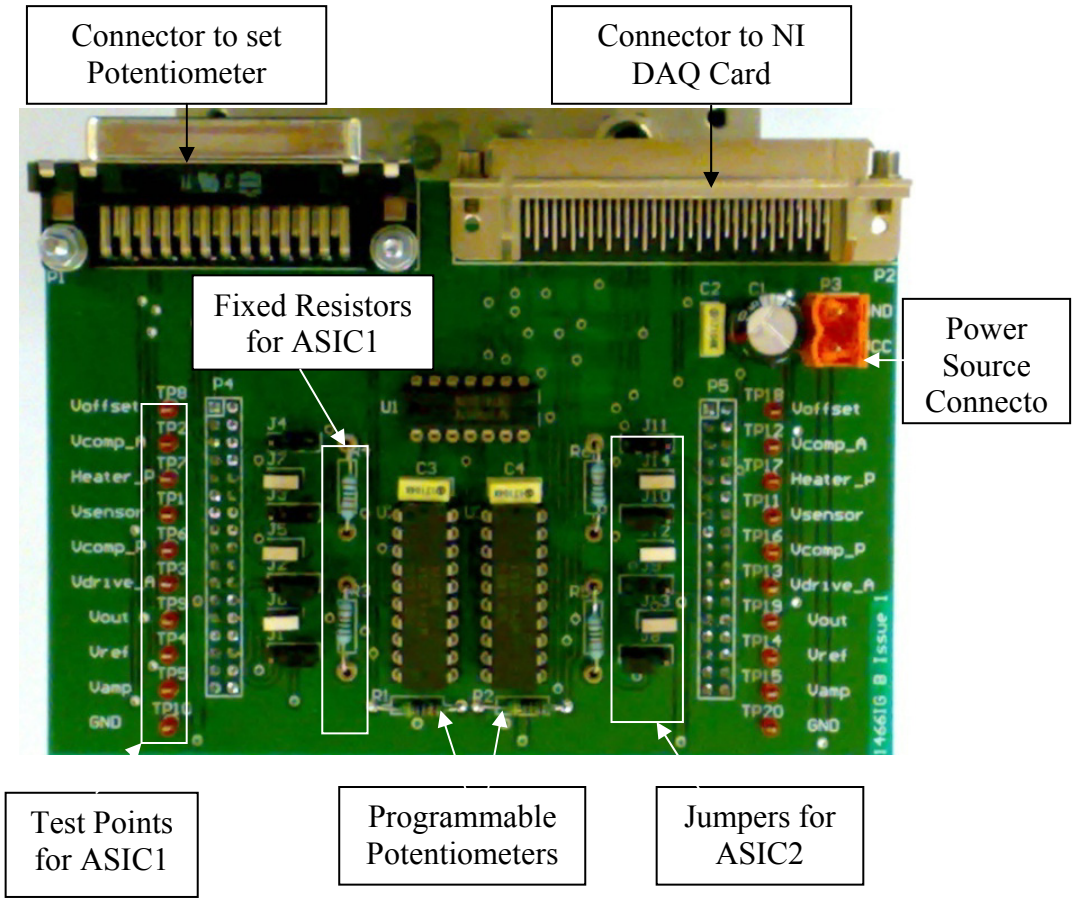

Figure 3.15 The Test Board (top view)

A detailed design description of the test board and the connecting PCB, including circuit schematic diagrams are given in Appendix A.

3.5.2. Testing Strategy and Durations

This part of the chapter describes the testing durations and the methodology. VOC tests were carried out on various combinations of chemosensors and for a variety of testing durations to observe the most optimum exposure time duration and results. Testing started with using devices with only one chemoresistor and a fixed resistor to calibrate the behaviour of an individual sensor. The next step involved introducing two chemosensors of the same basic linker structure in ratiometry. One of the two sensors was coated with a silicone gel to act as a partitioning layer. These two setups are considered as mono-type (uni-variate and bi-variate) sensors as all the chemoresistive sensors in a single device contained chemoresistors of the same material. Chemoresistors based on all three linker structure materials were tested in this arrangement of devices. The last phase was to test a polar linker structure with a non-polar linker structure based chemoresistor combined in one sensor device. The reason for doing so was to test the combined effects of two materials whose properties varied from each other in this manner. Au-NT and Au-HDT are only differentiated with the length of their linker chain, whereas Au-MAH has a polarised functional group included into the linker chain structure. It was expected that these devices would have negligible sensitivity for analytes which have similar results for the two chemoresistive materials in these duo-type devices. However, for analytes which differed in their sorption properties with the two chemosensor materials would benefit with a high degree of diversification between analyte outputs. Three different alcohols (methanol, ethanol, and propan-1-ol) were chosen to observe the device behaviour when exposed to polar analytes and the effect of increasing molecular size. Toluene was also tested as an aromatic non-polar molecule.

3.5.3. Mono-type & Duo-type devices

In this setup, three distinct kinds of devices were used. The first kind only used a single chemoresistor as part of the gas sensor circuit. In the second one of the two chemoresistors was encapsulated in a silicone gel. For the purpose of consistency it is always the passive sensor which is encapsulated by the silicone gel. The term ‘passive sensor’ refers to the position of the sensor rather than the presence of the silicone partitioning layer. Dow Corning 3145 RTV MIL-A-46146, was used as the non-corrosive silicone sealant to encapsulate the passive chemoresistor. After application the sealant gel was allowed to dry for 24 hours in air prior to any experiments. The

theoretical advantage of this setup is that both chemoresistors could be present in the same test chamber under similar environmental conditions. The change in response behaviour caused by the silicone partitioning layer should allow the sensor device to cancel out the environmental effect while responding to the difference in adsorption rates of the two chemosensors. Both the chemoresistors are subject to the same temperature changes and ageing times. This should minimise or nearly eliminate any drift effects caused by non-uniform ageing or non-test ambient condition changes during the testing procedure. The other chemoresistor was exposed directly to the VOC molecules without the presence of a partitioning layer. This chemoresistor will be referred to as the 'active sensor'.

A third type of devices called the Duo-type devices were made using two distinctly different chemoresistive sensor with the SRL 194 ASIC chip. The characterization of this type of devices is reported in chapter 6.

The first set of tests carried out analysed the AuNT and AuMAH hybrid devices, which were exposed to six different concentrations of Toluene, Ethanol, and Propan-1-ol vapours, with a total flow rate of 300 ml/min through the FIA station. Purified air was used as the carrier gas. A second round of tests was then carried out where the total flow rate through the test chamber was increased to 400 ml/min to reduce the sensor response time and to allow for validation and verification of corresponding chemoresistor data obtained from Sony Deutschland GmbH. Low (i.e. < 1000 ppm) as well as high concentrations (i.e. > 1000 ppm) of VOCs were used and the hysteresis between increasing and decreasing concentrations of the exposure analytes observed.

Various testing durations were tested. Analyte exposure duration of 20 minutes and a 'relaxation period' of 25 minutes during which the devices were exposed to pure carrier gas were found to be most effective in terms of observing the saturation value and returning to the baseline value from any particular exposure concentration.

3.5.4. FIA Test Station

The ASICs packaged with the chemoresistive sensitive material were exposed to the VOCs in a Fluid Injection Analysis (FIA) test station. The FIA test station allowed for the automated control of the exposure of vapours as well as manual control. The test station was used in both modes for the characterization of the chemoresistive

materials in combination with the ASICs. A detailed flow diagram of the FIA test station is given in Appendix B.

3.5.5. Vapour flow rate calculation.

The total flow of air and VOCs through the test station was governed by three Mass Flow Controllers (MFC: Brooks Mass Flow Controllers 5850 TR Series), and the exhaust measured by a Mass Flow Meter to account for any leakages. In order to convert the flow rates into VOC concentrations the Antoine vapour pressure equation was employed (Dean 1999), which uses a simple three parameter fit to experimental vapour pressures measured over a restricted temperature range. The equation for calculating analyte vapour concentration from vapour flow rates is derived in equation 3.4 to 3.8.

$$log_{10}\,(P_{analyte}) = A - \frac{B}{T+C} \tag{3.4}$$

Rearranging equation 3.4 we get,

$$P_{analyte} = 10^{A-(\frac{B}{T+C})} \tag{3.5}$$

$$Maximum\ analyte\ concentration = \frac{P_{analyte}}{P_{air}} \tag{3.6}$$

where P_{air} is taken as 760mmHg.

$$Anaylte\ vapour\ \% = \frac{Anaylte\ vapour\ flow\ rate}{Total\ flow\ rate} \tag{3.7}$$

$$Anaylte\ concentration = \frac{Maximum\ analyte\ concentration}{Anaylte\ vapour\ \%} \tag{3.8}$$

where, P is vapour pressure, T is temperature, and A, B, and C are "Antoine coefficients" that vary from substance to substance. The Antoine equation is accurate to a few percent for most volatile substances (with vapour pressures over 10 Torr).

The Antoine coefficients used over the course of this study are listed in the table below:

Analytes	*A*	*B*	*C*
Ethanol	8.32109	1718.1	237.52
Methanol	7.8975	1474.08	229.13
Propan-1-ol	7.84767	1499.21	204.64
Toluene	6.95464	1344.8	219.48
Water	16.54	3985	-39

Table 3.2 Antoine coefficients for analytes

A cooling bath (Neslab RTE-300) was used to keep the analytes at a constant temperature, usually 6°C.

3.5.6. Test durations

The FIA station allowed automated as well as manual control of the flow rates and exposure times of the VOC analytes. The total flow rate was kept at 300 ml/min for all monotype sensors. The duo-type tests were carried out at a higher flow rate of 400 ml/min. The change to 400 ml/min was made to reduce the device response time which was observed to be negligible (less than 30 seconds) considering the time required by the FIA test station was considerably longer when adjusting to a new vapour concentration (approximately 15 minutes).

Before the start of the experiment each sensor device was placed in the sealed stainless steel chamber at a constant temperature in the Dri Bloc heater for a minimum of six hours duration. During this time pure carrier gas was passed through the chamber to allow the sensors to lose any contaminant vapours. The humidity level at which the sensor device was to be exposed at was adjusted during this pre-test phase as well. This allowed the sensor devices as well as the FIA test station to get accustomed to the relative humidity levels.

Once the exposure sequence had begun, no further changes to the testing environment were made apart from those to the analyte flow rates. The sensor devices were exposed to the lowest concentration of the analyte first. The device exposure time was set to 20 minutes after which the FIA station switched to pure carrier gas to allow the sensor devices to return to the baseline values. An interval of 20-25 minutes between exposures was found sufficient to return the sensor device output to the

baseline value. During this device 'relaxation period' the flow rates through the mass flow controllers was adjusted to be ready for the next analyte concentration. A feedback loop with the humidity sensor in the FIA station allowed automatic adjustments of the flow rate controlling the relative humidity in the testing chamber. The sensor device was then exposed to the next higher concentration of the analyte.

This sequence was repeated till the maximum exposure analyte concentration was achieved. Once the highest test VOC concentration had been tested the applied test concentrations were reduced in steps in the reverse sequence till the lowest test concentration was reached. Using this entire testing sequence it was possible to observe any hysteresis in the sensor device response. Some studies have suggested using a randomised testing sequence to avoid sensor device drift. It was observed that a randomised sequence had two disadvantages. Firstly, it was not possible to plot the response hysteresis and secondly, if a low concentration was being tested after a high analyte concentration the residuals of the test analyte in the chemosensor film did not return the maximum sensor output. Studies have also suggested that completely randomised exposure sequences do not eliminate drift either. Experiments had to start with one of the highest test concentrations being applied first. This supports the second point mentioned above.

Once all the concentration tests for one test analyte were completed the sensor devices were exposed to pure carrier gas for approximately six hours before another VOC analyte could be tested. For tests carried out at higher temperatures the above procedure was repeated after allowing the sensor devices to stabilise at the higher temperature for at least six, and more usually twelve hours.

3.6. Data Analysis

The process of adsorption is the result of a number of analyte vapours forming a thin film on the surface of the chemoresistive films. Several empirical models have been developed to describe the adsorption process in resistive polymer based sensors (Gardner, J.W., Bartlett & Pratt 1995). For the purpose of this study the test chamber was said to be in equilibrium when the rate at which analyte vapours stick to the surface of the resistive sensors equates the rates at which these vapour molecules leave the surface of the polymer films. This can be represented in equation (3.9), where j_f and j_b are the forward and backwards rate constants, A is the adsorbed analyte species, { } represents an empty site, and $\{A\}$ represents an occupied site.

$$A + \{\ \} \underset{j_b}{\overset{j_f}{\leftrightharpoons}} \{A\} \tag{3.9}$$

The forward reaction rate, r_f, is proportional to the concentration of the target analyte, C, and the number of free sites, N, on the chemoresistive polymer. Hence the forward reaction rate can be given as:

$$r_f = j_f CN(1-\theta) \tag{3.10}$$

where θ is the fractional occupancy of the sites. The backwards reaction rate, r_b is proportional only to the concentration of sites containing the target species and can be represented as:

$$r_b = j_b N\theta \tag{3.11}$$

As at equilibrium the forward and backward reaction rates are equal (Ingleby 1999), the model for site occupancy can be described as:

$$\theta_\infty = \frac{J_a C_a}{1 + J_a C_a} \tag{3.12}$$

where C_a is the concentration of analyte A, and the binding constant, J_a, is given by the ratio of the forward and backward reaction rate constants (j_f / j_b) (Yang, X et al. 2001). This model is also known as the Langmuir adsorption isotherm.

The chemoresistive sensors respond to the adsorption of an analyte vapour by swelling and increasing the intermolecular tunnelling distance, hence resulting in an increase in the sensor film's resistance. Thus, it can be assumed that the increase in resistance is directly proportional to the site occupancy of the chemoresistive sensors.

$$\Delta resistance \propto \theta_{\infty} \tag{3.13}$$

Thus,

$$\Delta resistance \propto \frac{J_a C_a}{1+ J_a C_a} \tag{3.14}$$

Dividing the numerator and denominator on the right hand side this can be rewritten as:

$$\Delta resistance \propto \frac{C_a}{1/J_a+ C_a} \tag{3.15}$$

When $K = 1/J_a$ expression (3.15) becomes:

$$\Delta resistance \propto \frac{C_a}{K+ C_a} \tag{3.16}$$

At very low concentrations, when J_aC_a or C_a/K is much smaller than 1, the relationship shown in expression (3.14) can be approximated to a linear approximation as:

$$\Delta resistance \propto J_a C_a \tag{3.17}$$

From this model we can estimate the effects of the change in concentration on the change in the resistance of sensor. A lower K (or higher J_a) value would suggest that more vapour molecules are likely to bind with the sensor surface giving a more sensitive sensor, whereas, a higher K (or lower J_a) value would suggest weak binding forces

between the sensor surface and the vapour analyte giving a smaller change in resistance per unit change in concentration.

Joseph et al. have reported the Langmuir isotherm to be a good fit for the gold nano-particle chemoresistive sensors used in this study (Joseph, Y. et al. 2004). As the dynamic behaviour of these films to various VOCs has already been shown to be a good fit to the Langmuir plot, a limited number of concentrations (usually 3) were tested against previously untested VOCs to show that the films still behaved in a similar manner and that the effectiveness of the ratiometric principle.

Another isotherm which describes the adsorption of an analyte on a surface is the Freundlich isotherm. This isotherm relates the concentration of a solute on the surface of an adsorbent, to the concentration of the solute in fluid phase. It can be mathematically expressed as:

$$\frac{x}{m} = F_k p^{1/n_f} \tag{3.18}$$

or,

$$\frac{x}{m} = F_k C^{1/n_f} \tag{3.19}$$

where x is the mass of the adsorbate, m is the mass of adsorbent, p is the equilibrium pressure of the adsorbate, C is the equilibrium concentration of the analyte. F_k and $1/n_f$ are constants for a given adsorbate and adsorbent at a particular temperature.

For the purpose of this study it was assumed that the ratio of the mass of the adsorbate to the mass of the adsorbent was directly proportional to the change in resistance of the chemoresistive sensor films. Thus,

$$\Delta resistance \propto F_k C^{1/n_f} \tag{3.20}$$

When $n = 1/n_f$ expression (3.20) becomes:

$$\Delta resistance \propto F_k C^{n} \tag{3.21}$$

The Freundlich equation (Yang, C-h 1998) states that, at a constant temperature, the amount of adsorbate bound per unit weight of adsorbent, *x/m* (adsorption efficiency of the adsorbent) is a logarithmic function of the residual concentration in the fluid phase at equilibrium, *C*. As the resistance increase of the chemoresistive sensors is directly proportional to *x/m*, this implies that the amount of adsorbate adsorbed increases with an increase in analyte concentration. At larger concentrations of adsorbate, the amount adsorbed approaches a constant value. Thus, the gradient of the curve is greatest at low solute concentrations and decreases with solute concentration (Proctor & Toro-Vazquez 1996).

Although the Freundlich model is based on empirical concepts, the parameters of the equation, F_k and n, are relative indicators of adsorption capacity and energy of adsorption, respectively. If $C = 1$ expression (3.21) becomes:

$$\Delta resistance \propto F_k \tag{3.22}$$

implying that F_k can be regarded as coverage of the unit concentration. Considering the proportionality sign as equality and taking logarithms of both sides of the equation and differentiating, we have

$$\left(d(\Delta resistance)/\Delta resistance\right) \Big/ \left(d(C)/C\right) = n \tag{3.23}$$

leading to the empirical constant n being regarded as the rate of the increase in $\Delta resistance$ (in fraction) with increasing C (in fraction). Thus, these empirical constants (F_k and n) can be regarded as responsible for characterizing the adsorption capacity of the system and establish a relationship between the macroscopic behaviour of the adsorption system and microscopic properties of the adsorbed molecule.

As the data were fitted to the Langmuir, linear and Freundlich isotherms with only three experimental data points a high correlation coefficient could be obtained with such a small number of data points in a narrow experimental interval. However, repeated tests with a narrow margin of error support the data fit. The main purpose of using these isotherms was for showing their mathematical simplicity and significance of their empirical constants. The Langmuir isotherm, its linear approximation and the

Freundlich isotherm were mainly used as a means to compare the results of the ratiometric sensor devices and how they fared when fit to these three mathematical models.

3.7. Conclusions

In this chapter the design and fabrication of the smart ASIC chip as well as the VOC sensitive self-assembled gold nanoparticle alkyl-dithiol linker structures were discussed. Individual sections of the SRL 194 smart ASIC device were analysed and the advantages of the non-inverting ratiometric amplifier architecture, followed by the instrumentation amplifier and the Bessel low pass filter were reviewed. An overview of the general sensor device testing strategy for characterization of the smart gas sensors to various VOC analytes was also given. A description of the FIA test setup and the interface electronics was presented. An explanation of various mathematical models used to analyse device output data was also given.

The following chapter shows that the change in the resistive ratio of chemoresistive sensors is directly proportional to the change in the output of the smart gas sensors. In chapter 4 results of characterization tests for sensor devices formed with one chemosensor balanced by a standard resistor in the ratiometric setup are analysed. The characterization tests are carried out with ‘active’ sensor devices and compared with silicone encapsulated ‘passive’ sensor devices to observe the effects of the presence of the silicone sealant gel on the chemosensor.

3.8. References

Abeles, B, Sheng, P, Coutts, MD & Arie, Y 1975, 'Structural and electrical properties of granular metal films', *Advances in Physics*, vol. 24, no. 3, pp. 407-61.

Bethell, D, Brust, M, Schiffrin, DJ & Kiely, C 1996, 'From monolayers to nanostructured materials: an organic chemist's view of self-assembly', *Journal of Electroanalytical Chemistry*, vol. 409, no. 1-2, pp. 137-43.

Brust, M 1995, University of Liverpool.

Brust, M, Bethell, D, Schiffrin, DJ & Kiely, CJ 1995, 'Novel Gold-Dithiol Nano-Networks with Non-metallic Electronic Properties', *Advanced Materials*, vol. 7, no. 9, pp. 795-&.

Brust, M, Fink, J, Bethell, D, Schiffrin, DJ & Kiely, C 1995b, 'Synthesis and reactions of functionalised gold nanoparticles', *Journal of the Chemical Society-Chemical Communications*, no. 16, pp. 1655-6.

Brust, M, Walker, M, Bethell, D, Schiffrin, DJ & Whyman, R 1994, 'Synthesis of thiol-derivatized gold nanoparticles in a 2-phase liquid-liquid system', *Journal of the Chemical Society-Chemical Communications*, no. 7, pp. 801-2.

Cole, M, Ulivieri, N, Garcia-Guzman, J & Gardner, JW 2003, 'Parametric model of a polymeric chemoresistor for use in smart sensor design and simulation', vol. 34, pp. 865-75.

Covington, JA 2001, 'CMOS and SOI CMOS FET-based gas sensors', Dissertation/Thesis thesis.

Dean, JA 1999, *Lange's Handbook of Chemistry*, McGraw-Hill.

Evans, SD, Johnson, SR, Cheng, YLL & Shen, TH 2000, 'Vapour sensing using hybrid organic-inorganic nanostructured materials', *Journal of Materials Chemistry*, vol. 10, no. 1, pp. 183-8.

Faraday, M 1857, 'The Bakerian Lecture: Experimental Relations of Gold (and Other Metals) to Light', *Philosophical Transactions of the Royal Society of London*, vol. 147, pp. 145-81.

García-Guzmán, J 2005, 'Smart ratiometric ASIC chip for VOC monitoring', University of Warwick.

García-Guzmán, J, Ulivieri, N, Cole, M & Gardner, JW 2003, 'Design and simulation of a smart ratiometric ASIC chip for VOC monitoring', *Selected Papers from Eurosensors XVI*, vol. 95, no. 1-3, pp. 232-43.

Gardner, JW, Bartlett, PN & Pratt, KFE 1995, 'Modelling of gas-sensitive conducting polymer devices', *Circuits, Devices and Systems, IEE Proceedings* -, vol. 142, no. 5, pp. 321-33.

Han, L, Daniel, DR, Maye, MM & Zhong, CJ 2001, 'Core-shell nanostructured nanoparticle films as chemically sensitive interfaces', *Analytical Chemistry*, vol. 73, no. 18, pp. 4441-9.

Ingleby, P 1999, 'Modelling and Characterisation of Conduction Polymer Chemoresistors', University of Warwick.

Joseph, Y, Besnard, I, Rosenberger, M, Guse, B, Nothofer, HG, Wessels, JM, Wild, U, Knop-Gericke, A, Su, DS, Schlogl, R, Yasuda, A & Vossmeyer, T 2003, 'Self-assembled gold nanoparticle/alkanedithiol films: Preparation, electron microscopy, XPS-analysis, charge transport, and vapor-sensing properties', *Journal of Physical Chemistry B*, vol. 107, no. 30, pp. 7406-13.

Joseph, Y, Guse, B, Yasuda, A & Vossmeyer, T 2004, 'Chemiresistor coatings from Pt- and Au-nanoparticle/nonanedithiol films: sensitivity to gases and solvent vapors', *Sensors and Actuators B: Chemical*, vol. 98, no. 2-3, pp. 188-95.

Joseph, Y, Krasteva, N, Besnard, I, Guse, B, Rosenberger, M, Wild, U, Knop-Gericke, A, Schlogl, R, Krustev, R, Yasuda, A & Vossmeyer, T 2004, 'Gold-nanoparticle/organic linker films: self-assembly, electronic and structural characterisation, composition and vapour sensitivity', *Faraday discussions*, vol. 125, pp. 77-97; discussion 9-116.

Krasteva, N, Besnard, I, Guse, B, Bauer, RE, Mullen, K, Yasuda, A & Vossmeyer, T 2002, 'Self-assembled gold nanoparticle/dendrimer composite films for vapor sensing applications', *Nano Letters*, vol. 2, no. 5, pp. 551-5.

Krasteva, N, Guse, B, Besnard, I, Yasuda, A & Vossmeyer, T 2003, 'Gold nanoparticle/PPI-dendrimer based chemiresistors Vapor-sensing properties as a function of the dendrimer size', *Sensors and Actuators B-Chemical*, vol. 92, no. 1-2, pp. 137-43.

Leff, DV, Brandt, L & Heath, JR 1996, 'Synthesis and characterization of hydrophobic, organically-soluble gold nanocrystals functionalized with primary amines', *Langmuir*, vol. 12, no. 20, pp. 4723-30.

Neugebauer, CA & Webb, MB 1962, 'Electrical Conduction Mechanism in Ultrathin, Evaporated Metal Films', *Journal of Applied Physics*, vol. 33, no. 1, pp. 74-82.

Porter, MD, Bright, TB, Allara, DL & Chidsey, CED 1987, 'Spontaneously Organized Molecular Assemblies, 4. Structural Characterization of n-Alkyl Thiol Monolayers on Gold by Optical Ellipsometry, Infrared Spectroscopy and Electrochemistry', *Journal of the American Chemical Society*, vol. 109, no. 12, pp. 3559-68.

Proctor, A & Toro-Vazquez, JF 1996, 'The Freundlich isotherm in studying adsorption in oil processing', *Journal of the American Oil Chemists Society*, vol. 73, no. 12, pp. 1627-33.

Vossmeyer, T, Guse, B, Besnard, I, Bauer, RE, Mullen, K & Yasuda, A 2002, 'Gold nanoparticle/polyphenylene dendrimer composite films: Preparation and vapor-sensing properties', *Advanced Materials*, vol. 14, no. 3, pp. 238-+.

Vossmeyer, T, Joseph, Y, Besnard, I, Harnack, O, Krasteva, N, Guse, B, Nothofer, HG & Yasuda, A 2004, 'Gold-nanoparticle/dithiol films as chemical sensors and first steps towards their integration on chip', *Physical Chemistry of Interfaces and Nanomaterials Iii*, vol. 5513, pp. 202-12.

Vossmeyer, T, Katsikas, L, Giersig, M, Popovic, IG, Diesner, K, Chemseddine, A, Eychmueller, A & Weller, H 1994, 'CdS Nanoclusters: Synthesis, Characterization, Size Dependent Oscillator Strength, Temperature Shift of the Excitonic Transition Energy, and Reversible Absorbance Shift', *Journal of Physical Chemistry*, vol. 98, no. 31, pp. 7665-73.

Wohltjen, H & Snow, AW 1998, 'Colloidal metal-insulator-metal ensemble chemiresistor sensor', *Analytical Chemistry*, vol. 70, no. 14, pp. 2856-9.

Yang, C-h 1998, 'Statistical Mechanical Study on the Freundlich Isotherm Equation', *Journal of Colloid and Interface Science*, vol. 208, no. 2, pp. 379-87.

Yang, X, Chen, Q, Zhang, JS, An, Y, Zeng, J & Shaw, CY 2001, 'A mass transfer model for simulating VOC sorption on building materials', *Atmospheric Environment*, vol. 35, no. 7, pp. 1291-9.

Zhang, HL, Evans, SD, Henderson, JR, Miles, RE & Shen, TH 2002, 'Vapour sensing using surface functionalized gold nanoparticles', *Nanotechnology*, vol. 13, no. 3, pp. 439-44.

CHAPTER 4

4. Characterisation of 'Active' & 'Passive' Chemoresistive Devices

4.1. Introduction

This chapter discusses the results obtained with SRL 194 ASIC devices combined with chemoresistive sensors. The tests analysed in this chapter use one chemoresistor with one fixed resistor at a time. The terms *'active'* and *'passive'* refer to positions of the sensors and fixed resistors as defined in chapter 3 (see figure 3.11). This convention will be followed throughout the thesis, and is used regardless of whether there is a passivating coating on the sensor being mentioned or not.

These tests were carried out to characterise the behaviour of the chemoresistors when only one chemoresistive sensor is associated with the ratiometric ASIC. This chemosensor is balanced with a static or fixed resistor to complete the ratiometric arrangement of the non-inverting amplifier circuit. The results obtained in this chapter are used to verify the results reported for the test devices in chapters 5 (mono-type) and 6 (duo-type) both of which discuss bi-variate devices as two chemoresistors with variable resistances are used with one ASIC to form a sensor device. The ratiometric

limits of the ASIC were also tested and analysed in this chapter. This was carried out using standard fixed resistors and by varying one resistance at a time.

4.2. Determining Ratiometric Limitations

In order to proceed with chemoresistor device tests it was important to verify the limits of the resistance ratios (*rr*) within which the ASIC would operate. It was easier to select chemoresistors based on this information as the selection could be made keeping in view the expected change in the resistance of the chemoresistor. In this way saturation of the output voltage could be avoided.

The ASIC had initially been designed to work optimally with 10 kΩ resistors. Subsequent simulations have been reported by García-Guzmán (García-Guzmán 2005) for a chemoresistor operating range of 1 kΩ to 1 MΩ. However, these reported simulations assumed active and passive resistors to be always at parity with each other.

A resistance ratio of as close to 1 as possible was reported to be the safest starting point for a test in which the chemoresistors were to be exposed to VOCs. However, this resistance ratio would change during exposure to VOC as the resistances of the individual chemoresistors changed.

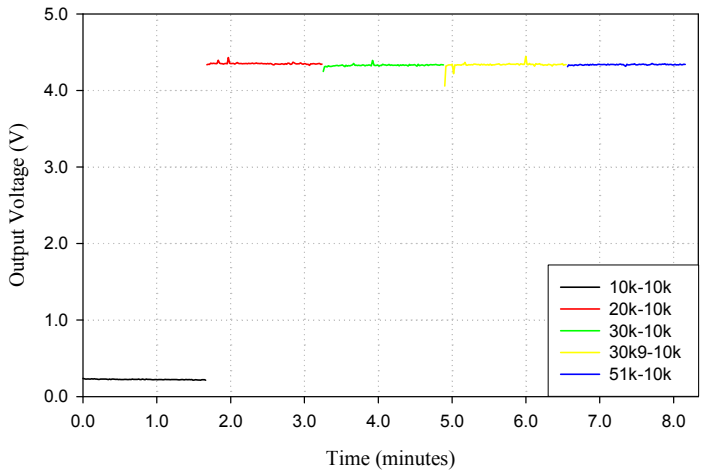

Figure 4.1 Increasing the active resistance from 10 - 51 kΩ

To test the ratiometric limitations of the ASICs, the jumper settings on the test boards were set to work with external fixed resistors. The gold ceramic packaged ASICs were placed in the sealed steel chamber and kept in the Dri-Bloc heater, described in chapter 3, at 30ºC for at least 6 hours prior to starting a test sequence.

To measure the operating limit of the resistor ratio one of the resistors was kept constant while the other one varied. Figure 4.1 shows the device behaviour when the active resistor is varied and the passive resistor is kept constant.

Active Resistance (kΩ)	Passive Resistance (kΩ)	Offset Resistance (kΩ)	V_{sensor} (V)	V_{offset} (V)	V_{ref} (V)	V_{out} (V)
10	10	17	2.43	2.40	1.21	0.21
20	10	17	4.96	2.39	1.21	4.35
30	10	17	4.96	2.41	1.21	4.33
39	10	17	4.96	2.40	1.21	4.35
51	10	17	4.96	2.41	1.21	4.35

Table 4.1 Resistance values and voltage outputs for 10 - 51 kΩ tests

The active resistance was increased from 10 kΩ to 51 kΩ. Saturation was achieved at 20 kΩ. Table 4.1 shows values of the active resistors and passive resistors and the associated output voltages. It can be seen that the output voltage reaches a saturation level as soon as the resistance ratio goes over 2. From simulations done by García-Guzmán (García-Guzmán 2005), the ideal reference voltage (V_{ref}) is expected to be 1.2 V. The measured value was observed to be slightly higher at 1.21 V which is within acceptable limits. The slight increase from the expected value exists because of the contact resistance of the circuitry and the measuring probe.

Previous simulations showed increasing rising and falling edge switching spikes when the operating resistances of the active and passive resistors were increased whilst the resistance ratio was kept at parity. The fixed resistance tests verify the simulated observations. To check for ASIC operation at high resistances the devices were tested starting at a resistance ratio of unity with both the resistances (active and passive) at 750 kΩ. Figure 4.2 shows the resulting voltage outputs. Operating with resistances over 750 kΩ the ASICs show good operational results with a high signal to noise ratio. Figure 4.2 also shows saturation reached at active-passive resistances of 2200-750 kΩ giving a maximum operating resistance ratio of approximately 3. The colours indicate a change of resistors. By increasing the active resistance the magnitude of the switching spikes were also observed to have increased giving a poorer signal to noise ratio. The instrumentation amplifier gain was noted to be 7. The figure shows the

output with a sampling frequency of 1 Hz. Increasing the sampling frequency shows the switching noise more clearly.

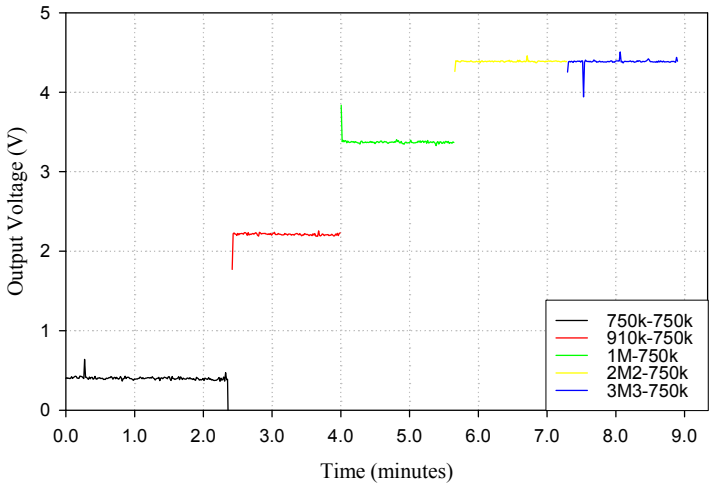

Figure 4.2 Increasing the active resistance from 750 kΩ - 3.3 MΩ

Using the voltage values for from table 4.2 in equation (3.1), the operating gain of the ASIC was calculated to be 7.37. The devices can be assumed to be saturated when the reference voltage, sensor voltage and output voltage do not match this gain value with a 10% error margin, using equation (3.1). The internal resistance of the offset circuit of the ASIC (R_{int}) can be calculated from equation (4.1).

$$R_{int} = R_{off}\left(\frac{V_{offset}}{V_{ref}} - 1\right) \tag{4.1}$$

Active Resistance (kΩ)	Passive Resistance (kΩ)	Offset Resistance (kΩ)	V_{sensor} (V)	V_{offset} (V)	V_{ref} (V)	V_{out} (V)
750	750	17	2.43	2.40	1.22	0.30
910	750	17	2.69	2.39	1.22	2.21
1000	750	17	2.85	2.39	1.22	3.37
2200	750	17	4.97	2.38	1.22	4.39
3300	750	17	4.97	2.38	1.22	4.39

Table 4.2 Resistance values and voltage outputs for 750 kΩ - 3.3 MΩ tests

Once the gain of the instrumentation amplifier is confirmed from equation (3.1), R_{int} can be verified with equation (4.2), which is derived by rearranging equations (2.9), (2.10) and (3.1). This gives an expression for the internal resistance R_{int} of the ASIC given in equation (4.2), which was calculated using the non-saturated voltage values to be 16.40 kΩ. Any differences that lie in the value of R_{int} calculated from both the equations gives the operational error of the circuit.

$$R_{int} = R_{off}\left(\frac{R_{act}}{R_{pas}} - \frac{V_{out}}{Gain \times V_{ref}}\right) \tag{4.2}$$

Equation (4.2) can be re-arranged to give an expression for the resistance ratio. This is an important value as during VOC exposure experiments it was not possible to measure individual resistances of the chemoresistors. This expression is given in equation (4.3).

$$rr = \frac{R_{act}}{R_{pas}} = \left(\frac{R_{int}}{R_{off}} + \frac{V_{out}}{Gain \times V_{ref}}\right) \tag{4.3}$$

This equation is preferred to expression (4.4) to calculate the resistance ratio as this shows the resistance ratio directly proportional to the output voltage, which is the measured output value for all the experiments. The disadvantage of expressions (4.4) is that it is dependent on the measurement of V_{sensor}, which could not be measured during exposure times.

$$rr = \frac{R_{act}}{R_{pas}} = \left(\frac{V_{sensor}}{V_{ref}} - 1\right) \tag{4.4}$$

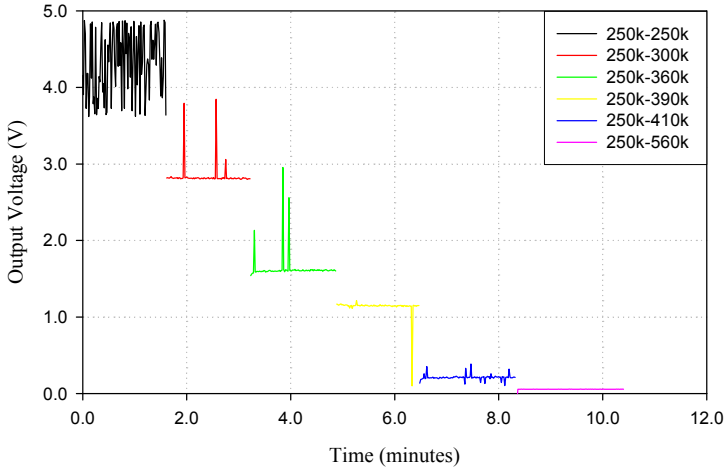

Figure 4.3 Increasing the passive resistance from 250 - 560 kΩ

The relationship between a varying passive sensor resistance and a fixed active sensor resistance is shown in equation (2.10) in chapter 2. The results shown in figure 4.3 are from a test when the active resistance was kept constant and the passive resistance was varied. The passive resistance is varied from 250 kΩ to 560 kΩ. When both the resistances were at parity at 250 kΩ, the offset resistance was set so that the output of the device was saturated at 4.33 V. By increasing the passive resistance, the voltage output of the ASIC device was reduced.

Active Resistance (kΩ)	Passive Resistance (kΩ)	*rr*	Offset Resistance (kΩ)	V_{sensor} (V)	V_{offset} (V)	V_{ref} (V)	V_{out} (V)
250	250	1.000	33	2.43	1.80	1.22	4.33
250	300	0.833	33	2.20	1.80	1.22	2.81
250	360	0.694	33	2.04	1.81	1.22	1.60
250	390	0.641	33	1.97	1.80	1.22	1.14
250	410	0.610	33	1.84	1.81	1.22	0.20
250	560	0.446	33	1.75	1.80	1.22	0.05

Table 4.3 Resistance values and voltage outputs for 250 - 560 kΩ tests

Table and figure 4.3 show the test device saturating at a resistance ratio of 0.4464, when the active and passive resistances were 250 kΩ and 560 kΩ, respectively.

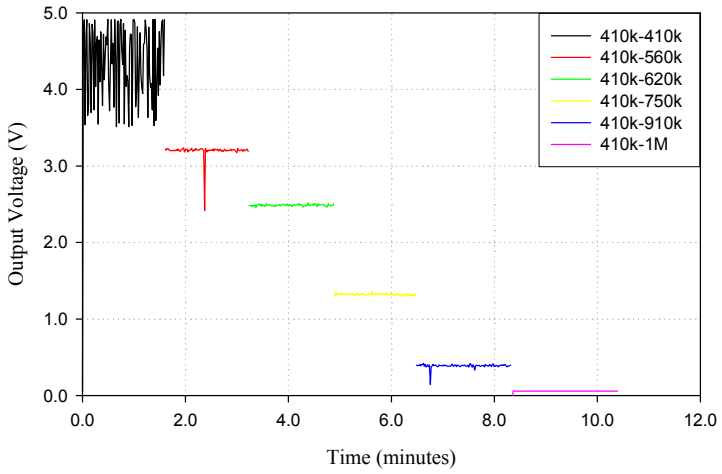

Figure 4.4 Increasing the passive resistance from 410 kΩ - 1 MΩ

Active Resistance (kΩ)	Passive Resistance (kΩ)	*rr*	Offset Resistance (kΩ)	V_{sensor} (V)	V_{offset} (V)	V_{ref} (V)	V_{out} (V)
410	410	1.000	33	2.43	1.80	1.21	4.36
410	560	0.732	33	2.24	1.80	1.21	3.21
410	620	0.661	33	2.14	1.80	1.21	2.48
410	750	0.547	33	1.98	1.80	1.21	1.32
410	910	0.451	33	1.85	1.80	1.21	0.38
410	1000	0.410	33	1.79	1.80	1.21	0.05

Table 4.4 Resistance values and voltage outputs 410 kΩ - 1 MΩ tests

Figure and table 4.4 show that the test device still responded to a change in resistance at a resistance ratio of 0.4506 and was saturated when it was reduced to a resistance ratio of 0.41. Using the results from table 4.3 it was determined that the device saturated between 0.4506 and 0.4464. The reciprocals of these values are 2.2193 and 2.2401. These values exceed the saturation value obtained from table and graph 4.1, which were approximately at a ratio of 2.0. However, to keep the devices within operable limits the maximum resistance ratio value of 2 and a minimum of 0.5 were used for all the experiments when choosing chemoresistors to be paired up with the ASICs.

4.2.1. Relationship of output voltage to chemosensor resistance

To determine the percentage change in resistance ratio when the chemoresistive sensors are exposed to various VOCs, the ASIC devices were packaged with one chemoresistive sensor and one standard fixed resistor. The tests were split between two stages. In the first stage, a variable resistance chemoresistive sensor was used in place of the resistor representing the *Active* sensor along with a fixed resistance *Passive* resistor. In the second stage, a chemoresistive sensor coated with a silicone gel was used in place of the passive resistor, while a fixed resistance standard resistor was used in place of the active sensor.

The response of the sensors was measured as a change of output voltage from the baseline value. When the active sensor's resistance was allowed to increase, the output voltage was expected to increase under exposure conditions. Thus, the change in output voltage can be calculated as

$$\Delta V_{out} = V_{out}' - V_{out} \tag{4.5}$$

where, V_{out}' is the voltage output under exposure conditions and V_{out} is the baseline output voltage prior to exposure. In equation (2.1), the resistance ratio (*rr*) was defined as the ratio of the active and passive resistors of the ASIC device. The change in *rr* is defined as the change in this ratio between exposure and non-exposure conditions.

$$\Delta rr = \frac{R_{act}'}{R_{pas}'} - \frac{R_{act}}{R_{pas}} \tag{4.6}$$

where, R_{act}' and R_{pas}' are the active and passive resistances under exposure conditions respectively. Using this definition and expression for the change in the output voltage can be given as

$$\Delta V_{out} = \left(Gain \times V_{ref}\right) \times \Delta rr \tag{4.7}$$

Here, *Gain* and V_{ref} are constants and only affected by ambient temperature changes as they are dependent on electronic circuitry rather than variable resistance chemical films. V_{ref} is a measured quantity which was measured using a voltmeter for each experiment. It is supposed to be around 1.2 V for all the experiments. The measured quantities are

usually around 1.21 V taking into account contact and circuit resistances. The gain is set prior to starting the experiment using the programmable potentiometers located on the test board PCB and controlled through LabVIEW software. For the experiments mentioned in this chapter it was set to the value of 7. The expression to calculate the change in the resistance of the exposed resistor with respect to *rr* is given in equation (4.8).

$$\frac{\Delta R_{act}}{R_{act}} = \frac{\Delta rr}{rr} \tag{4.8}$$

When the passive chemoresistive sensor coated with silicone is exposed to the analyte vapours, an increase in the resistance of these passive resistors is observed. This results in a reduction of the output voltage. A negative value of Δ*rr* simply reflects the fact that ΔV_{out} had a negative value due to a decrease in output voltage under exposure conditions. Equation (4.9) gives the expression for calculating the relative change in resistance with respect to *rr* under these conditions. For all of the experiments carried out in chapters 4 and 5 we are only concerned with the magnitude change of Δ*rr*, thus for all calculations it is |Δ*rr*| that is usually used.

$$\frac{\Delta R_{pas}}{R_{pas}} = -\frac{rr}{\Delta rr + rr} \tag{4.9}$$

The passive chemoresistors were coated with silicone gel. It was expected that this coating would have varying adsorption rates for the various analyte vapours (Grate & Abraham 1991; Li, J & Werth 2002; Yi-Ming Sun 1994); thus, acting like a partitioning layer or a chromatography medium. Accumulation of some of the VOC vapours in the silicone coating was expected to increase the output of the ASIC device to that vapour, hence, making the silicone coating act similar to a pre-concentrator.

When analysing Δ*rr* values in any of the empirical models, Δ*resistance* as discussed in chapter 3 was equated to Δ*rr*. This fits the output of the complete combined ratiometric device rather than just one chemoresistive sensor.

4.3. Chemoresistive Sensor Tests Results

The response of the three chemoresistive materials (Au-NT, Au-HDT and Au-MAH) was measured against exposure to vapours of ethanol, methanol, propan-1-ol and toluene in air. The response was measured at three different concentrations controlled by the flow rate of air through the VOC analyte solutions. Three test concentrations were considered to be sufficient as Joseph et al. have already shown the films to be good fits to the Langmuir model (Joseph et el., 2003). Other models, such as the Freundlich and the linear approximation to the Langmuir model were chosen for the purpose of comparison and their appropriateness to be used for these ratiometric devices. During the tests, the chemoresistive sensor devices were exposed to the VOC vapours for 20 minutes. This was followed by a relaxation period of 20 minutes during which the devices were exposed to the carrier gas (dry air). These durations were considered sufficiently long enough to allow the sensors to reach their maximum value at the exposure concentrations. The total flow rate of 300 ml/min through the device exposure chamber was maintained.

Initial tests were carried out at 0-2% relative humidity (rh) with additional tests at 38-40% rh. Tests were carried out at a Dri-Bloc heater temperature of 30°C. The cooling bath temperature was kept constant at 6°C. The exposure concentrations were controlled by controlling the air flow rate through the analyte samples, and calculated using Antoine's vapour pressure equation as explained in equations (3.4) to (3.8) (Dean 1999). Table 4.5 gives the volumetric flow rates and exposure concentrations of all the VOCs used in these set of experiments.

Methanol		Ethanol		Propan-1-ol		Toluene	
Flow rates (ml/min)	**Concentrations (ppm)**	**Flow rates (ml/min)**	**Concentrations (ppm)**	**Flow rates (ml/min)**	**Concentrations (ppm)**	**Flow rates (ml/min)**	**Concentrations (ppm)**
13	2423	9	728	12	301	9	386
76	14163	55	4449	70	1756	55	2360
138	25718	100	8089	127	3186	100	4291

Table 4.5 Test flow rates and concentrations

4.3.1. Au-NT 'Active' Sensor Tests

The detailed analysis and calculations for Δrr and $\frac{\Delta R_{act}}{R_{act}}$ of all the tests when the 'active' sensor was exposed to the VOC vapours is tabulated in table 4.6 along with the respective exposure concentrations of the vapours. These tests were carried out at a chamber temperature of 30°C and 0% rh.

Test Results for Au-NT Devices with Active Sensor Exposure					
VOC	**Concentrations (ppm)**	**ΔV_{out} (V)**	**Δrr (x10^{-3})**	**$\Delta R_{act}/R_{act}$ (x10^{-3})**	
Methanol Exposure Test	2423	0.055	6.49	6.87	Baseline = 0.975 V *rr* = 0.945
	14163	0.225	26.56	28.11	
	25718	0.385	45.45	48.10	
Ethanol Exposure Test	728	0.050	5.90	6.25	Baseline = 1.025 V *rr* = 0.945
	4449	0.115	13.58	14.37	
	8089	0.245	28.93	30.61	
Propan-1-ol Exposure Test	301	0.080	9.44	10.00	Baseline = 1.28 V *rr* = 0.947
	1756	0.200	23.61	24.99	
	3186	0.295	34.83	36.86	
Toluene Exposure Test	386	0.070	8.13	8.59	Baseline = 1.04 V *rr* = 0.947
	2360	0.225	26.13	27.59	
	4291	0.320	37.78	39.98	

Table 4.6 Response of Au-NT 'active' devices

Using the simplified linear approximation to the Langmuir model in equation (3.17), this data can be fit to a linear equation

$$\Delta rr = JC + \Delta rr_0 \tag{4.10}$$

where, J is the equilibrium constant and Δrr_0 is the error at 0 ppm of adsorbate analyte. The results are plotted in figure 4.5 with values for the intercept and the gradient given in table 4.7. The differences in these results show the distinction the Au-NT film makes between the different VOCs based on the gradient of the graph J. The gradient values of propan-1-ol and toluene show a close correlation giving a similar response per unit concentration of analyte. These gradients being much higher than those of ethanol and methanol also reflect the difference in response rate between propan-1-ol, ethanol and methanol. This characteristic can be attributed to an increasing affinity of Au-NT

material for the alcohol molecule with increasing molecular weight and size of the molecule. The increasing *J* values from methanol to propan-1-ol confirm that a larger adsorbate molecule is likely to occupy more adsorbant sites on the chemoresistive film resulting in greater change of resistance per unit of analyte concentration.

VOC	Δrr_0 (x10^{-3})	J (ppm^{-1}) (x10^{-6})
Methanol	2.581	1.673
Ethanol	2.319	3.125
Propan-1-ol	7.241	8.803
Toluene	6.190	7.598

Table 4.7 *y* intercept and gradient values for Au-NT 'active' devices

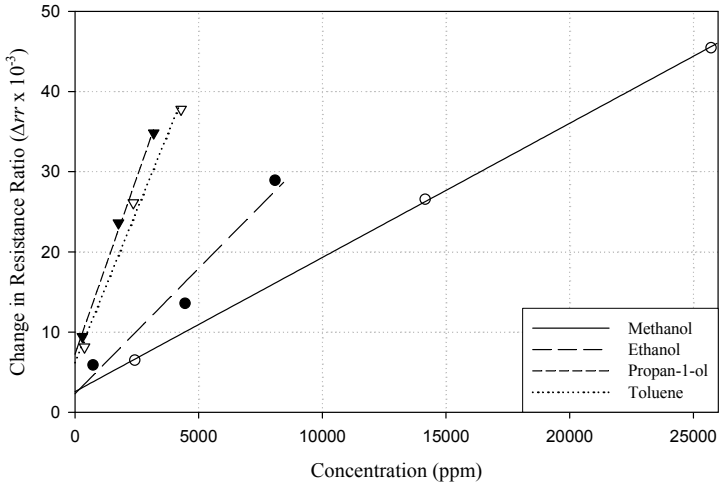

Figure 4.5 Linearly modelled results for 'active' sensor exposure tests for Au-NT device

Joseph et al. have shown results for Au-NT films exposed to water, ammonia and carbon monoxide have characteristics that match a Langmuir adsorption model (Joseph, Yvonne et al. 2004; Li, J & Werth 2002). Equation (4.11) was developed using the relation between resistance change and exposure concentrations shown in equation (3.16). A Langmuir fit plot using a one site saturation ligand binding model relating Δrr to the exposure concentrations (C in ppm) of the VOCs is shown in figure 4.6. The results show an increase in the resistance of the film as a result of exposure to the analytes. The responses measured for toluene and propan-1-ol were observed to be

considerably higher than those measured with methanol and ethanol for the same concentration levels. The isotherms show that toluene and propan-1-ol interact stronger with the film as compared to ethanol and methanol. The Langmuir relationship for these results is given by

$$\Delta rr = \frac{\alpha C}{K+C} \tag{4.11}$$

where α is a proportionality constant and K is ratio of the forward and backward reaction rate constants and C is the VOC concentration in ppm.

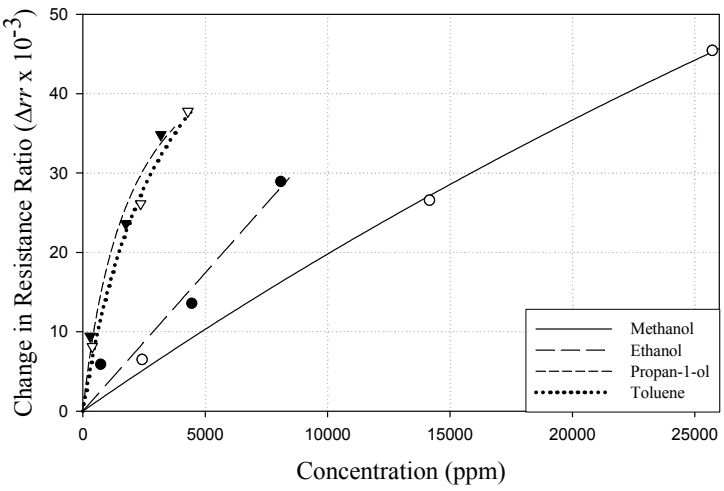

Figure 4.6 Langmuir modelled results for Δ*rr* against concentrations for 'active' Au-NT device

Table 4.8 lists the details of the relevant constants of the different analytes. With the stronger adsorption rate of toluene and propan-1-ol into the Au-NT film, the Langmuir model shows that these two analytes saturate the sensitive film at a much lower concentration than ethanol or methanol. As K is the ratio of backwards reaction rate constant to the forward reaction rate constant, the high K value of methanol and ethanol compared to the other two analytes also suggests that these analytes can more easily leave the surface of the chemoresistors and are adsorbed on the chemoresistive films through weak binding forces.

VOC	α (x10^{-3})	K (ppm) (x10^{3})
Methanol	249.35	115.973
Ethanol	11518543.893	3306614.554
Propan-1-ol	54.8211	1.992
Toluene	67.90	3.530

Table 4.8 Constants for a Langmuir adsorption model for Au-NT 'active' devices

4.3.2. Au-NT 'Passive' Sensor Tests

The tests mentioned for the 'active' sensors were repeated for the devices where only the 'passive' sensor was exposed to the analytes. These sensors were coated with a silicone gel layer, hence, the adsorption constants were expected to be modified. This silicone layer has a delaying effect on the response of the chemoresistors. The time taken to reach equilibrium at any given concentration was found to be much longer (between 1-3 minutes more) than before. The results for ΔV_{out}, Δrr and $\Delta R_{pas}/R_{pas}$ are tabulated in table 4.9.

Test Results for Au-NT Devices with Passive Sensor Exposure					
VOC	**Concentrations (ppm)**	**ΔV_{out} (V)**	**Δrr (x10^{-3})**	**$\Delta R_{pas}/R_{pas}$ (x10^{-3})**	
Methanol Exposure Test	2423	-0.10	-11.81	11.43	Baseline = 2.94 V rr = 1.045
	14163	-0.23	-27.15	26.68	
	25718	-0.305	-36.01	35.69	
Ethanol Exposure Test	728	-0.08	-9.44	9.12	Baseline = 2.94 V rr = 1.045
	4449	-0.19	-22.43	21.94	
	8089	-0.25	-29.52	29.07	
Propan-1-ol Exposure Test	301	-0.09	-10.63	10.27	Baseline = 2.93 V rr = 1.045
	1756	-0.19	-22.43	21.94	
	3186	-0.25	-29.52	29.07	
Toluene Exposure Test	386	-0.11	-12.99	12.62	Baseline = 2.92 V rr = 1.042
	2360	-0.27	-31.88	31.56	
	4291	-0.34	-40.14	40.07	

Table 4.9 Response of Au-NT 'Passive' Devices

The negative values of ΔV_{out}, Δrr are due to an increase in the resistance of the 'passive' resistors which represents the denominator resistance in the non-inverting amplifier circuit, resulting in a decrease in the output voltage. One of the observed effects of this silicone layer was that at lower concentrations (i.e. < 3000 ppm), the magnitude of the change in voltage output and the *rr* was higher than those of the uncoated 'active' sensor devices. Hence, it is safe to say that at lower concentrations, with the delayed response of the chemoresistors, the silicone coating has an amplifying effect on the final equilibrium values of ΔV_{out} and Δrr.

The absolute values of the data ($|\Delta rr|$) when fit into a Freundlich adsorption model (Li, J & Werth 2002; McCash 2001) are represented in figure 4.7 and the constants given in table 4.10. Equation (4.12) gives a modified form of the Freundlich isotherm in equation (3.21).

$$\Delta rr = F_k C^n \tag{4.12}$$

Here, C is the analyte concentration and F_k and n are constants calculated in table 4.10.

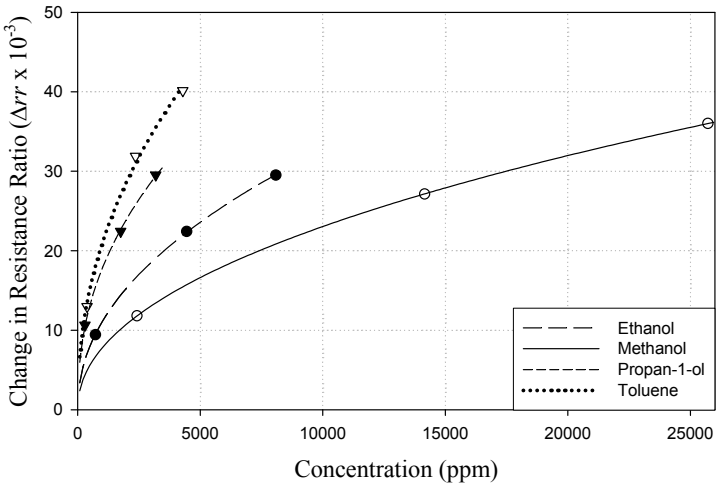

Figure 4.7 Freundlich modelled results for Δ*rr* against concentrations for 'passive' Au-NT device

From the constant F_k it can be seen that the increase in adsorbance between methanol and ethanol is nearly two-fold, which increases a further two-fold between ethanol and propan-1ol. This follows the same convention as the 'active' resistance uncoated Au-NT chemoresistor. An increase in the value of F_k suggests that the larger

molecule VOCs have the effect of a larger coverage of sensor surface per unit concentration of the VOC. The values of *n* which gives the rate of increase of change of resistance with increasing concentration are nearly the same for all the analytes.

VOC	F_k (ppm^{-n}) (x10^{-4})	n (x10^{-1})
Methanol	2.978	4.722
Ethanol	4.251	4.715
Propan-1-ol	8.720	4.361
Toluene	8.876	4.573

Table 4.10 Constants for the Freundlich adsorption model for Au-NT 'passive' devices

Plotting the same data with the Langmuir model (equation 4.11) gives the plot in figure 4.8. In case of both, the Freundlich and the Langmuir models, Δrr is assumed to be directly proportional to the weight adsorbed per unit weight of the adsorbent.

The Langmuir model shows a convergence of all VOC responses at a Δrr value of around 0.04 for the Au-NT passive devices. Comparing this with the active device responses it can observed that at higher concentrations, the passive device results converge to the active device results. However, at lower concentrations, the passive device results are approximately 60% higher for ethanol and methanol, but fairly similar for propan-1-ol and toluene. The delay in the response time to the VOCs suggests that the silicone film causes a slower adsorption of the analytes by acting as an obstacle between the chemoresistive film and the VOC vapours. This slows down the response of the chemical film but allows the vapour to build up on the silicone layer. This results in a higher response for ethanol, methanol and toluene at lower concentrations. As the concentrations are increased a high accumulation of the analyte in this coating causes it to saturate and the response of the device with the silicone coating begins to match that of the active sensor without the silicone film.

VOC	α (x10^{-2})	K (ppm) (x10^{3})
Methanol	4.565	8.058
Ethanol	3.730	2.482
Propan-1-ol	3.543	0.8061
Toluene	5.031	1.211

Table 4.11 Constants for the Langmuir model Au-NT 'passive' devices

The Langmuir constants in table 4.11 follow the trend shown by the active sensor devices. The values of K were significantly lower than the active devices for ethanol and methanol suggesting a substantial increase in the binding forces for these analytes. K for propan-1-ol is nearly the same for the active and silicone coated passive devices, whereas for toluene its reduced by almost 60%. This explains the higher response at lower concentrations with the silicone covering. The values for α decreased significantly for methanol and ethanol and came quite close to the values for propan-1-ol and toluene. Thus, the rate with respect to concentration with which the maximum concentration is reached was observed to be similar for all the analytes.

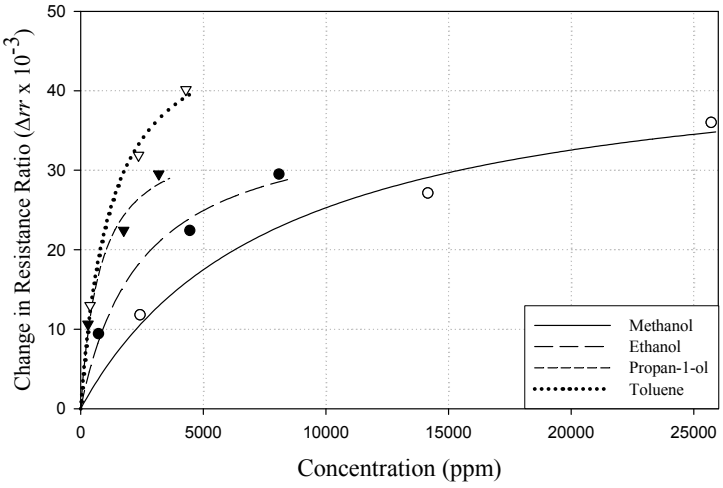

Figure 4.8 Langmuir modelled results for Δ*rr* against concentrations for 'passive' Au-NT device

4.3.3. Au-HDT 'Active' Sensor Tests

Table 4.12 shows the response characteristics of the active sensor based on the Au-HDT sensor resistor. The Au-HDT chemical films mainly differ from the Au-NT films in their chain length. The HDT polymer has a carbon chain length of 16 whereas

the NT polymer has a carbon chain length of 9. Vossmeyer et al. have shown the Au-HDT material to have a much higher response to toluene vapours than the Au-NT materials (Joseph et al. 2003). This is evident from the high gradient of the linear and Langmuir regression plots in figures 4.9 and 4.10.

Test Results for Au-HDT Devices with Active Sensor Variation					
VOC	**Concentrations (ppm)**	**ΔV_{out} (V)**	**Δrr ($x10^{-3}$)**	**$\Delta R_{act}/R_{act}$ ($x10^{-3}$)**	
Methanol Exposure Test	2423	0.03	3.54	3.35	Baseline = 1.38 V *rr* = 1.067
	14163	0.165	19.48	18.43	
	25718	0.285	33.65	31.83	
Ethanol Exposure Test	728	0.04	4.72	4.43	Baseline = 1.34 V *rr* = 1.057
	4449	0.12	14.17	13.28	
	8089	0.205	24.20	22.68	
Propan-1-ol Exposure Test	301	0.08	9.44	8.85	Baseline = 1.38 V *rr* = 1.067
	1756	0.20	23.61	22.13	
	3186	0.30	35.42	33.20	
Toluene Exposure Test	386	0.17	20.01	18.99	Baseline = 1.34 V *rr* = 1.057
	2360	0.55	64.94	61.43	
	4291	0.77	90.91	86.00	

Table 4.12 Response of Au-HDT 'Active' Devices

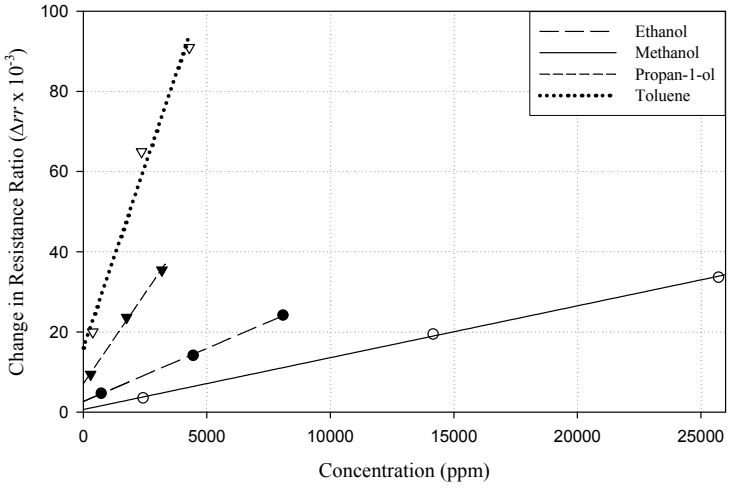

Figure 4.9 Linear model results for Δ*rr* against concentrations for active Au-HDT device

A clear distinction is observable between the results for toluene and propan-1-ol with the Au-HDT material. The increased chain length material shows a two to three

fold increment in the Δ*rr* response to toluene. The response to methanol is reduced by about 24%, and that of ethanol and propan-1-ol corresponds to those with the Au-NT material. The variation of the toluene and methanol responses shows an increase in the diversification of Δ*rr* output values by the chemoresistive film. For the Au-NT active sensor tests, the linear regression gradients of methanol, ethanol and propan-1-ol doubled between methanol and ethanol and then doubled again between ethanol and propan-1-ol. In case of the HDT active sensor tests, the gradient almost doubles between methanol and ethanol and then increases 3.5 times between ethanol and propan-1-ol. The gradient then doubles again between propan-1-ol and toluene. The high *J* value for toluene suggests much higher binding forces for the toluene vapours as compared with the other analytes. This gradient value can be used as a distinguishing factor between the different tested analyte vapours.

VOC	Δrr_0 (x10^{-3})	J (ppm^{-1}) (x10^{-6})
Methanol	0.3482	1.320
Ethanol	2.813	2.603
Propan-1-ol	6.709	9.248
Toluene	12.73	19.60

Table 4.13 *y* intercept and gradient values for Au-HDT 'active' devices

The Langmuir modelled plot in figure 4.10 shows the toluene vapours to have almost twice the response of closest other vapour, propan-1-ol. The respective coefficients for the plot are given in table 4.14.

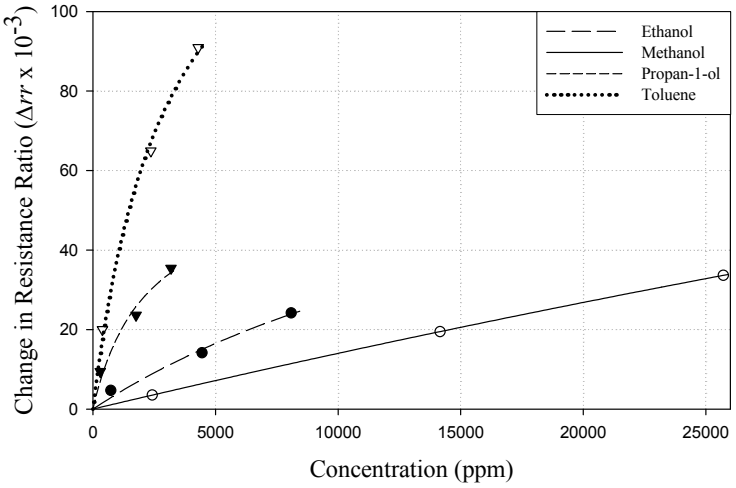

Figure 4.10 Langmuir modelled results for Δ*rr* against concentrations for active Au-HDT device

The decreasing value of the Langmuir coefficient *K* supports the observation made with the linear model of low surface binding forces for methanol and higher binding forces for the larger alcohol molecules and toluene. Comparing the constant values with those obtained from the Au-NT Langmuir isotherm fits there is nearly a 80% increase in the value of *K* for methanol suggesting a fall in the sensitivity of the film material to this analyte. The Langmuir constant *K* for the other analytes are almost the same for this film material. Other than methanol and toluene the other three analytes also show a stark fall in the α value which supports the observation of a high increase in response per unit concentration of the analytes.

VOC	α (x10^{-3})	*K* (ppm) (x10^{3})
Methanol	307.444	209.27
Ethanol	86.615	21.23
Propan-1-ol	58.115	2.208
Toluene	152.798	3.012

Table 4.14 Coefficient for a Langmuir adsorption model for Au-HDT 'active' devices

4.3.4. Au-HDT 'Passive' Sensor Tests

The response of the silicone coated passive device had no significant difference to the active device response results for toluene. This suggests that the silicone film is almost porous to the toluene vapour. This absence of any difference between the active

and passive results for toluene was also observed for the Au-NT devices. A significant impact on the ethanol results was noticed, where the response increased by as much as 300% at the lowest exposure concentrations and by about 30% at the higher concentrations. The Langmuir fit curves in figure 4.12 suggest that the Δ*rr* saturation value would still be lower than that of the active sensor devices.

Test Results for Au-HDT Devices with Passive Sensor Exposure					
VOC	**Concentrations (ppm)**	**ΔV_{out} (V)**	**Δrr ($x10^{-3}$)**	**$\Delta R_{pas}/R_{pas}$ ($x10^{-3}$)**	
Methanol Exposure Test	2423	-0.14	-16.53	17.092	Baseline = 2.96 *rr* = 0.9836
	14163	-0.19	-22.43	23.34	
	25718	-0.27	-31.88	33.49	
Ethanol Exposure Test	728	-0.13	-15.35	15.80	Baseline = 2.99 *rr* = 0.9868
	4449	-0.24	-28.34	29.56	
	8089	-0.3	-35.42	37.23	
Propan-1-ol Exposure Test	301	-0.135	-15.94	16.42	Baseline = 2.99 *rr* = 0.9868
	1756	-0.26	-30.70	32.11	
	3186	-0.33	-38.96	41.10	
Toluene Exposure Test	386	-0.17	-20.07	20.83	Baseline = 2.96 *rr* = 0.9836
	2360	-0.6	-70.84	77.61	
	4291	-0.83	-97.99	110.65	

Table 4.15 Response of Au-HDT 'Passive' Devices

The values given in table 4.15 show that methanol has a five-fold response increase at the lowest concentration. However, saturation was achieved quickly, and thus, at higher concentrations the regression output of the passive device nearly matched that of the active device. This suggests a high sorption rate for methanol into the silicone medium. But as the Au-HDT material forms weak bonds with the methanol molecules, once the sensor is near saturation, the |Δ*rr*| response does not change greatly. Propan-1-ol followed a similar response mechanism to methanol. The initial sorption at lower concentrations causes a greater change in *rr* than the active sensors. However, at higher concentrations, the response increase reduced to just 8% from an initial 77% increase from the active sensor values. The Freundlich and Langmuir plots with their relevant coefficients are given in plots figures 4.11 and 4.12 and tables 4.16 and 4.17 respectively. The response to toluene corresponded closely with that obtained for the unencapsulated active sensors.

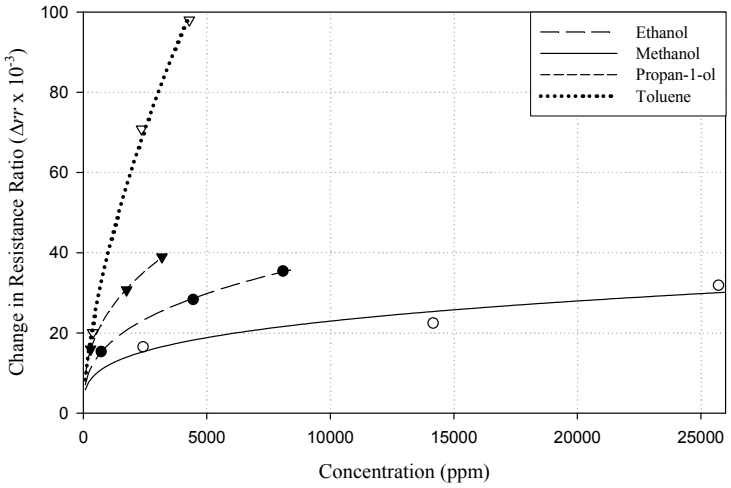

Figure 4.11 Freundlich modelled results for Δ*rr* against concentrations for passive Au-HDT device

The differences in the values of the Freundlich constant *n* show the separation between the analyte curves and the rate of increase of $|\Delta rr|$ with respect to increasing concentration, whereas the coefficient F_k represents the coverage of the adsorbate VOC molecules on the adsorbant chemoresistive sensor surface. The F_k coefficient values for the three alcohols are 5 times higher for methanol, 3 times higher for ethanol and almost twice for propan-1-ol when compared with the Au-NT silicone coated passive device results for the Freundlich fit. Toluene values for F_k were almost the same. A larger difference in the *n* values for the silicone coated passive Au-HDT material was observed. For the similar Au-NT device the *n* value was almost the same for all the analytes. With the Au-HDT material this value increased with the size of aanalyte molecule.

VOC	F_k (ppm^{-n}) (x10^{-3})	n (x10^{-1})
Methanol	1.656	2.854
Ethanol	1.528	3.488
Propan-1-ol	1.804	3.804
Toluene	0.5307	6.255

Table 4.16 Coefficients for the Freundlich adsorption model for Au-HDT 'passive' devices

When fit to the Langmuir model and compared with the Au-NT Langmuir constants, only toluene shows a significant difference (3 times the value) to the α values for Au-NT silicone coated passive devices suggesting a larger response rate for this analyte. As this value for toluene is almost the same as that for the uncoated active sensor device, this confirms the porosity of the silicone gel to toluene vapour.

The K values for propan-1-ol were 30% and for ethanol were 50% less than those for similar Au-NT devices, whereas for toluene this was 3 times higher. The value for methanol was observed to be almost the same as before. Comparing the values of this coefficient with the uncoated Au-HDT active sensor all the alcohols showed a significant reduction in the K values suggesting stronger binding forces for the alcohols with the silicone coating. The value for toluene was the same as that for the uncoated Au-HDT active device as expected.

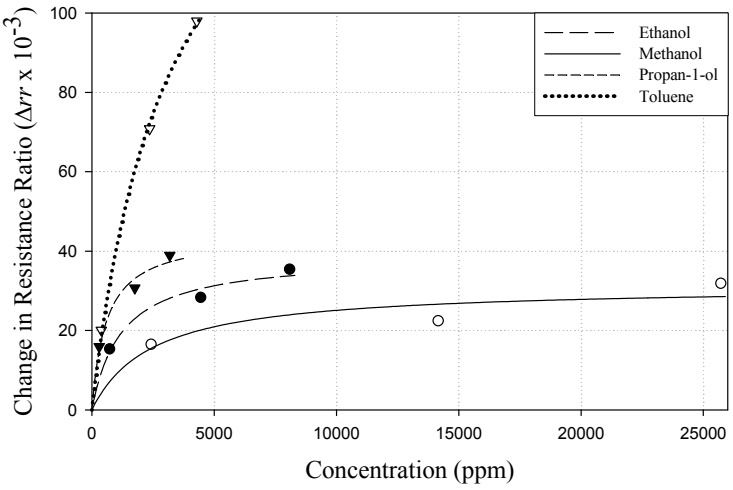

Figure 4.12 Langmuir modelled results for Δ*rr* against concentrations for passive Au-HDT device

VOC	α (x10^{-2})	K (ppm) (x10^{3})
Methanol	3.128	2.475
Ethanol	3.884	1.212
Propan-1-ol	4.412	0.5868
Toluene	16.92	3.169

Table 4.17 Coefficients for the Langmuir model for Au-HDT 'passive' devices

4.3.5. Au-MAH 'Active' Sensor Tests

Au-MAH is a polarised compound with an acetyl–amino–thiol (i.e. R–(NHCOSH)–) group at either end of the carbon chain of six carbons. The oxygen double bond makes the linker structure polarised and highly susceptible to form Van der Waals and hydrogen bonds with the alcohol and water molecules. Thus, it was expected from the response results of this material to have a large change in the resistance ratio (*rr*) for the three alcohols and water vapours, whereas the results for toluene should be similar to a response for a six chain carbon dithiol. Table 4.18 shows the response outputs for the Au-MAH active device.

Test Results for Au-MAH Devices with Active Sensor Variation					
VOC	**Concentrations (ppm)**	**ΔV_{out} (V)**	**Δrr ($x10^{-3}$)**	**$\Delta R_{act}/R_{act}$ ($x10^{-3}$)**	
Methanol Exposure Test	2423	0.1925	22.73	26.27	Baseline = 0.88 V *rr* = 0.865
	14163	0.605	71.43	8258	
	25718	0.9175	108.32	125.23	
Ethanol Exposure Test	728	0.208	23.56	28.39	Baseline = 0.88 V *rr* = 0.865
	4449	0.53	62.57	72.34	
	8089	0.73	86.19	99.38	
Propan-1-ol Exposure Test	301	0.23	27.16	35.18	Baseline = 2.04 V *rr* = 0.772
	1756	0.441	52.07	67.44	
	3186	0.591	69.78	90.39	
Toluene Exposure Test	386	0.06	7.08	9.18	Baseline = 2.04 V *rr* = 0.772
	2360	0.291	34.36	44.50	
	4291	0.426	50.30	65.15	

Table 4.18 Response of Au-MAH 'Active' Devices

Compared to the Au-NT device results, the table shows an increase of two to four times in the response to ethanol, 1.5-2.5 times rise in the response to methanol and nearly two fold rise in the response to propan-1-ol. The response to toluene at the highest concentrations went up by only 30%. However, at lower concentrations the toluene response was similar to that of the Au-NT device, as was expected. Figure 4.13 shows the linear regression of the analyte results. A distinct difference between this result and those obtained before for Au-NT and Au-HDT materials is the higher Δrr values obtained for propan-1-ol and ethanol compared with the response for the toluene vapour, which had so far given the highest response with the previous two materials.

The relationship between the size of the alcohol molecule and the strength of the Δ*rr* response still exists as propan-1ol causes the greatest change in the Δ*rr* values followed by ethanol and then methanol.

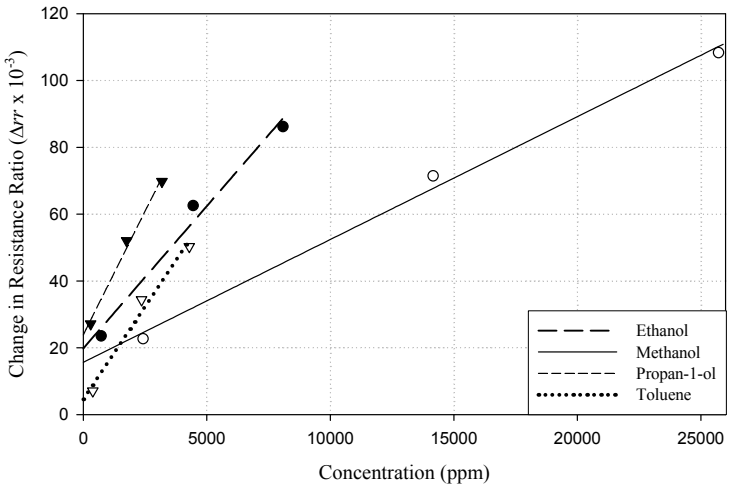

Figure 4.13 Linear model results for Δ*rr* against concentrations for active Au-MAH device

The values for the gradients and the y intercepts (Δrr_0) for the linear regression are given in table 4.19. The separation between the three alcohols can be observed from the difference in gradients *J*. As expected the gradient for the three alcohols is two to three times steeper than that observed for the Au-NT and Au-HDT materials. This steeper gradient is evidence of the MAH linker materials increase in surface binding forces for the polar alcohols. The increase in vapour binding forces increases with the polarity and size of the analyte molecules, allowing more of them to occupy a vacant site on the chemoresistive sensor's surface per unit concentration.

VOC	Δrr_0 (x10^{-3})	J (ppm^{-1}) (x10^{-3})
Methanol	15.665	3.675
Ethanol	19.784	8.516
Propan-1-ol	23.840	14.78
Toluene	4.595	11.08

Table 4.19 *y* intercept and gradient values for Au-MAH 'active' devices

The Langmuir model fitted plot is shown in figure 4.14. For the Au-NT and Au-HDT films the expected saturation Δ*rr* value for the three alcohols was around 0.04.

However, for the Au-MAH material this is observed to have increased to between 0.08 and 0.10. This is a direct consequence of the increase in the binding forces between the polar acetyl-amino group and the alcohols as discussed for the linear model. Furthermore, it can be seen from the plot that propan-1-ol, due to its larger molecule interacts more with the polymer film and achieves saturation more rapidly. As expected, propan-1-ol response is followed by ethanol and methanol in the given order. Compared withteh Au-NT material, the *K* value for the alcohols is 3 to 4 times less, whereas for toluene it is 1.5 times higher. This means that more of the alcohol vapours can bind to the surface of the sensor films and a higher forward reaction rate constant and viceversa for the toluene vapours. The toluene *K* value compared to the Au-HDT device is also 1.5 times higher for the same reason.

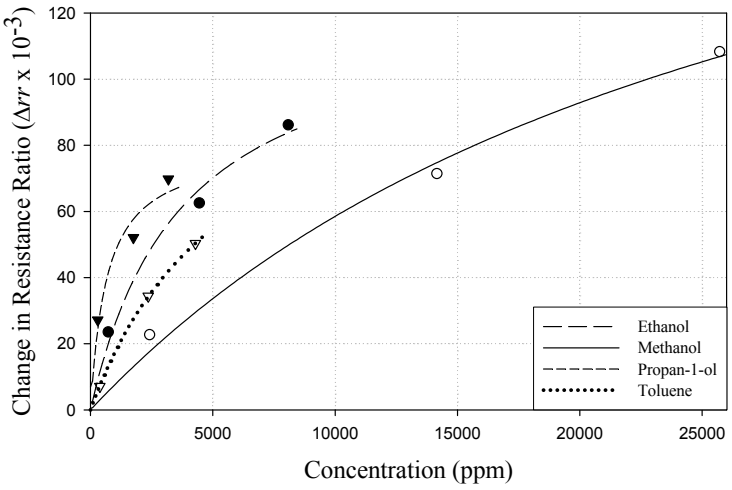

Figure 4.14 Langmuir model results for Δ*rr* against concentrations for active Au-MAH device

VOC	α (x10^{-1})	***K* (ppm)** (x10^{3})
Methanol	2.252	28.49
Ethanol	1.228	3.757
Propan-1-ol	0.7991	0.6787
Toluene	1.193	5.871

Table 4.20 Coefficient for a Langmuir adsorption model for Au-MAH 'active' devices

4.3.6. Au-MAH 'Passive' Sensor Tests

Table 4.21 shows the response of the silicone coated passive Au-MAH sensor to the various analytes. The response to ethanol, propan-1-ol, and toluene of the silicone coated passive sensors is much the same as the uncoated active sensor. A 70% increase at lower concentrations (i.e. < 3000ppm) reducing to a 7% increase in response at higher concentration (i.e. > 10000 ppm) of methanol vapours is observed. It must be noted even though the change in *rr* of the active and passive devices is fairly similar for ethanol, propan-1-ol and toluene, this Δ*rr* response is achieved by a smaller percentage change in the resistance of the exposed resistor.

Test Results for Au-MAH Devices with Passive Sensor Exposure					
VOC	**Concentrations (ppm)**	**ΔV_{out} (V)**	**Δrr ($x10^{-3}$)**	**$\Delta R_{pas}/R_{pas}$ ($x10^{-3}$)**	
Methanol Exposure Test	2423	-0.33	-38.96	39.35	Baseline = 2.79 V *rr* = 1.029
	14163	-0.73	-86.19	91.41	
	25718	-0.99	-116.88	128.14	
Ethanol Exposure Test	728	-0.23	-27.16	27.10	Baseline = 2.79 V *rr* = 1.029
	4449	-0.53	-62.57	64.75	
	8089	-0.72	-85.01	90.05	
Propan-1-ol Exposure Test	301	-0.19	-22.43	22.22	Baseline = 2.14 V *rr* = 1.032
	1756	-0.47	-55.49	56.82	
	3186	-0.65	-76.74	80.34	
Toluene Exposure Test	386	-0.06	-7.08	6.91	Baseline = 2.14 V *rr* = 1.032
	2360	-0.32	-37.78	38.00	
	4291	-0.43	-50.77	51.74	

Table 4.21 Response of Au-MAH 'Passive' Devices

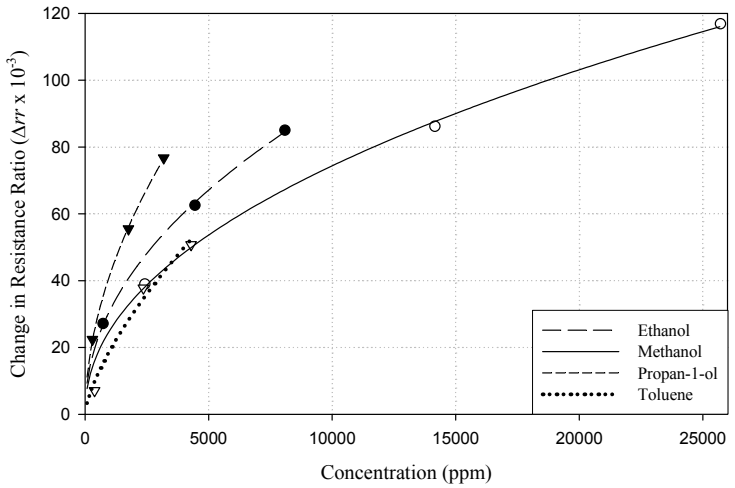

Figure 4.15 Freundlich modelled results for Δ*rr* against concentrations for passive Au-MAH device

Figure 4.15 shows the Freundlich model fitted plot of the Au-MAH passive sensor with the respective co-efficients given in table 4.22. The main advantage of using the silicone-coating with the Au-MAH material was observed to be the improved response to methanol while maintaining the distinction between the three alcohols. The *n* values of all the analytes was almost the same as those for the Au-NT material, suggesting that the rate of increase in the resistive response with increasing concentration is quite similar to the silicone coated passive Au-NT material. The F_k values of the silicone coated passive Au-MAH material were 3 times higher for methanol, 2.5 time higher for ethanol, 1.2 times higher for propan-1-ol and 5.5 times lower for toluene than those for the silicone coated passive Au-NT material. This suggests an improvement in the coverage per unit concentration with the alcohols and a reduction for toluene. The response to toluene, as with the Au-NT and Au-HDT material, is unaffected by the silicone gel coating compared with the uncoated active material. The silicone causes a delay in the transient response of the sensors as the analytes are absorbed into the gel barrier and reach the chemoresistive sensor film.

VOC	F_k (ppm^{-n}) (x10^{-3})	n (x10^{-1})
Methanol	0.9688	4.713
Ethanol	1.130	4.795
Propan-1-ol	1.104	5.254
Toluene	0.1586	6.933

Table 4.22 Coefficients for the Freundlich adsorption model for Au-MAH 'passive' devices

Figure 4.16 and table 4.23 show the Langmuir fit to the plot and the relevant constants of the fit respectively. The fit shows a close correlation between the methanol and toluene plots. However, taking note of the *K* values it can be noted that the value for methanol is twice that for toluene suggesting a weaker surface binding force. The value for methanol is less than a third than that for the uncoated active device, almost the same for ethanol, double for propan-1-ol and as expected almost the same for toluene. This means that the silicone layer increased the binding forces for the smaller alcohol molecule, while reducing the binding forces for the larger alcohol molecule. The effect of the silicone coating on the Au-HDT material was observed to be consistent with the results obtained for the previously discussed two materials showing little effect on the adsorption properties apart from a slight time delay in reaching the equilibrium value.

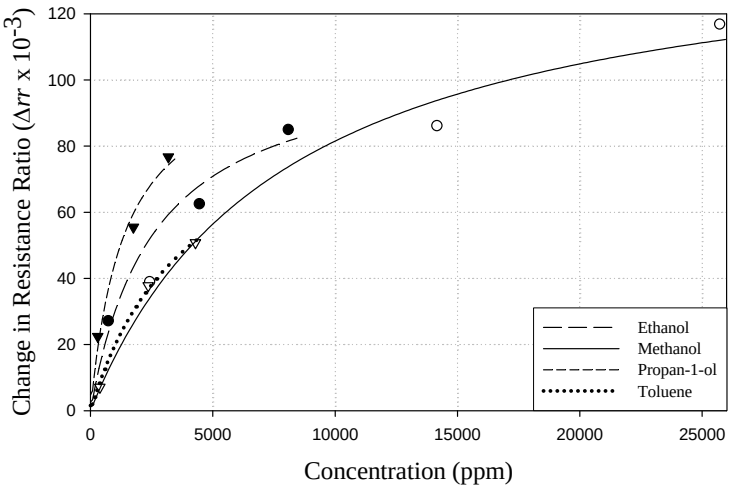

Figure 4.16 Langmuir modelled results for Δ*rr* against concentrations for passive Au-MAH device

VOC	α (x10^{-1})	K (ppm) (x10^{3})
Methanol	1.470	8.029
Ethanol	1.079	2.615
Propan-1-ol	1.067	1.390
Toluene	0.9982	4.061

Table 4.23 Constants for the Langmuir active model for Au-MAH 'passive' devices

4.4. Tests at 38% Relative Humidity (rh)

Tests with toluene and propan-1-ol were carried out at 38% rh to estimate the level of competition for vacant adsorption sites on two of the chemoresistive materials (Au-HDT and Au-MAH). The test concentrations were kept the same as for tests at 0-2% rh. The Au-HDT and Au-MAH devices were chosen to see differences in the effects of humidity between a non-polar and a polar sensor respectively.

4.4.1. Active Sensor Exposure Test at 38% rh for Au-HDT

Test Results for Au-HDT Devices with Active Sensor Exposure at 38% rh						
VOC	Concentrations (ppm)	ΔV_{out} (V)	Δrr (x10^{-3})	$\Delta R_{act}/R_{act}$ (x10^{-3})	α (x10^{-2})	K (ppm) (x10^{3})
Propan-1-ol Exposure Test	301	0.08	9.44	08.09	2.563	0.5403
	1756	0.16	18.89	16.19		
	3186	0.19	22.43	19.22		
Toluene Exposure Test	386	0.05	5.90	5.06	20.86	12.35
	2360	0.28	33.65	28.83		
	4291	0.46	53.72	46.03		

Table 4.24 Langmuir response of 'active' Au-HDT sensor at 38% rh

The results for Au-HDT tests show a 36% reduction in response to propan-1-ol and an approximate 50% reduction in response to toluene at higher humidity (table 4.24 and figure 4.17). This reduction is created by the water vapours occupying sorption sites on the chemoresistive film making it difficult for the VOCs to interact with the films. As the films are non-polar the sorption of the water vapour does not have any

significant affects on the resistance on the film, and simply acts as a barrier layer between the VOC vapour and the chemoresistive film.

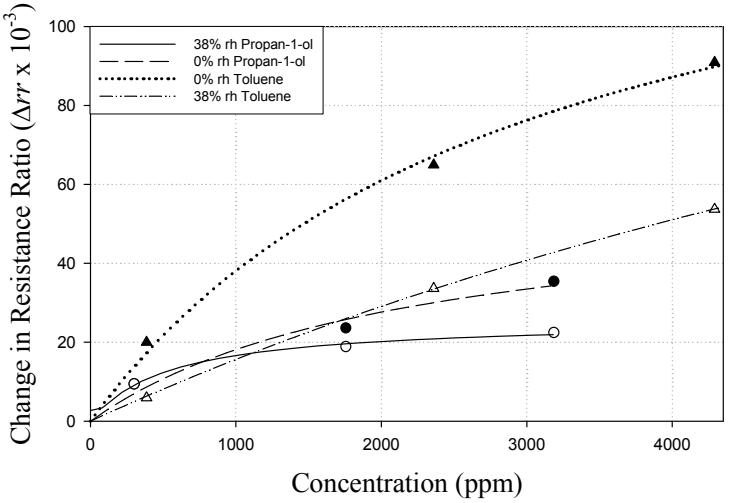

Figure 4.17 Langmuir modelled results for Δ*rr* against concentrations for active Au-HDT device (0% rh response comparison with 38% rh)

4.4.2. Passive Sensor Exposure Test at 38% rh for Au-HDT

A comparison of the results for 'passive' silicone coated sensors shows a close match between the results at 0% rh and at 38% rh (figure 4.18). Table 4.25 shows the values of ΔV_{out} Δrr and $\Delta R_{pas}/R_{pas}$ for these tests.

Test Results for Au-HDT Devices with Passive Sensor Exposure at 38% rh						
VOC	**Concentrations (ppm)**	**ΔV_{out} (V)**	**Δrr (x10^{-3})**	**$\Delta R_{pas}/R_{pas}$ (x10^{-3})**	**α (x10^{-2})**	**K (ppm) (x10^{3})**
Propan-1-ol Exposure Test	301	-0.05	-12.99	6.69	4.226	0.7540
	1756	-0.485	-27.74	68.96		
	3186	-0.73	-35.42	107.54		
Toluene Exposure Test	386	-0.05	-5.90	6.70	29.86	10.44
	2360	-0.48	-57.26	68.96		
	4291	-0.73	-86.19	107.54		

Table 4.25 Langmuir response of 'passive' Au-HDT sensor at 38% rh

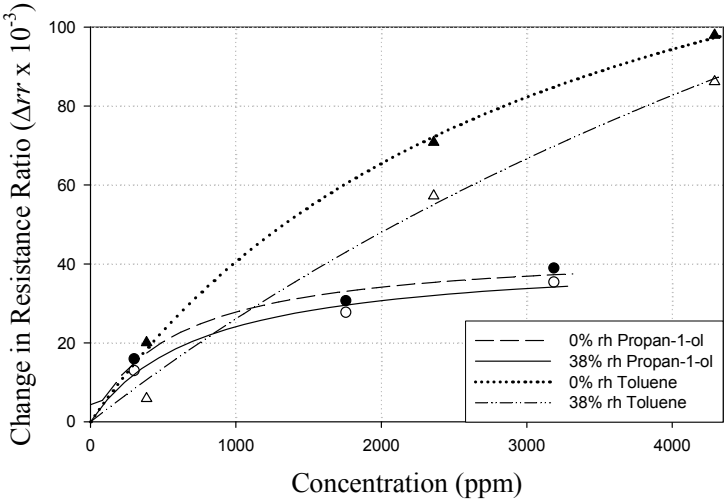

Figure 4.18 Langmuir modelled results for Δ*rr* against concentrations for passive Au-HDT device (rh response comparison)

As reported for the passive sensor results for the Au-NT and Au-HDT devices at 0% rh, the silicone coating is almost porous to the toluene vapours. However, the coating acts a sealant for water. Due to the high affinity of toluene for the chemoresistive film, it gets adsorbed onto the chemoresistive film without any competition from water molecules. As a result the Δ*rr* response nearly matches the response at 0-2% rh.

Examining a comparison between the propan-1-ol tests for passive Au-HDT device at 0% rh and 38% rh it can be seen from figure 4.18 that the outputs at the two humidities are almost similar. This follows the same logic as the toluene test. Once the water molecules are blocked by the silicone film, the device is able to respond to the analyte at the same levels as it would at 0% rh. The other alcohols are expected to respond in a similar fashion to propan-1-ol with decreasing affinity as the alcohol molecule size decreases.

4.4.3. Active Sensor Exposure Test at 38% rh for Au-MAH

Table 4.26 lists the outputs for toluene and propan-1-ol exposure results to the Au-MAH test device. The results show a high level of competition for sorption sites between the water molecules and propan-1-ol and toluene molecules leading to a decrease of 275% for propan-1-ol and 250% for toluene. This is due to the high polar

nature of the MAH linker chain which forms a strong bond with the hydroxyl group in the water molecule.

Test Results for Au-MAH Devices with Active Sensor Exposure at 38% rh						
VOC	**Concentrations (ppm)**	**ΔV_{out} (V)**	**Δrr (x10^{-3})**	**$\Delta R_{pas}/R_{pas}$ (x10^{-3})**	**α (x10^{-2})**	**K (ppm) (x10^{3})**
Propan-1-ol Exposure Test	301	0.1	11.81	12.10	2.300	0.3095
	1756	0.15	17.71	18.16		
	3186	0.19	22.43	23.00		
Toluene Exposure Test	386	0.04	4.72	4.84	1.518	1.217
	2360	0.07	8.26	8.47		
	4291	0.11	12.99	13.32		

Table 4.26 Response of Au-MAH at 38% rh and Langmuir constants

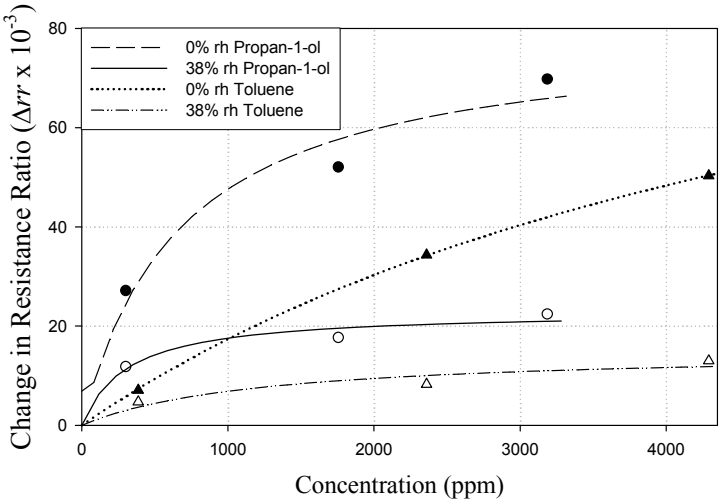

Figure 4.19 Langmuir modelled results for Δrr against concentrations for active Au-MAH device (rh response comparison)

4.4.4. Passive Sensor Exposure Test at 38% rh for Au-MAH

The results for the propan-1-ol exposure of the silicone coated passive Au-MAH device (section 4.3.6) confirms the slightly higher output with the silicone coating. However, contrary to expectation a 50-70% reduction in the Δrr response is observed while operating at 38% rh. A significant reason for this result could be the strong affinity of the polar MAH attracting the water molecule strongly enough to form a film of water on top of the silicone coating, and thus increasing the distance and reducing the possibility of a vacant site occupancy by the analytes on the chemoresistive

films *K* values confirm this as for propan-1-ol it is an order of a magnitude higher than that without the silicone coating and for toluene it is five times higher suggesting weaker binding forces between the analyte and the chemoresistive sensor.

Test Results for Au-MAH Devices with Passive Sensor Exposure at 38% rh						
VOC	**Concentrations (ppm)**	**ΔV_{out} (V)**	**Δrr (x10^{-3})**	**$\Delta R_{pas}/R_{pas}$ (x10^{-3})**	**α (x10^{-2})**	**K (ppm) (x10^{3})**
Propan-1-ol Exposure Test	301	-0.025	-2.95	3.50	5.614	3.429
	1756	-0.17	-20.07	22.85		
	3186	-0.225	-26.56	30.46		
Toluene Exposure Test	386	-0.03	-3.54	3.96	3.649	4.372
	2360	-0.115	-13.58	15.34		
	4291	-0.15	-17.71	20.10		

Table 4.27 Response of Au-MAH at 38% rh and Langmuir Constants

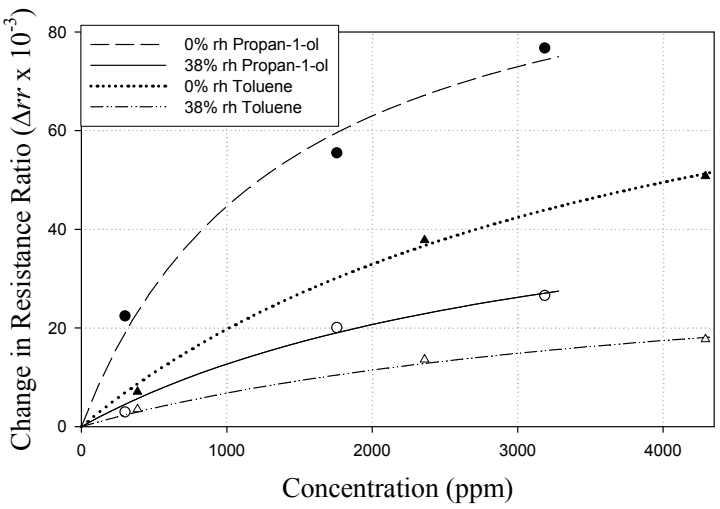

Figure 4.20 Langmuir modelled results for Δrr against concentrations for passive Au-MAH device (rh response comparison)

4.5. Effects of Chamber Temperature Variation on the Baseline Voltage

The circuit resistance of the ASIC and the data acquisition setup is related to the temperature of the circuit. To check the effects of temperature movements, the ASICs were connected to external resistors. This makes the changes to the chemoresistive materials irrelevant. However, ASIC devices made with two separate

resistive materials were chosen in order to look for consistency amongst the result and use one as a reference against the other. Increasing the chamber temperature from 26°C to 55°C showed an equivalent linear decline in the output voltage, and a linear increase in the offset voltage (figure 4.21). The reference voltage and sensor voltage were measured as well and were observed to be constant. The gradient of the decline of V_{out} is -0.025/°C. From relationship between V_{out} and V_{offset} given in equation (3.1) it can be seen that a rise in the offset voltage is directly responsible for a decline of the output voltage.

The temperature increase results in the resistance of the internal resistor of the offset circuit (R_{int}) to increase as given by equation (4.13).

$$\frac{\Delta R_{internal}}{\Delta T} = \frac{R_{offset}}{V_{ref}} (\Delta V_{offset}) \tag{4.13}$$

This gives a constant of 0.1016 kΩ/°C.

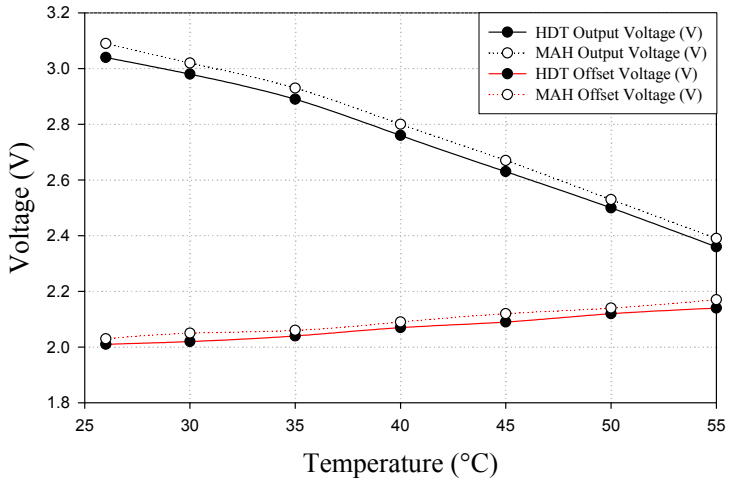

Figure 4.21 Relationship between output voltage and offset voltage with increasing temperature

4.6. Conclusions

This chapter identified the saturation limits of the ratiometric ASIC chip. These limits were measured to be roughly between 0.5 as the lower limit and 2.0 as the upper limit within a 10% error. For ideal operation, when choosing chemoresistor devices the ratio of their resistances must lie between these bounds with some room to be allowed for changes in *rr* from analyte vapour exposures. The ASIC was initially designed to operate with 10 kΩ active and passive resistors. However, it was shown that the ASIC operated at over 1 MΩ resistance as well, albeit with a slight deterioration of the signal at high *rr*. Using external resistors, the internal resistance of the offset circuit was calculated to be around 16 kΩ with a 5% error margin.

The Au-NT (with a nine carbon chain length), Au-HDT (with a sixteen carbon chain length) and Au-MAH (six carbon chain length with an acetyl-amino-thiol group at each end) chemoresistive sensors were individually characterized against four different analytes (ethanol, methanol, propan-1-ol and toluene) to increasing concentrations at 0-2% rh in this chapter. The change in the resistance ratio (Δrr) was taken as the response measure proportional to the analyte vapour concentration.

The tests with the Au-NT material based devices showed a higher adsorption of the propan-1-ol and toluene vapours than ethanol and methanol and a good return to baseline value. When used in the 'active' sensor setup and the response fit to a Langmuir adsorption model, the device shows a nearly overlapping output for the propan-1-ol and toluene vapours. However, the devices showed a good response rate and response diversification between ethanol, methanol and propan-1-ol responses.

For tests with silicone coated 'passive' Au-NT sensors a delay in the response to analytes was observed. This delay allowed for a greater separation of the responses at lower concentrations (i.e. < 3000 ppm), where the response differences were 33% between toluene and propan-1-ol, 36% between propan-1-ol and ethanol and 46% between ethanol and methanol. Here, toluene had the highest response output and methanol the lowest. A higher $|\Delta rr|$ value was observed at low concentrations, as compared to the active devices. However, this effect was reversed at high VOC concentrations where the response differences were almost eliminated.

Au-HDT devices were tested against the same criteria as the Au-NT devices to observe the effects of a longer chain length on the response output. This chemoresistive material had a high affinity for toluene with the response value being twice that for Au-

NT. The response to propan-1-ol and ethanol did not prove to be too different from the Au-NT values. The response to methanol was about 30% lower in the Au-HDT case. Thus, the previous issue in Au-NT of lack of separation between toluene and propan-1-ol responses, and the ethanol and methanol responses was eliminated by use of a longer chain length of the same monomer.

The Au-HDT passive results showed a similar characteristic to the Au-NT results in terms of the output saturation for ethanol, methanol and propan-1-ol. However, at concentrations less than 5000 ppm the device still gave significant separation between the three analytes. The ethanol result was 50% higher than the methanol response, and the propan-1-ol was 30% higher than the ethanol. Toluene response was 2.5 times the propan-1-ol response and could easily be distinguished from the other three analytes. A comparison with the Au-NT passive results showed a similar characteristic as the active responses of the two film materials. A comparison with the active device of the Au-HDT material showed a 10% higher response for toluene, a 50% higher response for ethanol and a 100% higher response for methanol. The silicone-coated passive devices were a better fit to the Langmuir curve than the uncoated active devices.

The Au-MAH chain structure was a polar monomer and it was expected to show a higher affinity for the alcohols as compared to the previous two non-polar linker structures. In the active configuration at concentrations less than 5000 ppm the ethanol and propan-1-ol responses were equivalent to each other, both being 25% higher than the response to toluene and 1.3 times the methanol response.

The passive Au-MAH device showed no significant increase to the response to ethanol or toluene compared to the active device, however, a 20% increase for propan-1-ol and a 50% increase on methanol was achieved.

The Au-HDT and Au-MAH materials were also tested against dependence on water vapour. Tests were run for toluene and propan-1-ol. The Au-HDT device showed a 60% drop in the response value for toluene and 50% drop for propan-1-ol when tested at 38% rh. This drop was eliminated when the devices were tested in the passive configuration due to the sealing effect of the silicone coating.

The Au-MAH sensor was expected to be more significantly affected by the presence of the water vapour in the vapour mixture due to the polar component in the linker chain. The response to toluene and propan-1-ol reduced nearly 3.5 times at 38% rh and 3000 ppm analyte concentration. In the passive sensor tests for the same material,

this drop was not as large as for the active devices. However, the silicone did not prove to be a sufficient sealant for this material and the 38% rh results were still 2.5 times lower than the results at 0-2% rh.

The stability of the electronics was tested by increasing the exposure chamber temperature form 26°C to 55°C. The results showed an increase in the resistance by 0.1016 kΩ/°C of the ASICs internal offset resistor.

The devices based on all three different materials in both the configurations provided with a good signal output with very little switching noise with data sampled at 1 Hz frequency, and a good return to baseline characteristic.

The following chapter discusses the characterization of a variation of monotype ratiometric devices which were assembled using two chemoresistors of the same material. The chemoresistors positioned in the passive resistor position were encapsulated in silicone sealant gel. These passive chemoresistors also respond to the VOC test vapours as discussed with the passive device tests in this chapter. This second type of monotype devices may be referred to as monotype bi-variate devices as both the active and passive chemoresistors change their resistances when exposed to the VOC vapours.

4.7. References

Dean, JA 1999, *Lange's Handbook of Chemistry*, McGraw-Hill.

García-Guzmán, J 2005, 'Smart ratiometric ASIC chip for VOC monitoring', University of Warwick.

Grate, JW & Abraham, MH 1991, 'Solubility interactions and the design of chemically selective sorbent coatings for chemical sensors and arrays', *Sensors and Actuators B: Chemical*, vol. 3, no. 2, pp. 85-111.

Joseph, Y, Besnard, I, Rosenberger, M, Guse, B, Nothofer, HG, Wessels, JM, Wild, U, Knop-Gericke, A, Su, DS, Schlogl, R, Yasuda, A & Vossmeyer, T 2003, 'Self-assembled gold nanoparticle/alkanedithiol films: Preparation, electron microscopy, XPS-analysis, charge transport, and vapor-sensing properties', *Journal of Physical Chemistry B*, vol. 107, no. 30, pp. 7406-13.

Joseph, Y, Guse, B, Yasuda, A & Vossmeyer, T 2004, 'Chemiresistor coatings from Pt- and Au-nanoparticle/nonanedithiol films: sensitivity to gases and solvent vapors', *Sensors and Actuators B: Chemical*, vol. 98, no. 2-3, pp. 188-95.

Li, J & Werth, CJ 2002, 'Modeling sorption isotherms of volatile organic chemical mixtures in model and natural solids', *Environmental Toxicology and Chemistry*, vol. 21, no. 7, pp. 1377-83.

McCash, EM 2001, *Surface Chemistry*, 1st edition edn, Oxford University Press, USA.

Yi-Ming Sun, JC 1994, 'Sorption/desorption properties of ethanol, toluene, and xylene in poly(dimethylsiloxane) membranes', *Journal of Applied Polymer Science*, vol. 51, no. 10, pp. 1797-804.

CHAPTER 5

5. Characterization of Mono-type Ratiometric Devices

5.1. Introduction

In chapter 4, chemoresistive sensors were characterized individually, while being ratiometrically paired up with a reference resistor. The characterization was carried out with the unencapsulated chemoresistor exposed to VOCs in the active specification, with a fixed resistor as the passive resistor. Tests were also carried out with the positions of the chemoresistor and the reference resistor reversed and the chemoresistor coated with a silicone gel (Dow Corning 3145 RTV MIL-A-46146). The paired resistors formed the ratiometric feedback loop of the non-inverting amplifier setup of the Warwick ASIC (SRL 194).

In this chapter, *two* identical chemoresistive sensors were paired up ratiometrically and connected to the SRL 194 ASIC device. Both chemoresistive sensors used to make one device were based on the same chemoresistive film, where the

active sensor was exposed directly to the VOC vapours and the passive sensor was exposed to the VOCs while being coated with the silicone sealant gel. Three different chemoresistive materials based on Au-nanoparticle alkylenedithiol linker structures, as discussed in chapter 3, were tested in this chapter. The exposure of the active as well as the passive sensor takes place simultaneously and the results obtained from the data acquisition setup were the resulting voltage output of the SRL 194 device dependent on the simultaneous shifts in the resistance ratio due to changes in the resistances of the active and passive chemoresistors.

In the mono-type ratiometric setup, both sensors were subjected to the same vapour and environmental conditions which allowed them to age equally. As it was always the ratio of the two sensors that accounted for the voltage output all ageing and drift effects were expected to be cancelled out giving the net output purely as a result of the resistance ratio changes (Δrr) from VOC exposure.

The behaviour of the individual silicone coated passive sensor, paired with a static resistor was shown in chapter 4. Despite this sealant coating, the resistance of the passive sensor responded to the presence of analyte vapours. It was observed that the silicone gel increases the time it takes for the VOC vapours to reach the chemoresistive film. This behaviour prevented absolute cancellation of the resistance changes of the two chemoresistive sensors. Usually the relative percentage increase in the 'passive' resistance was observed to be greater than the percentage increase in 'active' resistance at exposure concentrations less than 5000 ppm. This suggests that the non-reactive silicone film also responds dynamically through various sorption effects of the VOCs. These sorption effects are expected to modify the transient response of the chemoresistor film. However, the transient response can be ignored for the case of this study as the change in the resistance ratio (Δrr) of the active and passive chemosensors is measured at the τ_{90} equilibrium value (i.e. at 90% of the exposure duration) of a particular exposure concentration.

As the change in the resistance ratio was a combination of the simultaneous changes in the 'active' as well as the 'passive' chemoresistive sensors, the cancellation of effects due to ageing was achieved at the cost of a lower magnitude of voltage output and Δrr value. The relationship between the test device's resistance ratio change and change in voltage output is given in equation 4.7. As in the case of chapter 4, all calculations are based on the magnitude of voltage output or resistance ratio changes

(Δrr). Thus, the negative sign representing a reduction in voltage output due to a reduction in the value of *rr* is usually ignored and the $|\Delta rr|$ value taken.

5.2. Stability and Drift Tests

Before the devices could be tested against analyte vapours, they were tested for drift due to application of a DC voltage over several hours (e.g. a field-effect). The tests were carried out at ~3% rh and ~38% rh at which the devices were only exposed to the carrier gas. In both cases the FIA tests station was kept at the respective relative humidity level for over 12 hours before the tests were carried out, allowing the test station fixtures to adjust and stabilise at the relevant humidity level. The test devices were kept at 40°C in the sealed exposure chamber for these tests. The total flow rate for these tests was 300 ml/min.

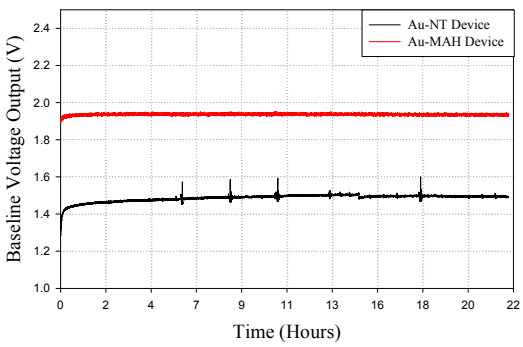

a) Baseline signals at 3% rh

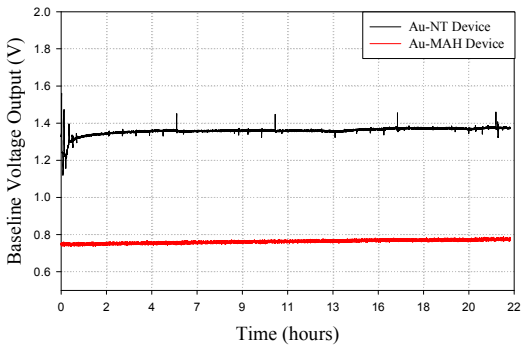

b) Baseline signals at 38% rh

Figure 5.1 Baseline voltage output over 22 hours at 3% rh and 38% rh for Au-NT and Au-MAH devices

Figures 5.1 a) and b) show the baseline output voltage of the Au-NT and Au-MAH devices at ~3% rh and ~38% rh over a 22 hour period. Some variation can be observed over the first 30 minutes of the tests as the FIA test station tries to stabilise the humidity setup. After that the two baselines drift negligibly (less than 0.01V). For the higher relative humidity test, the offset resistance of the Au-MAH devise was deliberately reduced (resulting in a reduction of the offset voltage) for the Au-MAH device to avoid saturation. This was done because the MAH material is highly sensitive to the hydroxyl molecule as explained in chapter 4.

5.3. Characterization of the Mono-type Hybrid Device

The three chemoresistive devices (Au-NT, Au-HDT and Au-MAH), based on dodecylamine stabilized gold nano-particles of 4 ± 0.8 nm diameter networked with an 1,***n*** alkylenedithiol chain (where ***n*** is the number of methylene units) were tested against different alcohol based analytes and toluene at various concentrations. Two of these materials have a methylene chain length of 9 and 16, respectively (Au-NT and Au-HDT), while a third has a chain length of 6 but includes a polar amide group in the backbone of the linker structure (Au-MAH). The tests for all three types of chemoresistors were run at two different humidities to observe any variation in output due to hydrophobic or hydrophilic behaviour. In addition to this, the tests for Au-NT and Au-MAH were repeated at two different temperatures (i.e. 30°C and 40°C) to observe the effect of temperature change on the hybrid mono-type ratiometric device output. Figure 5.2 shows a typical voltage output response for exposure to toluene and ethanol vapours at 40°C at ~38% rh (9853 ppm) and then again at ~3% rh (3000 ppm).

The following subsections describe the characterization and analysis using one material at a time in ratiometry. As observed in figure 5.2 the voltage output reduced as a result of exposure to all the analytes. Hence, all Δrr plots relative to exposure concentration show the *magnitude change* in resistance ratio, $|\Delta rr|$. The real values for Δrr were negative.

As can be seen from figure 5.2, the devices show an extremely good return to baseline value characteristic and a short post exposure recovery time for ethanol. Toluene recovery times were slightly longer (approximately 15 minutes) as it binds with the chemoresistive films more strongly than ethanol does.

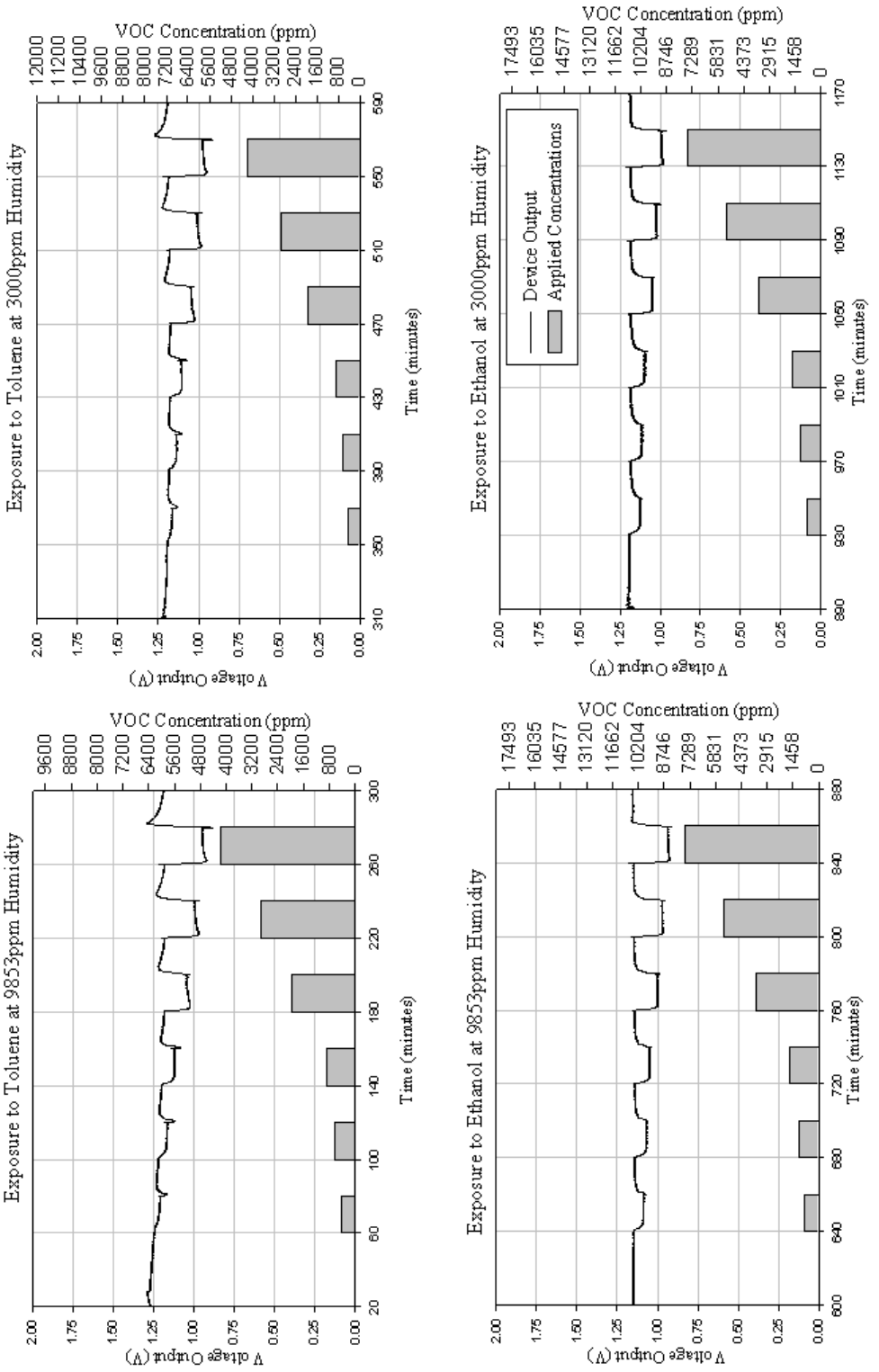

Figure 5.2 Typical responses of Au-NT device to Toluene and Ethanol vapour in air at 40°C.

5.4. Characterization of the Au-NT Devices

The Au-NT sensors were individually characterized in chapter 4 and were shown to have a high rate of adsorption for toluene. The resistance of the active and passive chemoresistive sensors chosen for the mono-type hybrid device characterization were in the range of 30-40 kΩ in ambient conditions. As this dithiol linker structure has a negligible dipole moment it does not have a strong affinity for alcohols or water. In chapter 4 it was observed that the adsorption rate increased with the size of the alcohol molecule. For the mono-type mono-variate hybrid devices the characterization tests for this material were carried out at six concentrations of ethanol and toluene. Both analytes were tested at two humidities, ~3% and ~38% rh. The devices were also exposed to three concentrations of propan-1-ol at ~38% rh. Table 5.1 shows the VOC vapour concentration levels at which this characterization was carried out.

Ethanol		Propan-1-ol		Toluene	
Flow Rates ml/min	**Concentrations (ppm)**	**Flow Rates ml/min**	**Concentrations (ppm)**	**Flow Rates ml/min**	**Concentrations (ppm)**
15	805	16	401	15	442
21	1127	81	2032	21	619
30	1610	162	4064	30	884
66	3542	162	4064	66	1946
99	5312	81	2032	99	2918
141	7566	16	401	141	4156

Table 5.1 Test flow rates and concentrations for Au-NT characterization

Figure 5.3 shows the Langmuir modelled plot of the exposure results for ethanol, propan-1-ol and toluene. There is a remarkable difference between these results and those obtained for the single active or the passive devices as seen in chapter 4. Comparing the results and figures 4.6 and 4.8 with figure 5.3 for the exposure results it can be observed that passive resistor dominates the characteristic of the net output for all three analytes. However, for propan-1-ol the active resistance reduces the effects of the passive resistance to some extent by pulling the gradient closer to the x-axis. The net voltage output showed a reduction in output at each exposure concentration. The Δrr values and their standard deviations are shown in table 5.2 and the magnitude Δrr have been plotted against the exposure concentrations of the VOCs in figure 5.3.

Ethanol (ppm)	Δ*rr* (x10^{-3})	± σ (x10^{-3})	Propan-1-ol (ppm)	Δ*rr* (x10^{-3})	± σ (x10^{-3})	Toluene (ppm)	Δ*rr* (x10^{-3})	± σ (x10^{-3})
805	-10.3	0.163	401	0.00	0.00	442	-5.22	0.386
1127	-11.4	0.535	2032	-11.1	0.5905	619	-8.98	0.519
1610	-13.7	0.523	4064	-18.9	0.5903	884	-12.6	0.829
3542	-20.7	0.940	4064	-17.7	0.5902	1946	-21.5	1.825
5312	-25.7	1.103	2034	-10.0	0.0204	2918	-28.6	2.707
7566	-30.9	1.271	401	0.00	0.0000	4156	-35.1	2.717

Table 5.2 Change in resistive ratios (Δ*rr*) for various analytes

Comparing these results with the exposure results for single chemoresistor tests presented in chapter 4, for ethanol the results obtained with the monotype hybrid device almost replicate the results for the passive sensor exposure results. However, in the case for the propan-1-ol and toluene exposure results the magnitude is fairly lower. The reduction is 30% for toluene and almost 50% for propan-1-ol. This is because the active sensor pulls the negative Δ*rr* value up resulting in a reduction of the net magnitude. A fair outcome of this compromise is the increased stability offered by the ratiometric hybrid device.

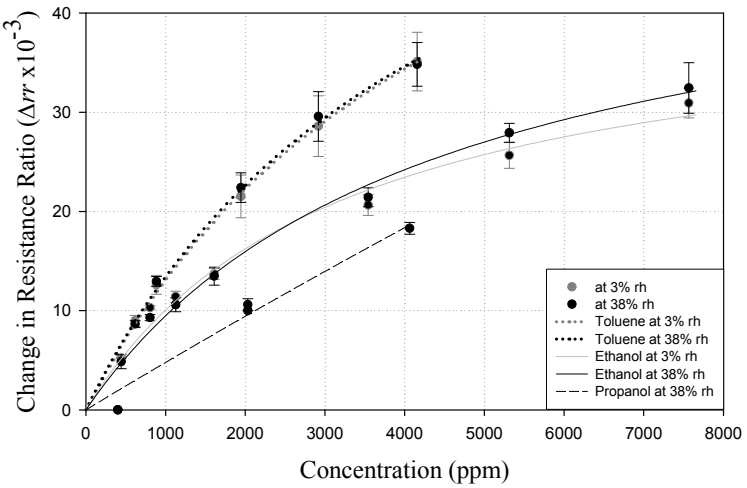

Figure 5.3 Au-NT response to toluene, ethanol and propan-1-ol at 30°C

The hybrid Au-NT device showed a high response to toluene. This is shown by the higher Δ*rr* curve than ethanol or propan-1-ol for the Langmuir fit. One of the most prominent features that could be observed with this hybrid device test was that the previously observed characteristic results dependant on alcohol molecule size was not

as apparent as before. Ethanol has a higher rate of adsorption than methanol, and propan-1-ol a higher rate than ethanol when tested with only one chemoresistor. Using a hybrid device the dynamic change in the *rr* values results in propan-1-ol to have a lower |Δ*rr*| value than ethanol due to shifts in the active and passive sensor resistances at the same time. A relatively larger increase in resistance of the active sensor resistance for propan-1-ol compared to that for ethanol resulted in a lower |Δ*rr*| value for propan-1-ol.

5.4.1. Dependence on Humidity

Table 5.3 shows the Langmuir constants for the Au-NT hybrid device with the respective plots in figure 5.3. The grey line represents the response at 3% rh, which in the case of ethanol and toluene overlaps with the black lines (representing the sensor response at 38% rh). This close correlation between the plots for the tests at the two humidities shows the hydrophobic nature of the Au-NT films due to absence of any polar component in the linker structure. This is also reflected in the nearly identical α and K values at the two humidities for ethanol and toluene.

VOC	α (x10^{-2})	K (ppm) (x10^{3})
Ethanol 3%	4.21	3.189
Ethanol 38%	5.02	4.289
Propan-1-ol 38%	31.77	65.180
Toluene 3%	7.53	4.764
Toluene 38%	7.33	4.465

Table 5.3 Constants of the Au-NT Langmuir Plot

5.4.2. Dependence on Temperature

The results shown in section 4.5 show a 0.25 V drop in output voltage for a rise in temperature of the exposure chamber by 10 °C. This also corresponds with a rise in the offset voltage by 0.1 V for the same temperature change. This drop in the output voltage was largely because of changes in the resistance of the circuitry as it heated up. The increase in the offset voltage was due to an increase in the internal resistance of the offset circuitry of the ASIC. Figures 5.4 (a), (b), (c) and (d) show the magnitude change in the Δ*rr* response between 30°C and 40°C for exposure results to ethanol and toluene. The real values of Δ*rr* were negative. The response results were calculated after adjusting for the drop in voltage output from the electrical circuit heating up.

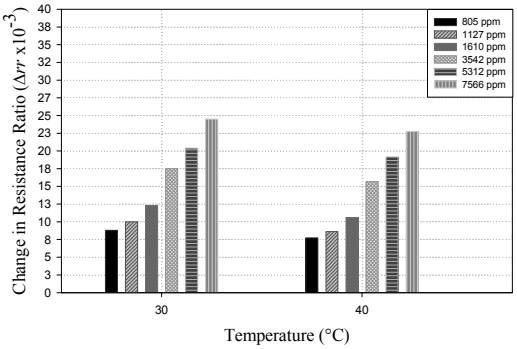

Figure 5.4(a) Au-NT Δ*rr* variation to ethanol between 30°C and 40°C at 2% rh

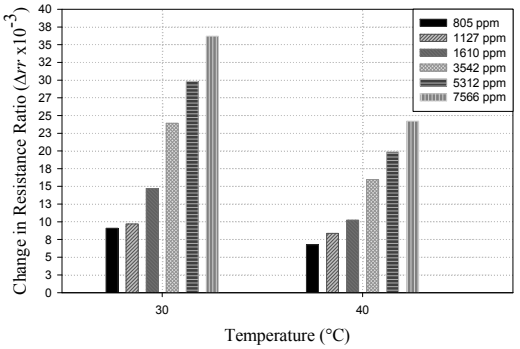

Figure 5.4(b) Au-NT Δ*rr* variation to ethanol between 30°C and 40°C at 38% rh

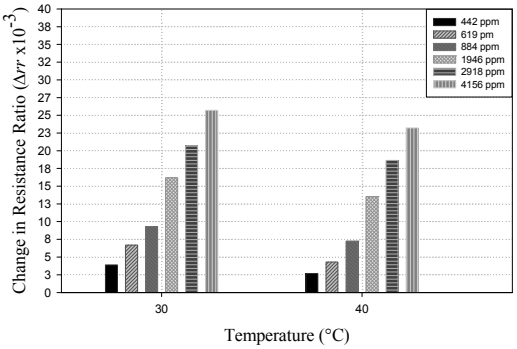

Figure 5.4(c) Au-NT Δ*rr* variation to toluene between 30°C and 40°C at 2% rh

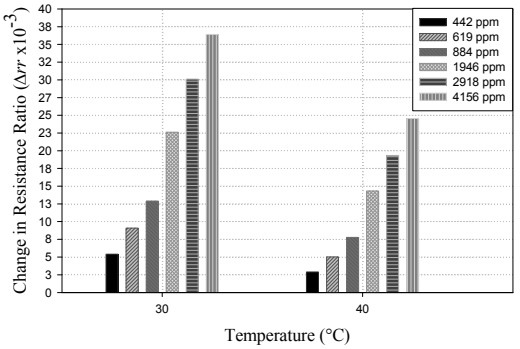

Figure 5.4(d) Au-NT Δ*rr* variation to toluene between 30°C and 40°C at 38% rh

The figures above show a drop in the Δ*rr* value with increasing temperature. At 38% rh it can be seen that the drop is more severe than at 2% rh. However, this dependence on exposure concentrations is absent when the same devices are tested at 2% rh. This suggests that the respective net *rr* change per ppm of analyte is lower at higher concentrations of each analyte at 38% rh and 30°C. It is also a clear indication of the relatively higher level of competition that exists between water and analyte molecules to access the chemoresistive films at 38% rh and 40°C. The Au-NT sensors being hydrophobic do not react to the presence of the water molecules. However, as the larger VOC vapours try to access the chemoresistive films, they are obstructed by the

smaller water molecules. It is important to remember that the net resistance ratio change is a function of the active and the passive sensor increasing in resistance simultaneously. Keeping in view that the real value of Δrr is negative and recalling from chapter 4

$$\Delta rr = \frac{R_{a2}}{R_{p2}} - \frac{R_{a1}}{R_{p1}} \tag{5.1}$$

where, R_{a2} and R_{p2} are the active and passive resistances under exposure conditions respectively, it can be seen that a relative increase in resistance of R_p to R_a is larger at 30°C than at 40°C. This difference in adsorption can be attributed to the presence of the silicone coating on the passive sensor. In addition to this, VOC adsorption is known to be effected by increasing temperatures (Chiang, Chiang & Huang 2001; Chuang et al. 2003; Pang et al. 2006).

5.5. Characterization of the Au-HDT Devices

The difference between the Au-NT and the Au-HDT sensor materials is that the Au-NT film has a methylene chain length of nine units while the Au-HDT material has a methylene chain length of sixteen units. Both the polymers end in a thiol molecule at either end of the chain. The effects of the increase in chain length on the rate of sorption and resistance change has been established by Joseph et al. and also observed in chapter 4 (Joseph et al. 2003; Joseph, Yvonne et al. 2004; Joseph, Y. et al. 2004). It was reported that the adsorptive properties of the polymer increase with an increasing number of carbons in the polymer chain. The physical effect that was observed to prove this was a higher percentage change in resistance for the larger polymer chain per ppm of analyte. This effect was confirmed by the results and analysis carried out in chapter 4. The resistance of the active and passive chemoresistive sensors chosen for the characterization were in the range of 40-60 kΩ in ambient conditions.

5.5.1. Tests at 0% rh

In this section, the effects between the two materials in a ratiometric setup are observed. Building up from the analysis carried out in sections 4.3.3, 4.3.4 and 5.3.1 the Au-HDT is tested against methanol, ethanol, propan-1-ol, toluene and water at 0% rh and 38% rh while maintaining a temperature of 30°C in the exposure chamber. The

concentrations at which the ratiometric devices were exposed at are given in table 5.4 below.

Methanol	Ethanol	Propan-1-ol	Toluene	Water
1817	789	301	386	327
10622	4732	1768	2381	1941
19288	8675	3198	4312	3507
10622	4732	1768	2381	1941
1817	789	301	386	327

Table 5.4 Exposure concentrations for sorption and desorption tests with Au-HDT

The devices were tested for adsorption/desorption effects by exposing them to increasing concentrations of the analyte followed by decreasing concentrations. The results are shown in figure 5.5 (a) and 5.5 (b) in Langmuir and linear model fitted plots. The device chamber was kept at a constant temperature of 30°C while maintaining moisture content of 0% rh. In figure 5.5 (b) the response to propan-1-ol plot is a linear regression plot and the respective coefficient and *y* intercept value are labelled accordingly in table 5.5.

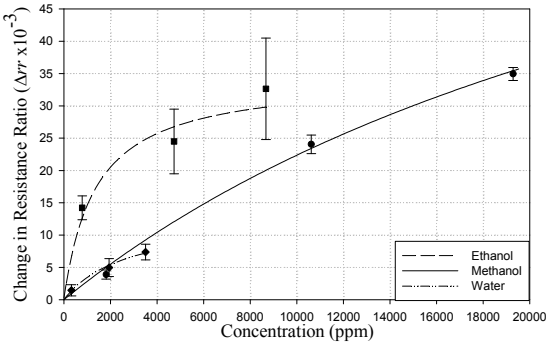

Figure 5.5 (a) Langmuir plot for Au-HDT response to methanol, ethanol and water at 30°C and 0% rh

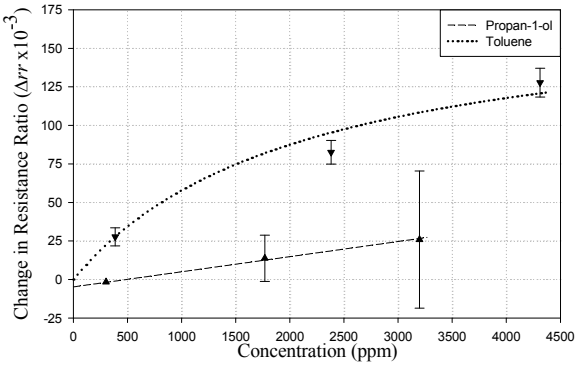

Figure 5.5 (b) Plot for Au-HDT response to propan-1-ol and toluene at 30°C and 0% rh

VOC	α (x10^{-2})	K (ppm) (x10^{3})
Methanol	9.56	32.766
Ethanol	3.45	1.367
Toluene	17.98	2.110
Water	1.29	2.747
Linear Constants	Δrr_0 (x10^{-2})	J (x10^{-6})
Propan-1-ol	-0.47502	9.8095

Table 5.5 Langmuir and linear constants for the Au-HDT device plots at 0% rh

Table 5.5 shows the respective constants for the plots given in figures 5.5 (a) and (b). As these results are from bi-variate ratiometric devices, the value of *K* is a function of the ratio of the *K* value for the active sensor and the passive sensor. Thus, a high *K* means that the active sensor has lower surface binding forces interacting with the analyte than the passive sensor. The reverse is true for low *K* values. In table 5.5 methanol has the highest *K* value in figure 5.5. From chapter 4 it is known that methanol has a stronger surface binding capability compared to ethanol and a much lower *K* value for the silicone coated passive sensor than the unencapsulated active sensor. Thus, in case of these bi-variate devices, methanol has stronger surface interaction with the passive silicone coated sensors resulting in a greater negative Δrr response and a much larger *K* value than ethanol. Propan-1-ol was linearly modelled as the response results did not converge for the Langmuir plot. In the linear fit the *J* gradient value is observed to be extremely small for this analyte therefore, the approximation given in equation (3.17) can be used. The small *J* value is a result of a larger response change on the passive sensor surface as compared to the active sensor surface.

The respective Δrr values for the sorption exposure cycle are given in table 5.6. The negative Δrr suggest that the passive sensor dominated during these tests. This suggests that the percentage change in the passive sensor resistance was greater than the active sensor.

Test Results for Au-HDT Devices			
VOC	**Concentrations (ppm)**	**Δrr (x10^{-3})**	**± σ (x10^{-3})**
Methanol Exposure Test	1817	-3.2	1.002
	10622	-25.5	2.087
	19288	-34.9	1.002
Ethanol Exposure Test	789	-14.2	2.588
	4732	-24.5	7.096
	8675	-32.6	11.100
Propan-1-ol Exposure Test	301	1.6	1.085
	1768	-13.8	2.504
	3198	-25.9	7.430
Toluene Exposure Test	386	-27.7	5.013
	2381	-82.6	7.281
	4312	-127.7	9.764
Water Exposure Test	327	-1.5	1.378
	1941	-5.0	1.569
	3507	-7.4	1.212

Table 5.6 Δ*rr* values for the Au-HDT sorption exposure cycle at 0% rh

The values obtained shown in table 5.6 and figures 5.5 (a) and (b) show a marked difference from the device characteristics shown in figures 4.9 - 4.12. Exposure to the ethanol vapour shows a sharp increase in the |Δ*rr*| value suggesting the device coming to a saturation value at 4,000 ppm. Methanol shows a comparatively slow sorption result, similar to the Au-HDT active device result but with a negative value. Due to the HDT material's hydrophobic nature the devices showed the least magnitude response to vapour exposure with water as expected.

The most distinctive difference from the tests carried out in chapter 4 and from the Au-NT results in section 5.3.1 was the result for propan-1-ol. With just one sensor exposed, the device output showed convergence at a resistance ratio change of 0.04 and could be fitted into a Langmuir plot. In the monotype bi-variate ratiometric device the regression plot did not converge at any particular value. Hence, a linear regression plot has been drawn. This can be considered to be a result of the active sensor reaching saturation value while, the passive sensor resistance continues to increase as it responds to the VOC vapour. The plot shows that the equilibrium for the active and passive sensors for propan-1-ol lies between the methanol and ethanol plots.

Toluene had shown the highest rate of *rr* change when only one of the two sensors was exposed. In the mono-type bi-variate device the Δ*rr* convergence value is similar to the results with single active or passive sensors but only negative in value. The

monotype ratiometric results for Au-HDT show a four-fold increase in response to toluene vapour as compared with the Au-NT device.

5.5.2. Dependence on Humidity

Figures 5.6 (a) and (b) show the Langmuir fitted plots for analyte tests at 38% rh. The respective constants of the plots are given in table 5.7. The plots show a larger $|\Delta rr|$ response for methanol and ethanol as compared to results for the same analytes at 0% rh as shown in the previous section. The increase is around 50% for methanol and about 30% for ethanol. Comparatively, the net Δrr values differ minutely from the 0% rh value for propan-1-ol and toluene following no particular trend. As was the case for the propan-1-ol response at 0% rh, the K value for (or $1/J$ in case of the linear regression) is fairly large, however, a conversion of results was achieved. This may be so as the water vapour makes it more difficult for the chemoresistor film coated with the silicone to respond to VOC vapour. Methanol, ethanol and toluene show results along the same order of magnitude as shown by results at 0% rh.

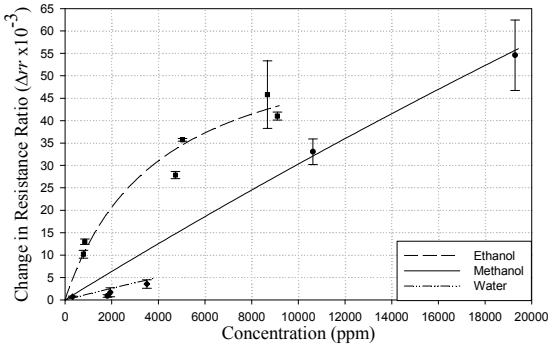

Figure 5.6 (a) Langmuir Plot for Au-HDT response to methanol, ethanol and water at 30°C and 38% rh

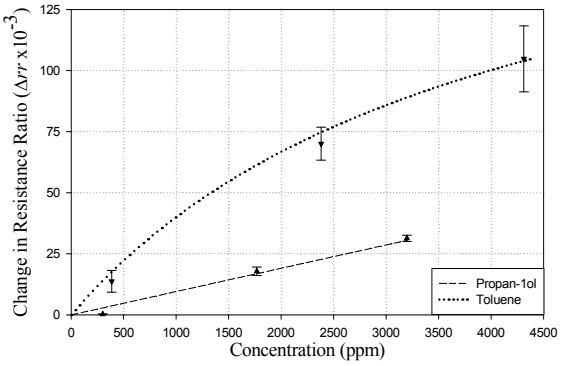

Figure 5.6 (b) Langmuir Plot for Au-HDT response to propan-1-ol and toluene at 30°C and 38% rh

VOC	α (x10^{-2})	K (ppm) (x10^{3})
Methanol	56.18	175.343
Ethanol	6.24	4.051
Propan-1-ol	4127.85	4325.0
Toluene	20.07	4.012
Water	7.28	54.125

Table 5.7 Constants for the Au-HDT Langmuir plots at 38% rh

Table 5.8 shows the change in the resistive ratio in the sorption cycle of the tests. The negative values suggest a greater percentage change in the resistance of the passive sensor as compared to the active sensor. The Δ*rr* values for all the exposures are negative with the exception of propan-1-ol at the lowest exposure concentration as the water film on the passive sensor silicone layer acts as a greater inhibiting factor at this concentration than on the active sensor where no silicone layer is present.

Test Results for Au-HDT Devices			
VOC	**Concentrations (ppm)**	**Δ*rr* (x10^{-3})**	**± σ (x10^{-3})**
Methanol Exposure Test	1817	-0.9	0.417
	10622	-33.1	4.007
	19288	-54.6	11.100
Ethanol Exposure Test	789	-10.2	0.917
	4732	-27.9	0.851
	8675	-45.8	8.234
Propan-1-ol Exposure Test	301	0.3	0.0835
	1768	-17.8	2.504
	3198	-31.3	1.753
Toluene Exposure Test	386	-13.8	3.843
	2381	-70.1	6.305
	4312	-104.8	12.000
Water Exposure Test	327	-0.7	0.167
	1941	-1.7	1.419
	3507	-3.6	1.336

Table 5.8 Δ*rr* values for the Au-HDT sorption exposure cycle at 38% rh

Figure 5.7 shows the resistance ratio change plots at two different humidities for exposure to all the analyte vapours as bar charts. The Au-HDT material, similar to the Au-NT material, was not expected to show a strong dependence on humidity. The lack of a particular upward or downward trend in these results validates this expectation.

There are at least two mechanisms which pull the results in the positive or negative directions. If the resistance of the active sensor increases more than the passive sensor, the net Δrr value is positive. Otherwise it is negative. The change in Δrr value is determined by the rate of sorption/desorption at the chemoresistor surface.

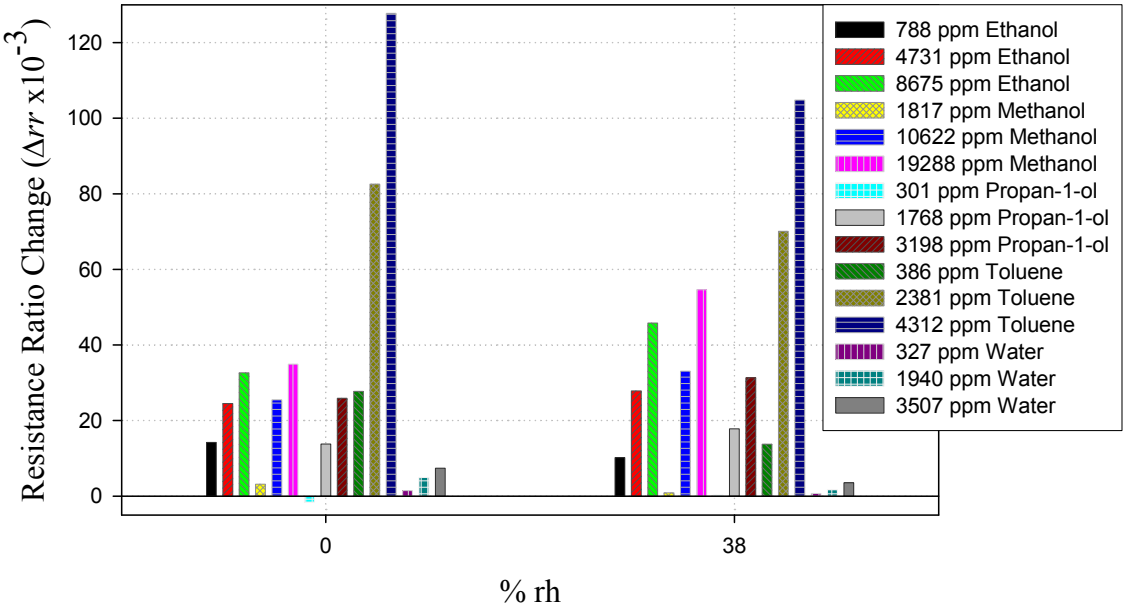

Figure 5.7 Change in resistance ratio (Δrr) of Au-HDT with respect to Change in rh at 30°C at 0% rh and 38% rh

Toluene shows the greatest reduction in the magnitude response at higher relative humidity. The three alcohols show a very slight increase in the response magnitude, especially at the higher concentrations (the plot shows the magnitude values. See table 5.8 for real values). This implies that the active resistance increases in resistance more than the passive resistance at a relative humidity of 38%. As the water molecules form a significantly high concentration compared to the analyte molecules at these concentrations, the smaller water molecules and the silicone deny the alcohol molecules access to the chemoresistive film. However, as the active sensor is uncoated and has very little sorption capacity for water, due to the nature of the Au-HDT material, the change occurring in the passive film sensor outdoes the change in the active sensor resistance. Propan-1-ol is an exception to this case as at the lowest concentration of 301 ppm at 38% rh it shows the active resistance changing more relative to the passive resistance. In the case presented here, the balancing effect of the active sensor results in

a much smaller net change in the Δ*rr* value. Keeping in mind that the error margin for this reading was between 6-10% this variation from the norm can be counted as notable but negligible.

At higher analyte concentrations, all three alcohols, apart from propan-1-ol at the highest concentration, show an increasingly negative Δ*rr* result. This implies that at higher concentrations the analyte molecules regain their dominance in the water/analyte vapour mixture and cause a greater change in the resistance of the passive resistor as compared to the active resistance of the respective test devices. The increase in the relative change in Δ*rr* value per unit concentration these analytes shows a higher relative dependence on the analyte vapours as compared with the water vapours.

In chapter 4 it was confirmed that the silicone film does not affect the rate of sorption of toluene vapour into the chemoresistive film. At 38% rh, the respective results at the 3 vapour concentrations show a reduction in the |Δ*rr*| value by 50% at the lowest concentration and 20% at the higher concentrations. Thus, at higher humidities the active sensor has a greater percentage change in the resistance as compared with the single passive sensor setup.

In terms of scale, the test with water shows the smallest change in resistance ratio as compared with the other VOC vapours. The change is half an order of magnitude less than that for the three alcohols and one and a half orders of magnitude compared with the toluene. It was also observed that the active sensor shows a greater change in resistance at 38% rh compared with at 0% rh. This was expected as the silicone forms a good sealant against water vapours. Thus, allowing the active sensor to contribute more significantly to the net result. However, the overall Δ*rr* value is still dominated by the change in the resistance of the passive sensor hence giving negative Δ*rr* values. A possible reason for the larger silicone coated passive sensor may be from the swelling effect of the silicone which causes the chemoresistive film below it to stretch and hence result in an increase in resistance.

5.6. Characterization of the Au-MAH Devices

The Au-MAH film material consisted of dodecylamine stabilized gold nano-particles of 4 ± 0.8 nm diameter networked with an alkylenedithiol chain of 6 carbon atoms. Other than the methlylene chain length the other difference between the Au-MAH and the Au-HDT and Au-NT materials is the presence of a polar amide group in the alkylenedithiol linker structure backbone (Vossmeyer et al. 2004). Vossmeyer et al. have shown that the presence of this amide group lowers the sensitivity to the non-polar toluene. This was verified in chapter 4. The amide group was also expected to have greater magnitude response to the polar water and alcohol molecules as compared with the previous two film materials tested. In this section the Au-MAH material has been tested in a ratiometric setup with the SRL 194 device. As with the other two materials analysed in this chapter, the active chemoresistive sensor was left uncovered and interacted with the VOC vapours directly, whereas the passive sensor was coated with the permeable silicone gel. The resistances of the active and passive chemoresistive sensors chosen for the characterization were in the range of 90-120 kΩ in ambient conditions. Figure 5.8(a) shows a convergent Langmuir fitted plot for methanol, ethanol and toluene at a chamber temperature of 30°C and 0% rh. Comparing with the Au-HDT device that has the same exposure conditions, the two alcohols show an increase in magnitude response of 100% whereas, there is a slight reduction in the Δrr response value for toluene. There is a large overlap between the results for toluene and ethanol even though toluene has twice the K value than ethanol. Table 5.9(a) shows the plot constants for ethanol, methanol and toluene.

The results for exposure to propan-1-ol and water did not converge to any particular value. Hence, the linear regression of these results is plotted in figure 5.8(b). The respective y-intercept (Δrr_0) and gradient values (J) are given in table 5.9(b). The linear approximation is also justifiable due to the extremely small value of J, which satisfies the conditions of equation (3.17). If the K value is taken as $1/J$ for propan-1-ol it comes to 51.22×10^3 which suggests that the passive sensor has much larger adsorption than the active sensor for propan-1-ol.

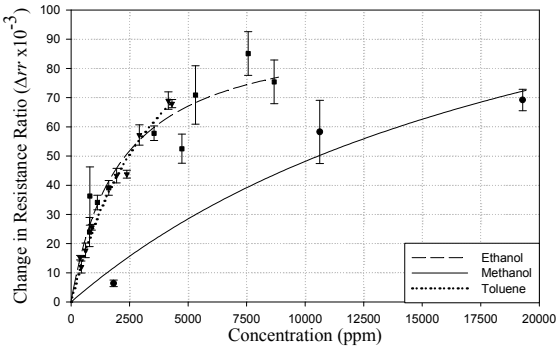

Figure 5.8(a) Langmuir plot for change in resistance ratio (Δ*rr*) of Au-MAH at 30°C and 0% rh

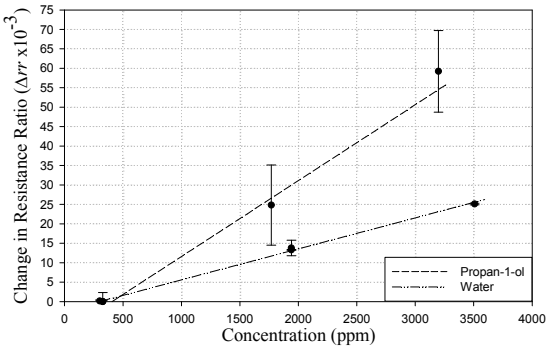

Figure 5.8 (b) Linear regression for change in resistance ratio (Δ*rr*) of Au-MAH at 30°C and 0% rh

VOC	α (x10^{-2})	K (ppm) (x10^{3})
Methanol	15.62	22.417
Ethanol	9.53	2.099
Toluene	13.22	4.024

Table 5.9(a) Constants for the Au-MAH Langmuir Plots at 0% rh

VOC	Δrr_0 (x10^{-3})	J (x10^{-6})
Propan-1-ol	-7.9277	19.521
Water	-2.3797	7.9720

Table 5.9(b) Constants for the Au-MAH linear regression plots at 0% rh

From the tests it was observed that at the lowest concentrations of 301 ppm and 327 ppm for propan-1-ol and water respectively, the devices had a negligible voltage response. It can be assumed that at these concentrations the response at the active and passive chemoresistor surfaces nearly cancel out each other. As with the case with the Au-NT and Au-HDT devices, the passive sensors dominated the device output. Table 5.10 shows the Δ*rr* response results when the devices were exposed to ascending concentrations of the analytes. The negative Δ*rr* values suggest a larger increase of resistance in the passive sensor as compared with the active sensor. As observed from the Langmuir fit and linear regression plots, the three alcohols show a doubling of the change in resistance ratio values. Compared to Au-HDT toluene has a reduction in

output of approximately 40%. Water shows the most dramatic increase in Δ*rr* by increasing three fold.

Test Results for Au-MAH Devices			
VOC	**Concentrations (ppm)**	**Δ*rr* (x10^{-3})**	**± σ (x10^{-3})**
Methanol Exposure Test	1817	-8.0	3.848
	10622	-58.3	9.721
	19288	-69.2	3.001
Ethanol Exposure Test	789	-24.0	1.202
	4732	-52.5	6.930
	8675	-75.4	7.354
Propan-1-ol Exposure Test	301	-0.5	0.289
	1768	-24.8	11.60
	3198	-59.2	11.60
Toluene Exposure Test	386	-15.2	2.431
	2381	-43.8	1.298
	4312	-68.0	1.258
Water Exposure Test	327	0.0	0.417
	1941	-13.8	2.824
	3507	-25.1	0.275

Table 5.10 Δ*rr* values for the Au-MAH sorption exposure cycle at 0% rh

5.6.1. Dependence on Humidity

Figure 5.9 shows the changes in Δ*rr* values with an increase from 0% to 38% rh. The plots show the response results at three ascending concentrations of each analyte. The general trend is observed to be a significantly large reduction in the magnitude response at the higher relative humidity and an increase in the decline of magnitude with increasing analyte concentration. The only exceptions to this rule are propan-1-ol and water at the lowest test concentrations. Both these analytes had a negligible Δ*rr* response at 0% rh and have only a slightly larger magnitude response at 38% rh. An increase in the negative response at the lowest concentrations of propan-1-ol and water implies a greater change in the resistance of the passive resistor at 38% rh than at 0% rh. But this is the exception and not the rule.

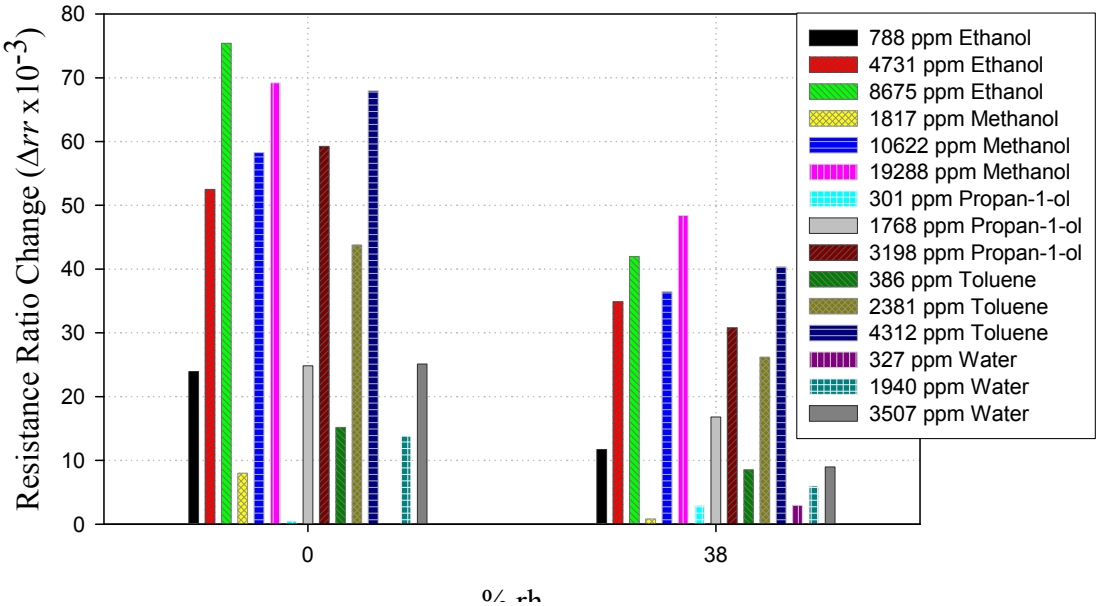

Figure 5.9 Change in resistance ratio (Δ*rr*) of Au-MAH with respect to change in rh at 30°C

For most of the results at higher humidity, the mixture of VOC vapour in humidity is attracted by both the active and passive chemoresistors. Adsorption is facilitated by the attraction of the amide linker chain for the polar analytes resulting in increased competition for vacant sites between water and VOC. Whereas, on the passive sensor the water forms a film on top of the silicone coating preventing a large change in the resistance of the film. As described before, some swelling of the silicone film may occur which can be the reason for a larger relative change to the passive sensor resistance due to stretching causes by the swelled up silicone. Also the dielectric effect of the silicone film between two polar media, i.e. between the water and alcohol molecules (-OH group) and the polar chemoresistive film, may contribute to a change in resistance of the silicone coated passive sensor. As a result most of the test results show a negative value for change in resistance ratio. The reason for a decrease in magnitude as compared to at 0% rh is that at the higher relative humidity the active sensor has a greater resistance change but still not as large a change as that of the passive sensor.

5.6.2. Dependence on Temperature

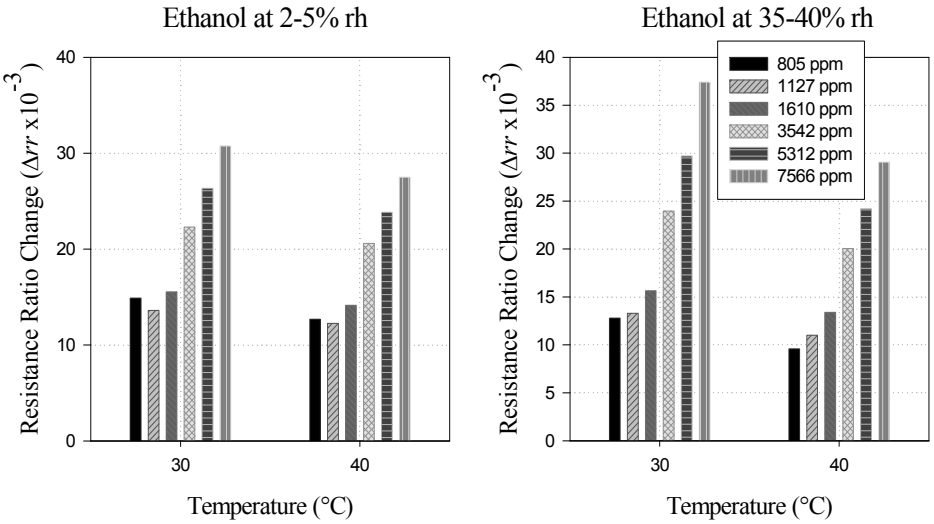

Figure 5.10(a) Change in resistance ratio (Δ*rr*) of Au-MAH to ethanol exposure with respect to change in temperature

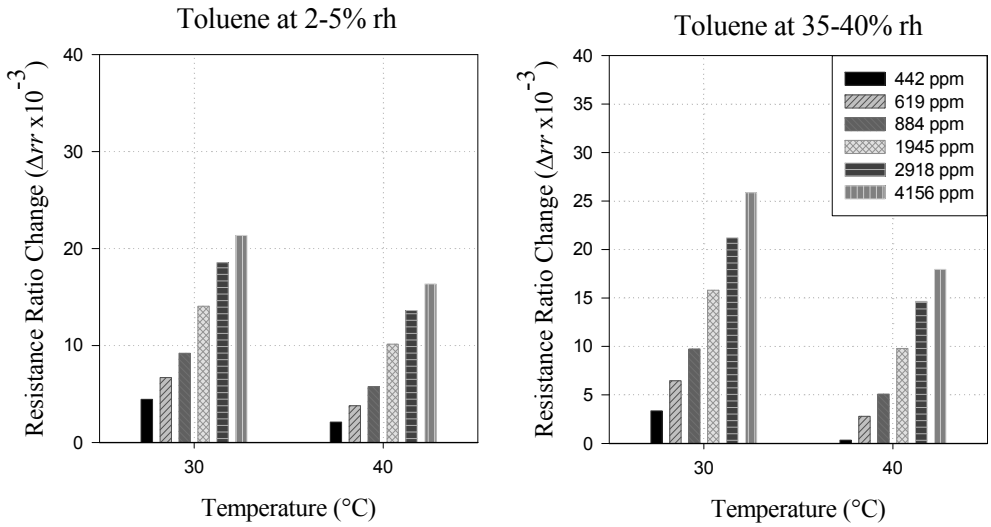

Figure 5.10(b) Change in resistance ratio (Δ*rr*) of Au-MAH to toluene exposure with respect to change in temperature

Figures 5.10(a) and (b) show the change in Δ*rr* value when the temperature of the exposure chamber is increased from 30°C to 40°C for ethanol and toluene respectively. The results were plotted after correcting for the drop in circuit resistance with increasing chamber temperature. For the results obtained at 2-5% rh it can be observed that the

drop in resistance ratio change at 40°C is approximately the same for all the exposure concentrations of the analyte. The average drop in Δrr value is 2×10^{-3} for ethanol and 4×10^{-3} for toluene at 2-3% rh.

A greater drop in response to exposures at 35-40% rh was observed. It was also observed that the drop in response increases at the higher concentrations. The range of Δrr drop was observed to be between 2.5-8 $\times 10^{-3}$ for ethanol and between 3-7 $\times 10^{-3}$ for toluene. This increased dependence on analyte concentration at the higher humidity occurs because of the increased competition between the water vapours and the analyte vapours for sorption sites on the chemical film, as observed in figure 5.9. The general trend for the Δrr value is a reduction in magnitude at higher temperature. This shows that at higher temperature the active sensor has better net cancellation effects of the passive sensor output as relatively less adsorbate vapours interact with the silicone coated passive sensor.

5.7. Difference in Effects of High and Low Resistance Chemoresistors at 0% rh and 30°C

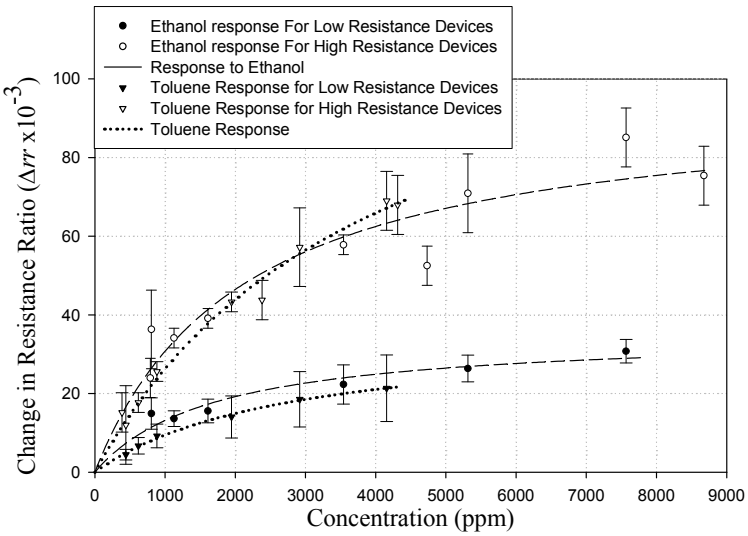

Figure 5.11 Comparison of Au-MAH Devices Based on High Resistance and Low Resistance Chemoresistive Sensors

	VOC	α (x10^{-2})	K (ppm) (x10^{3})
Low Resistance Devices	Ethanol	3.54	1.690
	Toluene	3.55	2.762
High Resistance Devices	Ethanol	9.53	2.100
	Toluene	13.22	4.024

Table 5.11 Langmuir constants for Au-MAH ethanol and toluene at 0% rh 30°C

Tests were conducted with devices based on two types of Au-MAH sensors. The only difference between the two sensors was the difference in their resistances. The two pairs had the active and passive sensors in the 50-60 kΩ and the 90-120 kΩ ranges with the former being classified as the low resistance device and the latter as the high resistance device respectively. A stark difference between the Δ*rr* responses of the two sets of devices was observed, as seen in figure 5.11 and table 5.11. The higher resistance devices showed a net Δ*rr* change 2-3 times greater than that of the low resistance device. The results for toluene and ethanol exposure were close to each other and hence, matched the behaviour of other Au-MAH devices. The reason for this significant difference in the behaviour of the two sets of sensors is that the high resistance devices have a greater range of resistance change available to them and go

through a greater percentage change in resistance of the passive device, compared to the low resistance devices. Also the compensation effect of the active sensor is limited. The slightest difference between the respective changes of resistances between these sensors is amplified through the electronics and results in a greater device output. The presence of the silicone layer allows the active and passive sensors to increase their resistances during exposures at different rates. Hence, the high resistance devices result in a much higher Δrr response as compared with the low resistance devices.

5.8. Response Curve Shape Analysis

An important feature of the response results of the sensor devices was the shape of the sensor device response curve. The response curve shape was a direct result of the reactions taking place on the surface of the active as well as the passive sensor simultaneously. As both of the sensors (active and passive) were resistive sensors for all the test devices, the impact of adsorption onto the sensor surface was an increase in resistance of the individual sensor. Both sensors making the test device were connected to each other through the ASIC as resistors in a non-inverting amplifier circuit. Thus, the rate of adsorption at individual sensor surface played an important factor in determining the shape of the device output.

Figure 5.12 a) shows the typical device response to 3542 ppm of ethanol and 1946 ppm of toluene, both resulting from an analyte flow rate of 66 ml/min. The decrease in voltage output was a result of the passive sensors resistor increasing more than the active sensor. The passive sensor was faster in responding to the toluene vapour at the beginning of the exposure time, making the devices reached a minimum value (as the device output decreased during exposure times) within 150 seconds of coming into contact with the vapour. As the active sensor continued to adsorb the vapour the result was a slight bulge at the beginning of the exposure time and a device equilibrium being reached almost 15 minutes after the start of the device exposure. At the end of the exposure time, there was a slight inverted peak which was a result of the active sensor losing the adsorbed vapour much faster than the passive sensor initially. However, as the passive sensor began to lose its adsorbed toluene vapour its rate of desorption surpassed that of the active sensor, causing the peak at the end of the exposure time. The response rate characteristics for ethanol for the active and passive sensors were fairly comparable as there were no sharp peaks present. The passive sensor, however, changed

its resistance more than that of the active sensor as shown by the decrease in output voltage.

Figure 5.12 b) shows the response characteristic of an Au-HDT based mono-type bi-variate sensor device to methanol, ethanol, propan-1-ol, toluene and water vapours at 10622 ppm (76 ml/min) , 4732 ppm (78 ml/min), 1768 ppm (94 ml/min), 2381 ppm (74 ml/min) and 1941 ppm (83 ml/min) respectively. The figure shows an initial peak for all the analytes as a result of rapid resistance increase of the active sensor relative to the passive sensor. This was followed by a smooth reduction in the output voltage caused by a gradual increase of the passive sensor resistance to reach an active to passive sensor equilibrium value. Toluene, methanol and ethanol showed the sharpest shift to equilibrium as propan-1-ol had a high response value at the active sensor which reduced the magnitude of the response, and water had very low adsorbance in the hydrophobic Au-HDT material. At the end of the exposure time there was an inverted peak caused by the rapid desorption at the active sensor. The inverted peak reached its lowest value at 90 to 100 seconds (fastest for methanol and slowest for toluene) after the analyte exposure was switched off showing the response delay effect of the silicone coating. It should be noted that toluene had a much higher magnitude response. Therefore, the axis was reduced in scale to match with the magnitude of the other analytes.

Figure 5.12 and c) shows the response characteristic of an Au-MAH bi-variate sensor device. The device characteristics were quite similar to those of the Au-HDT device. The major differences were the sharp response of the toluene passive sensor and the reduced magnitude of response to this vapour. This was an expected outcome as the Au-MAH sensor was more attracted to the polar alcohol and water molecules. That is why the highest initial peak was for water as the resistance of the active sensor increased sharply, followed by a more gradual increase in resistance of the silicone coated passive sensor. At the end of the exposure sequence there was an inverted peak like for the Au-HDT material, however, the device responded to all the analytes in an almost synchronous fashion. Toluene, showed the fastest time to reach 90% of the maximum magnitude change (τ_{90}) at 200 seconds.

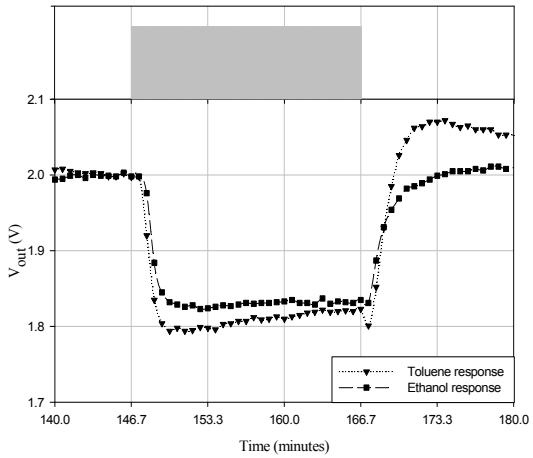

a) Typical response of the Au-NT device to Toluene and Ethanol

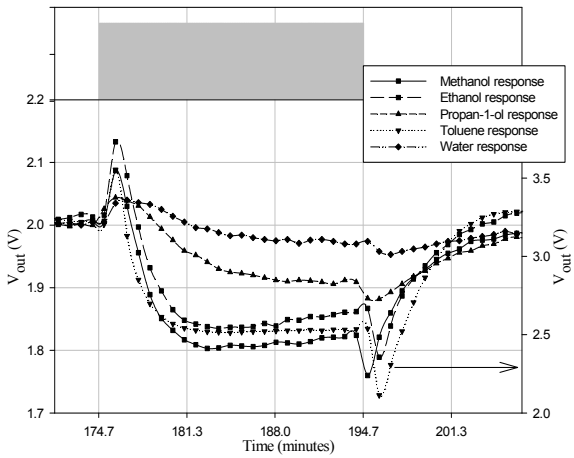

b) Typical response of the Au-HDT devices to Methanol, Ethanol, Propan-1-ol, Toluene and Water

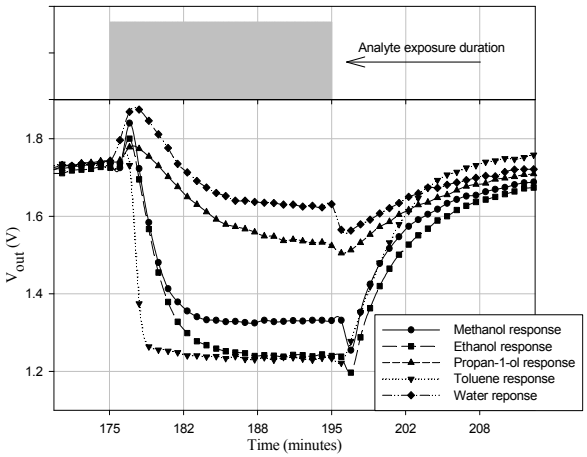

c) Typical response of the Au-MAH devices to Methanol, Ethanol, Propan-1-ol, Toluene and Water

Figure 5.12 Typical response of the three Monotype Bi-variate Sensor devices to various VOCs at 0% rh and 30°C showing the differences between the shapes of the response curves

In chapter 4 equation (4.7) it was shown that the magnitude voltage response, ΔV_{out}, was a function of the relative resistance change response, Δrr. Thus, the time to reach 90% of the saturation value during exposure durations (τ_{90ON}) and the time to

reach 90% of the baseline value after exposure to analyte has been switched off (τ_{90OFF}) can be determined from the following equations:

$$V_{out}(t) = V_{out(0)} + \Delta V_{out(1)} \left[exp\left(\frac{-t}{\tau_{90ON1}}\right)\right] \quad (5.2)$$

$$V_{out}(t) = V_{out(0)} + \Delta V_{out(1)} \left[1 - exp\left(\frac{-t}{\tau_{90OFF1}}\right)\right] \quad (5.3)$$

These equations are valid for when the response voltage output reduces during exposure times and increases to a baseline value after exposure to analyte has been switched off. For the cases when the voltage response behaves in the opposite manner, equations (5.2) and (5.3) need to be reversed for τ_{90ON} and τ_{90OFF}. A second order equation using $\Delta V_{out(2)}$ could be used to obtain τ_{90ON2} and τ_{90OFF2} for a better fit to the test data.

Linear discriminant analysis (Weiss & Kulikowski 1991) can be applied to the data collected from multiple runs of each analyte and each device. Here, each analyte at a particular concentration or flow rate can be considered as a different class, (i.e. C_m for methanol, C_e for ethanol, C_p for propan-1-ol, C_t for toluene and C_w for water). To create the probability matrix it is necessary to calculate the conditional probability of a particular analyte given that we have obtained any of the following variables, i.e. the magnitude response ΔV_{out} (here referred to as M) at that particular concentration or flow rate, the Langmuir coefficient K, and the switch on and switch off times, τ_{90ON} and τ_{90OFF}. Once these observations and the relevant conditional probabilities are known for each class the probability matrix can be constructed as shown in table 5.12.

Variable	C_m	C_e	C_p	C_t	C_w
M	$P(C_m\|\ M)$	$P(C_e\|\ M)$	$P(C_p\|\ M)$	$P(C_t\|\ M)$	$P(C_w\|\ M)$
K	$P(C_m\|\ K)$	$P(C_e\|\ K)$	$P(C_p\|\ K)$	$P(C_t\|\ K)$	$P(C_w\|\ K)$
τ_{90ON}	$P(C_m\|\ \tau_{90ON})$	$P(C_e\|\ \tau_{90ON})$	$P(C_p\|\ \tau_{90ON})$	$P(C_t\|\ \tau_{90ON})$	$P(C_w\|\ \tau_{90ON})$
τ_{90OFF}	$P(C_m\|\ \tau_{90OFF})$	$P(C_e\|\ \tau_{90OFF})$	$P(C_p\|\ \tau_{90OFF})$	$P(C_t\|\ \tau_{90OFF})$	$P(C_w\|\ \tau_{90OFF})$

Table 5.12 Probability matrix for each of the analytes

In a case where the tested analyte is unknown then to determine which analyte is being tested in a particular test run we take the product of the conditional probability of one of the analytes (or classes in this case) given that we have the respective variable output and the corresponding variable as the weighting factor and then sum up for all

the variables. The analyte or class which has the largest sum is thus taken to be the analyte under investigation. This provides a thorough method for being able to discriminate between the analytes based on statistical evidence calculated from the device output. For example, equations (5.4) and (5.5) can be used to determine whether a result from an unknown analyte run is methanol or ethanol when the device response time is nearly the same. Table 5.12 gives the hypothetical values for the case when in 60% of the cases when the given device magnitude response is 0.03 V the analyte is methanol, otherwise its ethanol. Similarly in this example, in 80% of the cases when the *K* value is 32000 ppm, the analyte is methanol otherwise ethanol. The switch on and switch off times have an equal likelihood for either of the two analytes. The probability matrix for this data can be given as follows:

Variable		C_m	C_e
M	0.03 *V*	0.6	0.4
K	32000 *ppm*	0.8	0.2
τ_{90ON}	400 *sec*	0.5	0.5
τ_{90OFF}	500 *sec*	0.5	0.5

Table 5.13 Example for Linear Discriminant Analysis

$$\boldsymbol{X_m = \left(M * P(C_m|M)\right) + \left(R * P(C_m|K)\right) + \left(\tau_{90ON} * P(C_m|\tau_{90ON})\right) + \left(\tau_{90OFF} * P(C_m|\tau_{90OFF})\right)} \quad (5.4)$$

$$\boldsymbol{X_e = \left(M * P(C_e|M)\right) + \left(R * P(C_e|K)\right) + \left(\tau_{90ON} * P(C_e|\tau_{90ON})\right) + \left(\tau_{90OFF} * P(C_e|\tau_{90OFF})\right)} \quad (5.5)$$

From equation (5.4) we have X_m as 26.0 $\times 10^3$ and X_e as 6.9 $\times 10^3$. Thus, it can be determined that the analyte under investigation is methanol. It is important to note that if the analyte were ethanol which has almost the same τ_{90ON} and τ_{90OFF} times, the values for *K* and *M* and subsequently, the values for the conditional probabilities would have been considerably different, and thus, would have given a higher value for X_e.

5.9. Conclusions

In this chapter the three chemoresistive materials (Au-NT, Au-HDT and Au-MAH) were tested in a ratiometric setup as part of the non-inverting amplifier circuit of the SRL 194 device. Each test device was made with two chemoresistive sensors of the same vapour-sensitive material. The active sensor was exposed directly to the VOC vapours whereas, the passive sensor was coated with a silicone gel. All three devices were tested in the range of 0-5% rh and then at 35-38% rh to observe dependence of device output on humidity presence. All three devices were tested at a device chamber temperature of 30°C. The Au-NT and Au-MAH devices were further tested at a chamber temperature of 40°C. Before starting any analyte tests one Au-NT and one Au-MAH device were tested for over 12 hours to observe any drift from application of a DC voltage. The devices showed a negligible drift effect of 0.01V over the test time period.

Langmuir fitted plots, and where necessary linear regression plots, were drawn for the test results of all the devices. For each of the analytes a straight line fit rather than a convergence curve for a particular value of Δrr meant a longer time for the device to reach its equilibrium value. Two kinds of equilibria were required to be reached. The first one is the equilibrium between the rates of sorption and desorption of the analytes at individual chemoresistive sensor surfaces. The second equilibrium is between the rates of adjustment of the active sensor resistance relative to the passive senor resistance.

As observed in chapter 4 the passive sensors took a slightly longer time to respond to an analyte and to reach the equilibrium value at a certain concentration compared with the active device. This was due to the silicone coating on the passive sensors which delayed the contact time to the sensitive film by approximately 10 seconds for the alcohols. The combination of the active and silicone coated passive sensors was expected to reduce drift and ageing effects while giving a lower magnitude output for the devices.

The Au-NT hydrophobic material showed a result comparable with the singular passive device result seen in chapter 4 for ethanol. The results for propan-1-ol and toluene showed a reduction in net response of 30% and 50%, respectively, at 0% rh. The Au-HDT showed four-fold increase to the response for toluene vapour, compared with the Au-NT results. The highest $|\Delta rr|$ value was observed for toluene, followed by

propan-1-ol, ethanol, methanol and then water. However, the propan-1-ol showed a lower net $|\Delta rr|$ value than ethanol at the lowest exposure concentrations. The hydrophilic Au-MAH material showed a 100% increase in the $|\Delta rr|$ response to alcohols and a 20% reduction in the response results to toluene when compared with the Au-HDT results. A linearization of the response results to propan-1-ol was observed for all three films materials as a result of the equilibrium dynamics of the active and passive sensor resistance shifts. In case of the Au-MAH devices it was also observed that devices made from chemoresistive sensors of ~105 kΩ ± 15%, showed twice the $|\Delta rr|$ response to ethanol and toluene at 0%rh as well as 38% rh, as compared to test devices made from sensors of 55 kΩ ± 10%.

Comparison of the temperature dependence results of the Au-NT and Au-MAH materials when tested at 30°C and then at 40°C showed a reduction of 2.5×10^{-3} $|\Delta rr|$ units for ethanol and toluene with Au-NT material and a reduction of 2.5 and 5×10^{-3} $|\Delta rr|$ units for ethanol and toluene respectively for the Au-MAH material at 0-5% rh. At 35-38% rh, a greater reduction in the net $|\Delta rr|$ value was observed with increasing analyte concentration due to the competition between water and analyte vapour for sorption sites on the chemoresistive material.

An analysis of the device response curves was also carried out to observe any distinguishing factors between the analyte vapours for the three materials. It was observed that the response rates and magnitude responses for the individual analytes could be used as identifying factors for the analytes. The response time was noted to be fairly long (usually between 200 to 800 seconds) which made these devices unsuitable for rapid detection uses. However, these devices could still be used where the changes in conditions were expected to occur over a longer period and a long term monitoring device was required.

In the following chapter bi-variate duo-type ratiometric device test results are analysed and explained. These devices are formed by combining a non-polar and a polar chemoresistive sensor material in ratiometric arrangement in one test device.

5.10. References

Chiang, Y-C, Chiang, P-C & Huang, C-P 2001, 'Effects of pore structure and temperature on VOC adsorption on activated carbon', vol. 39, no. 4, pp. 523-34.

Chuang, CL, Chiang, PC, Chang, EE & Huang, CP 2003, 'Adsorption--Desorption Rate of Nonpolar Volatile Organic Compounds onto Activated Carbon Exemplified by C[sub 6]H[sub 6] and CCl[sub 4]', *Practice Periodical of Hazardous, Toxic, and Radioactive Waste Management*, vol. 7, no. 3, pp. 148-55.

Joseph, Y, Besnard, I, Rosenberger, M, Guse, B, Nothofer, HG, Wessels, JM, Wild, U, Knop-Gericke, A, Su, DS, Schlogl, R, Yasuda, A & Vossmeyer, T 2003, 'Self-assembled gold nanoparticle/alkanedithiol films: Preparation, electron microscopy, XPS-analysis, charge transport, and vapor-sensing properties', *Journal of Physical Chemistry B*, vol. 107, no. 30, pp. 7406-13.

Joseph, Y, Guse, B, Yasuda, A & Vossmeyer, T 2004, 'Chemiresistor coatings from Pt- and Au-nanoparticle/nonanedithiol films: sensitivity to gases and solvent vapors', *Sensors and Actuators B: Chemical*, vol. 98, no. 2-3, pp. 188-95.

Joseph, Y, Krasteva, N, Besnard, I, Guse, B, Rosenberger, M, Wild, U, Knop-Gericke, A, Schlogl, R, Krustev, R, Yasuda, A & Vossmeyer, T 2004, 'Gold-nanoparticle/organic linker films: self-assembly, electronic and structural characterisation, composition and vapour sensitivity', *Faraday discussions*, vol. 125, pp. 77-97; discussion 9-116.

Pang, P, Guo, J, Wu, S & Cai, Q 2006, 'Humidity effect on the dithiol-linked gold nanoparticles interfaced chemiresistor sensor for VOCs analysis', *Sensors and Actuators B: Chemical*, vol. 114, no. 2, pp. 799-803.

Vossmeyer, T, Joseph, Y, Besnard, I, Harnack, O, Krasteva, N, Guse, B, Nothofer, HG & Yasuda, A 2004, 'Gold-nanoparticle/dithiol films as chemical sensors and first steps towards their integration on chip', *Physical Chemistry of Interfaces and Nanomaterials Iii*, vol. 5513, pp. 202-12.

Weiss, SM & Kulikowski, CA 1991, *Computer Systems that Learn*, Morgan Kaufmann Publishers, Inc.

CHAPTER 6

6. Characterization of Duo-type Ratiometric Chemoresistive Devices

6.1. Introduction

The 'duo-type' ratiometric devices discussed in this chapter were constructed with one polar chemoresistive sensor and one non-polar chemoresistive sensor. The three chemoresistive materials (Au-NT, Au-HDT and Au-MAH) used to make these ratiometric devices were individually characterized in chapter 4. In this chapter these chemoresistive materials are tested in ratiometric pairs of polar (Au-MAH) and non-polar (Au-HDT and Au-NT) materials. Three different pair arrangements of these materials were tested. Active/Passive pairs of Au-MAH/Au-NT, Au-MAH/Au-HDT, and Au-HDT/Au-MAH, respectively, have been tested and analysed. Unlike in chapters 4 and 5, the passive sensor in each duo-type hybrid devices was not encapsulated in the silicone sealant and the term merely reflects the position of the sensor in the device.

It was expected that two sensor materials with similar sensitivities to a specific analyte would result in a reduced or nearly net zero resistance ratio change (Δrr) as the increase in the resistance of the active resistor would be equalled, or nearly matched, by the increase in resistance of the passive resistor. On the other hand, any differences in the sorption properties of the active and passive resistors would be amplified through the ratiometric ASIC circuitry. The Δrr values calculated in this chapter represent the 'real' value (i.e. including negative values) as opposed to the magnitude response as shown in the previous chapters. The reason for this is that as the response of these duo-type devices depends on the adsorption characteristics of the individual sensors, some devices may show a shift from a net positive Δrr value at low concentrations to a net negative value at higher concentrations of the analyte or vice versa. This quality is expected as the sorption rates differ at different concentration levels of the VOC vapours. The ageing effects of the chemoresistors were expected to be cancelled out as the test devices were assembled from chemoresistors belonging to the same production batch. They would also see the same humidity, and as long as their response was linearly correlated, then this effect would also be cancelled out.

6.2. Characterization of the Au-MAH/Au-NT Hybrid Device

The Au-MAH/Au-NT devices had the polar hydrophilic Au-MAH material in position of the active resistor and the non-polar hydrophobic Au-NT material as the passive resistor of the non-inverting amplifier circuit of the ASIC (SRL device 194). The resistance ratio (*rr*) of the test devices was in the range of 1.00 to 1.10 with active and passive resistances in the range of 70-75 kΩ and 65-70 kΩ, respectively. The devices were tested at six different concentrations of ethanol and toluene at approximately 2% rh and then again at approximately 38% rh. The tests were first carried out at a chamber temperature of 30°C and then repeated at 40°C.

Ethanol		Toluene	
Flow Rates mln/min	**Concentrations (ppm)**	**Flow Rates mln/min**	**Concentrations (ppm)**
15	805	15	442
21	1127	21	619
30	1610	30	884
66	3542	66	1946
99	5312	99	2918
141	7566	141	4156

Table 6.1 VOC flow rates and exposure concentrations for Au-MAH/Au-NT device tests

Table 6.1 shows the concentration determining flow rates and VOC concentrations at which the test devices were exposed to the VOC vapour. The devices were exposed to the above VOC concentrations for a period of 20 minutes and then exposed to only the carrier gas for 20-25 minutes during which the chemoresistors were able to return to their baseline resistances.

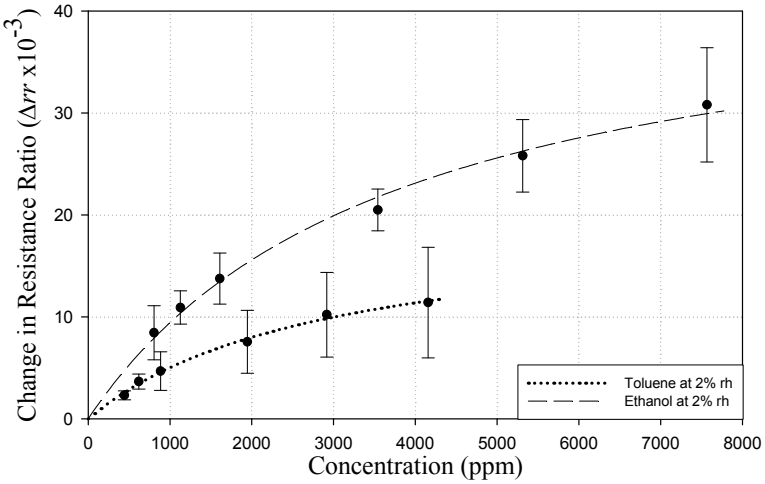

Figure 6.1 Response of an Au-MAH/Au-NT device to toluene and ethanol vapour in air at 30°C and 2% rh

Figure 6.1 shows the characteristic Langmuir model fitted plot of the Au-MAH/Au-NT device when exposed to ethanol and toluene vapour at 30°C and ~2% rh. In chapter 4, it was observed that the Au-MAH material's response to ethanol vapour was nearly 3 times the Au-NT response at 8089 ppm and almost 4 times at the lowest exposure concentration of 728 ppm as a result of the polar nature of the Au-MAH film material. During exposure to toluene vapour, the Au-MAH material had shown a nearly 50% higher response than the Au-NT material. These characteristics led to net positive Δ*rr* values calculated for the Au-MAH/Au-HDT duo-type devices and the response observations are tabulated in table 6.2 below.

Test Results for Au-MAH/Au-NT Duo-type Devices					
VOC	**Concentrations (ppm)**	**ΔV_{out} (V)**	**Δ*rr* (x10^{-3})**	**± σ (x10^{-3})**	**Initial Pre-test Values**
Ethanol Exposure Test	805	0.072	8.44	2.083	*rr* = 1.1
	3542	0.174	20.50	1.416	
	7566	0.261	30.80	2.093	
Toluene Exposure Test	442	0.020	2.30	0.323	*rr* = 1.1
	1946	0.064	7.56	0.612	
	4156	0.096	11.40	1.373	

Table 6.2 Response of Au-MAH/Au-NT devices at 30°C and 2% rh

As the Au-MAH material is more responsive than the Au-NT material to ethanol and toluene vapour, the net Δ*rr* is positive for all exposure concentrations of the

VOCs. Compared to the Au-MAH device in chapter 4, a reduction in the magnitude Δrr value is observed as a result of the increase in resistance of the passive resistor sensor. As the relative resistance increase of the passive resistor is less than that the resistance increase of the active resistor due to the respective adsorption properties of the materials, the net Δrr is positive. The duo-type device response value is between 30-50% of the Δrr value for Au-MAH for exposure to ethanol and 25% for exposure to toluene vapours. The response values are almost the same as compared to Au-NT response to ethanol and 30% lower as compared to the same material's response to toluene. The larger reduction in exposure to toluene occurs as the two constituent materials of the duo-type device have a nearly comparable response rate to this VOC vapour when tested in mono-type or individual chemoresistive sensor setups.

VOC	α ($x10^{-3}$)	K (ppm) ($x10^{4}$)
Ethanol	44.7	3.740
Toluene	19.7	2.917

Table 6.3 Constants of the Au-MAH/Au-NT Langmuir plots at 30°C and 2% rh

The resulting difference from this can be observed in figure 6.1 where the toluene response curve is at almost 50% the value of the ethanol response curve. Comparing this with the Au-MAH active device response curves in figure 4.14 the advantage of utilizing the Au-NT sensor's characteristics in combination with the Au-MAH material are obvious. The Au-NT sensor results in section 4.3.1 show an overlap in the ethanol and toluene results which was avoided in this duo-type device by combining it with the Au-MAH material to make one device. The Au-NT sensor in the duo-type device separates the response curves of the Au-MAH device at the cost of a reduction in magnitude response. The regression constants for the Langmuir fit are given in table 6.3 for the respective analytes. The large K value suggests a small change in the resistance ratio and thus a smaller magnitude response.

6.2.1. Dependence on Humidity

The Au-MAH/Au-NT test devices were exposed to six concentrations of ethanol and toluene vapour in air at ~2% rh and then again at ~38%rh at 30°C. The tests were repeated at 40°C to observe any changes in the device output dependent on

temperature. Figures 6.2 (a) and (b) show the effect of an increase in the relative humidity content of the exposing vapour.

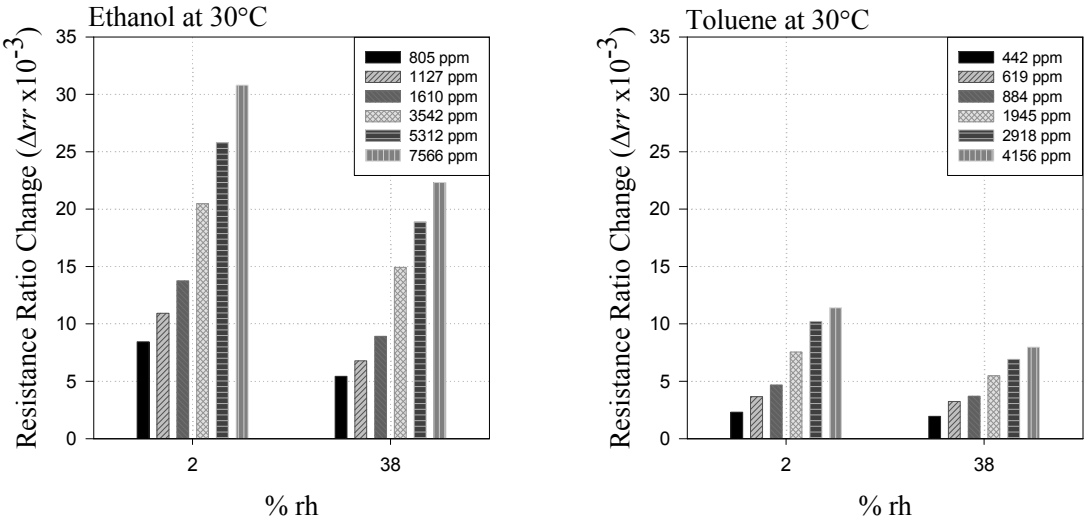

Figure 6.2 Change in resistance ratio (Δ*rr)* of Au-MAH/Au-NT with respect to change in rh at 30°C. (a) Response to ethanol, (b) Response to toluene

From the figures above it can be scene that at higher relative humidity the magnitude response of the duo-type device reduces by almost 25% on average. The loss in magnitude response is more prominent at higher concentrations of the analyte.

The Au-NT device is known to be hydrophobic from the test results in chapter 5 and as reported by Joseph et al. (Joseph et al., 2004). The Au-MAH device is known to have a lower affinity for toluene and a higher affinity for alcohols and water as compared to the Au-NT material (Vossmeyer et al. 2004). Thus, the drop in magnitude response at the higher humidity occurs as a result of two mechanisms. Firstly, the increase in resistance of the passive chemoresistor reduces the magnitude effect of the response generated by the active chemoresistor. Secondly, there is higher competition between the water molecules and the VOC molecules for binding sites on the chemosensors' surfaces. In the scenario tested here, the large VOC molecules at 38% rh have to occupy the same sites on the sensor surfaces as the water molecules. The water molecules generating the humidity have an advantage as the baseline value of the devices was determined once the testing environment had been stabilised at 38% rh. Thus, the water molecules had occupied most of the binding sites by the time the test analyte was introduced to the test environment. All Δ*rr* calculations at ~38% rh exclude

the initial baseline jump from 0% rh to 38% rh values and only show the change in resistance ratio values between the 38% rh baseline value and the analyte saturation value at any particular test concentration. This effect reduces the Δ*rr* value sensitivity at higher relative humidity.

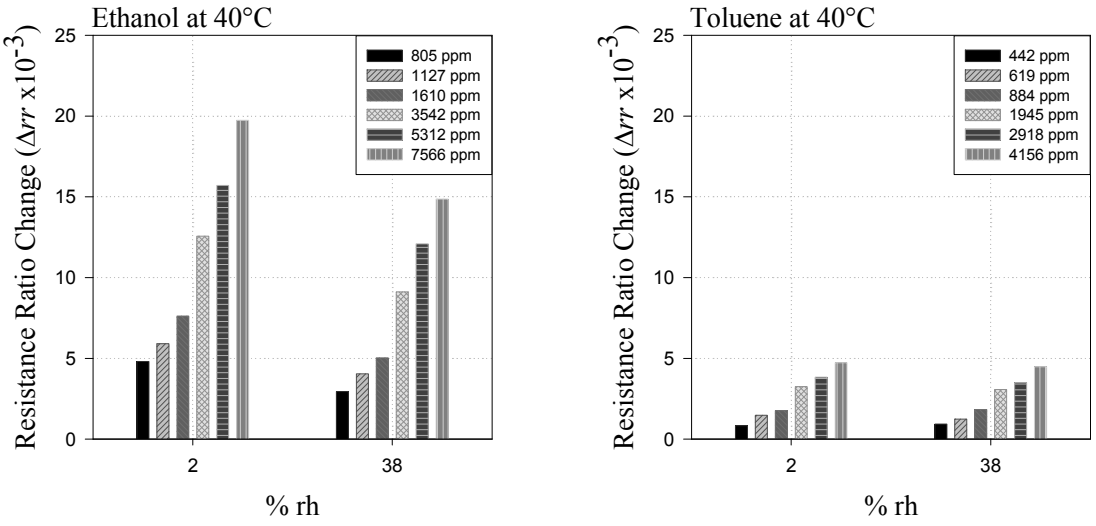

Figure 6.3 Change in resistance ratio (Δ*rr*) of Au-MAH/Au-NT with respect to change in rh at 40°C. (a) Response to ethanol, (b) Response to toluene

The drop in magnitude response at higher humidity is not as dramatic as for the mono-type ratiometric Au-MAH devices discussed in chapter 5. The Au-NT passive sensor is able to reduce the magnitude response reduction that occurs due to the presence of humidity. This stabilising effect is observed even more when the devices are tested at 40°C as shown in figure 6.3. The effect occurs at the cost of lower magnitude response to the VOC vapour. The Au-MAH chemoresistive sensor's affinity for polar molecules is able to shift the net Δrr value in the positive direction. In the mono-type Au-MAH devices the reduction in response was almost 50% at the highest concentrations at 30°C. In the duo-type case, the reduction is about 30%. It will be seen in the following subsection, that the rise in operating temperature results in a drop in magnitude response as well.

6.2.2. Dependence on Temperature

The tests for the Au-MAH/Au-NT duo-type devices for response to ethanol and toluene vapours at 2% rh and 38% rh were repeated at 40°C to observe any effects of the increase in temperature on device response. Figures 6.4 and 6.5 show the change in response of the Au-MAH/Au-NT devices between 30°C and 40°C at ~2% rh and ~38% rh respectively. The trend shows a reduction in device Δ*rr* value output of approximately 35% for ethanol and 50% for toluene on average with the temperature increase to 40°C.

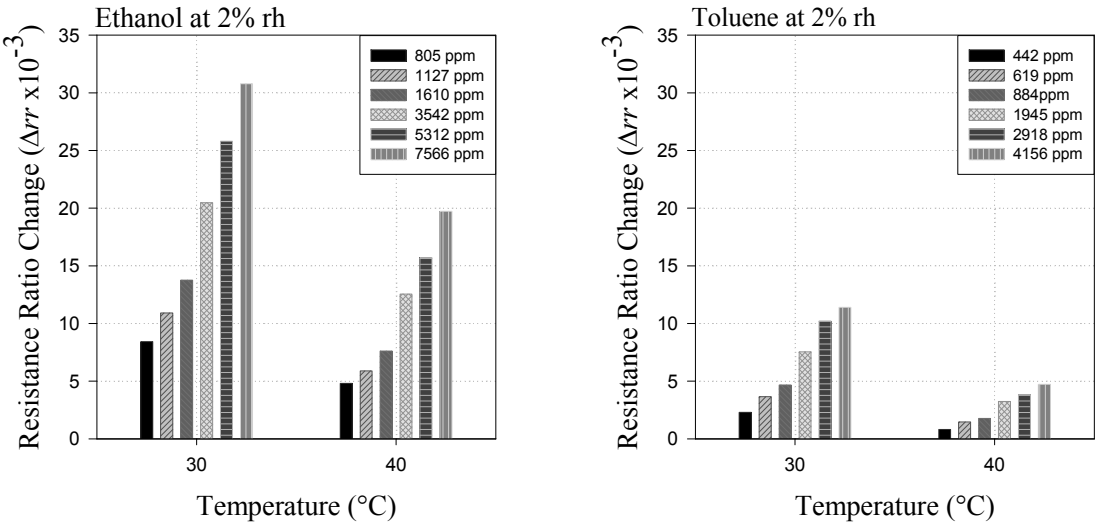

Figure 6.4 Change in resistance ratio (Δ*rr*) of Au-MAH/Au-NT with respect to change in temperature at 2% rh. (a) Response to ethanol, (b) response to toluene

As with the humidity tests, the devices were stabilised at 40°C for several hours before they were exposed to the test analytes. The response was measured from the baseline stabilised at 40°C and then compared with the results obtained for the same concentration exposure at 30°C. Using this method the changes in the resistance of the data acquisition PCB and cables is eliminated. The reduction in magnitude response is observed to be stronger at higher analyte concentrations as can be seen by the bar charts. Hence, it can be said that the reduction in response (Δ*rr*) to an increase in temperature is directly related to the changes in VOC concentration. Figure 6.5 shows the effect of temperature at ~38% rh. The effect is similar to that at 2% rh suggesting that the change

in humidity is a less significant factor in terms of response dependence as compared to the change in temperature.

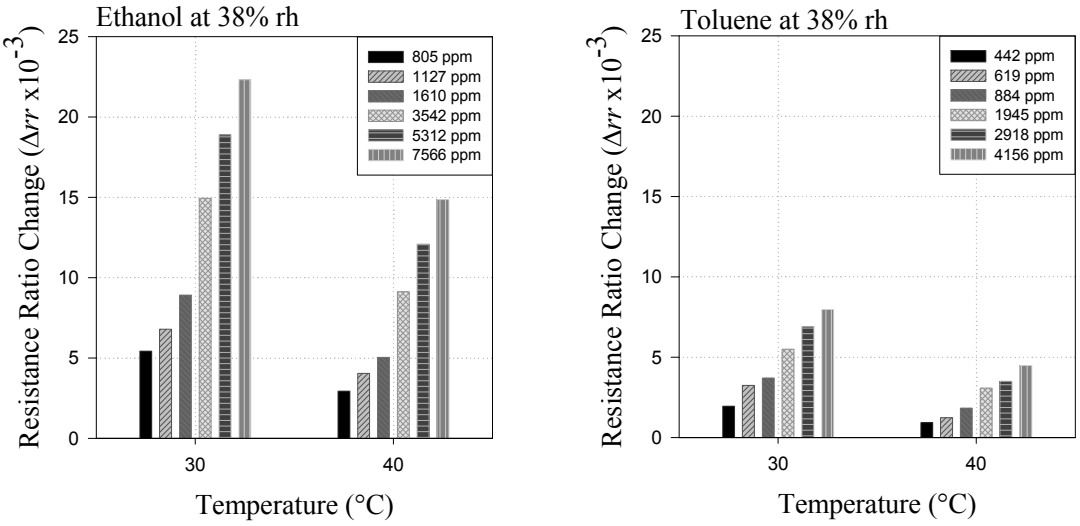

Figure 6.5 Change in resistance ratio (Δ*rr*) of Au-MAH/Au-NT with respect to change in temperature at 38% rh. (a) Response to ethanol, (b) Response to toluene

6.3. Characterization of the Au-MAH/Au-HDT Hybrid Device

The Au-HDT material replaces the Au-NT material as the passive sensor for the devices tested in this section. The Au-HDT material has a 16 unit alkylene chain length as compared to the Au-NT material, which have a chain length of 9 units. The effects of this change were discussed in chapters 4 and 5 whilst characterizing devices based on individual sensors and mono-type ratiometric devices. Recalling from chapter 4 this material has a higher affinity for toluene vapour with a 100% increase in Δrr values and a 30% lower response rate for methanol.

Duo-type devices of the formation of Au-MAH/Au-HDT are tested at 30°C here. The test devices are exposed to three VOCs and are tested at three concentrations of the analytes at 0% rh. The respective test analyte flow rates and concentrations are given in table 6.4 (a). These analyte concentrations were first increased in the given order and then stepped down in the reverse order. The resulting static outputs are shown in figure 6.6 with the error bars showing the difference between test results when concentrations were being increased and then later decreased. The standard deviations between the results are given in table 6.6. Propan-1-ol and toluene were tested at 38% rh and the respective flow rates and concentration are given in table 6.4 (b). The plots shown here are a Langmuir fit to the data.

Methanol		Ethanol		Water	
Flow rates (ml/min)	**Concentrations (ppm)**	**Flow rates (ml/min)**	**Concentrations (ppm)**	**Flow rates (ml/min)**	**Concentrations (ppm)**
13	1817	13	789	14	327
76	10622	78	4732	83	1941
138	19288	143	8675	150	3507

Table 6.4(a) VOC flow rates and exposure concentrations for Au-MAH/Au-HDT device tests

Propan-1-ol		Toluene	
Flow rates (ml/min)	**Concentrations (ppm)**	**Flow rates (ml/min)**	**Concentrations (ppm)**
16	301	12	386
94	1768	74	2381
170	3198	134	4312

Table 6.4(b) VOC flow rates and exposure concentrations for Au-MAH/Au-HDT device tests

Figure 6.6 shows the test results for ethanol, methanol and water at 30°C and 0% rh. The active/passive resistance values were 120/100 kΩ. The Δ*rr* values are positive for all the analytes as the Au-MAH active chemoresistor changes its resistance more than the Au-HDT chemoresistor. This was the expected result from the analysis in chapter 4. The figure shows that water and ethanol reach saturation much quicker than methanol. Ethanol also has a higher response than water. This is reflected in the high *K* values given in table 6.5.

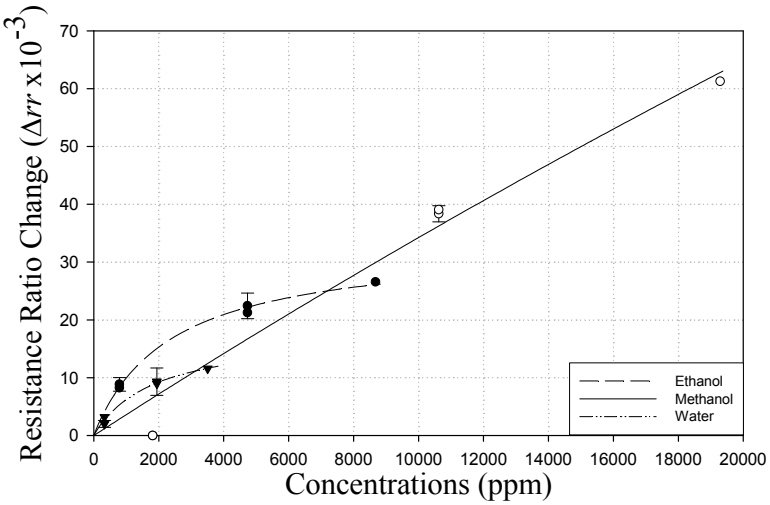

Figure 6.6 Response of an Au-MAH/Au-HDT devices to ethanol, methanol and water vapour at 30°C and 0% rh

VOC	α (x10^{-3})	K (ppm) (x10^{3})
Methanol	615.5	169.795
Ethanol	33.2	2.339
Water	17.8	1.871

Table 6.5 Constants of the Au-MAH/Au-HDT Langmuir plots at 2% rh

The reason behind the higher response rate and a lower saturation rate for methanol is that the Au-MAH has a higher response rate than the Au-HDT device for this analyte leading to a net higher response rate of the duo-type device. Thus, the device makes use of the difference between the response rates of the two constituent chemoresistors to give a distinctive result. The property of the slower saturation rate is carried forward from the individual sensors where the smallest alcohol analyte had the smallest saturation rate. Table 6.6 gives the response values at specific concentrations of the three analytes.

	Test Results for Au-MAH/Au-HDT Duo-type Devices				
VOC	**Concentrations (ppm)**	**ΔV_{out} (V)**	**Δrr (x10^{-3})**	**$\pm \sigma$ (x10^{-3})**	**Initial Pre-test Values**
Methanol Exposure Test	1817	0.00	0.00	0.000	*rr* = 1.2
	10622	0.325	38.4	0.501	
	19288	0.519	61.3	0.000	
Ethanol Exposure Test	789	0.075	8.86	0.417	*rr* = 1.2
	4732	0.190	22.4	0.835	
	8675	0.225	26.6	0.000	
Water Exposure Test	327	0.017	2.01	0.835	*rr* = 1.2
	1941	0.079	9.33	0.250	
	3507	0.098	11.6	0.000	

Table 6.6 Response of Au-MAH/Au-HDT devices at 2% rh

6.3.1. Dependence on Relative Humidity

The Au-MAH/Au-HDT duo-type devices were tested at 38% rh against vapour concentrations of methanol, propan-1-ol and toluene. Table 6.7 summarises the results obtained for three specific concentrations of the analytes. In these results propan-1-ol shows a unique behaviour.

	Test Results for Au-MAH/Au-HDT Duo-type Devices				
VOC	**Concentrations (ppm)**	**ΔV_{out} (V)**	**Δrr (x10^{-3})**	**$\pm \sigma$ (x10^{-3})**	**Initial Pre-test Values**
Methanol Exposure Test	1817	0.02	2.66	1.044	rr = 1.2
	10622	0.28	33.1	5.176	
	19288	0.40	47.2	0.000	
Propan-1-ol Exposure Test	301	0.03	3.54	0.000	rr = 1.2
	1768	0.10	11.8	2.087	
	3198	0.04	4.72	0.000	
Toluene Exposure Test	386	-0.08	-8.86	7.931	rr = 1.2
	2381	-0.35	-41.3	14.20	
	4312	-1.12	-132.2	0.000	

Table 6.7 Response of Au-MAH/Au-HDT devices at 38% rh

The Δrr response for propan-1-ol increases initially and at the highest exposure concentration it falls. This can be explained by re-examining the results of the relevant materials analysed in chapter 4. Propan-1-ol has significantly different adsorption rates for the Au-MAH and Au-HDT materials. The propan-1-ol response to Au-MAH is thrice in magnitude to the Au-HDT response and reduces to only twice in magnitude at the higher concentration. At the highest concentration the Δrr response to propan-1-ol given by Au-MAH is much higher than Au-HDT. But the reduction in response of the hydrophilic Au-MAH caused by the presence of the water vapours causes the response value to change in direction at the highest concentration. This is because the Au-MAH is overwhelmed by the presence of the presence of the water vapours whereas, the Au-HDT material is hydrophobic. This effect creates a large separation between the response rates for methanol and propan-1-ol as can be seen in figure 6.7.

Table 6.8 shows the constants of the Langmuir fit to the data. The nature of the dynamics between the active and passive sensors meant that the data for propan-1-ol and toluene could not be fit to a Langmuir model. A quadratic equation fit, in equation (6.1), was plotted for these analytes and their constants and coefficients represented in table 6.8.

$$\Delta rr = \Delta rr_0 + LC + MC^2 \tag{6.1}$$

Here Δrr_0 is the error at the origin, and L and M are equation constants reflecting the rate of response per unit analyte vapour concentration. As the net Δrr

output is negative a negative value for either *L* or *M* suggests greater dominance of the passive chemoresistor. This explains the toluene response. From results in chapter 4 it is known that the Au-HDT material has twice the response magnitude of the Au-MAH sensor material. As the Au-HDT chemoresistor forms the passive resistor in the duo-type arrangement under discussion the net effect is a negative increase in the response with increasing exposure concentrations of the analyte. Furthermore, the results showed an exponential negative increase in the Δrr value with increasing VOC concentration as can be seen in figure 6.7. This exponential increase occurs as the ratio of the relative resistance value increase of the Au-HDT chemoresistor compared to the Au-MAH increases with increasing concentrations of the analyte.

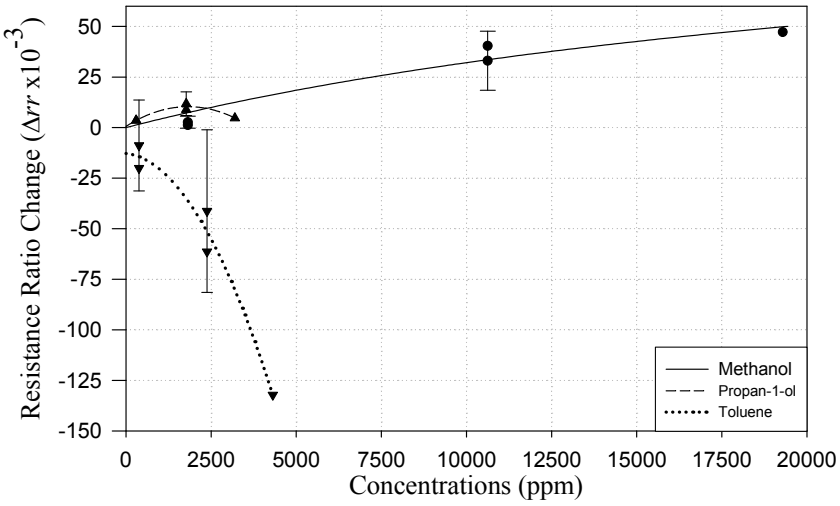

Figure 6.7 Response of an Au-MAH/Au-HDT devices to methanol, propan-1-ol and toluene vapour at 30°C and 38% rh

VOC			
Methanol (Langmuir fit)	α = 123.1 x10^{-3}	**K (ppm)** = 28.36 x10^{3}	
Propan-1-ol (Quadratic fit)	Δrr_0 = 0.579 x10^{-3}	**L (ppm^{-1})** = 10.73 x10^{-6}	**M (ppm^{-2})** = -2.95 x10^{-9}
Toluene (Quadratic fit)	Δrr_0 = 12.8 x10^{-3}	**L (ppm^{-1})** = -2.001 x10^{-6}	**M (ppm^{-2})** = -5.958 x10^{-9}

Table 6.8 Constants of the Au-MAH/Au-HDT plots at 38% rh

Comparing the device results for exposure to methanol at 0% rh and then at 38% rh the duo-type device showed remarkable stability. At the lowest exposure

concentration at 0% rh the device had shown no response to the analyte vapour. However, at higher analyte concentrations a slight decrease in magnitude response was observed with increase in concentration. However, the fall in magnitude response was limited to about 20%. Figure 6.8 shows the dependence of the device magnitude response on the presence of humidity. This decrease in magnitude response occurs as the vacant sorption sites on the Au-MAH sensor surface get occupied with water vapour sensors and the Au-NT sensor increases in resistance pulling down the net magnitude of the response. However, the binding forces on the Au-MAH surface between the analyte and the sensor material are strong enough to keep the response on the positive side. This suggests a relatively greater change in the Au-MAH resistance than the Au-HDT resistance as expected from results in chapter 4.

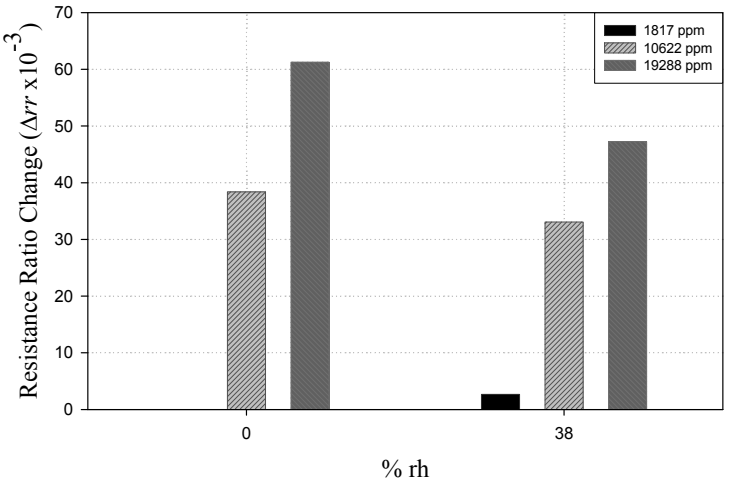

Figure 6.8 Change in resistance ratio (Δrr) response to methanol with respect to change in rh at 30°C.

6.4. Characterization of the Au-HDT/Au-MAH Hybrid Device

The third arrangement of the duo-type devices tested employed the Au-HDT chemoresistor as the active resistor and the Au-MAH resistor as the passive resistor in a ratiometric arrangement with the SRL 194 ASIC chip. All the tests were carried out at 30°C. The devices were initially tested at 0% rh against ethanol, methanol, propan-1-ol, toluene and water. The test concentrations are given in table 6.9.

Methanol	Ethanol	Propan-1-ol	Toluene	Water
Concentrations (ppm)	Concentrations (ppm)	Concentrations (ppm)	Concentrations (ppm)	Concentrations (ppm)
1817	789	301	386	327
2313	1025	1768	2381	1941
10622	4732	3198	4312	3507
13524	6152			
19288	8675			
24556	11280			

Table 6.9 Exposure concentrations for Au-HDT/Au-MAH device tests at 0% rh

As this arrangement of the duo-type device simply reverses the active and passive chemoresistor sensor positions discussed in the previous section, the characteristic plots were expected to show the exact opposite properties as observed for the Au-MAH/Au-HDT device. Hence, a positive net response instead of a negative one for toluene and a negative net response result for ethanol, methanol and water was expected. The devices were tested at 0% rh for their response to all five analyte vapours. The resulting Langmuir fit characteristic plots are given in figure 6.9.

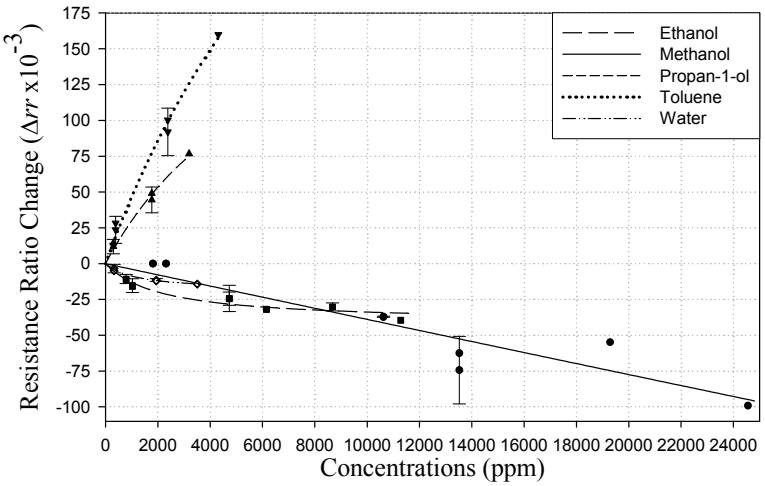

Figure 6.9 Characteristic plot of Au-HDT/Au-MAH devices for exposure to ethanol, methanol, propan-1-ol, toluene and water at 30°C and 0% rh

For the Au-MAH/Au-HDT arrangement only ethanol, methanol and water were tested at 0% rh. Comparing these plots for the two devices it can be seen that the Au-HDT/Au-MAH device gives the x-axis reflection of the results obtained for the Au-MAH/Au-HDT device. The Δ*rr* values at particular exposure concentrations are given in table 6.10. This behaviour is similar to what was expected for the ethanol, methanol and water vapour analytes. Toluene and propan-1-ol were only tested at 38% rh for the Au-MAH/Au-HDT, where toluene gave an exponential negative increase in Δ*rr* values with increasing analyte concentration. In the Au-HDT/Au-MAH 0% rh tests, the data for all the different analytes moves towards saturation rather than increase exponentially and is a perfect Langmuir fit.

Test Results for Au-HDT/Au-MAH Duo-type Devices					
VOC	**Concentrations (ppm)**	**ΔV_{out} (V)**	**Δrr ($x10^{-3}$)**	**$\pm \sigma$ ($x10^{-3}$)**	**Initial Pre-test Values**
Methanol Exposure Test	1817	0.00	0.00	0.000	*rr* = 1.07
	10622	-0.31	-37.1	0.167	
	19288	-0.46	-54.9	8.348	
Ethanol Exposure Test	789	-0.09	-10.7	1.174	*rr* = 1.07
	4732	-0.21	-24.4	2.115	
	8675	-0.26	-30.2	1.002	
Propan-1-ol Exposure Test	301	0.10	11.9	1.753	*rr* = 1.07
	1768	0.38	44.5	3.172	
	3198	0.65	76.6	0.000	
Toluene Exposure Test	386	0.20	23.6	3.318	*rr* = 1.10
	2381	0.78	92.0	5.886	
	4312	1.36	160.0	0.000	
Water Exposure Test	327	-0.03	-3.42	1.085	*rr* = 1.07
	1941	-0.10	-11.5	0.417	
	3507	-0.12	-14.3	0.000	

Table 6.10 Response of Au-HDT/Au-MAH devices at 0% rh

The Langmuir coefficients of the plots in figure 6.9 are given in table 6.11. Here it can be seen from the extremely large *K* value for methanol and the negative α coefficient for water, methanol and ethanol, the dominance of the passive sensor over the active one. The constants for propan-1-ol and toluene reflect a higher response result for toluene which has a higher *K* value than propan-1-ol. This also suggests that the Au-HDT active sensor had stronger adsorption of the analytes as compared to the Au-MAH passive sensor.

VOC	α ($x10^{-3}$)	*K* (ppm) ($x10^{3}$)
Methanol (inverted)	-7900	2020
Ethanol (inverted)	-41.1	2.13
Propan-1-ol	243.4	7.13
Toluene	570.4	11.29
Water (inverted)	-18.9	1.17

Table 6.11 Langmuir coefficients of the Au-HDT/Au-MAH plots at 0% rh

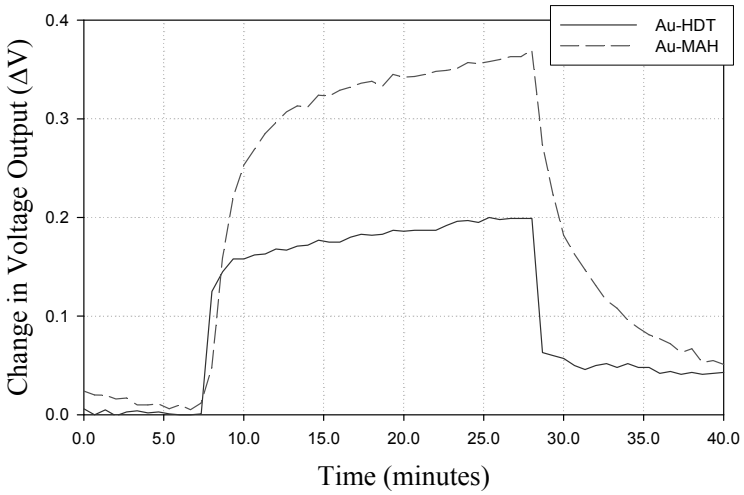

Figure 6.10 Voltage response curves for individual Au-HDT and Au-MAH sensors at 0% rh

When tested with Au-MAH chemoresistors and Au-HDT chemoresistors individually, tests with propan-1-ol gave twice the Δ*rr* output values with Au-MAH as compared with the Au-HDT material. From this it was expected that propan-1-ol should give a net negative result with the Au-HDT/Au-MAH material. However, the results are quite the opposite. The reason for this effect is not completely understood, however, a possible factor could be the rate of adsorption of the two materials. As seen in figure 6.10, the Au-HDT material shows a sharp increase in the voltage response at the start of the exposure, whereas, the Au-MAH response is more gradual. Even though the voltage change and resistance ratio change results are calculated at the end of the exposure cycle, any differences between the net resistance changes is amplified by the SRL 194 ASIC. Analysis of the transient response for propan-1-ol shows a degradation of the signal with propan-1-ol vapour. This degradation is even more pronounced for tests at 38% rh.

The duo-type results for the Au-HDT/Au-MAH device at 38% rh did not satisfy the Langmuir adsorption model. In figure 6.11 the methanol plot is produced by linear regression and the propan-1-ol and toluene plots are quadratic model fits to the data. Table 6.12 gives the respective coefficients of the relevant plots.

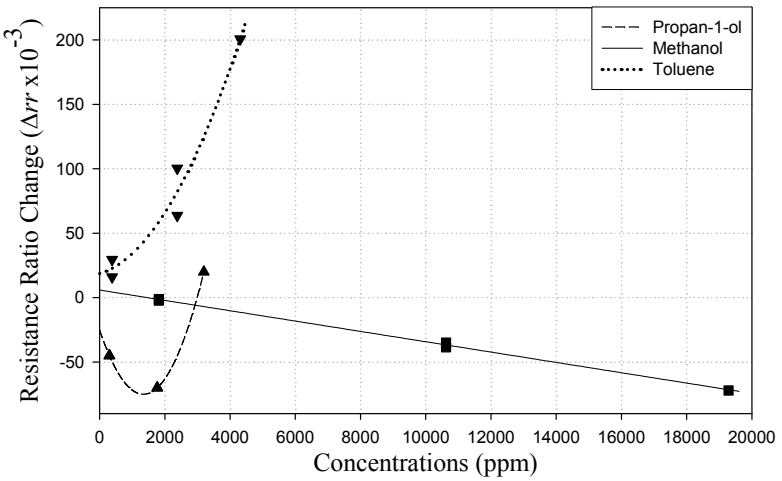

Figure 6.11 Characteristic plot of Au-HDT/Au-MAH devices for exposure to methanol, propan-1-ol and toluene at 30°C and 38% rh

VOC	Coefficients		
Methanol (Linear fit)	Δrr_0 = 5.87 x10^{-3}	$\boldsymbol{L}$ (ppm^{-1}) = -4.01 x10^{-6}	
Propan-1-ol (Quadratic fit)	Δrr_0 = -25.2 x10^{-3}	$\boldsymbol{L}$ (ppm^{-1}) = -0.742 x10^{-6}	$\boldsymbol{M}$ (ppm^{-2}) = 0.276 x10^{-9}
Toluene (Quadratic fit)	Δrr_0 = 18.7 x10^{-3}	$\boldsymbol{L}$ (ppm^{-1}) = 7.3768 x10^{-6}	$\boldsymbol{M}$ (ppm^{-2}) = 8.0785 x10^{-9}

Table 6.12 Coefficients of the Au-HDT/Au-MAH plots at 38% rh

As with the device results at 0% rh, it can be seen that these results are x-axis reflection of the Au-MAH/Au-HDT device results at 38% rh for exactly the same reasons. The toluene and propan-1-ol exponential increase occurs as the binding sites on the Au-MAH sensor's surface are already occupied by the water molecules responsible for maintaining higher relative humidity. At 38% rh, the introduction of the toluene and propan-1-ol vapours activates the response from the hydrophobic Au-HDT chemoresistor leading to an exponential increase. The initial drop in the propan-1-ol response till 1756 ppm occurs as the relative change in the resistance of the Au-MAH material exceeds that of the change in resistance of the Au-HDT material. However, this balance is overturned as the analyte concentration is increased. The tests were carried out by stepping up the concentrations in the first instance and then stepping down the exposure concentrations. It was observed that there was negligible hysteresis present in case of all the analytes. From the transient behaviour of the device to propan-1-ol

vapour it is expected that the device would saturate only slightly in the positive. At higher concentrations the competition to pull the dynamic equilibrium by the respective sensors (up for active and down for passive sensor) between the chemoresistors is expected to increase. The *M* coefficients of the quadratic fits have an extremely low value of the order of 10^{-9} which shows the low dependence of the resistance change on the square for the vapour concentration. The relatively larger *L* coefficient for toluene suggests that the behaviour of the device can be approximated to a linear model. Whereas, the negative nature of the *L* coefficient for propan-1-ol gives it a parabolic nature.

6.4.1. Dependence on humidity

The effect of response change between 0% rh and 38% rh was observed whilst keeping the exposure chamber temperature constant at 30°C. Figure 6.13 shows the resulting plots. It was observed that tests with methanol vapour showed no particular effects of humidity on the magnitude response of the device apart from the slight response observable at the lowest concentration of the higher rh. Toluene had a 20-35% reduction in response at the two lower test concentrations. However, at the highest concentration there was a 25% increase in the device response magnitude. Propan-1-ol showed a general decrease in magnitude response. However, this decrease had a range of 75%-250% dependent on the adsorption rate effect discussed earlier, and moved the response from a net positive value at the two lower concentrations to a net negative value.

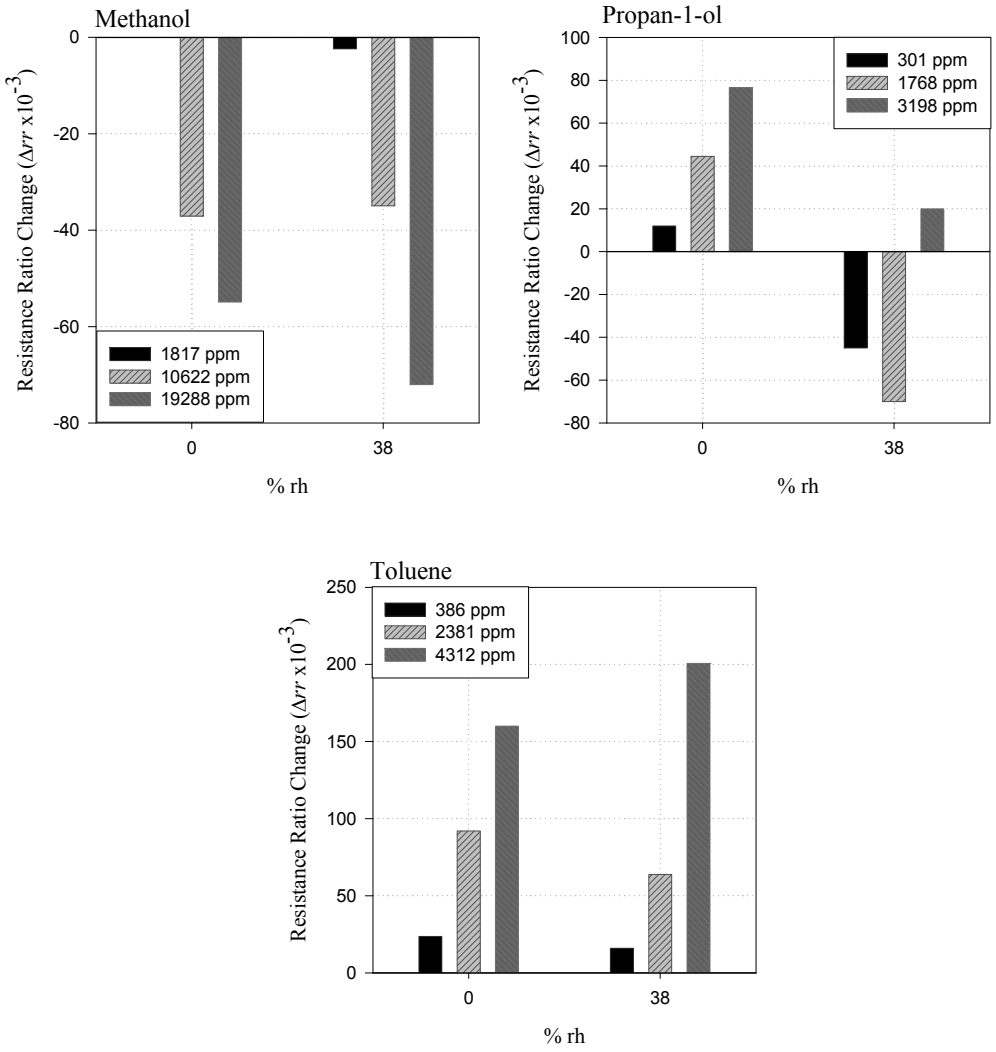

Figure 6.12 Change in resistance ratio (Δ*rr*) to methanol, propan-1-ol and toluene with respect to change in rh at 30°C.

6.5. Response Curve Shape Analysis

As with the mono-type device response curves described in the previous chapter this section analyses the response shapes of three duo-type devices to various VOCs. It is important to remember that in these duo-type devices neither of the resistive sensors had any silicone coating on them and hence, the surface reaction rates and the device response rates were a direct result of the interaction between the vapour molecules and the chemoresistive sensors, unhindered by any partition layer. The final device output indicates the increase in the resistance of the active sensor as a ratio relative to the resistance increase of the passive sensor.

Figure 6.13 a) shows the typical device response to 3542 ppm of ethanol and 1946 ppm of toluene, both resulting from an analyte flow rate of 66 ml/min. The increase in voltage output was a result of the active sensors resistor increasing relatively more than the passive sensor resistance. The response rate characteristics for ethanol and toluene were observed to be similar as the response curves can almost overlap each other. Hence, the device showed very little differentiation between the responses to the two analytes. The active Au-MAH was faster in responding to the analyte vapours at the beginning of the exposure time, making the devices reach a maximum value within 200 seconds of coming into contact with the vapour. As the passive Au-NT sensor did not saturate at this point and continued to adsorb the analyte vapour the result was a slight bulge at the beginning of the exposure time followed by a reduction in the magnitude voltage output as the device moved towards equilibrium. This was where the response curves for the two analytes differed the most. The passive Au-NT sensor increased in resistance (after the initial peak) more for ethanol than for toluene causing a separation between analyte response curves. Equilibrium was reached almost 15 minutes after the start of the device exposure. At the end of the exposure time, there was a sharp peak which was the result of the passive sensor losing the adsorbed vapour much faster than the active sensor initially. An inverted bulge was observed right after the exposure duration finished which lasted for another 15 minutes. The bulge occurred as the active sensor resistance reduced more than the passive sensor and during the rest of these 15 minutes both sensors negotiated with each other to reach the baseline equilibrium value.

Figure 6.13 b) shows the response characteristic of an Au-HDT/Au-MAH based duo-type bi-variate sensor device to methanol, ethanol, propan-1-ol, toluene and water vapours at 10622 ppm (76 ml/min) , 4732 ppm (78 ml/min), 1768 ppm (94

ml/min), 2381 ppm (74 ml/min) and 1941 ppm (83 ml/min) respectively. The results of this duo-type device were distinctly different from those of the Au-HDT monotype device shown in chapter 5 as the voltage output here was split between those analytes that increased the output voltage as the device was exposed to the vapours and those analytes that decreased voltage output as the device was exposed to the vapours. This separation of results between the analytes occurred due to the greater affinity of the Au-HDT material for propan-1-ol and toluene as compared to the Au-MAH material for the same analytes. The opposite was true for methanol, ethanol and water which were more attracted to the polar MAH sensor than the non-polar Au-HDT.

The response to methanol was a reduction in voltage output. The device output voltage changed rapidly (within 120 seconds) for this analyte to 83% of the peak value. After this there was a gradual decrease in output voltage and equilibrium between the active and passive sensors was reached 16 minutes into the exposure routine. Compared to the methanol response ethanol had a much more gradual change in voltage output to the equilibrium value. This was an indication of the growing hold of the active Au-HDT material on the larger alcohol molecules. The time to reach 90% of the maximum magnitude change of device output (τ_{90}) was approximately 400 seconds. The response of the Au-HDT sensor increased relatively more than the Au-MAH material with larger alcohol molecules resulting in a net increase in voltage output with propan-1-ol. The response showed a sharp increase to a maximum value followed by a gradual decrease to an equilibrium value almost 17 minutes into the exposure duration.

The response to the non-polar toluene was observed to have a net increase in voltage output and also showed the largest magnitude response compared to all the other analytes. This outcome was a direct result of the strong binding forces between the non-polar toluene molecule and the hydrophobic Au-HDT film material as shown in chapter 4. The curve showed a smooth increase to the maximum voltage output with τ_{90} being reached in 500 seconds. No significantly large peaks were observed at the beginning or end of the exposure sequence. The device returns to its baseline value in 600 seconds after the analyte vapour was switched off.

The polar water molecule had a greater affinity for the hydrophilic Au-MAH material. Hence, the resulting output was a net decrease in voltage from the device during exposure. There was an initial small peak observed as the Au-HDT responded to the higher humidity content of the exposure air. However, the magnitude of this peak was negligible. The equilibrium value for water was reached fairly quickly compared to

the other analytes (within 200 seconds). The magnitude response for the water vapour concentration was fairly small and showed that the device can cope with testing conditions with higher humidity content.

Figure 6.13 and c) shows the response characteristic of an Au-MAH/Au-HDT bi-variate sensor device. This device basically had the active and passive sensor materials reversed from the test shown in figure 6.13 b). Therefore, the expected outcome was an inverse of the results seen for the Au-HDT/Au-MAH device. Only methanol, ethanol and water were tested at 10622 ppm (76 ml/min), 4732 ppm (78 ml/min) and 1941 ppm (83 ml/min) respectively. The magnitude of the device output was observed to decrease with increasing alcohol molecule size. Methanol response showed a smooth increase to its peak value with τ_{90} reached in less than 400 seconds. As the Au-HDT material began to attract the larger ethanol molecule the result was a much lower magnitude change and twice the time to reach the τ_{90} value. The time taken to return to baseline was observed to be much longer than the Au-HDT/Au-MAH device and was noted to be around 15 minutes for the two alcohols. As with the previously mentioned device, water had a much sharper response time. τ_{90} was reached in almost 50 seconds. The time taken to return to the baseline value was also considerably less than the alcohols at less than 300 seconds.

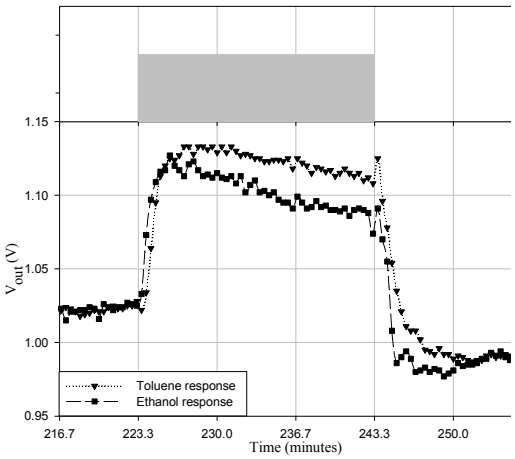

a) Typical response of the Au-MAH/Au-NT device to Toluene and Ethanol

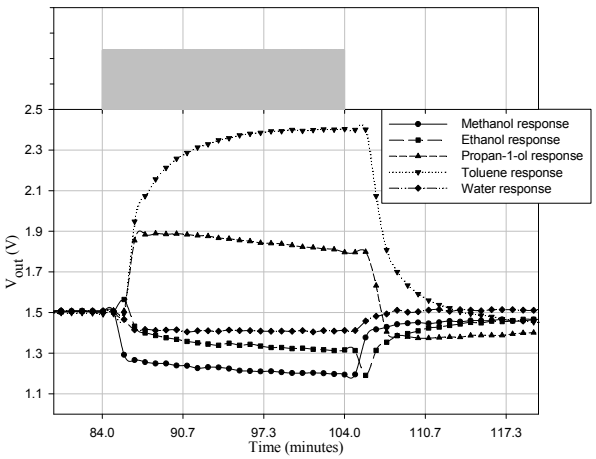

b) Typical response of the Au-HDT/Au-MAH devices to Methanol, Ethanol, Propan-1-ol, Toluene and Water

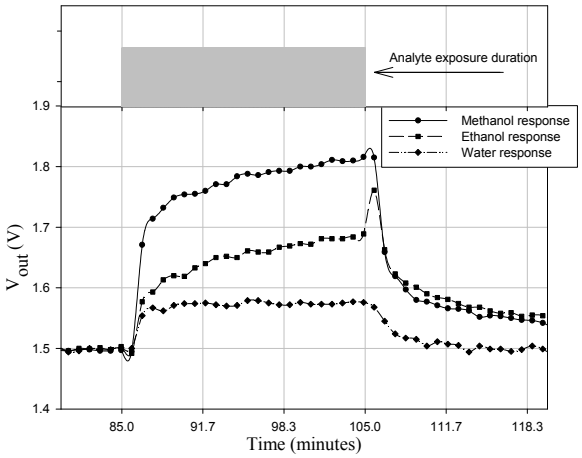

c) Typical response of the Au-MAH/Au-HDT devices to Methanol, Ethanol, and Water

Figure 6.13 Typical responses of various Duo-type Bi-variate Sensor devices to various VOCs at 0%rh and 30°C showing the differences between shapes of the response curves

Linear discriminant analysis, as explained in section 5.8 and equations (5.2) to (5.5) in chapter 5, can also be applied to these duo-type device results. For the case where, the device output during exposure increases during analyte vapour exposure time, equations (5.2) and (5.3) need to be reversed to obtain τ_{90ON} and τ_{90OFF}. A significant difference between the results obtained for these duo-type devices and those for the mono-type devices is that whereas, the voltage output generally tends to be reduced for the bi-variate mono-type devices, these duo-type device results could go either way. This gives the option of pre-classifying the device results into groups of analytes that are likely to cause an increase in voltage output and those that are likely to cause a decrease in voltage output. Once this is known the rest of the calculation to identify the analyte being examined is the same as the example given in equations (5.4) and (5.5). To be able to perform this analysis several runs of the same test with several different test devices are needed for statistical accuracy.

6.6. Conclusion

In this chapter three duo-type arrangements were tested utilizing the combination of one polar material based chemoresistive sensor (Au-MAH) and one non-polar material based chemoresistive sensor (Au-NT and Au-HDT), as the active and passive resistors in the ratiometric setup of the SRL 194 ASIC device. The Au-MAH/Au-NT, Au-MAH/Au-HDT and Au-HDT/Au-MAH device arrangements were tested against increasing concentrations of five different analytes with at ~0% rh and at ~38% rh.

The Au-MAH/Au-NT device showed improved separation between the toluene and ethanol plots allowing better identification of the analytes as compared to just the Au-MAH or the Au-NT chemosensors on their own. A ~30% fall in magnitude response was observed when tested at 38% rh. By increasing the operating temperature from 30°C to 40°C the impact of humidity was reduced to a 20% fall for ethanol and almost negligible for toluene.

Au-MAH/Au-HDT devices were tested against ethanol, methanol and water at 0% rh and methanol and propan-1-ol at 38% rh. It was observed that water and ethanol had a lower net Δrr response but a faster rate of saturation than methanol. The devices when exposed to propan-1-ol vapour at 38% rh showed an initial increase in Δrr response but as the exposure concentration was increased, the increase in the Au-HDT device resistance resulted in a net decrease in the total device output.

The Au-HDT/Au-MAH devices gave a response which was the x-axis reflection of the Au-MAH/Au-HDT devices. It was observed that the Au-HDT device was not able to pull down the propan-1-ol response into the negative despite having a greater percentage resistance change to the analyte than Au-MAH when tested individually with this analyte. With the introduction of water vapour to increase relative humidity to 38% rh, it was observed that the toluene response which had moved towards saturation and gave a perfect Langmuir fit at 0% rh fit, a quadratic model fit was found to suit the data more due to the water vapour reducing the response output of the Au-MAH chemosensor relatively to the Au-HDT chemosensor. Between methanol, propan-1-ol and toluene only propan-1-ol showed a significant change in device response behaviour from an increase in relative humidity from 0% rh to 38% rh.

The analysis of device response curves was also carried out to observe any distinguishing factors between the analyte vapours for the three different combinations

of polar and non-polar chemoresistive sensor materials. It was observed that the response rates, magnitude responses and the direction of the response for the individual analytes could be used as identifying factors for the analytes as some analytes caused an increase in the voltage output while others caused the voltage output to decrease . The response time was noted to be longer than the devices tested in chapter 5. It was proposed that these distinguishing factors combined with the pre-grouped conditional probabilities according to response direction could be used in linear discriminant analysis to identify the VOC vapours being analysed.

The polar/non-polar and non-polar/polar duo-type devices offered a wider spread of response results thus offering a greater spectrum of response results in magnitude and positive or negative direction for each of the analytes tested. Even though none of the tested devices resulted in absolute cancellation of the balancing chemosensor the response to some of the analytes were significantly reduced in magnitude, such as that of the Au-MAH/Au-NT device to toluene at 0% rh. It was observed that as the net magnitude response of the devices to analyte vapour was reduced, so was the dependence of the character of the devices on changes in relative humidity and temperature. The ideal operating temperature was determined to be 40°C at which the effects of rh changes on the device output were observed to be minimal.

The following chapter summarises the observations made in this research project and presents a conclusion to the thesis.

6.7. References

Joseph, Y, Guse, B, Yasuda, A & Vossmeyer, T 2004, 'Chemiresistor coatings from Pt- and Au-nanoparticle/nonanedithiol films: sensitivity to gases and solvent vapors', Sensors and Actuators B: Chemical, vol. 98, no. 2-3, pp. 188-95.

Vossmeyer, T, Joseph, Y, Besnard, I, Harnack, O, Krasteva, N, Guse, B, Nothofer, HG & Yasuda, A 2004, 'Gold-nanoparticle/dithiol films as chemical sensors and first steps towards their integration on chip', Physical Chemistry of Interfaces and Nanomaterials Iii, vol. 5513, pp. 202-12.

CHAPTER 7

7. Conclusions & Further Work

7.1. Overview

The main purpose of this research was to show the effectiveness of using the ratiometric principles to counter common problems, such as drift and low device life expectancy, associated with chemical sensors. A novel low-cost gas sensor system, based on chemoresistive sensors was developed and analysed in this study. The device was required to be capable of showing repeatable measurements for polar and non-polar VOCs with some level of discrimination between them in a test environment. It was expected that there would be some effect of humidity on the chemical sensors, hence, a sensor with as low as possible effects to changes in ambient temperature and relative humidity on the output of the sensor device while offering increased stability in the device output was required. Self-assembled gold nanoparticle linked alkyl-dithiol chemoresistors were selected as the chemosensors and were operated in a ratiometric arrangement. Previous work at Warwick University resulted in the fabrication of a smart ratiometric ASIC chip (SRL 194) which formed the electronic circuitry of the sensor device. This ASIC was fabricated under the Europractice IC Manufacturing Service for €2476 for a batch of 20, hence, keeping the device costs fairly low compared to other

handheld gas sensor systems. The ratiometric architecture of the SRL 194 ASIC was based on a non-inverting amplifier circuit and under ideal conditions was expected to reduce the effects of ageing, drift and offer stability in the device output when tested at different temperatures and relative humidity.

Three different self assembled gold nanoparticle linked alkyl-dithiol chemosensors were combined with the SRL 194 device to form the chemoresistive component of the non-inverting amplifier. The chemoresistive films could be modified to respond specifically to certain groups of VOCs. Two of the dithiol chemosensors had a non-polar resistive film component and differed from each other in the chain length of the alkyl units. The third chemosensor included a polar acetylamino group in the backbone of the linker structure. The architecture of the SRL 194 ASIC offered the opportunity to utilize the different properties of the chemosensors in a ratiometric array.

The objective of the research was to test and characterize the novel hybrid smart gas sensor system for different VOCs and observe the effects of changes in temperature and relative humidity on the response of the sensor device. The three materials characterized in this study were: Au-nanoparticle 1,9 nonanedithiol (Au-NT), Au-nanoparticle 1,16 hexadecane-dithiol (Au-HDT), and 2-mercapto-N-[6-(2-mercapto-acetylamino)-hexyl]-acetamide (Au-MAH). The sensor devices were characterized in three different types of arrangements. The first arrangement involved the use of only one chemosensor balanced by a precision reference resistor chosen to give a resistance ratio of 1.0. Depending on which resistor the chemosensor replaced in the non-inverting amplifier, the sensor was referred to as either the *active* or the *passive* monotype sensor device. The sensor devices formed with passive chemosensors had the chemosensor surface covered with a silicone sealant gel (Dow Corning 3145 RTV MIL-A-46146). These devices were tested under the same conditions as the active sensor devices.

The second type of devices tested were the *mono-type* bi-variate devices, in which both the active and passive resistors used were of the same chemoresistive material. The passive sensor in this case was covered with the same silicone sealant used previously for the individual passive sensor characterization.

The third type of devices manufactured were the *duo-type* devices where one polar and one non-polar chemosensor were combined in the ratiometric array to form one sensor device. The silicone sealant was not applied to any of the chemoresistors in the duo-type arrangement.

All three types of sensor devices showed a fairly slow response rate and were only usually tested with analyte concentrations between 300 to 10000 ppm. With the obtained response rates the sensors were found unsuitable for monitoring air quality to protect human life. However, these sensors were sufficiently good enough to monitor the ambient air for industrial systems that were susceptible to catching fire in the presence of the required activation energy for high concentrations of combustible hydrocarbons such as alcohols and toluene.

7.2. Review of Aims and Objectives

All the objectives set for this study were met. A brief summary of the work carried out to this effect is listed below:

a) The SRL 194 ASIC device was successfully integrated with three different gold nanoparticle alkyl-dithiol chemoresistive sensors. The integrated sensor chips were positioned inside the ceramic packaging with the SRL 194 ASIC and hence, were subjected to the same temperature and test environment conditions as the ASIC.

b) Change in the output voltage was determined to be entirely dependent on the change in the resistance ratio of the chemosensors. Hence, Δrr was taken as the measure for device response.

c) The integrated devices were characterized individually with one chemosensor at a time against methanol, ethanol, propan-1-ol and toluene vapours in air at 30°C and 0% rh.

d) The effects of encapsulating the chemosensor with a silicone sealant gel were observed. It was found that this partitioning layer resulted in amplification of the sensor device output at exposure concentration under 3000 ppm. At higher analyte concentrations no significant effects of the silicone gel were observed.

e) The results of the single sensor un-encapsulated (active) and the encapsulated (passive) chemosensor devices were found to fit a Langmuir sorption model. The results of the active devices were compared with a linear regression and the results of the passive sensors were found to fit a Freundlich sorption model.

f) The mono-type arrangement allowed the ratiometric setup to be characterized, using two chemosensors of the same material balancing each other in one sensor device. Application of the silicone sealant gel on one of the two chemosensors allowed the differences in the sorption properties of the two chemosensor films to be amplified while nearly cancelling the effects of temperature. The magnitude response results from the mono-type devices were found to fit the Langmuir adsorption model.

g) The duo-type arrangement allowed for the characterization of sensor devices based on a combination of a polar and a non-polar chemoresistive sensor material. This arrangement resulted in reduced response rate and response magnitude to the various VOCs compared to the single sensor and the mono-

type devices, but offered a wider spread of the effective change in resistance ratios produced by the different analyte vapours.

h) The most suitable regression models for the different VOCs were identified and plotted for the duo-type devices for the three different polar/non-polar arrangements.

i) A linear discriminant analysis was suggested which could be used to identify a particular vapour under investigation given the distinguishing factors obtained from static data analysis.

The SRL 194 ASIC design incorporates eight FET switches that invert the applied potential at the terminals of the chemoresistive material to avoid drift and polarisation associated with application of DC voltage over long periods of time. There was a possibility that at the high frequency of switching the polarity the gold nanoparticle linker structure based chemoresistive films, where the gold particles provide the conductivity in the chemosensors, could result in a short-circuited chemoresistive sensor. All the tests carried out showed that the gold nanoparticle chemoresistors were fully compatible of operating with the ASIC chip. Tests on the internal circuitry of the ASIC showed that the ASIC was able to operate in a resistance ratio range of 0.5 to 2 with a 10% error margin. The internal resistance of offset circuit of the SRL 194 ASIC was determined to be ~16 kΩ within a 5% error margin. It was calculated that the internal resistance of the offset circuitry of the SRL 194 ASIC had an increase in resistance of *ca*. 101.6 Ω/°C when the ambient temperature of the sensor device was increased.

The ratiometric setup offered increased stability to the device output. Drift due to long term exposure to DC voltage was reduced to negligible 0.01 V over a 12 hour period. All the tests carried out for characterization exposed the sensor devices to successively increasing concentrations of the analyte vapours rather than a randomised exposure strategy which is known to reduce device drift due to residual analyte remaining in the chemoresistive sensor film. Despite using successively increasing analyte concentrations the devices showed a negligible drift of the baseline. The repeatability of the devices was tested by exposing them to first increasing concentrations and then decreasing concentrations. The resulting hysteresis was also noticed to be negligible and within the device error margin of 10%.

7.3. Characterization of Gold Nanoparticle based Sensor Devices

The different types of sensor devices were characterized by testing them against various VOCs in air. The test temperature and relative humidity were varied for some of the tests to observe the stability effects of the ratiometric setup. The following subsections summarise all the characterization objectives explored. The tabulated results for changes in magnitude response at 38% rh or at 40°C are given relative to the values obtained for tests at 0-3% rh and 30°C.

7.3.1. Characterization of Mono-variate Sensor Devices

The first type of sensor devices based on single sensors (active or passive) were characterized with ethanol, methanol, propan-1-ol, and toluene vapour at 30°C and 0% rh. The devices were also tested for effects of humidity by testing the Au-HDT and Au-MAH devices at ~38% rh for exposure to toluene vapours. Table 7.1 summarises the characteristics of the active sensor (with no silicone encapsulation) devices, when exposed to 1000 ppm of each of the analytes.

Active Sensor Device / **VOCs**	**Au-NT (Δrr x 10^{-3})**	**Au-HDT (Δrr x 10^{-3})**	**Au-MAH (Δrr x 10^{-3})**
Methanol	2.18	1.50	7.82
Ethanol	6.74	3.99	26.3
Propan-1-ol	18.6	18.4	48.1
Toluene	15.3	38.8	17.7
Effect of Humidity Increase to 38% rh at 30°C		-10.6% (Prop)	-63% (Prop)
		-58.6% (Tol)	-61% (Tol)

Table 7.1 Characterization of active sensor devices at 1000 ppm

Table 7.1 lays clear the advantages of the three chemoresistive materials over each other when tested with the different VOCs. Each material showed a higher $|\Delta rr|$ response to the analyte with increasing size of the alcohol molecule. The magnitude response to toluene increased as the length of the linker structure increased. The inverse of this characteristic is also true for the magnitude response to alcohols when comparing Au-NT and Au-HDT materials. A large drop in magnitude response occurred as the

devices were tested at ~38% rh. The Au-HDT device had a limited magnitude response drop relative to the Au-MAH device. In the latter material's sensor device it was observed that the analyte adsorption sites were overwhelmingly occupied by competing water molecules instead of the VOCs.

Passive Sensor Device / **VOCs**	**Au-NT (Δrr x 10^{-3})**	**Au-HDT (Δrr x 10^{-3})**	**Au-MAH (Δrr x 10^{-3})**
Methanol	5.15	9.16	16.6
Ethanol	10.9	23.9	30.4
Propan-1-ol	19.8	28.1	45.3
Toluene	23.1	41.4	20.1
Effect of Humidity Increase at 30°C		-12.5% (Prop)	-71% (Prop)
		-35.1% (Tol)	-65.6% (Tol)

Table 7.2 Magnitude response of passive sensor devices at 1000 ppm

The advantage of using the silicone gel coating can be observed from the data values in table 7.2. The silicone gel coating magnitude response results were higher for the Au-NT and Au-HDT devices, the response results of the latter having being increased several times. However, the coating shows little effect on the Au-MAH device results apart from with exposure to methanol. The silicone coating was found to be most useful at analyte concentrations less than 5,000 ppm which was encouraging for real-world application.

The main conclusions drawn from the device characteristics over the range of VOC exposure concentrations are listed below:

The Au-NT Device

a) The Au-NT active material showed a strong and closely matching adsorption coefficient for propan-1-ol and toluene. Ethanol and methanol had lower adsorption coefficients and the device responded relatively slowly to changes in the vapour concentrations of these analytes.

b) The silicone sealant introduced a delay in the response time to the VOC vapours. This resulted in an increase in separation of the response results of the

sensor device to different analytes, and hence greater selectivity at concentrations less than 3,000 ppm.

Au-HDT Device

a) The overall result of the chain length increase between the Au-NT and Au-HDT devices was a greater separation between the analyte magnitude responses than the Au-NT based sensor.

b) The silicone sealed devices showed a more uniform separation between the analytes and were a better fit to the Langmuir curve.

Au-MAH Device

a) The addition of the polar acetyl-amino link in Au-MAH increased the magnitude responses of the material to alcohols three to four times the Au-NT levels. Response to toluene was increased by only 30% at 5000 ppm (upper limit) of analyte and remained unaffected at 386 ppm.

b) Application of the silicone sealant to the passive Au-MAH sensor increased the magnitude response to methanol by 50% and propan-1-ol by 20% at concentrations greater than 5,000 ppm.

7.3.2. Characterization of Mono-type Bi-variate Ratiometric Sensor Devices

The ratiometric monotype devices based on the three different gold nanoparticle film materials were characterized for exposure to several concentrations of ethanol, methanol, propan-1-ol, toluene and water concentrations at *ca.* 0-5% rh at 30°C. The devices were then tested for the effects of change of relative humidity from *ca.* 3% rh to *ca.* 38% rh. The devices were also tested for the effects on device response from changes in temperature from 30°C to 40°C.

Table 7.3 summarizes the response results of the three different devices tested when exposed to VOC vapour concentrations of 1,000 ppm. The characteristic magnitude response results are given for the devices when tested at 30°C at 0-5% rh. When exposed to the VOC vapours at a higher relative humidity or temperature, the comparative change in magnitude response to tests at 30°C at 0-5% rh are also given in this table. The most significant observation made with the monotype devices was the

dominance of the passive sensor over the active sensor to give net negative value to response results.

Mono-type Sensor Device / **VOCs**	**Au-NT (Δrr x 10^{-3})**		**Au-HDT (Δrr x 10^{-3})**	**Au-MAH (Δrr x 10^{-3})**	
Methanol			3.04	7.14	
Ethanol	10.5		14.8	31.4	
Propan-1-ol	5.06 (38% rh)		5.60	11.9	
Toluene	13.6		58.4	27.9	
Water			3.62	5.72	
Effect of Humidity Increase from 3% to 38% rh at 30°C	-6.2% (Eth)		12.7% (Meth)	-47.7% (Meth)	
			-11.5% (Eth)	-55% (Eth)	
	2.9% (Tol)		73% (Prop)	-31.8% (Prop)	
			-26.4% (Tol)	-39.1% (Tol)	
			-60.8 % (Wat)	-25.6% (Wat)	
Effect of Temperature Increase from 30°C to 40°C	-21.4% (Eth) (3% rh)	- 30% (Eth) (38% rh)		38.2% (Eth) (3% rh)	-29% (Eth) (38% rh)
	-42.2% (Tol) (3%rh)	-38.8% (Tol) (38%rh)		-77% (Tol) (3%rh)	-67.2% (Tol) (38%rh)

Table 7.3 Magnitude response of mono-type sensor devices at 1000 ppm

The above table only shows the magnitude response for all the devices to make it easy to compare with individual sensor device results. The response results were dependent on the net change of the resistance ratio of the active and passive chemosensors. The results showed a greater change in resistance of the silicone coated passive chemosensor compared to the active chemosensor. It can be concluded that the silicone partitioning layer has an effect similar to a pre-concentrator on the sensor films.

It was observed with the Au-NT and Au-MAH devices that the stability of the device over a change in relative humidity improved as the device operating temperature was increased to 40°C. The Au-HDT device reported a relative increase in magnitude response when exposed to methanol and propan-1-ol vapours and a relative decrease in magnitude response when exposed to the other three VOCs at 38% rh. The Au-MAH device reported a reduction in response at higher humidity for exposure to all the tested analytes. It was observed that even though the magnitude response compared to individual chemosensor based devices reduced predominantly, a generalized rule is

difficult to make as at some occasions the magnitude was much higher than the single sensor devices. Other observations for these devices are listed below:

a) Au-NT device's response to ethanol, methanol and propan-1-ol vapours showed nearly perfect Langmuir fits. As the resistances of the active and passive sensors adjust at the same time, the device saturation rate was a sum of the saturation rates of the two chemosensors.

b) The Au-HDT device compared to the Au-NT device showed an almost fourfold increase in response to toluene, followed by a 60% increase in propan-1-ol response.

c) The polar Au-MAH devices showed a 100% increase in response to the alcohols and a 20% reduction in the response to toluene compared to the Au-HDT device.

d) The Au-MAH devices proved susceptible to changes in humidity, with the drop in magnitude response proportional to the analyte test concentration.

e) The Au-MAH devices assembled from chemoresistors of ~105 kΩ showed twice the magnitude response to those assembled with chemoresistors of 55 kΩ.

f) Analysis of the response curve shape with respect to time showed the activity at chemosensor surfaces immediately after analyte exposure was switched on and off. These response curves were also analysed to observe the response rates which could be used in linear discriminant analysis to identify a pre-characterized test analyte vapour.

7.3.3. Characterization of Duo-type Ratiometric Sensor Devices

The characterization of duo-type devices used one polar and one non-polar chemosensor with the SRL 194 ASIC to form the ratiometric sensor device. Three types of duo-type sensors were tested in the following active/passive arrangements: Au-MAH/Au-NT, Au-MAH/Au-HDT, and Au-HDT/Au-MAH. As the two chemosensors forming the device had different adsorption characteristics the duo-type devices offered a wider spectrum of response results. The previous types of sensors discussed either had all their response results on the positive side or the negative side. The duo-type devices were unique to give a positive response to some analytes and a negative value to others.

Table 7.4 summarizes the response results of the three different devices tested when exposed to VOC vapour concentrations of 1,000 ppm.

It was expected from the duo-type devices that this arrangement would cause a severe reduction in the magnitude response of the devices compared to single sensor devices. Even though an effect of the combination of the two sensors had been observed, the final response results lay somewhere between that of the individual chemoresistive materials.

Duo-type Sensor Device	**Au-MAH/Au-NT (Δrr x 10^{-3})**		**Au-MAH/Au-HDT (Δrr x 10^{-3})**	**Au-HDT/Au-MAH (Δrr x 10^{-3})**
VOCs				
Methanol			3.94	-4.20
Ethanol	9.84		10.6	-13.8
Propan-1-ol			7.08 (38% rh)	31.9
Toluene	5.22		-24.5 (38% rh)	49.5
Water			6.58	-9.07
Effect of Humidity Increase from 3% to 38% rh at 30°C	-35.2% (Eth)		14% (Meth)	-135% (Meth)
	-21.2% (Tol)			-329% (Prop)
				-7.9% (Tol)
Effect of Temperature Increase from 30°C to 40°C	-46.6% (Eth) (0% rh)	-33.6% (Eth) (38% rh)		
	-61.19% (Tol) (0% rh)	-61.8% (Tol) (38% rh)		

Table 7.4 Response of duo-type sensor devices at 1000 ppm

The wide spectrum of response results ranging from negative to positive response result values made it easier to identify various VOC analyte groups. The combination of the polar and non-polar chemosensors brought together the advantageous elements of the two chemosensors into one device. The effects of humidity on device magnitude response were almost eliminated when the devices were operated at a temperature of 40°C. It was also observed that at higher relative humidity the characteristic plots did not fit the Langmuir model anymore. A summary of the benefits offered by these devices is as follows:

a) The polar Au-MAH material maintains its dominating affinity to the alcohol molecules. Between ethanol, methanol and water, the two alcohols have the highest saturation rate with ethanol leading the response rate by 100% to methanol for the Au-MAH/Au-HDT device.

b) Increase in relative humidity has a remarkable effect on the propan-1-ol and toluene responses with the Au-MAH/Au-HDT device. The response to propan-1-ol comes down from a peak at ~2,000 ppm as propan-1-ol's affinity for Au-HDT increases relative to the water molecule occupied Au-MAH chemosensor. Similarly the toluene response changes from a Langmuir fit to an exponential fit.

c) The Au-HDT/Au-MAH device reported results which were almost the exact x-axis reflection of the Au-MAH/Au-HDT device with the exception of propan-1-ol vapour exposure.

d) By analysing the shape of the response curve with respect to time it was possible to observe several distinguishing factors between the device responses including response rates and direction of magnitude response. A modification of the linear discriminant analysis model for mono-type devices was suggested for easier identification of pre-characterized analyte vapours.

7.4. General conclusions

Three different types of chemoresistor based sensor devices were successfully characterized and the effects of changes in relative humidity and temperature on device magnitude response studied. Under ideal conditions the active and the passive chemosensors would have matching resistances and a net *rr* value of 1.0. This was difficult to achieve in practice because of device to device variation. However, despite the differences in the resistances of the chemosensors all the sensor devices showed repeatable results within an error margin of 10%. The devices showed good operability and extremely good signal to noise ratio with chemoresistors of the order of 1 kΩ to 1 MΩ despite being originally designed for operating with 10 kΩ resistors. The test devices were robust with very little variation in the quality of the device output over the course of 18 months.

The characterization tests showed that the ideal operating temperature of the devices was 40°C, where the effects of relative humidity change were least felt. However, this increased stability came at the cost of device magnitude response. Hence, a compromise between device magnitude response, response rate and device stability needed to be achieved depending on usage requirements.

The ratiometric configuration of the chemosensors resulted in devices with good return to baseline properties and an extremely low hysteresis. Most of the tested configurations showed a good fit to the Langmuir model when relative humidity effects are negligible.

The effects of applying a silicone sealant gel on the chemoresistive sensors were observed. It was noticed that the silicone was permeable to all the tested analytes and behaved similar to a pre-concentrator when exposure concentrations were less than 3,000 ppm. At higher concentrations the silicone was observed to reach a saturation value and had a tendency to converge all the responses to the different analytes.

Novel configurations of the ratiometric sensor array tested in this study resulted in a wide spectrum of response results with various analyte results grouped together with either positive or negative value of the response magnitudes. This spread of responses was achieved without reducing the magnitude response of the sensor devices greatly. The smart ratiometric gas sensors characterized over the course of this study required minimal post-processing steps for the device output. A linear

discriminant analysis model was presented which could be used to identify pre-characterized analyte vapours.

7.5. Further Work

This study focused on characterizing the gold nanoparticle based sensor with individual VOCs and observe the effects of relative humidity and temperature changes. This has opened up the opportunity for the work to be extended in other future projects. Other prospective projects that may arise from this work are listed below:

a) The duo-type arrangement offers the opportunity for the sensor array to be characterized with mixtures of gases. This work can also be extended to characterizing and identifying odours and hence incorporate more e-nose elements into the device.

b) The current characterization of the device reported results to an accuracy of 10%. Greater statistical analysis can improve this error margin. Pattern recognition techniques such as PCA and MLP can be included in the post-processing step offering greater discrimination between analyte vapours and smells.

c) The data acquisition part of the circuit can be integrated onto a single CMOS chip or hybrid chip to be suitable for a portable hand-held instrument.

d) The on-chip heating element of the SRL 194 ASIC can be characterized and the effects of using on chip heating as an alternative to using a Dri-bloc heater can be determined.

e) The SRL 194 ASIC device has on chip inter-digitated electrodes. A fully hybrid device can be manufactured by depositing the chemoresistive film directly onto these electrodes. This requires post-CMOS gold bump bonding onto the aluminium (metal3) layer. The process is a standard wafer-level one and has been used elsewhere (Strandjord et al., 2002; Yau et al., 2004). Aluminium metal is unsuitable for use in chemical sensors and so a post-CMOS process is essential for practical application of the chip. The relatively low temperature deposition process of the polymer coatings is compatible with CMOS technology and can be carried out post-CMOS.

f) The effects of depositing chemoresistive material on various shapes of electrodes integrated with the ASIC device can be observed.

g) The ratiometric arrangement can be improved by using a suitable sealant material which allows one of the two chemoresistive films to act as the reference while the other one responds to the test vapours. Humidity dependence will be removed if the sealant material is pervious to water vapours but not the analyte vapours. Temperature dependence can be removed if the sealant material has the same thermal behaviour as the chemoresistive film material.

h) The duo-type characterization results have opened up the possibility of further exploration of configurations based on similar principles. Arrays based on chemoresistors more distinctly different from each other can be tested and the effects of combining more diverse resistors into one sensor can be characterized.

i) Novel nano-biosensor materials have shown promise in following the principles of the mammalian olfactory system (Gomila et al. 2006). Combining such materials in a ratiometric array may offer a close match to the sensitivity of the mammalian olfaction.

7.6. References

Gomila, G, Casuso, I, Errachid, A, Ruiz, O, Pajot, E, Minic, J, Gorojankina, T, Persuy, MA, Aioun, J, Salesse, R, Bausells, J, Villanueva, G, Rius, G, Hou, Y, Jaffrezic, N, Pennetta, C, Alfinito, E, Akimov, V, Reggiani, L, Ferrari, G, Fumagalli, L, Sampietro, M & Samitier, J 2006, 'Advances in the production, immobilization, and electrical characterization of olfactory receptors for olfactory nanobiosensor development', Sensors and Actuators B-Chemical, vol. 116, no. 1-2, pp. 66-71.

Strandjord, AJG, Popelar, S & Jauernig, C 2002, 'Interconnecting to aluminum- and copper-based semiconductors (electroless-nickel/gold for solder bumping and wire bonding)', Microelectronics Reliability, vol. 42, no. 2, pp. 265-83.

Yau, EWC, Gong, JF & Chan, P 2004, 'Al surface morphology effect on flip-chip solder bump shear strength', Microelectronics Reliability, vol. 44, no. 2, pp. 323-31.

Appendix A: Layout of Data Acquisition Setup

This appendix contains the design layout of the Connecting PCB and the Test Board.

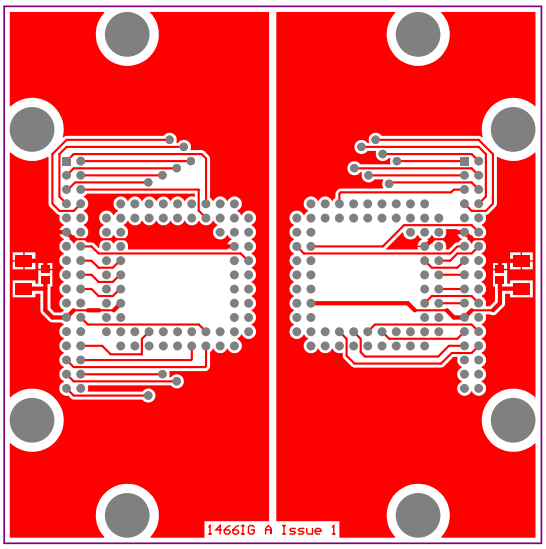

Figure 1 Tope view of the Connecting PCB

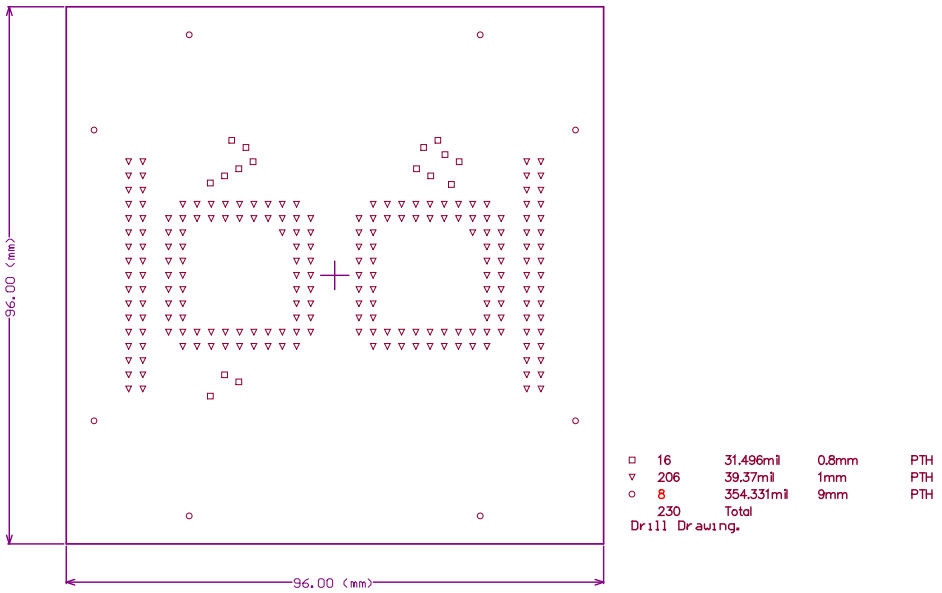

Figure 2 Dimensional layout of drill holes in the Connecting PCB

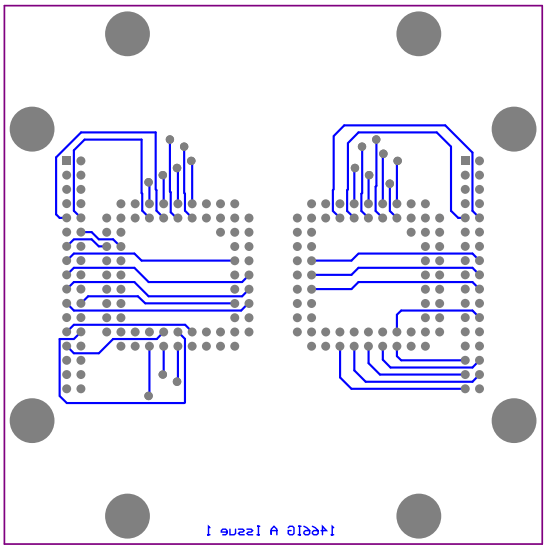

Figure 3 Bottom view of the Connecting PCB

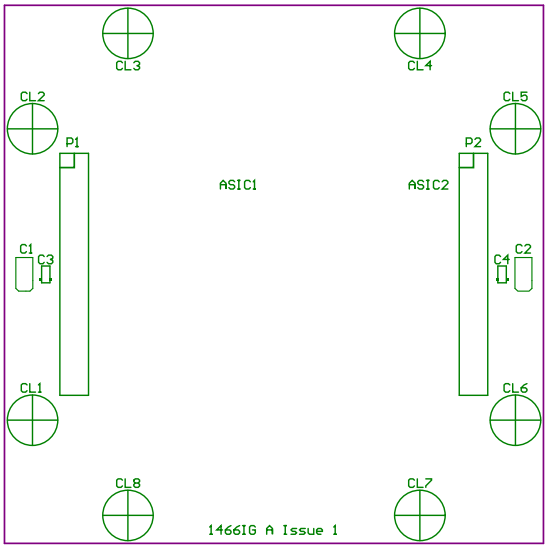

Figure 4 Dimensional layout of drill holes in the Connecting PCB for screws and connectors

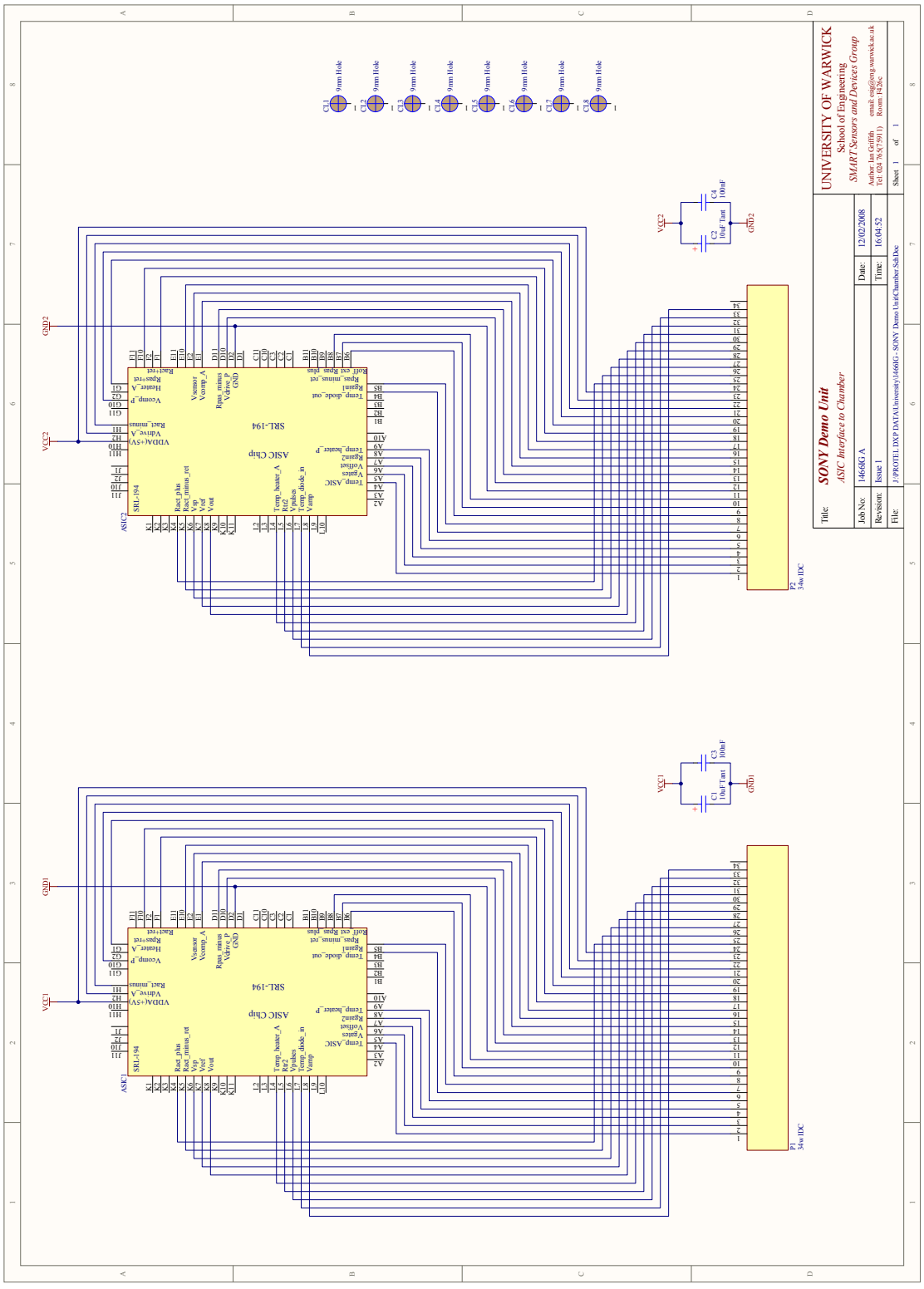

Figure 5 Pin and Wire Connections of the Connecting PCB

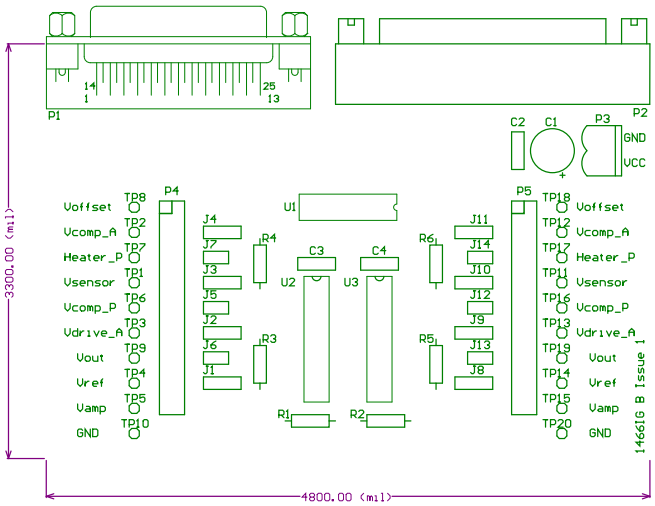

Figure 6 Component layout of the Test Board

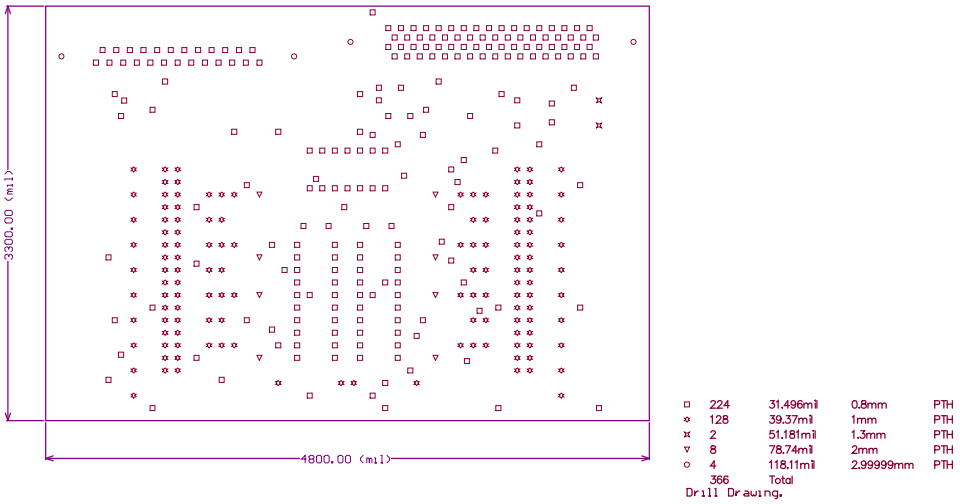

Figure 7 Drill dimensions of the Test Board

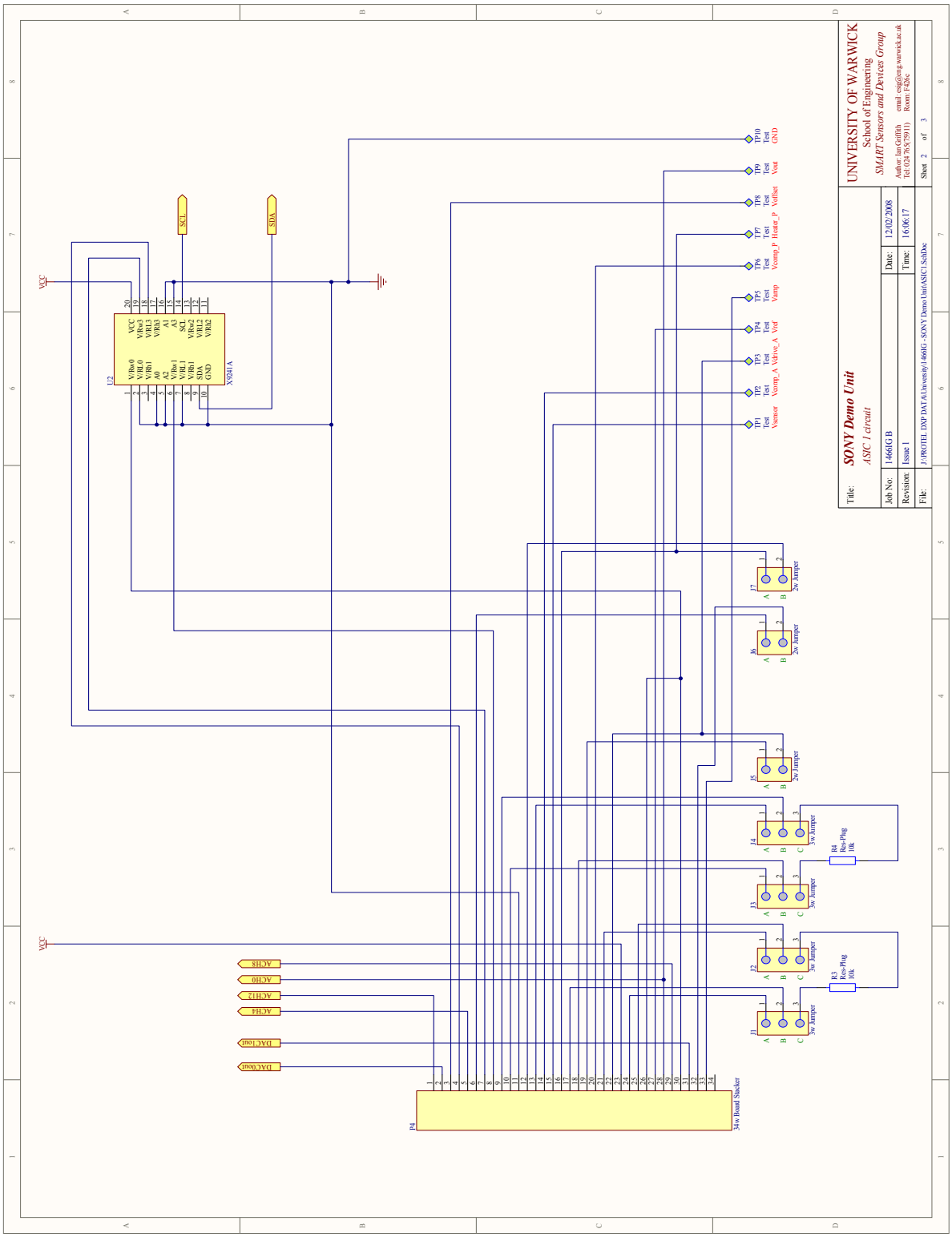

Figure 8 Pin and Wire Connections for ASIC1 on the Test Board

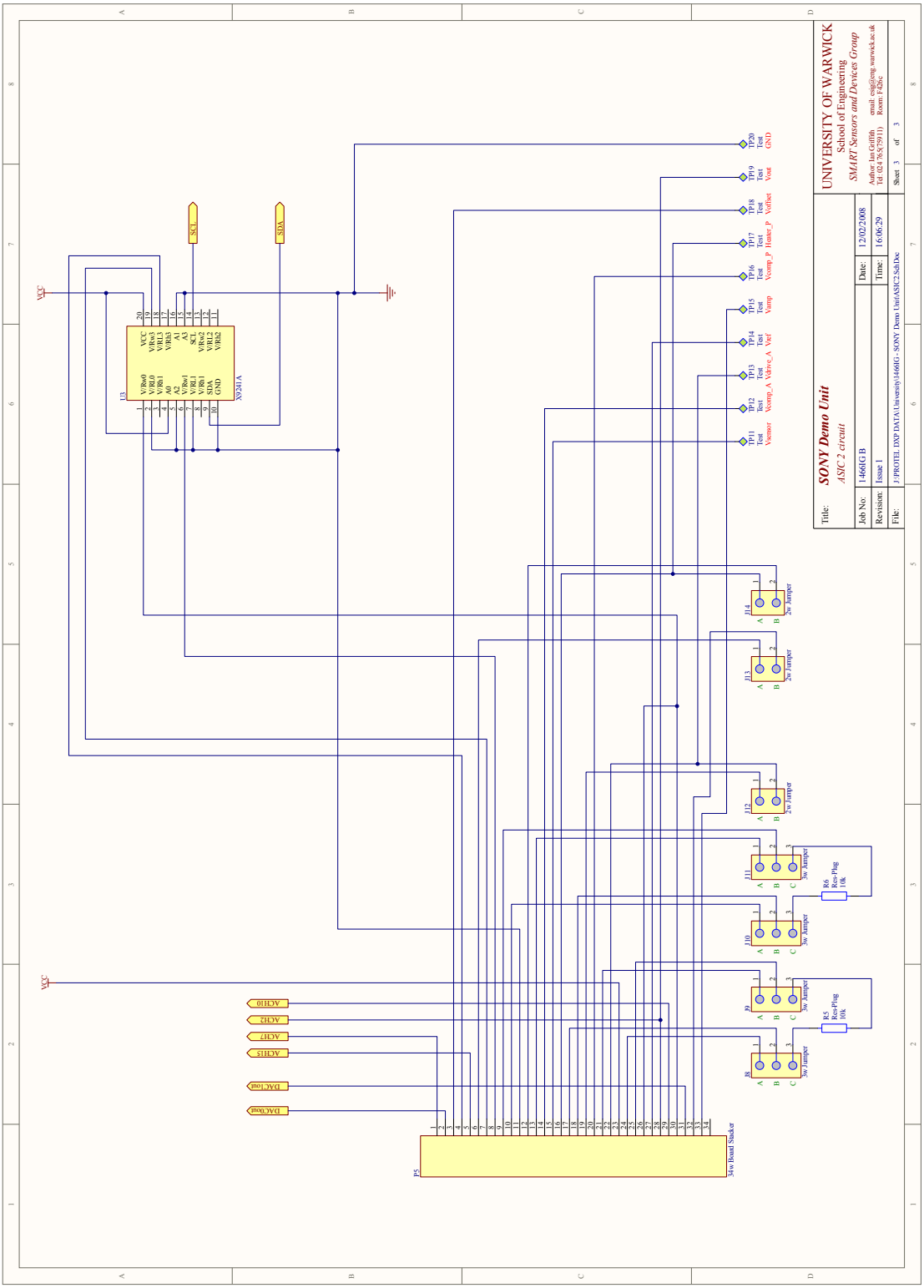

Figure 9 Pin and Wire Connections for ASIC2 on the Test Board

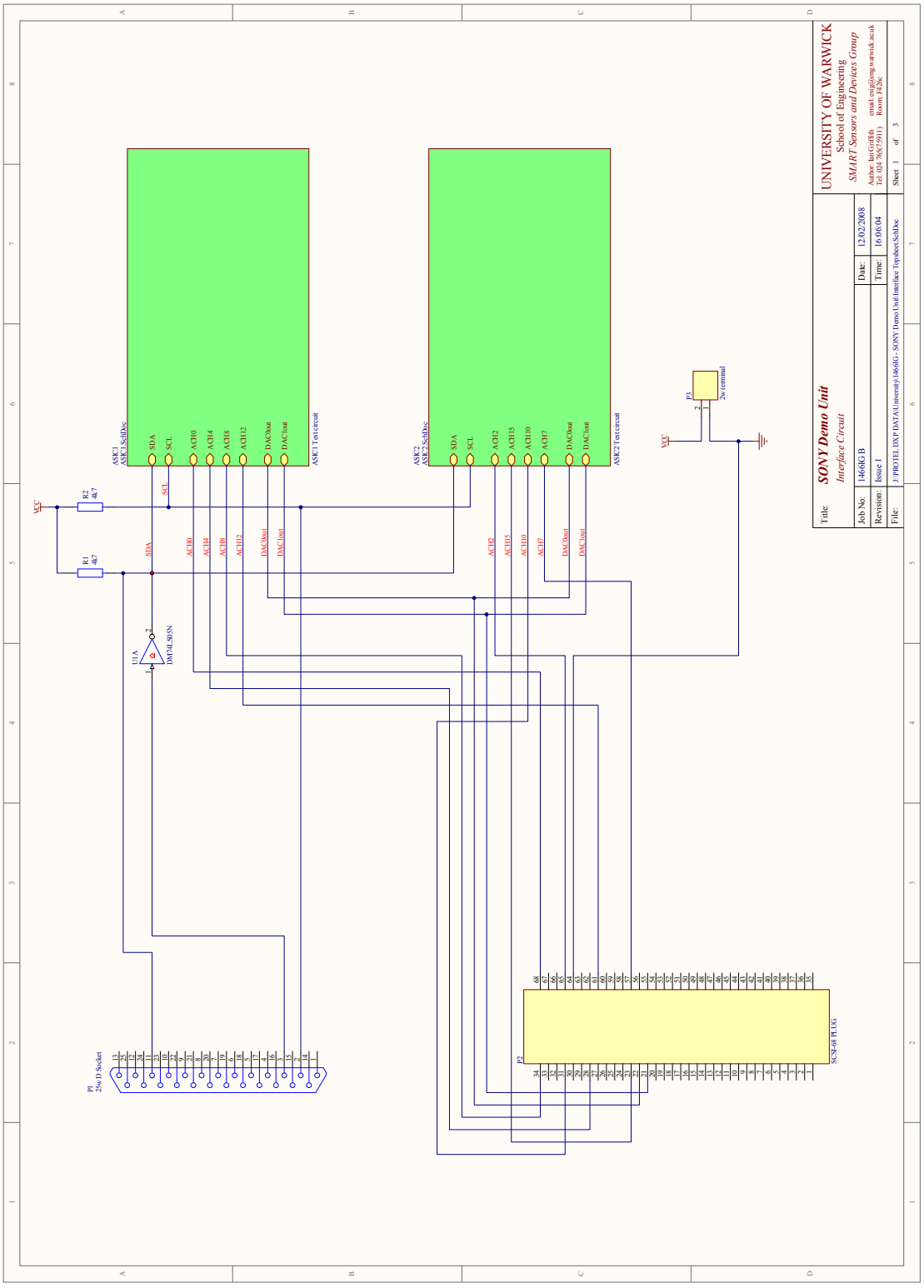

Figure 10 Pin and Wire Connections between NI-DAQ, Parallel Port Interface connectors and ASIC1 and ASIC2

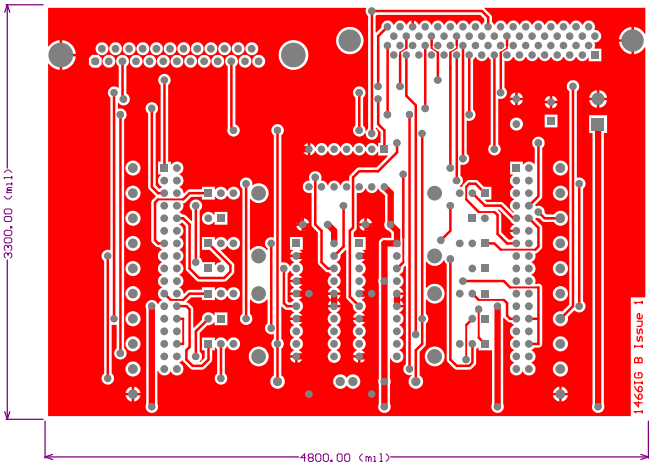

Figure 11 Top view of the Test board

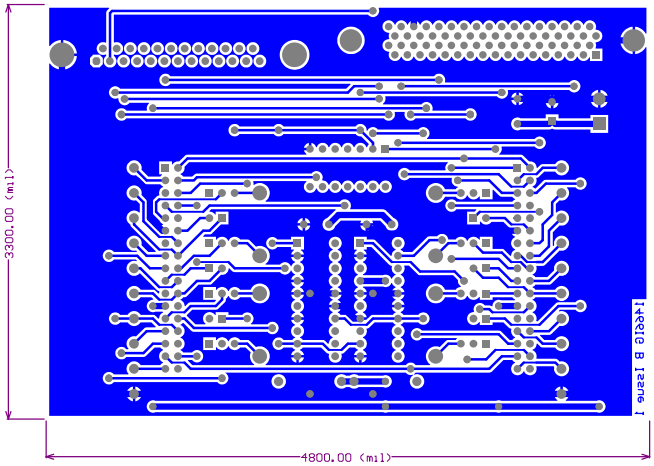

Figure 12 Bottom view of the Test board

Appendix B: Schematics of Flow Injection Analysis Test Station

This Appendix lists all the components that form the Flow Injection Analysis test station. Table 1 defines the key to all the symbols used in the design schematic for the test station. Figure 1 gives a schematic overview of the FIA station. The details of the FIA test station have been published by Covington (Covington, James A. 2001).

Symbol	Part	Supplier	Details
	Compressed Air Source, Type L Bottle	BOC Gases Ltd.	Compressed cylinder containing low grade dry air. Pressure is controlled by a single stage regulator.
	Particulate Matter Filter	Lee Products Ltd. TCFA120135A	Filters which trap particles with diameter greater than 35 μm.
	Mass Flow Controller (1, 2 and 3)	Brooks Instruments B.V.	Model TR 5850. 0 to 300 ml/min flow range. Each MFC consists of a flow controller, override valve and flow meter.
	Non–return Value	Lee Products Ltd. TKLA950113D	Used after each MFC to prevent backward flows in the system due to pressure differentials or MFC failure.

	Non-return Valve	The West Group	Viton non-return valves, resistant to sample vapours
	Solenoid Valves NC	The West Group. ET2-12H	Low power solenoid values with 5 V_{DC} switching voltage.
	Bubbler	Fisons Scientific Equipment Ltd. BTF-900-150S	250 ml Drechsel (gas washing) bottle and head with grade 1 sinter.
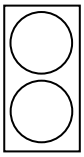	Refrigeration unit	Neslab RTE-300D	Refrigeration unit, temperature range 200^{o}C to – 40^{o}C (± 0.1 ^{o}C).
	Mixing Chamber	N/A	Stainless steel mixing chamber manufactured at Warwick University to mix the sample vapour and the water vapour and deliver it to a single output.
	Flow Meter	Brooks Instruments B.V.	Model TR5850, to measure output flow of system
	Flow Meter	Honeywell	Flow meter, Honeywell

		AWM3300	AWM3300.
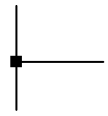	Stainless Steel 316 Tubing	Metal Supermarket	3 mm O.D. (1 mm I.D.) tubing used wherever possible within the equipment.
	PTFE Tubing	Economatics Ltd.	3 mm O.D. (1 mm I.D.) tubing used where needed.
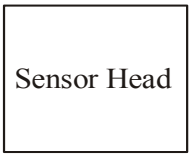	Sensor Chamber		Custom designed and manufactured sensor chamber.
	Multi-blok Heater	Cole Parmer. E-03129-02	Second heater for the mixing chamber.
	Dri–bloc™ heater	Techne Ltd.	Dri–block heater Model DB-2D allowing programmable temperatures to be set in a range from room temperature to 105 ºC, with long–term stability within 0.1 ºC.

Table 1 Symbol key and Explanation

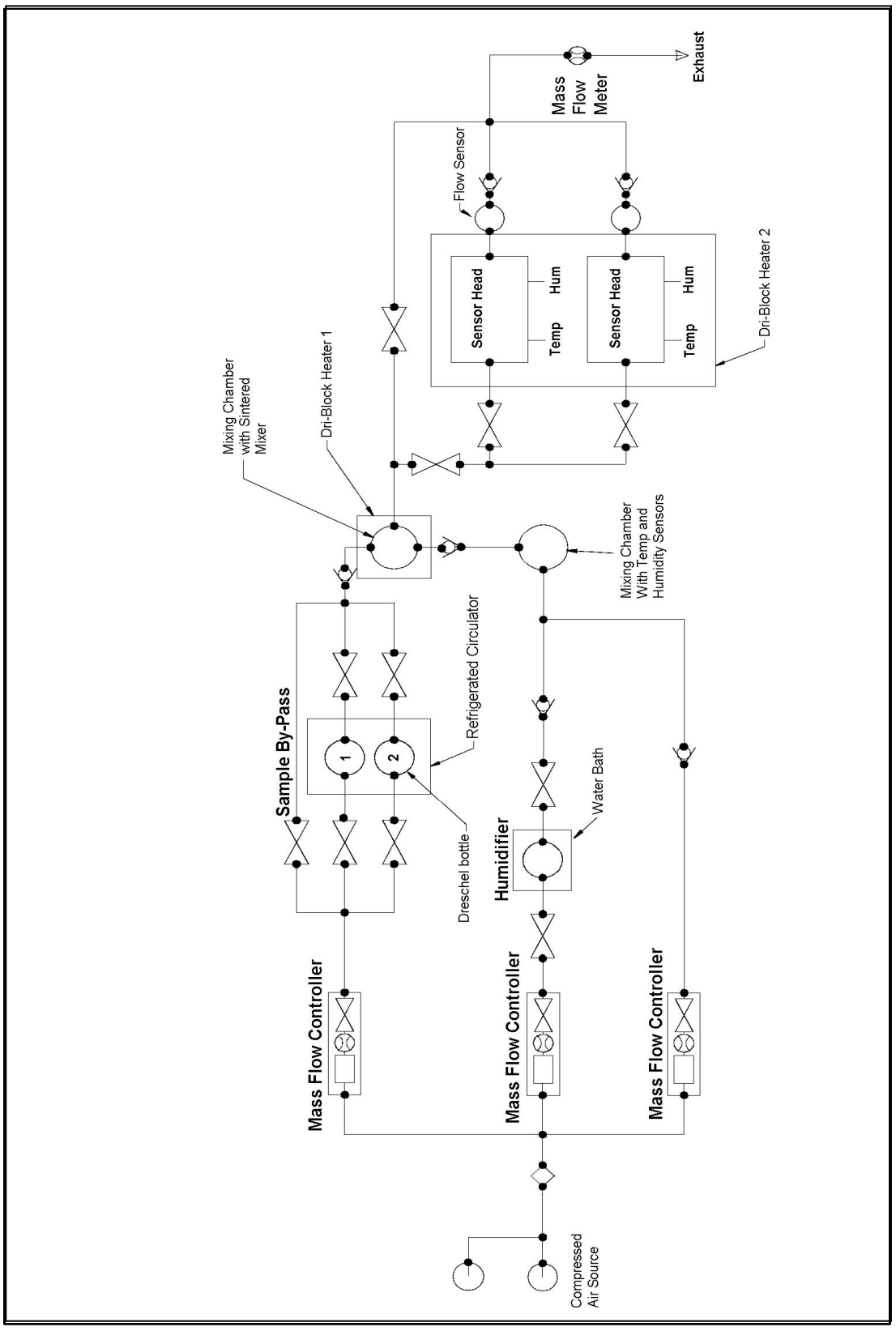

Figure 1 Schematic Overview of the FIA station